University of Durham

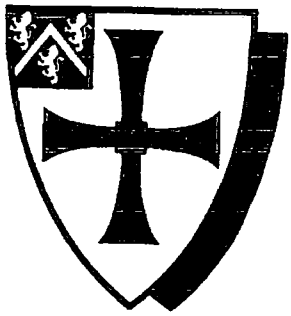

Computer simulations of liquid crystals

Melanie Joanna Cook

Chemistry Department

University of Durham

October 2000

Submitted in partial fulfillment of the

requirements for the degree of

Doctor of Philosophy

Abstract

Computer simulations of liquid crystals

Melanie Joanna Cook

Molecular simulations performed on modern computers provide a powerful tool for the investigation of both static and dynamic properties of liquid crystals. In this thesis several properties of liquid crystal mesogens have been investigated using state-of-the-art Monte Carlo (MC) and molecular dynamics (MD) simulation techniques.

The helical twisting power, β_M, determines the pitch of the chiral nematic phase produced when a nematic liquid crystal is doped with a low concentration of chiral solute molecules. A new simulation technique that allows the prediction of both the sign and the magnitude of β_M is described. The method employs fully atomistic MC simulations of a chiral dopant molecule in the presence of a twisted nematic solvent composed of Gay-Berne particles. Eighteen different chiral dopant molecules were examined and in all cases the results were in good agreement with existing experimental data.

The Kirkwood correlation factor, g_1, has been evaluated for the molecules PCH5, PCH5-Cl, me5NF and GGP5Cl using MD simulations in the pre-transitional region of the isotropic phase. The calculations employed an all-atom force field, which was developed specifically for liquid crystal molecules. PCH5 and me5NF were seen to favour anti-parallel dipole alignment whereas, PCH5-Cl and GGP5Cl preferred a parallel arrangement of the molecular dipoles. With the exception of GGP5Cl, the simulations gave g_1 values that were in accordance with existing experimental dielectric measurements. Detailed analysis of the MD trajectories showed that certain molecular pair configurations were preferred in the bulk and indicated which molecular groups were responsible for the stabilization of these configurations.

Equilibrium molecular dynamics simulations were carried out in order to evaluate the rotational viscosity coefficient, γ_1, for a Gay-Berne mesogen using two independent analysis techniques. The methods gave consistent results, which were comparable to experimental data for real mesogens of similar shape and size.

Acknowledgements

I would like to take this opportunity to thank a great many people who have helped me in the three years of this research. Without their help this thesis would never have been written. Firstly, I wish to express my many thanks to the Engineering and Physical Sciences Research Council (EPSRC) for the grant of a quota award and to Merck UK Ltd and Merck Darmstadt Ltd for converting this quota award into a CASE award, therefore, allowing this research to take place. I would also like to thank the University of Durham Computer Centre for the use of their computing facilities, the Edinburgh Parallel Computing Centre (EPCC) for time on their Cray T3E and Merck UK Ltd for the gift of a DEC 433 a.u. workstation.

From an academic view point, there are several people who I have much to thank for their input into this PhD thesis. Dr Lydia Heck for her invaluable assistance with all matters computational. My colleagues, past and present, in the Computational Chemistry group at Durham for providing an interesting environment in which to work, particularly Dr Carl McBride, who's wit, support and encouragement, kept me sane throughout my first year. Above all, my most sincere thanks go to Dr Mark Wilson, my supervisor, whose immense enthusiasm for the subject of computer simulation of liquid crystals has rubbed off on a great many students. Fortunately, I am one of them. His influence during my undergraduate study was critical in my choice to stay at Durham and by doing so he has helped revolutionise the image of computational chemists within Durham. His support and encouragement as a supervisor and a friend are something for which I am eternally grateful.

Outside the university I would like to say a big 'Thank you' to Deerness Valley Gym Club and all the members thereof, for not only taking up the majority of my free time, but also for making my time in Durham a happy one. Special thanks must be given to my coaches, Karl Wharton and Stuart Thompson. However, without a shadow of a doubt I owe a huge debt of gratitude to Kathryn and Cassie, my partners. Without them, I would never have achieved my ambition of a place back in the Great Britain Gymnastics Squad.

From a personal perspective, I owe a huge debt of thanks to my family for their on-going love and support throughout my upbringing. This work is as much a credit to them as it is to me. Also my boyfriend, James, who has given me much love and patience throughout, especially in my final year. Thank you for your help and love.

Declaration

The material contained within this thesis has not previously been submitted for a degree at the University of Durham or any other university. The research reported within this thesis has been conducted by the author unless indicated otherwise.

Melanie J. Cook

October 2000

To Mum and Dad.

CONTENTS

LIST OF FIGURES

LIST OF TABLES

CHAPTER

1

Introduction to liquid crystals

1.1 A brief history of liquid crystals

1.1.1 The "discovery"

For many years it was customary to think of matter as existing in three states: solid, liquid or gas, but it is now known that this is not strictly correct. In particular, certain organic materials do not show a single transition from a solid to a liquid phase, but rather a series of transitions involving new phases. The properties exhibited by these new phases are intermediate between those of a liquid and those of a crystal and for this reason they are often termed *liquid crystal* phases. A more accurate name, however, is *mesophase*, meaning intermediate phase.

The first observation of this breakdown in conventional thinking was provided by the Austrian born botanist, Friedrich Reinitzer. Reinitzer's main interest was the function of cholesterol in plants. In 1888 he observed a strange phenomenon associated with the melting behaviour of pure crystals of cholesterol benzoate

[1, 2]. Reinitzer noted that at 145.5 °C the cholesterol benzoate crystals melted to form a cloudy liquid which at the higher temperature of 178.5 °C cleared to form a transparent liquid. He also observed some of the same colour effects that had been reported by earlier scientists working on cholesterol derivatives: a blue colour briefly appeared upon cooling when the clear liquid turned cloudy and a blue violet colour occurred just before the cloudy liquid crystallized. Whether or not Reinitzer was the first to truly *discover* liquid crystal phases is debatable. His observation and description of the melting behaviour (i.e two melting points) of cholesterol benzoate opened up a line of inquiry that turned out to be extremely fruitful. He described what he saw in a way that posed many of the right questions for future investigations. For example, if the solid phase melted at 145.5 °C then what was melting at 178.5 °C? Might this be a form of matter other than the solid or the liquid phase? For this reason Reinitzer is usually recognized as the *discoverer* of liquid crystal phases. The substance that Reinitzer observed is now recognized as a chiral nematic liquid crystal phase i.e a mesophase. The study of such mesophases has attracted a great deal of interest over recent years.

Another scientist who played a major role in the discovery of liquid crystals was Otto Lehmann, a German physicist [3–5]. At the time of Reinitzer's discovery, Lehmann was studying the crystallization properties of various substances. Lehmann had constructed a heating stage for his polarizing microscope which allowed him to observe the crystallization of materials as the temperature was slowly lowered. This instrument allowed him to make one of the most important early contributions to the field of liquid crystals. Such devices are still widely used today. Reinitzer knew of the work of Lehmann and saw a connection between his observations and what Lehmann was reporting. He therefore, sent some of his sample to Lehmann who carried out many studies using his heating stage microscope. Lehmann described Reinitzer's substance, along with many of his own samples, in a variety of ways during this time period. Initially, he called them soft crystals which were almost fluid, but later this was replaced by the term crystalline fluids. He finally became convinced, however, that the cloudy liquid was a uniform fluid phase, which affected polarized light in a manner similar to crystals and not liquids. This combination of characteristic flow properties, like a liquid, and optical properties, like a crystal, finally led Lehmann to label these

substances *liquid crystals* a term still in use today.

1.1.2 After the "discovery"

Lehmann remained an extremely influential character in the field of liquid crystals until his death in 1922. Later in life he turned his attention away from the naturally occurring cholesterol derivatives, where the whole story had begun, and focussed his attention on synthetic materials [6]. Lehmann was also partially responsible for introducing the field of liquid crystals into France. The culmination of this effort was the classification scheme suggested by George Friedel in 1922 [7]. Friedel proposed the currently accepted description of liquid crystal phases, which involves the idea of molecular ordering. This lay to rest the numerous other suggestions as to the origin of liquid crystallinity. His classification scheme consisted of the use of words, such as, nematic, cholesteric and smectic to describe the different phases observed. Finally, liquid crystal phases were being accepted as a new state of matter. Friedel was also responsible for the introduction of the term mesophase, which even today is the preferred and widely used name for liquid crystals.

In the period between 1922 and World War 2 the work carried out on liquid crystals was mainly concerned with their elastic properties, X-ray studies, and the effects of electric and magnetic fields. The *degree of order* was described using an order parameter S. This was an important step since the description of orientational order in a liquid crystal phase is a very complicated task without such a parameter.

After World War 2 the interest in liquid crystals all but disappeared. It has been suggested that this was due to the fact that all the problems concerning liquid crystals had been solved. Also there was an apparent lack of any practical applications for liquid crystals. However, in the late 1950's two German physicists Wilhelm Maier and Alfred Saupe [8, 9] did make one important development in the field of liquid crystals. They formulated a microscopic mean field theory for nematic liquid crystal mesophases. As a result, for the very first time, liquid crystal researchers possessed a theory that predicted the behaviour of the nematic phase starting from realistic characteristics of the individual molecules. Despite

this, and other important work, liquid crystals continued to be thought of as a novelty and hence were largely ignored.

Whatever the reason for the lack of interest in liquid crystals after World War 2, the situation changed shortly before 1960. During this period a few individuals in the United States, Great Britain and the Soviet Union undertook a general re-examination of liquid crystal phases, in the hope of learning more about their molecular structure, optical properties and technological possibilities. Progress was swift and substantial as it became apparent that liquid crystalline substances had the ability to detect extremely small changes in temperature, mechanical stress and chemical environment. The door was suddenly opened to a large number of possible applications. This work, together with the synthesis of the very first stable, room temperature nematic liquid crystal phase *p*-methoxybenzylidene-*p*-*n*-butylaniline, (MBBA) [10–12], and the development of the first liquid crystal display (LCD) gave the whole enterprise a new practical purpose.

1.1.3 The "present" day

Stimulated by the excitement of the development of the first LCD, the 1970's and 1980's saw an explosion in the volume of liquid crystal research. Scientifically, liquid crystals are an important phase and have played an important role in increasing our understanding of how molecules behave co-oporatively. Technologically, liquid crystals have become part of our daily lives, first appearing in wristwatches and pocket calculators, but now being used for displays in all sorts of instrumentation, including portable computers and televisions. Initially the advantage of liquid crystal display devices over other systems was their low power consumption and small size. However, liquid crystal displays now compete with other technologies for attractiveness, ease of viewing, cost and durability. Liquid crystals, nowadays, are not just being looked at for display technologies but also for their use as thermo-chromic materials [13] and data storage mediums [14]. Progress in our understanding of liquid crystals is also aiding developments in other areas such as cell biology. It now seems certain that the field of liquid crystals is set for further expansion in the future.

It is important to note that Reinitzer was an Austrian botanist and Lehman was a German physicist, and therefore, the discovery of liquid crystals represented collaboration between scientists representing two scientific disciplines from two different countries. From the very beginning, liquid crystal research has been a multidisciplinary, international field. A fact that has grown truer with time and is still a hallmark of the field today.

1.2 Liquid crystal phases

In order to understand the significance of these new states of matter, it is necessary to first recall the distinction between a *crystal phase* and a *liquid phase.* The most obvious difference is that the molecules in a crystal are highly ordered whereas those in a liquid are not. In a crystal the molecules can be thought of as having both long range positional and orientational order, in the sense that the molecules are constrained to occupy specific sites in a three dimensional periodic lattice. If on the other hand these degrees of order are completely lost, then an isotropic liquid arises, which has only short range positional order and no orientational order.

We know that most crystals transform directly into the liquid phase on heating, so that the long range positional and orientational order of the molecules is destroyed simultaneously. If the constituent molecules have pronounced anisotropy of shape, the disappearance in one, two, or three dimensions of the long range translational periodicity in the crystal may precede the collapse of the long range orientational order. This results in the occurrence of intermediate phases known as *liquid crystals* and *plastic crystals* (see figure 1.1) [15, 16].

Molecules in liquid crystal phases tend to be fluid-like because they have lost some or all of the long range positional order. They do, however, maintain some degree of orientational order, but the amount of order is quite small compared to that of a crystal. In contrast to liquid crystal phases, that always possess orientational order and sometimes positional order, there is yet another phase of matter termed *plastic crystals.* Plastic crystals are solid phases which lack the orientational order of crystals but still retain the long range positional order.

They tend to be formed by molecules with spherical symmetry so that they can rotate freely along one or more of their molecular axes, even though their centres of mass are fixed in a lattice. Methane and carbon tetrachloride are typical examples of compounds that form plastic crystals.

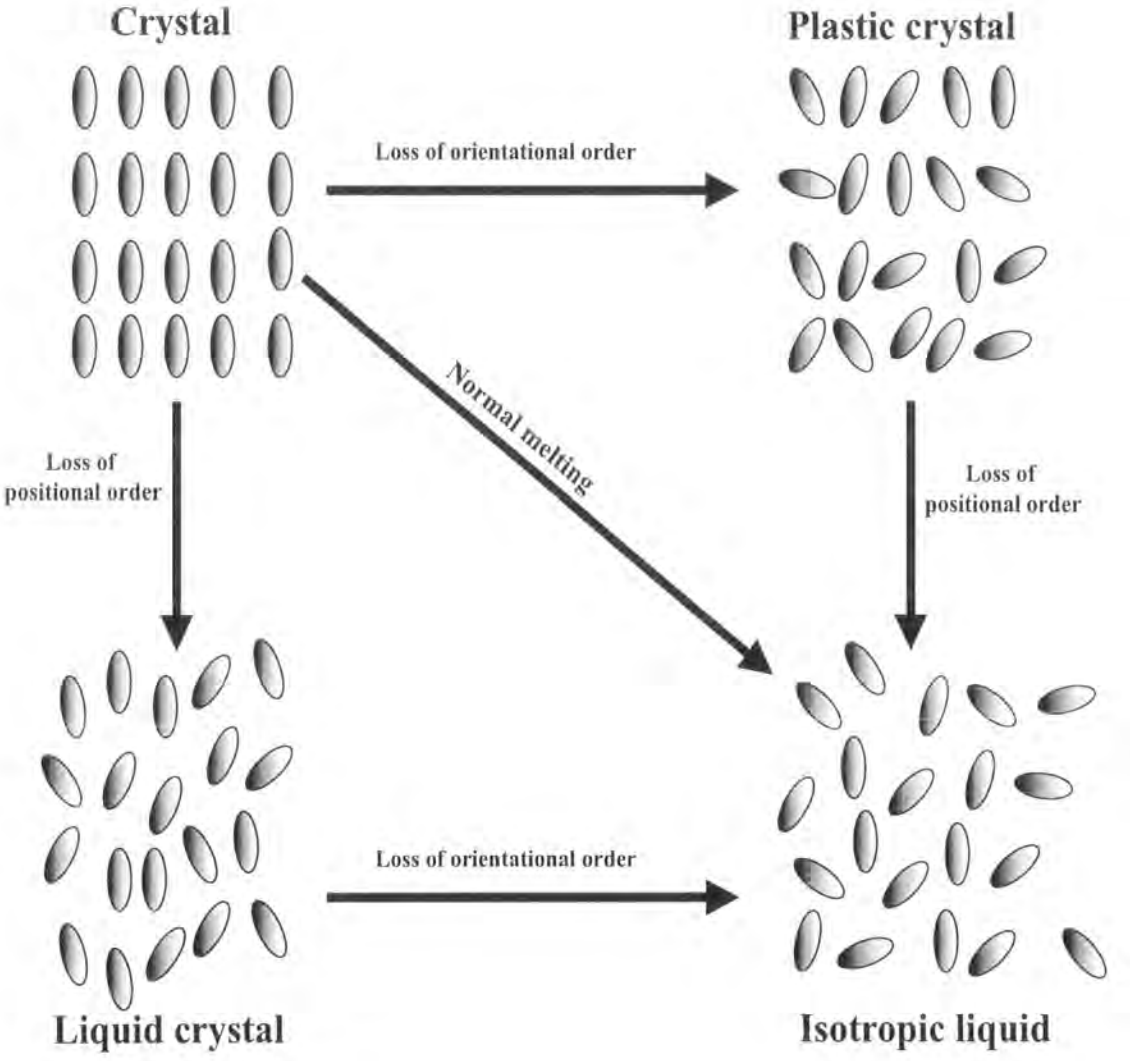

Figure 1.1: Positional and orientational order in crystals, liquids and mesophases.

1.3 Types of liquid crystals

Transitions to liquid crystal phases may be brought about in two different ways. The first method relies on a purely thermal process and results in a class of mesophases which are termed *thermotropic liquid crystals*. The second method arises when two different substances are mixed together. In the second case, different mesophases are formed not only as a consequence of changing the temperature but also as the concentration of one component of the mixture is varied. This latter method results in a class of mesophases, called *lyotropic liquid crystals*.

1.3.1 Thermotropic liquid crystals

Thermotropic liquid crystals form directly as a mesogenic material is heated up from its crystalline state. Their phase behaviour can be described simply in terms of what happens with respect to a single parameter, temperature. An important characteristic of thermotropics is that the transition from one phase to another occurs at a particular characteristic temperature for each mesogen. The transition from mesophase to isotropic liquid is termed the clearing temperature, T_c. Thermotropic liquid crystal phases can be further sub-divided depending on their degree of orientational and positional order. The majority of pure compounds exhibiting thermotropic mesomorphism have one distinctive feature in common, namely the rod-like shape of the molecule. Mesophases of rod-like molecules, termed *calamitic mesogens*, are classified broadly into three types: nematic, cholesteric (chiral nematic), and smectic.

Nematic Mesophase

The simplest thermotropic liquid crystal phase formed by rod like molecules is the nematic phase (figure 1.2). The nematic liquid crystal phase is characterized by having no long range positional order but a high degree of orientational order. The long axis of the molecules in a nematic phase tends to point along a preferred direction in space as the molecules undergo diffusion. This preferred direction is referred to as the director, and is represented by a unit vector $\mathbf{n}$.

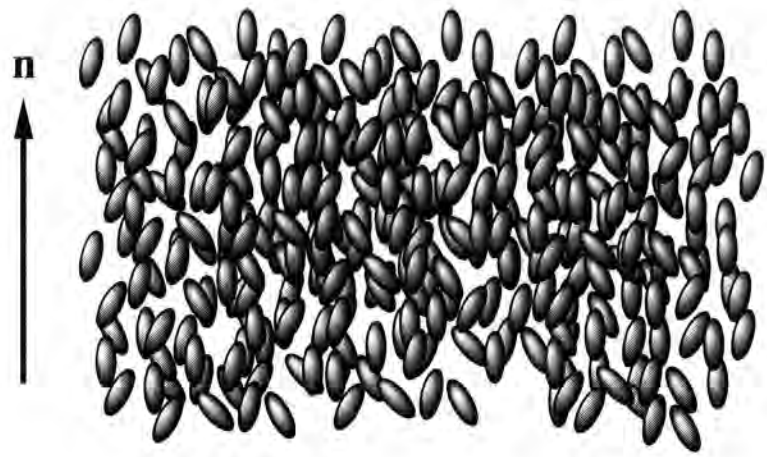

Figure 1.2: Schematic diagram of a nematic phase.

Cholesteric Mesophase

Closely related to the nematic phase is the cholesteric mesophase (figure 1.3). The term cholesteric is a historical term and comes from the fact that the first compounds found to exhibit such phases were derivatives of cholesterol. The modern name for these phases is *chiral nematic*, which is much more precise. Like nematic liquid crystals, chiral nematics have no long range positional order but do have orientational order, which is again described by a director, **n**. The main difference between a chiral nematic phase and a nematic phase is that the chiral nematic phase is composed of optically active molecules. As a result the structure acquires a spontaneous macroscopic twist about an axis perpendicular to the director. Consequently, a helical structure of pitch P is induced. The size of the pitch induced depends on the twisting power of the chiral molecule and for a large number of molecules, the size of the pitch is comparable to the wavelength of visible light. As a consequence of this, selective reflection of incident white light can occur and, therefore, chiral nematics appear intensely coloured. The pitch and hence the colour is temperature dependent. This property of chiral nematics has led to their use in a wide variety of applications. These include medical thermography, fever thermometers, hot warning indicators, as well as novelties such as *stress* and *mood* sensors.

If we have two chiral nematic enantiomers of a particular material present in equal amounts (racemic mixture) then it transpires that the resultant material is

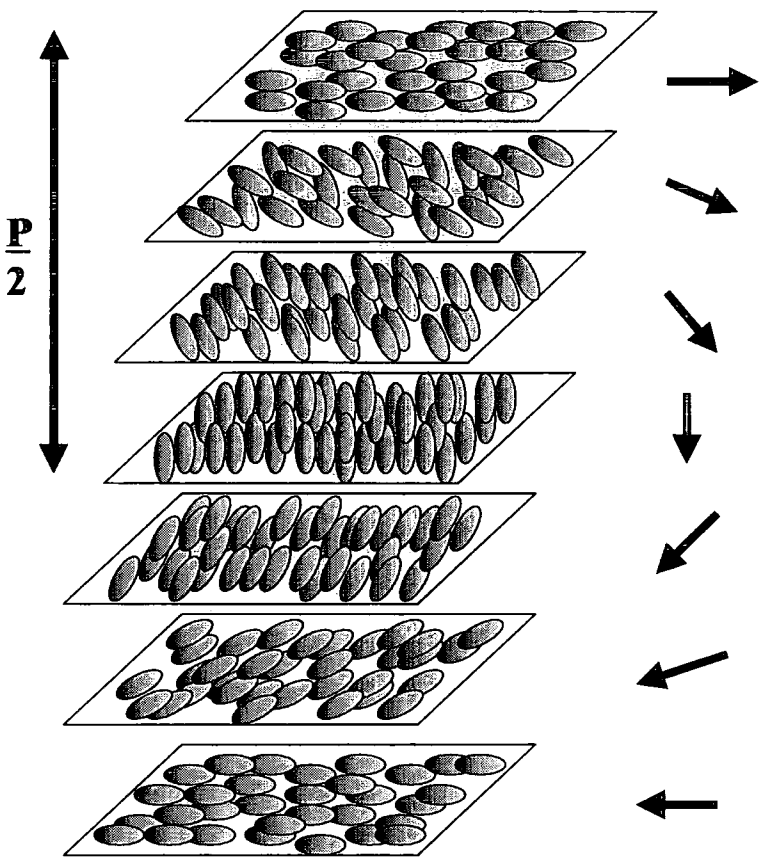

Figure 1.3: Schematic diagram of a chiral nematic (cholesteric) phase.

achiral with a helix of infinite pitch, and therefore, exhibits not a chiral nematic phase but a pure nematic phase. We can therefore, see that a nematic phase is simply a chiral nematic of infinite pitch.

Smectic Mesophase

The third type of mesophase is termed a smectic phase. Smectic phases differ from nematic phases in that they have some degree of positional order in addition to the orientational order [17]. Smectic liquid crystals have stratified structures and a variety of molecular arrangements are seen within each stratification. Examples of two smectic phases are shown in figures 1.4 and 1.5. In a smectic A phase (figure 1.4) the molecules are arranged with the mean orientation of the molecular long axis normal to the layers, and the molecular centres in each layer irregularly spaced in a *liquid like* fashion. The smectic C phase (figure 1.5) differs from the

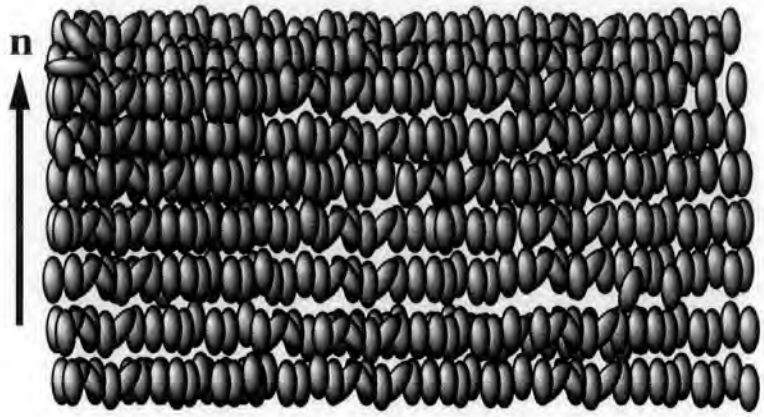

Figure 1.4: Schematic diagram of a smectic A phase.

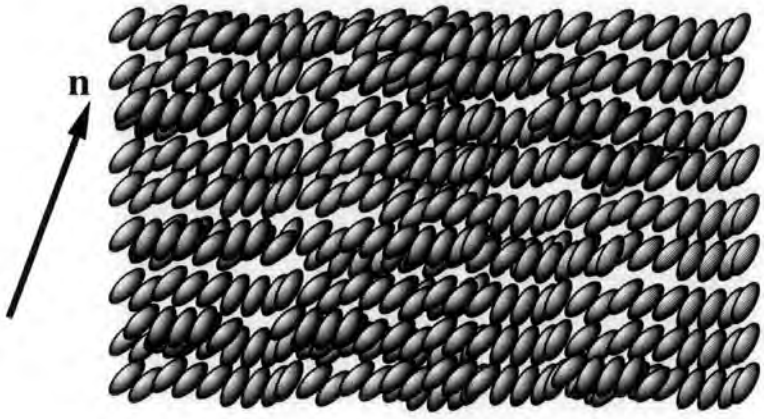

Figure 1.5: Schematic diagram of a smectic C phase.

smectic A phase in that the molecules within each layer are inclined with respect to the layer normal. This tilt angle differs from one material to another and is also temperature dependent. Many other smectic modifications have been found, but the detailed molecular arrangements are not known with certainty for all of them. Chiral versions of all the tilted smectic phases are also known to exist [18]. In these phases the director rotates around the cone generated by the tilt angle as the position along the normal to the layers is varied.

So far the entire discussion has been devoted to thermotropic liquid crystal phases formed by rod-like molecules (calamitic mesogens). The reason for this is simple; these are the most common liquid crystal phases and therefore the most

well known. However, in 1977 it was discovered that disk-like molecules also exhibit liquid crystalline behaviour, in which the axis perpendicular to the plane of the molecule tends to orient along a specific direction. These phases and the molecules that form them are called *discotic liquid crystals* [19]. As with rod-like molecules different discotic mesophases have been observed namely, nematic, chiral nematic, and columnar.

Nematic discotic mesophase

Again the simplest discotic phase is the nematic mesophase, shown in figure 1.6. In this phase the molecules have no positional order but do have some orientational order, with the short axis of the molecules (i.e. the axis perpendicular to the plane) preferentially orientating along a single direction, which characterises the director, **n**.

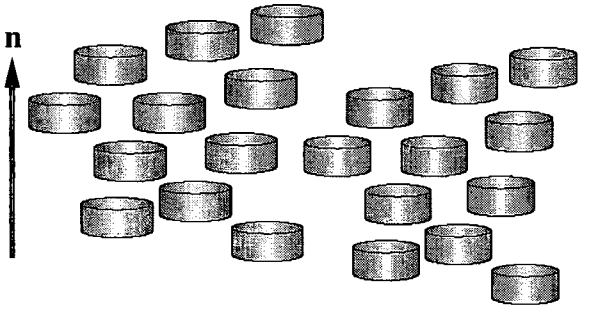

Figure 1.6: Schematic diagram of a discotic nematic phase.

Chiral nematic discotic mesophase

Chiral nematic discotic liquid crystals also exist. The structure of these phases are identical to the chiral nematic phases formed by rod-like molecules. That is, the director adopts a helical structure by rotating about an axis perpendicular to the director.

Columnar or smectic discotic mesophase

Positional order in discotic liquid crystals displays itself by the tendency of the molecules to arrange themselves in columns. These columns then tend to arrange themselves in a two-dimensional lattice, which can be either rectangular

or hexagonal. These phases are called columnar phases and a typical example of a columnar phases is shown in figure 1.7. However, it must be noted that the molecules within a columnar discotic liquid crystal phase are positioned quite randomly in the stack.

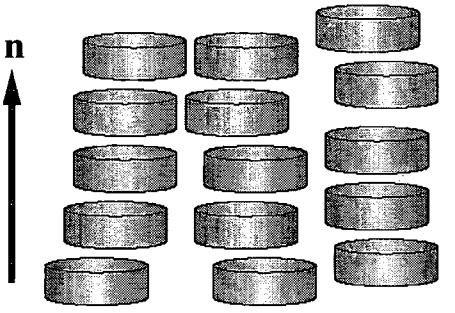

Figure 1.7: Schematic diagram of a discotic columnar phase.

Polymer liquid crystals

Thermotropic liquid crystals can also be formed by certain types of polymers. Polymer liquid crystals [20] can broadly be classified into two groups, main chain (MCLCP) and side chain (SCLCP), although mixed side chain/main chain polymers also exist. The names *main chain* and *side chain* refer to the positions of the mesogenic group within the polymer framework.

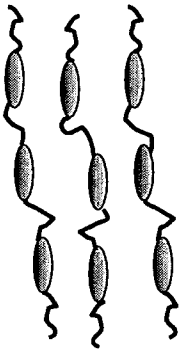

Figure 1.8: Schematic diagram of a main chain liquid crystal polymer.

If the mesogenic unit is within the main polymer chain, as shown in figure 1.8, this is referred to as a MCLCP. If the mesogenic unit is suspended from the main

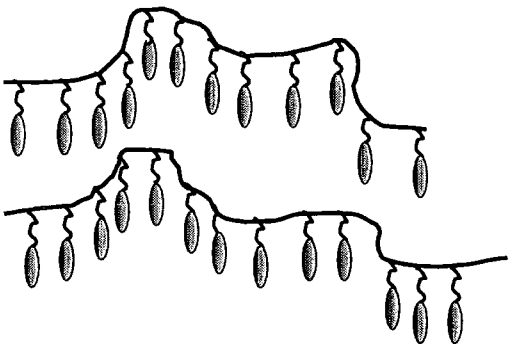

Figure 1.9: Schematic diagram of a side side chain liquid crystal polymer.

chain, as in figure 1.9, it is referred to as a SCLCP. The thermotropic mesophases formed by polymers arise due to the interactions of these mesogenic groups in a similar manner to that observed in low molecular weight thermotropics. The phase types formed by polymer liquid crystals are therefore, exactly the same as those formed by low molecular weight systems, that is, nematic, cholesteric, and smectic.

The range of different thermotropic liquid crystal phases is very large and a particular molecule may well exhibit more than one mesophase. Usually as the temperature is increased the degree of order in a material is reduced. Consequently, the expected order of a material that shows a whole series of mesophases is crystal, smectic phases with high order (smectic C), smectic phases with low order (smectic A), nematic and finally isotropic liquid. This order occurs for almost all materials, although not all materials exhibit each one of the phases. However, exceptions to this rule have been discovered in certain compounds.

The first observations of materials that did not show this sequence of transitions were in binary mixtures and later a similar effect was seen for pure compounds at elevated pressures. In these materials the order of the phase transitions is crystal to nematic to smectic to nematic to isotropic liquid. The second lower temperature nematic is referred to as the re-entrant phase. It should be noted that re-entrant behaviour is an unusual phenomenon and as a consequence is not well understood at present.

1.3.2 Lyotropic liquid crystals

The phase behaviour of lyotropic liquid crystals is governed by two parameters, temperature and solvent concentration. Lyotropic phases are formed by amphiphilic molecules, which usually consist of a hydrophilic *head* group at one end with a hydrophobic *tail* group at the other. Amphiphilic molecules form liquid crystal mesophases that are slightly different from the calamitic and discotic thermotropic liquid crystals. In appropriate polar solvents at low concentrations, amphiphilic molecules can go into solution. As the concentration of amphiphilic molecules increases then one of two possible structures begins to form. If the amphiphilic molecules have a strong polar head group relative to the non-polar part of the molecule then they arrange themselves into roughly spherical aggregates, with the polar groups on the outside and the hydrocarbon chains pointing towards the centre. This structure is known as a *micelle* and is stable provided the amphiphilic material is above a certain concentration known as the *critical micelle concentration.* If the head group is not highly polar compared to the rest of the molecule then spherical vesicles tend to form, which consist of double layers of amphiphilic molecules, called *bilayers* . It should be noted that similar structures form if a non-polar solvent is used, but in this case, the arrangement of the amphiphilic molecules in the micelle and vesicle structures are inverted and hence the name *inverted structures* is used.

If the concentration of the amphiphilic material is increased to approximately 50% then the micelles and bilayers combine to form larger structures, such as hexagonal, cubic and lamellar [21,22]. The hexagonal phase (figure 1.10) is formed from long cylindrical rods of amphiphilic molecules, which pack into an hexagonal array. The lamellar phase is composed of flat bilayers separated from each other by uniform amounts of water. These form at even higher concentrations (figure 1.11). One less common phase that occasionally forms at concentrations between the hexagonal and the lamellar phases is the cubic phase. The cubic phase is composed of spherical micelles packed together to form a cubic lattice. Two important classes of material that exhibit lyotropic mesomorphism are soaps and phospholipids. This thesis will not be concerned with lyotropic systems but will be confined to the structure and physical properties of thermotropic liquid crystals.

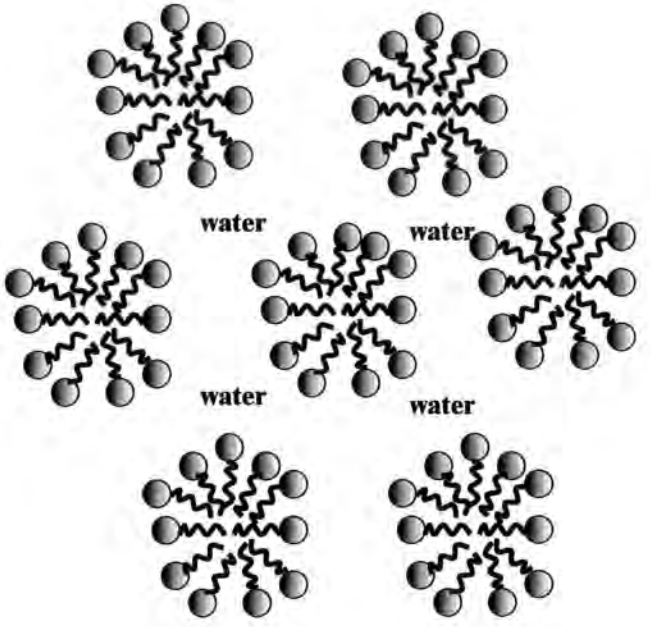

Figure 1.10: Schematic diagram of the hexagonal phase.

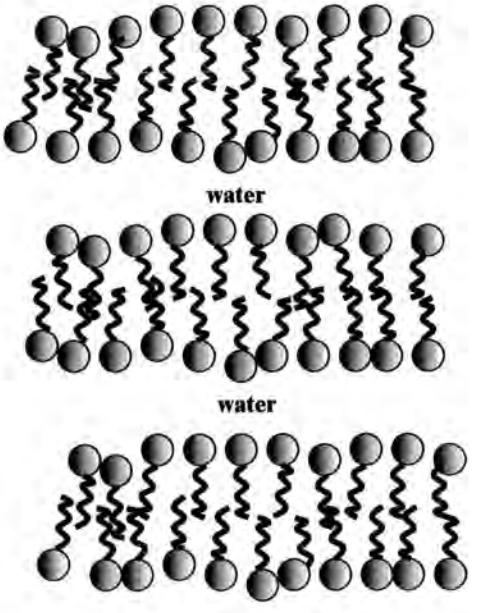

Figure 1.11: Schematic diagram of the lamellar phase.

1.4 Properties of Liquid crystals

1.4.1 Order parameter

Liquid crystal phases are characterized by their degree of orientational order. Qualitatively, the degree of order is expressed by saying that a liquid crystal mesophase is more ordered than an isotropic liquid but less ordered than a crystal. The question arises of how the degree of orientational order can be quantified?

Since the molecules are not fixed in space, one is forced to describe the orientational order as some form of average. If the assumption is made that the molecules can be approximated by rods of cylindrical symmetry, then the average alignment of the long molecular axes is given by a unit vector, $\mathbf{n}$, called the director. In order to characterize the degree of orientational order, one defines an order parameter, S. For a given configuration of N molecules, the order parameter, S, is written as

$$S = \frac{1}{N}\sum_{i=1}^{N} P_2(\hat{\mathbf{u}}_i \cdot \mathbf{n}), \tag{1.1}$$

where $\hat{\mathbf{u}}_i$ is the unit vector specifying the orientation of the long axis of molecule i and P_2 is the second Legendre polynomial, $P_2(\cos x) = 1/2(3\cos^2 x - 1)$. The director could be determined by maximising S with respect to rotations of $\mathbf{n}$, but it is more straight forward to proceed by writing,

$$S = \mathbf{n}.\mathbf{Q}.\mathbf{n} \tag{1.2}$$

where $\mathbf{Q}$ is an ordering matrix with the elements

$$Q_{\alpha\beta} = \frac{1}{2N}\sum_{i=1}^{N}(3\hat{\mathbf{u}}_{i\alpha}\hat{\mathbf{u}}_{i\beta} - \delta_{\alpha\beta}), \tag{1.3}$$

with $\delta_{\alpha\beta}$ the Kronecker δ and $\alpha, \beta = x, y, z$ referring to the space fixed axes. The problem of identifying the director is then reduced to diagonalising the ordering matrix. The largest positive eigenvalue is taken to be the order parameter, S, and the corresponding eigenvector to be the director $\mathbf{n}$, as proposed by Zannoni

[23]. An alternative method of calculating the order parameter was proposed by Eppenga and Frenkel [24]. This states that the order parameter is, $S = -2\lambda_0$, where λ_0 is the *middle* eigenvalue of the ordering matrix. This method often helps to distinguish the nematic from the isotropic phase in the vicinity of the phase transition, since the former definition leads to small positive values of S in the isotropic phase of the order $N^{-1/2}$, whereas the latter is of the order N^{-1}, fluctuating about zero. Clearly, this becomes more significant as the nematic-isotropic phase transition weakens.

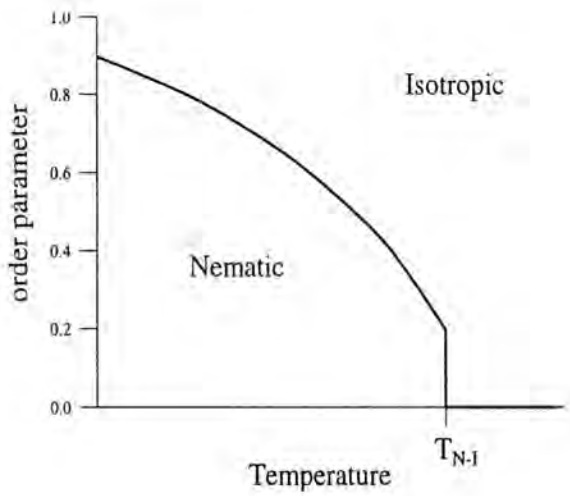

Figure 1.12: Variation of order parameter with temperature for a typical nematic phase.

Both methods show that in the isotropic phase at equilibrium and in the presence of no external orientating fields the order parameter is equal to zero ($S = 0$). However, under equivalent conditions in the nematic phase the order parameter takes a value of approximately 0.3, close to the nematic-isotropic phase transition (T_{N-I}). As the temperature is lowered further the order parameter increases to a maximum value of 0.8, just before a transition to a smectic or solid phase. Figure 1.12 shows a graph of the order parameter versus temperature for a typical nematic liquid crystal phase. It should be noted that the order parameter goes discontinuously to zero at T_{N-I} indicating a first order phase transition.

So far we have considered mesogens that can be assumed to be perfectly cylindrical. Real molecules are not perfectly cylindrical in shape and this can

sometimes lead to errors in the determination of S. However, for the most part molecules are well approximated by cylindrical symmetric rods.

1.5 Relationship between molecular structure and molecular properties

Considerable work has gone into synthesising and studying many different types of liquid crystal mesogens over the years. Despite this, there is still a poor understanding of why small changes in molecular structure can dramatically alter the physical properties of mesophases. The structure-property problem in liquid crystals is complicated by several factors. Firstly, liquid crystal molecules are drawn from a wide variety of chemical classes, such as, organic, inorganic, metals, and polymers. A second practical problem (for simulation) is that mesogenic molecules are moderately large, containing at least several tens of atoms, and several different atomic species. Thirdly, liquid crystal molecules tend to be flexible (at least in part), which leads to conformational freedom. Finally, mesogens tend to contain both dipolar and polarizable functional groups that gives rise to specific material properties. It is the study of all these factors by experimental and theoretical means, which will provide the key to understanding the physical properties exhibited by liquid crystals. It is hoped eventually, that a detailed knowledge of structure-property relationships will lead to the design of new and better materials.

In principle, some structure-property problems are surmountable by real experiments, which provide an insight into the molecular structure of liquid crystal molecules. However, when designing new materials it is desirable to have some sense of how a material will behave before it is synthesized. In this respect, experiment does not yet afford a predictive capability. In this context, reliable computer simulations can take on increased significance. In the longer term it is hoped that molecular simulations of liquid crystals [25, 26] will become sufficiently predictive to optimise desired physical properties. Thereby removing the need for costly, time consuming *trial and error* synthesis of mesogens. In this way predictive simulations would become a routine tool in the design of novel

new materials. As a step towards this goal, several powerful techniques are now available. For example, quantum mechanical studies can be used to develop realistic interaction potentials for mesogenic molecules [27]. Simulations of simple potential models can be used to study how changes in shape and attractive interactions influence phase behaviour [28,29], and statistical mechanical methods can be used to calculate key material properties, such as, elastic constants, viscosities, diffusion coefficients etc.

Having identified the basic problems which exist in understanding molecular structure-property relationships in liquid crystal mesogens, it is possible to outline a series of aims for this thesis.

1.6 Scope of thesis

The aim of this thesis is to employ computer simulation techniques to predict specific molecular properties of real liquid crystal mesogens. Where computationally possible, fully atomistic potential energy functions have been employed. This enables a comparison to be drawn continuously between the computational results and experimentally measured values. Consistency between the two sets of results provide confidence that the form of the computational model employed is correct. Throughout, the course of this thesis the consequence of employing accurate force field potential parameters is considered and this is given particular emphasis in chapter 4 where a novel liquid crystal force field is developed. Eventually, it is hoped that this force field model will be further developed to such an extent that it can be employed in a purely predictive sense. This will aid in the design of new materials with the desired molecular properties prior to synthesis. The rest of the work presented in this thesis is focussed on areas of liquid crystal research which at the present time are of great commercial interest.

In chapter 3 the effects of doping a twisted nematic liquid crystal phase (represented by a single site Gay-Berne potentials) with a chiral solute molecule (represented by a fully atomistic potential) is explored. The calculations provide a means of predicting both the direction of twist induced by a chiral dopant dissolved in a nematic solvent and also the magnitude of that twist.

In chapter 5 the preference for local parallel or anti parallel dipole correlation

in the bulk phase is investigated for the molecules PCH5, PCH5-Cl, me5NF and GGP5Cl. Commercially, there is considerable interest in molecules which have a Kirkwood correlation factor greater than 1 as this leads to a low threshold voltage for electro-optical switching in display devices. Therefore, particular reference is paid to analysing the simulation trajectories in order to assess why these molecules behave so differently.

Finally, the rotational viscosity coefficient of a nematic liquid crystal phase is investigated via molecular dynamic simulations of a simple Gay-Berne potential (chapter 6). In recent years a range of methods to evaluate this rotational viscosity coefficient have been developed. Several simulation techniques are described, and the suitability of the techniques employed are discussed.

In the course of these investigations a variety of simulation techniques have been employed and these are outlined, along with some technical aspects of computer simulation, in the next chapter.

CHAPTER

2

Introduction to computer simulations

2.1 The first computer simulation

The first computer simulation studies of a liquid were able to test only highly idealized models. The pioneering studies of two dimensional hard spheres reported in 1953 made use of one of the most powerful computers then available, MANIAC [26], and employed the *Metropolis Monte Carlo* [30] method, which is still widely used. However, the system size was limited to a few hundred particles. Today, the exact same calculations could be performed on a desktop computer in a matter of minutes. Both the size and the complexity of systems open to simulation study have grown immensely in the last 40 years. The latest generation of supercomputers allow simulations involving tens of thousands of particles, interacting via a continuous fully atomistic potential to be performed. These massively parallel machines, such as the *Cray T3E*, vastly outperform the state-of-the-art machines of just a few years ago. Most of the studies reported here have been performed on individual workstations (Silicon Graphics or DEC

alpha machines), allowing the study of 10^4 particles with reasonable comfort. With increasing computer power, the variety of model systems studied and the range of techniques available to the simulator have grown, allowing computer simulations to enhance our understanding in many theoretical and experimental contexts. Therefore, the importance and popularity of computer simulations in chemistry has dramatically increased, and looks likely to continue to do so in the near future, with the development of even more powerful computers.

2.2 Computer simulations of liquid crystals

The remarkable properties of liquid crystal molecules have caught the attention of both experimentalists and theoreticians. Studies of these materials have resulted in significant contributions being made to the wider field of phase transitions and critical phenomena. Computer modelling and simulation have played a valuable part in bridging the gap between experiment and theory, with the essential techniques of molecular mechanics, molecular dynamics and Monte Carlo methods now well established [25, 31].

By necessity, theoretical studies tend to be based on simple models, reducing the number of physical features, but aiming to retain those that are essential to the behaviour of interest. Often, even highly idealized models [30] cannot be solved exactly, and approximations must be made. By *exact* one means that a complete specification of the microscopic properties of the system (masses of atoms, molecular geometry, etc.) leads directly to a set of macroscopic properties of experimental interest (equations of state, structural order parameters, etc). This makes it difficult to judge the validity of the model by direct comparison with experimental data. Discrepancies between the experimental and theoretical results indicate that the theoretical treatment is inadequate or that the model itself misses some essential feature.

It is, at this point that computer simulations are of great importance. Essentially *exact results* can be obtained for a given model, exposing inappropriate approximations in an analytical approach. Furthermore, the underlying model itself can be tested by comparing the simulated results with those obtained from real experiments. Once a model has been shown to provide a good description of

a physical system, it can ultimately be used to understand why systems behave as they do. Another advantage of computer simulations is that they can often be used to determine molecular properties that cannot be measured directly by experimental techniques, by investigating parts of parameter space not readily accessible to experimentalists. However, predictions at this level are only possible if an extremely good model of the molecular interactions is employed.

In liquid crystals, computer simulations act as a bridge, by providing a direct route between the microscopic details of the chemical system (intermolecular interactions) and the macroscopic properties of experimental interest, (such as order parameters and transport coefficients). While computer simulations of liquid crystals are based on the same general Monte Carlo and molecular dynamics techniques used for liquids, they present a number of additional challenges:

- Many of the interesting phenomena associated with liquid crystals occur over long time and length scales.
- The reduced symmetry of these phases makes the description of structure and dynamics quite complicated.
- Liquid crystal molecules are difficult to model in a realistic way as they often contain both flexible and rigid fragments, polar and/or polarizable groups and are anisotropic.

2.3 Model potentials

The important properties of liquid crystal phases cover a wide range of time and length scales. At one extreme, we are interested in the ordering of molecules over 100's or 1000's of Angstroms (mesogenic regime). In the opposite limit, we are interested in the molecular geometry and the detailed electronic structure of individual molecules (microscopic regime). Ultimately, these molecular properties determine the condensed phase behaviour. In some cases, however, the inter and intra-molecular regimes are separable in that it is possible to discuss the origin of several liquid crystalline phases using very idealised representations of molecular structure and bonding.

Simulation studies of liquid crystal molecules began in the early 1970's [32,33] with lattice models. Subsequently, considerable research has been carried out in

two main areas: *hard body* and *soft body* potential models. Both these molecular models are efficient to implement in computer simulations and can be used to study a whole range of fundamental material properties of the liquid crystalline state.

2.3.1 Hard bodies

The simplest molecular models for liquid crystals represent the mesogens as hard rigid rods, ellipsoids or spherocylinders. The requirement that the molecules are hard bodies implies that no two molecules can inter-penetrate. Apart from this constraint, there are no other intermolecular interactions present. Investigations of systems of hard bodies were largely motivated by Onsager's predictions [34] that excluded volume effects can be sufficient to induce liquid crystalline ordering. The molecular origin of this excluded volume interaction lies in the fact that the electron clouds on adjacent molecules cannot overlap. Therefore, repulsive forces dominate at short distances. This short range repulsion is itself sufficient to give rise to a variety of orientationally ordered phases. Since, there is no source of attractive interactions in these models, phase behaviour is determined purely by molecular shape and density, not by temperature. Consequently, in the strictest sense, these systems do not exhibit thermotropic transitions though many of the phases that are seen are those that arise in a typical thermotropic mesogen.

The idealised pair potential for a hard sphere system [28] is extremely simple and takes the form shown in figure 2.1. Rigid body simulations use highly efficient algorithms, and have done much to increase our understanding of, for example, the role of molecular shape in the formation of liquid crystal mesophases. Simulation studies of hard spheroidal particles have indicated a phase diagram with approximate prolate/oblate symmetry about the hard sphere system. This system shows two phases exist, an isotropic fluid and a crystal [35]. Where the axial ratio of the particles exceeds about 3 (or 1/3), a nematic phase is also observed, but no smectic phases are noted. However, if hard spherocylinders are employed instead, with an axial ratio (length/width) of approximately 4, then a smectic A phase is observed [36]. The full range of phases shown by these hard particles is what has made them intrinsically an interesting topic of research. Hard particle

models do provide many useful insights into the nature of real liquid crystals. Nevertheless, due to the simplicity of the potential they do suffer from many deficiencies.

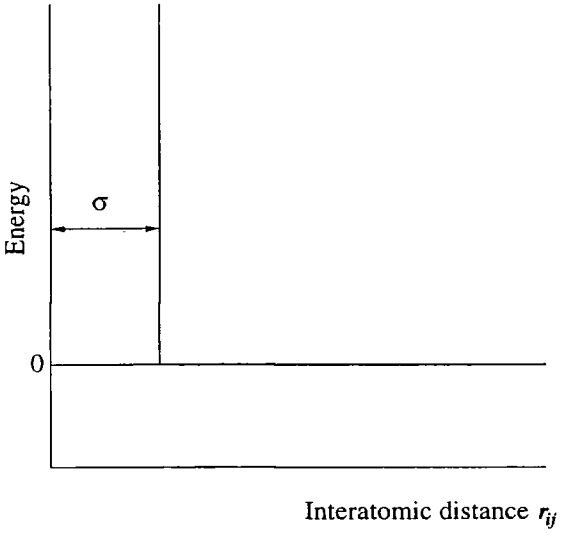

Figure 2.1: Idealised hard-sphere pair potential.

2.3.2 Soft bodies

Despite the success of hard particle models, it is generally recognized that both repulsive and attractive interactions make a significant contribution to the phase behaviour of real mesogens. Consequently, the last few years have seen a large number of simulations carried out on liquid crystal mesogens using continuous *soft* potentials. In general, two methods have been popular. In the first approach, simplified molecular potentials have been employed. These seek to approximate the dominant features of mesogenic interactions, such as, molecular shape anisotropy by a single site potential. Such models have no obvious relationship to any real system but are extremely useful because their simplicity enables simulations to be performed on large numbers of molecules. Simple models of this type have been highly successful in predicting the formation of a number of liquid crystal phases, leading to the development of techniques for the calculation of key bulk properties. One of the best known simple soft body potentials is the Gay-Berne model [29], where the interaction energy is based on a generalization of

the isotropic Lennard-Jones potential (see figure 2.2). Depending on parameterisation, the Gay-Berne potential can be used to model molecules with different shape anisotropies and different attractive interactions. However, it is difficult to represent the structure of real, flexible molecules by a Gay-Berne mesogen without a dramatic simplification of molecular structure.

An alternative molecular model, that is increasingly employed in computer simulations of liquid crystals, is the *molecular mechanics force field* model [31]. Such a model, seeks to represent the molecular structure of the mesogen as accurately as possible. A series of simple potential energy functions situated on each atom are used to describe both the non-bonded interaction energy between separate atomic sites and the intra-molecular interactions within the molecule. Together these potential energy functions make up the *molecular mechanics force field* for a particular molecule. This approach aims to make accurate predictions about mesophase behaviour for *real* systems based purely on a knowledge of the molecular structure.

The Gay-Berne potential

The creation of the Gay-Berne potential owes much to the work of Corner in his pioneering development of pair potentials for molecules [37]. He noted that the Lennard-Jones potential (equation 2.1) provides a good description of the short range attractive and repulsive interactions between atoms,

$$U_{ij}^{\mathrm{LJ}} = 4\epsilon_{ij}\left[\left(\frac{\sigma_{ij}}{r_{ij}}\right)^{12} - \left(\frac{\sigma_{ij}}{r_{ij}}\right)^{6}\right] \tag{2.1}$$

where ϵ_{ij} defines the well-depth, and σ_{ij} represents the separation of the centres of the atoms at which the attractive and repulsive terms in the potential cancel out.

It was suggested by Corner that the same function could in fact be used to describe the interaction between molecules provided that the parameters ϵ_{ij} and σ_{ij} were allowed to vary with the molecular orientations of the molecules as well as their intermolecular separation. Corner attempted to develop analytical

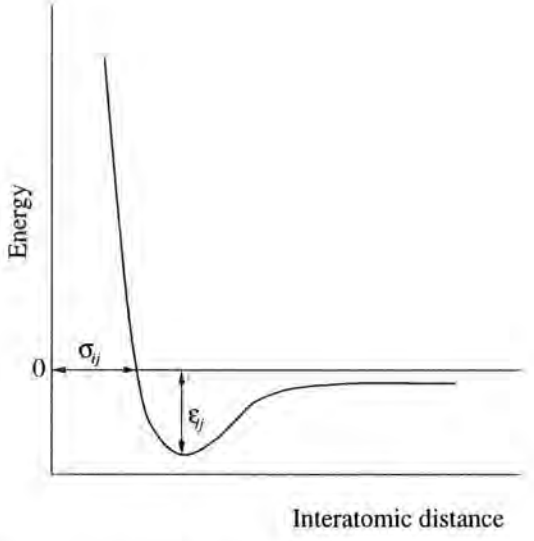

Figure 2.2: The Lennard-Jones potential.

functions for this dependence of ϵ_{ij} and σ_{ij}, but they were not suitable for the large shape anisotropies required in order to observe liquid crystalline behaviour.

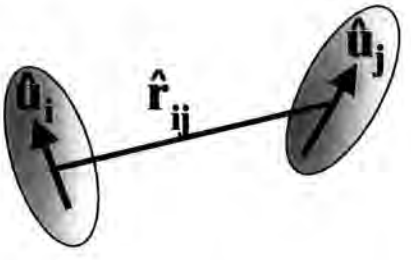

Figure 2.3: Diagram defining the orientation vectors for two adjacent Gay-Berne molecules.

Many years later Berne and Pechukas proposed a new model [38], namely the Gaussian overlap model (GO model). This model employed the idea that the interaction between two identical ellipsoidal molecules is governed by the extent to which their Gaussian distribution functions overlap. From the expression of the overlap they evaluated a range parameter which was taken to be the contact distance σ_{ij} and a strength parameter which was set equal to the well depth ϵ_{ij}. If the orientations of the two rod like molecules is denoted by the unit vectors $\hat{\mathbf{u}}_i$, $\hat{\mathbf{u}}_j$ and the orientation of the intermolecular separation is given by the unit

vector $\hat{\mathbf{r}}_{ij}$ (as shown in figure 2.3) then the expression for the angular dependence on the contact distance is

$$\sigma(\hat{\mathbf{u}}_i, \hat{\mathbf{u}}_j, \hat{\mathbf{r}}_{ij}) = \sigma_0 \times \left[1 - \chi\left(\frac{(\hat{\mathbf{r}}_{ij}\cdot\hat{\mathbf{u}}_i)^2 + (\hat{\mathbf{r}}_{ij}\cdot\hat{\mathbf{u}}_j)^2 - 2\chi(\hat{\mathbf{r}}_{ij}\cdot\hat{\mathbf{u}}_i)(\hat{\mathbf{r}}_{ij}\cdot\hat{\mathbf{u}}_j)(\hat{\mathbf{u}}_i\cdot\hat{\mathbf{u}}_j)}{1-\chi^2(\hat{\mathbf{u}}_i\cdot\hat{\mathbf{u}}_j)^2}\right)\right]^{-\frac{1}{2}} \tag{2.2}$$

where χ is the molecular anisotropy and is given by,

$$\chi = \left[\frac{\kappa^2 - 1}{\kappa^2 + 1}\right]. \tag{2.3}$$

κ is equal to the ratio, σ_{ee}/σ_{ss} of the contact distances σ_{ee} and σ_{ss} for particles in a end-to-end and side-by-side arrangement respectively. It follows then, that for a sphere χ vanishes while for an infinitely long rod it is 1 and for an infinitely thin disc it is -1. The scaling parameter σ_0 is the side-by-side contact distance for a pair of rods. A much simpler expression is used to define the angular dependence of the well depth

$$\epsilon(\hat{\mathbf{u}}_i, \hat{\mathbf{u}}_j, \hat{\mathbf{r}}_{ij}) = \epsilon_0 \left[1 - \chi^2(\hat{\mathbf{u}}_i\cdot\hat{\mathbf{u}}_j)\right]^{-\frac{1}{2}}. \tag{2.4}$$

The Gaussian overlap model suffers from two main difficulties which lead to certain unphysical features [39]. Firstly, the observation that the width of the attractive well varied with the molecular orientations was unrealistic. Secondly, the prediction that the well depth depends only on the relative orientations of the two particles and not on their relative orientation with respect to the intermolecular separation. These difficulties were addressed by a number of workers [40,41] and culminated in the development of the Gay-Berne potential model (GB model) [29],

$$U_{ij}^{\mathrm{GB}} = 4\epsilon_0^{\mathrm{GB}}[\epsilon^{\mathrm{GB}}(\hat{\mathbf{u}}_i, \hat{\mathbf{u}}_j)]^{\nu}[\epsilon'^{\mathrm{GB}}(\hat{\mathbf{u}}_i, \hat{\mathbf{u}}_j, \hat{\mathbf{r}}_{ij})]^{\mu} \times \left[\left(\frac{\sigma_0^{\mathrm{GB}}}{r_{ij} - \sigma(\hat{\mathbf{u}}_i, \hat{\mathbf{u}}_j, \hat{\mathbf{r}}_{ij}) + \sigma_0^{\mathrm{GB}}}\right)^{12} - \left(\frac{\sigma_0^{\mathrm{GB}}}{r_{ij} - \sigma(\hat{\mathbf{u}}_i, \hat{\mathbf{u}}_j, \hat{\mathbf{r}}_{ij}) + \sigma_0^{\mathrm{GB}}}\right)^{6}\right]. \tag{2.5}$$

Several major modifications were employed in the Gay-Berne model in order to address the deficiencies of the Gaussian overlap model outlined above. Firstly,

to remove the angular variation of the width of the attractive well they changed the functional form from a dependence on the scaled distance (r_{ij}/σ_{ij}) to a shifted scaled separation R, where

$$R = \left[\frac{r_{ij} - \sigma_{\mathrm{ij}}(\hat{\mathbf{u}}_i, \hat{\mathbf{u}}_j, \hat{\mathbf{r}}_{ij}) + \sigma_0}{\sigma_0}\right]. \tag{2.6}$$

Secondly, the independence of the well depth on the molecular orientation $\hat{\mathbf{u}}_i$ and $\hat{\mathbf{u}}_j$ with respect to the intermolecular separation $\hat{\mathbf{r}}_{ij}$ was removed by constructing a new strength parameter

$$\epsilon^{\mathrm{GB}}(\hat{\mathbf{u}}_i, \hat{\mathbf{u}}_j, \hat{\mathbf{r}}_{ij}) = \epsilon_0 \epsilon^{\mathrm{GB}}(\hat{\mathbf{u}}_i \cdot \hat{\mathbf{u}}_j)^{\nu} \epsilon'^{\mathrm{GB}}(\hat{\mathbf{u}}_i, \hat{\mathbf{u}}_j, \hat{\mathbf{r}}_{ij})^{\mu}, \tag{2.7}$$

where

$$\epsilon'^{\mathrm{GB}}(\hat{\mathbf{u}}_i, \hat{\mathbf{u}}_j, \hat{\mathbf{r}}_{ij}) = \left[1 - \chi'\left(\frac{(\hat{\mathbf{r}}_{ij} \cdot \hat{\mathbf{u}}_i)^2 + (\hat{\mathbf{r}}_{ij} \cdot \hat{\mathbf{u}}_j)^2 - 2\chi'(\hat{\mathbf{r}}_{ij} \cdot \hat{\mathbf{u}}_i)(\hat{\mathbf{r}}_{ij} \cdot \hat{\mathbf{u}}_j)(\hat{\mathbf{u}}_i \cdot \hat{\mathbf{u}}_j)}{1 - \chi^2(\hat{\mathbf{u}}_i \cdot \hat{\mathbf{u}}_j)^2}\right)\right] \tag{2.8}$$

and

$$\chi' = \left[\frac{\kappa'^{1/\mu} - 1}{\kappa'^{1/\mu} + 1}\right]. \tag{2.9}$$

κ' provides a measure of the anisotropy in the well-depth for rod-like molecules in the ratio $\epsilon_{ss}/\epsilon_{ee}$, where ϵ_{ss} and ϵ_{ee} are the well depths when the molecules are side-by-side and end-to-end respectively. The scaling parameter ϵ_0 is the well depth when the molecules are in the cross configuration. We should note that in the limit κ and κ' tend to unity then χ and χ' vanish and the Gay-Berne potential reduces to the Lennard-Jones potential given in equation 2.1.

Invariably, the Gay-Berne potential depends on four parameters, κ, κ', μ and ν [42]. Depending on the values given to these parameters then there are an infinite number of Gay-Berne potentials. The original form of the potential specified by Gay and Berne was designed to mimic the pair potential for a molecule consisting of a linear array of four equidistant Lennard-Jones sites with $\kappa = 3$. A value of 3 was chosen for κ as this is the minimum length to breadth ratio required in order to observe liquid crystalline behaviour in real systems. This procedure gave κ'

=5, ν= 1 and μ= 2. A typical graphical representation of the potential is to plot the distance dependence of the potential for particular orientations of the two ellipsoidal molecules, as shown in figure 2.4. There are several important features shown in figure 2.4.

- The contact distances change dramatically from a small value when the rod like molecules are side-by-side to a large value when they are end-to-end.
- The depth of the attractive potential well also changes significantly, being large when the molecules are side-by-side and small when they are end-to-end.
- The attraction is weak for the cross arrangement but becomes stronger when the molecules are in the side-by-side configuration.

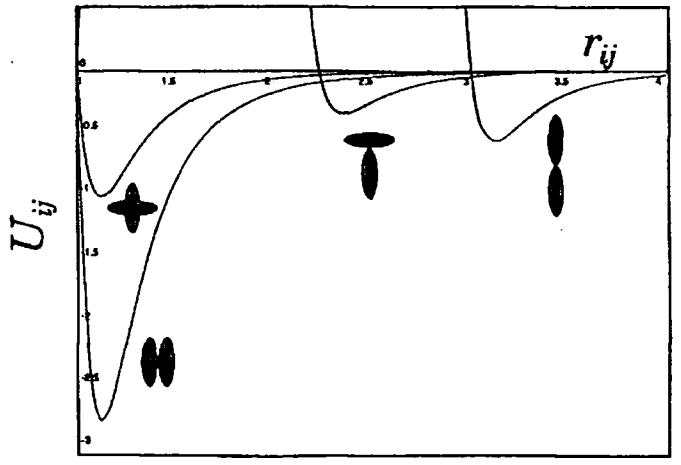

Figure 2.4: The distance dependency of the Gay-Berne potential (κ = 3, κ' =5, ν= 2 and μ= 1).

In a wide range of reported simulation studies, the Gay-Berne model has been shown to exhibit stable nematic and smectic mesophases. The work of de Miguel *et al* [43] has provided an approximate phase diagram for a Gay-Berne system with parameters κ = 3, κ' =5, ν= 1 and μ= 2 which indicates a stable nematic and smectic B phase. Other parameters have also been studied. Luckhurst *et al* [44] found that a system simulated with values κ = 3, κ' =5, ν= 2 and μ= 1 (shown in figure 2.4) showed a smectic A phase as well as a nematic and smectic B phase. Berardi *et al* [45] worked with the parameters κ = 3, κ' =5, ν= 3 and μ= 1 and found the existence of a nematic and smectic B phase. Many aspects of the Gay-Berne mesogen have been studied in addition to its phase behaviour, for

example, the behaviour of solute molecules in a Gay-Berne solvent [46], elastic constants [47,48], viscosity coefficients [49,50], thermal conductivity [51] and the behaviour in confining geometries [52].

The molecular mechanics force field model

Although liquid crystalline phases can be formed from entirely rigid units such as rods and ellipsoids, it is well known that all liquid crystal molecules are partially flexible, and can change their shape in a variety of ways. Therefore, extension of the rigid-rod theories and models has been the object of considerable effort for several years. It has become clear that relaxing the assumption of molecular rigidity has a profound effect on the mesophase behaviour.

The incorporation of molecular flexibility into a simulation model is made possible by employing a molecular mechanics force field [53,54]. This approach seeks to represent the molecular structure of the molecule as faithfully as possible by representing both the intermolecular and intra-molecular interactions at an atomic level. Typically, in a molecular mechanics force field, the molecule is represented by a series of simple potential energy functions situated on each of the atomic sites. Usually a separate energy function exists for each flexible degree of freedom such as bond stretching, angle bending and torsional angle deformation; as well as for each non-bonded interaction. Coupling all these potential energy functions together produces a molecular mechanics force field for the molecule of interest,

$$\begin{aligned} E \;=\; & \sum_{\text{bond}} E_{bond} + \sum_{\text{angle}} E_{angle} + \sum_{\text{dihedral}} E_{dihedral} \\ & + \sum_{non-bonded} E_{elec} + E_{vdw} + \ldots\ldots \end{aligned} \tag{2.10}$$

It should be stressed that each of the individual mathematical functions in equation 2.10 are in no way unique. In fact, each force field that is developed employs an analytical form that includes parameters which are carefully optimised to provide the best fit between experimental, structural and energetic data for a particular class of molecules. As a consequence it is possible that a wide range of additional terms may be needed in the model. Depending on the molecule, these

may include hydrogen bonding terms, or further terms to describe the coupling between bond stretching and bond bending distortions.

At present there are a number of parameterized functional forms of the force field available for atomistic simulations. These include CHARMM [55, 56], AMBER [57–61], MMFF94 [62–66], OPLS (Optimised Potential for Liquid Simulations) [67–72], and Allinger's MM(1-4) series of force fields [73–76].

The hybrid Lennard-Jones/Gay-Berne model

Computational studies of flexible liquid crystal molecules vary widely in the approximations they employ. Molecular models reported in the literature have varied from hard spheres joined by flexible links to fully atomistic treatments of mesogens. The hybrid Lennard-Jones/Gay-Berne model is an interesting variant of the fully atomistic force field model described above. It arises when rigid sections of the mesogen are replaced by a simpler potential such as the Gay-Berne model. Models of this type provide considerable savings in computer time by eliminating many of the pairwise non-bonded interactions associated with the rigid core, which is now represented by a single site potential. The molecular mechanics force field for this hybrid Lennard-Jones/Gay-Berne model takes the form

$$\begin{aligned} E = & \sum_{\text{bond}} E_{bond} + \sum_{\text{angle}} E_{angle} + \sum_{\text{dihedral}} E_{dihedral} \\ & + \sum_{\text{non-bonded}} E_{elec} + \sum_{\text{non-bonded}} E_{LJ-LJ} \\ & + \sum_{\text{non-bonded}} E_{LJ-GB} + \sum_{\text{non-bonded}} E_{GB-GB}. \end{aligned} \tag{2.11}$$

Here, E_{bond}, E_{angle}, and $E_{dihedral}$ are the stretch, bend and torsional interaction energies. The terms E_{LJ-LJ}, E_{LJ-GB}, E_{GB-GB} represent the non-bonded interaction energies for two particles i and j. The form of the interaction energy E_{LJ-LJ}, and E_{GB-GB} have already been discussed. E_{LJ-LJ} is the interaction energy for an inter-particle separation r_{ij} given by the Lennard-Jones 12:6 potential (equation 2.1), and E_{GB-GB} represents the orientational dependent interaction energy for two Gay-Berne particles [29]. The Gay-Berne/Lennard-Jones interaction, E_{LJ-GB}, is based on the work of Cleaver *et al.* [77] who derived a generalized

potential for two non-equivalent particles. Accordingly, for a rod-sphere interaction, the potential is written as

$$U_{ij}^{\mathrm{LJ/GB}} = 4\epsilon_0^{\mathrm{LJ/GB}}[\epsilon^{\mathrm{LJ/GB}}]^{\mu}(\hat{\mathbf{u}}_j, \hat{\mathbf{r}}_{ij}) \times \left[\left(\frac{\sigma_0^{\mathrm{LJ/GB}}}{r_{ij} - \sigma^{\mathrm{LJ/GB}}(\hat{\mathbf{u}}_j, \hat{\mathbf{r}}_{ij}) + \sigma_0{}^{\mathrm{LJ/GB}}}\right)^{12} - \left(\frac{\sigma_0^{\mathrm{LJ/GB}}}{r_{ij} - \sigma^{\mathrm{LJ/GB}}(\hat{\mathbf{u}}_j, \hat{\mathbf{r}}_{ij}) + \sigma_0{}^{\mathrm{LJ/GB}}}\right)^{6}\right], \tag{2.12}$$

where, in the limit of one of the particles being spherical, gives new range and strength parameters, respectively:

$$\sigma^{\mathrm{LJ/GB}}(\hat{\mathbf{u}}_j, \hat{\mathbf{r}}_{ij}) = \sigma_0[1 - \chi\alpha^{-2}(\hat{\mathbf{r}}_{ij} \cdot \hat{\mathbf{u}}_j)^2]^{-\frac{1}{2}} \tag{2.13}$$

and

$$\epsilon^{\mathrm{LJ/GB}}(\hat{\mathbf{u}}_j, \hat{\mathbf{r}}_{ij}) = \epsilon_0[1 - \chi'\alpha'^{-2}(\hat{\mathbf{r}}_{ij} \cdot \hat{\mathbf{u}}_j)^2] \tag{2.14}$$

with

$$\frac{\chi}{\alpha^2} = \frac{l_j^2 - d_j^2}{l_j^2 + d_i^2} \tag{2.15}$$

and

$$\frac{\chi'}{\alpha'^2} = 1 - \left(\frac{\epsilon_{ee}}{\epsilon_{ss}}\right)^{\frac{1}{\mu}}. \tag{2.16}$$

The hybrid Gay-Berne/Lennard-Jones model provides considerable savings in computer time over fully atomistic models. As a consequence, this method opens the way for simulations of complex systems, such as polymer liquid crystals.

2.4 Simulation methods

2.4.1 Molecular mechanics

Molecular mechanics is the simplest and the most commonly used molecular modelling technique. It focuses on the low energy structures of molecules, which

correspond to an energy minima in the molecular mechanics force field used to represent the molecule. Once an appropriate force field model has been chosen the aim of molecular mechanics is to optimise the molecular geometry of the molecule of interest by minimizing E, in equation 2.10. The molecular mechanics approach will be discussed in detail in chapter 4 and so here only the basics of the technique are described.

A typical molecular mechanics calculation consists of the following stages:

- Build a trial molecular structure.
- Minimize the energy of the trial structure producing a minimum energy conformation.
- Undertake a search for other energy minima by adjusting the dihedral angles within the molecule and re-minimizing the steric energy for each conformation.

The final result of this process is a series of potential energy minima, one of which corresponds to a global energy minima and therefore represents the lowest energy conformation of the molecule. For liquid crystal molecules a large number of energy minima exist and therefore, finding the global minima and characterizing the molecular structure is extremely difficult. Even with the development of new techniques for conformational searching, the problem of energy minimization on a multi-dimensional surface is still difficult. For complicated molecules it is not possible to guarantee that all the relevant conformations have been found.

One way of avoiding the multi-minima problem which occurs with molecular mechanics is to apply a more sophisticated technique which is capable of sampling the force field energy E without the need to home in on a particular minimum energy conformation. There are two well established methods for doing this: Monte Carlo (MC) and molecular dynamics (MD). Both approaches make use of the same types of potential energy functions used in molecular mechanics but are designed to sample conformational space such that a Boltzmann distribution of energies is generated. In the Monte Carlo method, averages are taken over configurations generated according to an appropriate probability density, whereas in molecular dynamics a sequence of configurations is generated according to Newton's equations of motion for the system allowing time averages to be measured.

2.4.2 Monte Carlo techniques

The Monte Carlo simulation method occupies a special place in the history of molecular modelling as it was the technique used to perform the very first computer simulation of a molecular system. In this section a brief summary of this technique will be given.

The aim of the Monte Carlo technique is to explore phase space in order to determine a useful equilibrium average of some thermodynamic property, A. In principle this can be achieved by evaluating the integral,

$$< A >= \int A(\mathbf{r})\mathrm{P}(\mathbf{r})\mathrm{d}(\mathbf{r}) \tag{2.17}$$

$P(\mathbf{r})$ is the Boltzmann weighted probability, that is, the probability of obtaining the configuration $\mathbf{r}$ and is given by,

$$P(\mathbf{r}) = \frac{\exp[-E(\mathbf{r})/k_{\mathrm{B}}\mathrm{T}]}{\int \exp[-E(\mathbf{r})/k_{\mathrm{B}}\mathrm{T}]\mathrm{d}(\mathbf{r})} \tag{2.18}$$

where $E(\mathbf{r})$ is the internal energy, $\mathbf{r}$ indicates all possible states of the system of interest, and the denominator represents the configurational integral. The main problem in calculating these integrals is that they cannot be evaluated analytically. However, the solution to the integrals could be found by sampling different configurations of the system in order to provide an indication of all the possible states. In its crudest formulation, calculations of the configurations of a system could be generated by making random changes to the positions of the species present, together with the orientations and conformations where appropriate. From the energies calculated at each move it would be possible to obtain estimates of $A(\mathbf{r})\mathrm{P}(\mathbf{r})$ which could be averaged to obtain $< A >$. This approach, however, is clearly flawed since each configuration makes an equal contribution to the configurational integral. Since $P(\mathbf{r})$ is proportional to the Boltzmann factor, $\exp[-E(\mathbf{r})/k_{\mathrm{B}}\mathrm{T}]$, only configurations with low energies will make a significant contributions to $P(\mathbf{r})$. Unfortunately, in reality a large number of configurations have an extremely small Boltzmann factor due to high energy overlaps between the particles. This reflects the nature of the phase space sampled, most of which corresponds to non physical configurations with high energies. Thus, only a small proportion of phase space corresponds to low energy configurations, where there

are no overlapping particles, and it is these low energy regions that correspond to physically observed phases such as solid, liquid, etc. Therefore, many of the configurations generated will have little or no influence, hence, proper sampling will not been achieved.

This sampling problem was solved with the development of a technique known as *Importance sampling*, which is the essence of the Metropolis Monte Carlo method [30]. The Metropolis Monte Carlo method has become so widely adopted that in the simulation and modelling communities it is usually referred to as the *Monte Carlo* method. Fortunately, there is rarely any confusion with the simple Monte Carlo method. The crucial feature of the Metropolis Monte Carlo method is that it biases the generation of configurations towards those that make the most significant contribution to the configurational integral. Specifically, it generates states with a Boltzmann probability and then counts each of them equally. By contrast the simple Monte Carlo integration method generates states with equal probability (both high and low energy) and then assigns them a Boltzmann weight.

In practice the simulation must have a procedure for moving between configurations in such a way that at the end of the simulation, each state has occurred with the appropriate probability. This is achieved by setting up, what is known as a Markov chain. This enables a representative portion of phase space to be sampled in a reasonable number of moves. A Markov chain satisfies two conditions:

- The outcome of each trial belongs to a finite set of possible outcomes called phase space.
- Each trial depends only on the outcome of the trial that immediately precedes it.

2.4.3 Metropolis Monte Carlo method

A Monte Carlo program for the simulation of an atomic fluid is quite simple to construct. At each Monte Carlo step in the simulation a new configuration is generated. This is carried out by making a random change to the co-ordinates of a single randomly chosen atom, whose maximum displacement in any one

direction is given by δr_{max}. (For molecules, random changes can be made to the Cartesian co-ordinates, but it is often more efficient to make changes to the internal co-ordinates.) After the trial move has been made the energy of the new state E_{new} is calculated and compared to the energy of the old configuration E_{old}. If the energy of the new configuration is lower than its predecessor ($E_{new} < E_{old}$), then the new configuration is accepted and used as a starting point for the next iteration. However, if the energy of the new configuration is greater than its predecessor ($E_{new} > E_{old}$), then the new move is accepted if the Boltzmann factor, $\exp(-(E_{new} - E_{old})/k_B T)$, is greater than a random number chosen between 0 and 1. If this condition is not met then the new configuration is rejected and the initial configuration is retained for the next trial move. The size of the move at each iteration is governed by the maximum displacement δr_{max}. This is an adjustable parameter whose value is chosen so that approximately 50% of the attempted trial moves are accepted. If the maximum displacement is too small then many moves will be accepted but the states explored will all be very similar and the phase space will be explored very slowly. On the other hand, if it is too large then many trial moves will be rejected and this will lead to unfavourable overlaps of phase space. Therefore, it is normal to adjust the maximum displacement automatically while the program is running in order to achieve value for money in terms of representative sampling per unit of computer time. Alternatively, a common practice in Monte Carlo simulations is to select the particles to move sequentially rather than randomly. This cuts down on the amount of random number generation and is an equally valid method.

Monte Carlo simulations normally consist of an equilibration phase followed by a production phase. During equilibration appropriate thermodynamic and structural quantities such as the total energy, order parameters, etc, are monitored until they achieve a stable value after which the production phase will commence.

2.4.4 Monte Carlo simulations of rigid molecules

The Monte Carlo technique is most easily implemented for atomic systems because it is only necessary to consider the translational degrees of freedom. How-

ever, if the system is molecular then implementation becomes more difficult as the trial move must now incorporate combined translational and orientational moves. For rigid non spherical molecules it is usual to translate and rotate one molecule during each Monte Carlo step, and then the joint displacement is accepted or rejected. The translational part of the move is carried out by randomly displacing the centre of mass of a molecule, where the maximum displacement is governed by the adjustable parameter δr_{max}. The orientational moves of the molecule are, however, described in terms of Euler angles [78].

Euler angles

Euler angles are a simple way of describing the orientation of a molecule, using three angular co-ordinates θ, ϕ, ψ. The Euler angles are defined in terms of a sequence of rotations of a set of Cartesian axes about the origin. The first rotation is through an angle (measured counter clockwise) ϕ about the z axis. This is followed by a rotation θ about the new x axis, and the final rotation is through an angle ψ about the new z axis (see figure 2.5).

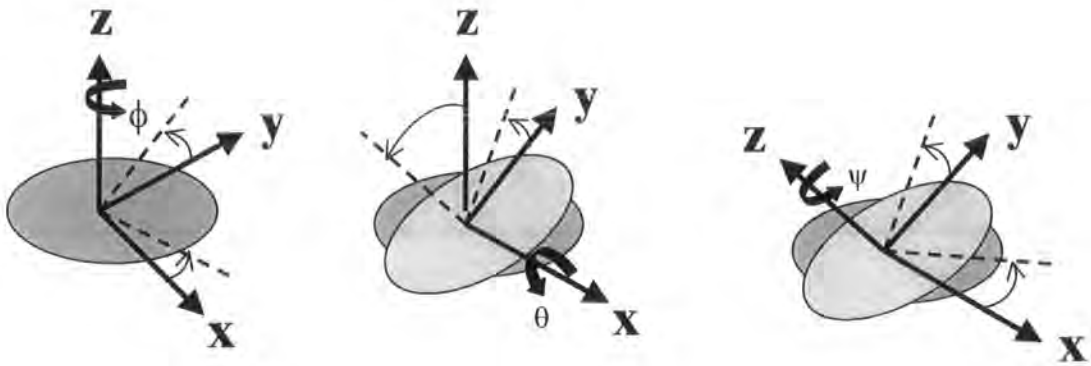

Figure 2.5: Schematic representation of the Euler angles.

A change in orientation is achieved when the Euler angles are randomly changed by small amounts. For example, if a vector $\mathbf{v}$ defining an axis of rotation is moved according to the full rotation matrix $\mathbf{A}$ (which is the product of the individual rotation matrices) then the new position of $\mathbf{v}$ (denoted as $\mathbf{v}_{\text{new}}$) is

given by equation 2.19,

$$\mathbf{v_{new}} = \mathbf{A}\mathbf{v_{old}} \tag{2.19}$$

where the matrix $\mathbf{A}$ is

$$\mathbf{A} = \begin{pmatrix} \cos\phi\cos\psi - \sin\phi\cos\theta\sin\psi & \sin\phi\cos\psi + \cos\phi\cos\theta\sin\psi & \sin\theta\sin\psi \\ -\cos\phi\sin\psi - \sin\phi\cos\theta\cos\psi & -\sin\phi\sin\psi + \cos\phi\cos\theta\cos\psi & \sin\theta\cos\psi \\ \sin\phi\sin\theta & -\cos\psi\sin\theta & \cos\theta \end{pmatrix}. \tag{2.20}$$

There are of course other ways of describing rotations, perhaps not as intuitively obvious, but often more convenient for numerical problem solving. One particularly useful method is to use *quaternions* [78]. A quaternion is a four dimensional vector, whose components can be specified in term of the Euler angles

$$\begin{aligned} q_1 &= \sin(\theta/2)\cos((\phi-\psi)/2), \\ q_2 &= \sin(\theta/2)\sin((\phi-\psi)/2), \\ q_3 &= \cos(\theta/2)\sin((\phi+\psi)/2), \\ q_4 &= \cos(\theta/2)\cos((\phi+\psi)/2). \end{aligned} \tag{2.21}$$

The quaternion components are normalised, with $\sum_{m=1,4} q_m^2 = 1$, so that the inverse relation can be obtained. The Euler angle rotation matrix can now be specified in terms of quaternions

$$\mathbf{A} = \begin{pmatrix} q_1^2 + q_4^2 - 1/2 & q_1q_2 + q_3q_4 & q_1q_3 - q_2q_4 \\ q_1q_2 - q_3q_4 & q_2^2 + q_4^2 - 1/2 & q_2q_3 - q_1q_4 \\ q_1q_3 + q_2q_4 & q_2q_3 - q_1q_4 & q_3^2 + q_4^2 - 1/2 \end{pmatrix}. \tag{2.22}$$

The benefits of quaternions is obvious from the rotation matrix in equation 2.22. There are no trigometric functions present, which are computationally expensive to calculate.

One difficulty with the Monte Carlo method for molecular systems is that there are a number of parameters governing the maximum translational and orientational displacements of the molecule during a move. As with atomic Monte Carlo calculations the acceptance parameters are adjusted in order to achieve an acceptance ratio of approximately 50%. However, in order to achieve this a sensible balance between the translational and rotational displacement parameters must be obtained by trial and error for a particular simulation.

2.4.5 Monte Carlo simulations of flexible molecules

Rotation of non-rigid molecules are often difficult to perform successfully unless the system is small, or some of the internal degrees of freedom are frozen out. The simplest way to generate a new configuration is to perform random changes to co-ordinates of individual atoms combined with translational and orientational moves of the entire molecule. Unfortunately, it is often found that even very small atomic displacements are required in order to achieve an acceptable acceptance ratio, which means that phase space is covered extremely slowly. For example, even small movements away from an equilibrium bond length will cause a large increase in the overall energy. Therefore, it is usual to freeze out some of the *hard* degrees of freedom such as bond stretches. For large molecules, even small internal bond rotations can cause large movements of atoms down the chain. Consequently, flexible molecules in a dense fluid can require specialist Monte Carlo methods.

2.4.6 Molecular dynamics techniques

The classical molecular dynamics method relies on solving Newton's equations of motion for a system of N particles (atoms) interacting via an appropriate potential energy function. The equations of motion are solved with respect to the forces that are present, according to Newton's second law of motion ($F = ma$).

$$\frac{d^2\mathbf{r}_i}{dt^2} = \frac{\mathbf{F}_i}{m_i}. \tag{2.23}$$

$\mathbf{F}_i$ is the force acting on each member of the system and is calculated from

$$\mathbf{F}_i = -\Delta E_i, \tag{2.24}$$

where E_i is the potential energy of site i. In order to obtain the dynamical behaviour of the entire system the second order differential equation must be solved for every particle in the system. This results in a set of successive configurations of the system that specify how the positions and velocities of the particles in the system vary with time. This method is distinct from the Monte Carlo technique, which requires outside intervention in the form of a random move in the system in order to produce a change. In molecular dynamics all the changes result from within the system.

The first molecular dynamics simulation of a condensed phase was performed using a hard-sphere model. In this model the spheres move at constant velocity in a straight line between collisions. All collisions are perfectly elastic and occur when the separation between the centres of the spheres equals the sphere diameter. The new velocities of the colliding spheres are calculated by applying the principles of conservation of momentum. The collisional dynamics of hard particles require quite a different treatment to those involving a smoothly varying potential.

In realistic models of intermolecular interactions, the force on each particle will change whenever the particle changes its position, or whenever any of the other particles with which it interacts change position. Under the influence of a continuous potential the motions of all the particles are coupled together, giving rise to a many bodied problem that can not be solved analytically. Therefore, for a continuous potential, *finite-difference* methods of solving ordinary differential equations of motion are needed.

The essential methodology behind the finite-difference algorithm is that time is broken down into a series of discrete steps, of length δt. The equations of motion are solved at successive values of time. The total force on each particle in the configuration at a time t is calculated as the vector sum of its interactions with all other particles. From the force, the accelerations of the particles can be determined which in turn are combined with the positions and velocities at a

time t to calculate the positions and velocities at a time $t + \delta t$. During the time step the force is assumed to be constant. Once the new positions and velocities are determined the new forces acting on the particles can be determined leading to new positions and velocities at a time $t + 2\delta t$ and so on.

2.4.7 Integration algorithms

There are many algorithms available for integrating the equations of motion using finite-difference methods. Many of these assume that the positions and dynamical properties (velocities, accelerations) can be approximated as a Taylor series expansion.

Leap-frog algorithm

The *leap-frog* algorithm [79] is a typical finite-difference algorithm that is commonly used for atomic systems

$$\begin{aligned} \mathbf{r}(\mathrm{t} + \delta\mathrm{t}) &= \mathbf{r}(\mathrm{t}) + \delta\mathrm{t}\mathbf{v}(\mathrm{t} + 1/2\delta\mathrm{t}), \\ \mathbf{v}(\mathrm{t} + 1/2\delta\mathrm{t}) &= \mathbf{v}(\mathrm{t} - 1/2\delta\mathrm{t}) + \delta\mathrm{t}\mathbf{a}(\mathrm{t}). \end{aligned} \tag{2.25}$$

To implement the leap-frog algorithm, the velocities $\mathbf{v}(\mathrm{t} + 1/2\delta\mathrm{t})$ are first calculated from the velocities at a time $(t - 1/2\delta t)$ and the accelerations at a time t. The positions $\mathbf{r}(\mathrm{t} + \delta\mathrm{t})$ are then deduced from the velocities calculated, together with the positions at time $\mathbf{r}(\mathrm{t})$. A further calculation is still required to find the velocities contemporaneous with the positions

$$\mathbf{v}(\mathrm{t}) = \frac{1}{2}[\mathbf{v}(\mathrm{t} + 1/2\delta\mathrm{t}) + \mathbf{v}(\mathrm{t} - 1/2\delta\mathrm{t})]. \tag{2.26}$$

This algorithm is numerically precise, as it explicitly includes the velocity. However the main disadvantage of this algorithm is that the positions and velocities are not synchronized.

For atoms the translational motion of the centre of mass is the sole concern, while, for anisotropic molecules rotation about the centre of mass must also be considered. There are a number of ways in which the rotational dynamics can be integrated, although the most common method is the rotational form of the leap-frog algorithm suggested by Fincham [80–85]. If the anisotropic particle is

axially symmetric and represented by a unit vector $\mathbf{u}$ along its molecular long axis, then the equations of motion for $\mathbf{u}$ and $\mathbf{v} = \dot{\mathbf{u}}$ can be solved using

$$\begin{aligned} \mathbf{v}(\mathrm{t} + 1/2\delta\mathrm{t}) &= \mathbf{v}(\mathrm{t} - 1/2\delta\mathrm{t}) + \delta\mathrm{t}\left[\frac{\mathbf{g}^{\perp}(\mathrm{t})}{\mathrm{I}} + \lambda(\mathrm{t})\mathbf{u}(\mathrm{t})\right], \\ \mathbf{u}(\mathrm{t} + \delta\mathrm{t}) &= \mathbf{u}(\mathrm{t}) + \delta\mathrm{t}\mathbf{u}(\mathrm{t} + 1/2\delta\mathrm{t}), \end{aligned} \tag{2.27}$$

where I is the moment of inertia, $\mathbf{g}_i^{\perp}$ is the *perpendicular turning force* defined by

$$\mathbf{g}_i^{\perp} = \mathbf{g}_i - (\mathbf{g}_i.\mathbf{u}_i)\mathbf{u}_i, \tag{2.28}$$

with the torque about the centre of mass given by,

$$\mathbf{u}_i \times \mathbf{g}_i = \tau_i, \tag{2.29}$$

$\lambda(t)$ is the undetermined multiplier which is introduced in order to maintain a constant bond length, and is denoted as,

$$\lambda(t)\delta t = -2\mathbf{u}(\mathrm{t} - 1/2\delta\mathrm{t}).\mathbf{u}(\mathrm{t}). \tag{2.30}$$

2.4.8 Monte Carlo or molecular dynamics

The choice between Monte Carlo and molecular dynamics depends solely on the phenomena under investigation. However, the two simulation methods can differ in their ability to explore phase space. A Monte Carlo simulation often gives rise to a rapid convergence of the thermodynamic properties of simple molecules, but may explore phase space of large molecules very slowly due to the need for small steps. The ability of Monte Carlo methods to make non-physical moves can significantly enhance its capacity to explore phase space. Monte Carlo fares well in simulations of isolated molecules, where there are a number of energy minima separated by high energy barriers. However, molecular dynamics may not be able to cross these barriers and so conformations will not occur according to the correct statistical weight. Therefore, molecular dynamics is most useful for exploration of the local phase space. It also has the ability to provide information on dynamical properties which are not usually available from Monte Carlo simulations.

2.5 General practicalities

2.5.1 Periodic boundary conditions

A major obstacle in the simulations of bulk liquids is that a large fraction of molecules lie on the surface and will experience quite different forces from those in the bulk. This problem is overcome by implementing periodic boundary conditions. The use of periodic boundary conditions has been used for many years as a standard technique for measuring the bulk properties whilst simulating a microscopic system. The simulation box containing all the particles in the system is considered as the centre of an infinite array of simulation boxes, as indicated in figure 2.6. In general, the stored particle co-ordinates in a simple simulation remain in the central simulation box. However, should a particle cross the face of the box during the simulation then attention is switched to the corresponding image particle entering the box at the opposite face, allowing the number of particles in the central simulation box to remain constant. The minimum image correction is always used in conjunction with periodic boundaries. Each particle interacts with the nearest periodic image of a neighbouring site, whether this is in the same simulation box or another adjacent box. The usual cuboidal periodic boundary conditions have been applied throughout this thesis with the exception of chapter 3, where special twisted periodic boundary conditions (section 3.2.2) have been employed in the calculation of the helical twisting powers. The use of periodic images can be problematic for some systems. For example, the longest wavelength fluctuations that can occur in the simulation are restricted to the size of the simulation box. This is a major problem in the vicinity of a phase transition.

2.5.2 Constraint dynamics

Special techniques have been developed to handle the dynamics of a molecular system in which certain degrees of freedom are constrained, normally bond lengths, while others remain free to evolve under the influence of the intermolecular and intra-molecular forces. It is desirable to constrain bond lengths during a molecular dynamics simulation because bond stretching motion occurs at high

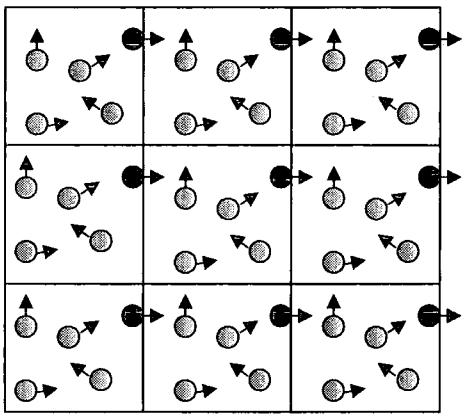

Figure 2.6: Periodic Boundary Conditions.

frequencies, therefore, the exchange of energy between bond stretches and other degrees of freedom can be rather poor. In addition, the elimination of bond stretching motion from a simulation allows much longer time steps to be taken during the integration of the equations of motion. The technique employed to constrain the bond lengths involves solving the equations of motion for one time step in the absence of constraint forces, then, subsequently it is possible to determine the correct atomic positions such that they satisfy the condition that the bond length is within some tolerance of its original value. There are several algorithms that perform this task, and the one used throughout this thesis is called SHAKE [85]. The SHAKE algorithm goes through the constraints one by one, adjusting the co-ordinates so as to satisfy each constraint in turn. The procedure is iterated until all constraints are satisfied within a given tolerance [31].

2.5.3 Ensembles

In this thesis all the Monte Carlo simulations sample states from the canonical (NVT) ensemble (see chapter 3). This corresponds to a system at constant volume with a constant number of particles. On the other hand, molecular dynamics simulations are traditionally performed in the micro-canonical (NVE) ensemble, which corresponds to an isolated system at constant energy. This type of calculation has been discussed in section 2.4.6. However, molecular dynamics simulations are often employed to carry out simulations in NVT and NpT ensem-

bles. In theory thermodynamic results can be transformed between ensembles but this is only true in the limit of infinite system size. Several different methods of prescribing thermostat and barostat algorithms exist in molecular dynamics [86] and these are briefly outlined in the following sections, 2.5.4 and 2.5.5.

2.5.4 Constant temperature (NVT)

Simulations involving constant temperature calculations are important when determining how the behaviour of a system changes with temperature. The temperature of a system is related to the time average of the kinetic energy, and therefore an obvious way to alter the temperature of the system is to scale the velocities accordingly. This can easily be achieved by simply multiplying the velocities by a factor λ at each time step [87] where $\lambda = (T/T_{current})^{-1/2}$, T is the required temperature and $T_{current}$ is the current temperature.

Berendsen thermostat

One method developed in order to maintain a constant temperature is to couple the system to an external heat bath that is fixed at the desired temperature [88]. This leads to a straight forward adaption of the molecular dynamics method. The heat bath acts as a source of thermal energy, supplying or removing heat from the system as appropriate. In practice, this is achieved by randomly selecting a new velocity from a Maxwell-Boltzmann distribution at intervals. The velocities of all the particles are scaled at each time step, so that the rate of change of temperature is proportional to the difference in temperature between the bath and the system.

$$\frac{dT(t)}{dt} = \frac{\delta t}{\tau}(T_{bath} - T(t)) \tag{2.31}$$

Where the scaling factor, λ for the velocities is now,

$$\lambda = \left[1 + \frac{\delta t}{\tau}\left(\frac{T_{bath}}{T(t))} - 1\right)\right]^{\frac{1}{2}} \tag{2.32}$$

τ is the coupling parameter characteristic of the relaxation time of the system and its value determines how strongly the heat bath and the system are coupled together. If the collisions with the bath are infrequent then the energy fluctuations will occur slowly, and the temperature fluctuations will occur much as in

conventional molecular dynamics. However if the collisions occur too frequently then the rate at which phase space is explored will be extremely slow. This relatively simple method has the advantage that it permits the system to fluctuate about the desired temperature. However, it does not generate rigorous canonical averages because the velocity scaling prolongs any temperature scaling among the components of the system. So although the overall temperature of the system is at the desired value individual components could have extreme values.

Nosé-Hoover thermostat

An alternative technique used to treat the dynamics of a system in contact with a thermal reservoir is to include the reservoir as an integral part of the system, represented by an additional degree of freedom, s. This is the approach taken in the Nosé-Hoover thermostat [89]. This method allows the energy to flow dynamically from the reservoir to the system and back. The whole technique is much like controlling the volume of a sample by using a piston. The reservoir has both a potential energy, $(f+1)k_BT\ln s$, and a kinetic energy, $\left(\frac{Q}{2}\right)\left(\frac{ds}{dt}\right)^2$; where f is the number of degrees of freedom in the physical system, T is the desired temperature and Q is the thermal inertia parameter which can be thought of as the fictitious mass of the extra degree of freedom. The magnitude of Q determines the coupling between the reservoir and the real system, and so influences the temperature fluctuations. For example, if the value of Q is large then the flow of energy is slow. In the limit of infinite Q conventional molecular dynamics is regained and there is no energy exchange between the reservoir and the real system. However, if Q is too small then the energy oscillates and this leads to equilibration problems. It was suggested by Nosé that Q should be proportional to $fk_{\mathrm{B}}\mathrm{T}$.

2.5.5 Constant pressure (NpT)

Many experimental measurements are made under conditions of constant temperature and pressure, and so simulations in the isothermal-isobaric (NpT) ensemble are most directly relevant to experimental data. The size and the shape of the simulation cell must be dynamically adjusted by coupling the system to a barostat

in order to achieve the desired average pressure. Two commonly used approaches are the Berendsen and Nosé-Hoover algorithms.

Berendsen barostat

Berendsen [88] described a relatively simple technique for coupling to a pressure bath which is analogous to the temperature bath in the NVT ensemble. The method requires that an extra term is added into the equations of motion in order to produce a pressure change. The rate of change of pressure is given by

$$\frac{dP(t)}{dt} = \frac{1}{\tau}(P_{bath} - P(t)). \tag{2.33}$$

where τ is the coupling constant, P_{bath} is the pressure of the *bath* and $P(t)$ is the actual pressure at time t. During the simulation the volume of the simulation box is scaled by a factor λ which is equivalent to scaling the atomic co-ordinates by a factor $\lambda^{1/3}$,

$$\lambda = 1 - \frac{\delta t}{\tau}(P_{bath} - P(t)). \tag{2.34}$$

This expression can be applied isotropically (scaling all volume equally in all three directions) but it is better to apply the scaling anisotropically (scale the volume independently in each axis).

Nosé-Hoover barostat

Another popular method is the Nosé-Hoover barostat [89]. This method involves incorporating an extra degree of freedom into the system, corresponding to the volume of the box. The potential energy associated with this degree of freedom is PV where P is the desired pressure and V is the volume of the system. There is also an associated kinetic energy, $1/2Q(dV/dt)^2$, which can be thought of as a piston of mass, Q acting on the system. A piston of small mass gives rise to rapid oscillations in the box, whereas a large mass has the opposite effect. An infinite mass returns the simulation to a normal molecular dynamics calculation. During the simulation the volume of the system varies and the average volume is determined by a balance between the internal pressure of the system and the desired external pressure.

2.6 Use of simulation techniques

In the following chapters, the simulation techniques described in this chapter will be employed in order to calculate specific molecular properties of liquid crystal mesogens. In chapter 3, Monte Carlo simulations in the NVT ensemble are carried out, with specially adapted periodic boundary conditions, in order to compute the helical twisting power of a liquid crystal chiral dopant. In chapters 5 and 6 molecular dynamics simulations are performed. These involve atomistic NpT simulations for the calculation of the Kirkwood correlation factor, and NVE simulations for the axially symmetric particles used to calculate the rotational viscosity respectively.

CHAPTER

3

Calculation of the Helical Twisting Power (HTP) for liquid crystal chiral dopants

3.1 Introduction

The helical twisting power determines the pitch of the chiral nematic phase produced when a nematic liquid crystal is doped with a low concentration of chiral solute molecules. In a *nematic* liquid crystal phase the molecular orientations have a preferred direction of alignment that is given by the director $\mathbf{n}(\mathbf{r})$. If a chiral solute is then added to the nematic phase, a uniform helical twist of the director is induced (as shown in figure 3.1), such that,

$$\mathbf{n}(\mathbf{r}) = (\cos\phi(z), \sin\phi(z), 0), \qquad \frac{\delta\phi}{\delta z} = k = \text{constant}. \tag{3.1}$$

Here the helical twist is about the z-axis and the resulting *chiral nematic phase* is characterized by its wavenumber k, or, alternatively, by the helical pitch P ($P = 2\pi/k$).

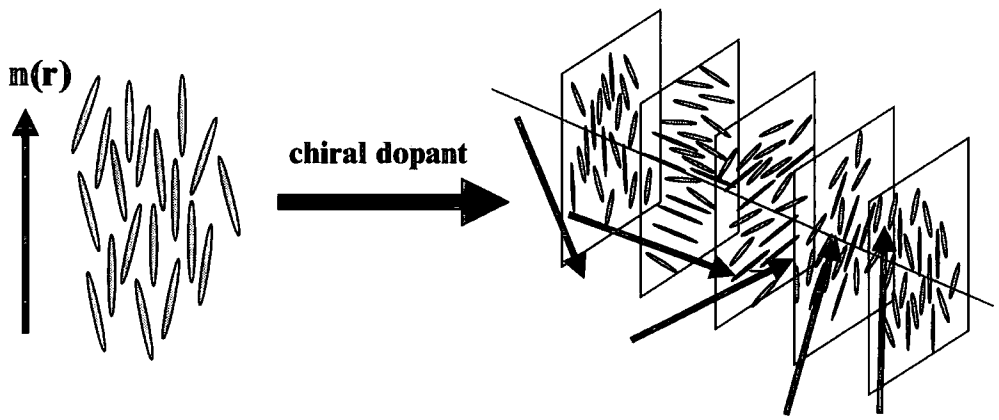

Figure 3.1: Schematic representation of HTP.

Experimental measurements have shown that different chiral materials exhibit widely different abilities to twist a nematic phase. This effect can be quantified by defining a *macroscopic helical twisting power*, β_{M} [90]

$$\beta_{\mathrm{M}} = (P c_w r)^{-1}, \tag{3.2}$$

where c_w is the weight concentration of chiral dopant and r defines the enantiomeric purity of the dopant. Depending on the material concerned, the sign of β_{M} can be either positive or negative indicating the presence of a right-handed or left-handed helix, respectively. Two pure enantiomers of the same material will always have the same magnitude of β_{M} but opposite signs.

Recently, there has been considerable commercial interest in the synthesis of materials with high β_{M} values. The reason for this is that such materials have potential applications in chiral nematic films for electro-optic displays, polarization sensitive polymer films [91], and thermally addressed display materials [92]. As often occurs with other liquid crystalline properties, small changes in molecular structure can give rise to large changes in β_{M}. The physical origin of this effect is due to changes in the solute-solvent interactions which are induced by changes

in the structure of the chiral solute [93, 94]. The question that therefore arises is whether or not reliable values of β_M can be predicted theoretically to aid the design of chiral dopants with high twisting powers that are desired for commercial products.

3.2 Theory

3.2.1 Microscopic helical twisting power, β

At low dopant concentrations there is a linear relationship between the chiral solute concentration and the equilibrium helical wave vector k_0. Using the de Gennes definition [90],

$$k_0 = \frac{2\pi}{P} = 4\pi\beta\rho \tag{3.3}$$

where $\rho = N/V$ is the number density of the chiral dopant molecules and the constant of proportionality β is defined as the *microscopic* helical twisting power of the solute [90]. For a uniformally twisted nematic phase or *chiral nematic,* with a helical wave vector k, the elastic part of the free energy is written relative to the undistorted state as

$$\Delta F = \frac{1}{2} V K_2 k^2. \tag{3.4}$$

However, if a uniformally twisted nematic phase, with wave vector, k, arises due to a nematic phase being doped with small numbers (N_+ and N_-) of a chiral dopant, producing a microscopic helical twisting power of $\pm\beta$, then the elastic part of the free energy can be written as [95],

$$\Delta F = \frac{1}{2} V K_2 \left(k - \frac{4\pi\beta}{V} [N_+ - N_-] \right)^2 \tag{3.5}$$

where V is the volume of the system and K_2 is the twist elastic constant of the solvent. Following the work of Allen [95], in the limit of infinite dilution

($N_-, N_+ \rightarrow 0$). The free energy difference can therefore, be written as the difference in chemical potential

$$\mu_- - \mu_+ = \frac{\partial F}{\partial N_-} - \frac{\partial F}{\partial N_+} = 8\pi\beta K_2 k \tag{3.6}$$

so that,

$$\beta = \frac{\Delta\mu}{8\pi K_2 k}. \tag{3.7}$$

This expression is only valid for vanishingly low dilutions and in the low k limit. It allows the determination of the microscopic helical twisting power, β from a measurement of the chemical potential difference between two enantiomers in a twisted nematic phase.

3.2.2 Twisted Periodic Boundary Conditions

Twisted periodic boundary conditions are a novel set of boundary conditions which allow a twisted nematic liquid crystal phase to be simulated [96]. They work by allowing the simulation of one quarter of a turn of the helical director in the length of one cuboidal box. The convention adopted is that the x and y co-ordinates of image particles in a neighbouring box are rotated by $+\pi/2$, in the $+z$ direction, with respect to those in the central box. Therefore, when a particle leaves a box through the $+z$ or -z face it is replaced by an image entering at the opposite face with its x and y co-ordinates rotated through $+\pi/2$ or -$\pi/2$ respectively. This convention incorporates a helical twist into the simulation, such that the helix produced has a pitch of four times the box length, as shown in figure 3.2. For a twisted nematic phase the lack of translational order means that there are no undesirable consequences arising from perturbing the centre of mass of the molecule in this way.

Previously, Allen [95] and Camp [97] obtained values of β from the chemical potential difference defined in equation 3.7, for a system consisting of two touching hard prolate ellipsoids of axial ratio $e = 5$ within a fluid of similar monomeric ellipsoids. The simulations use twisted periodic boundary conditions [96] whereby molecules in the neighbouring simulation box ($+z$ direction) are rotated through

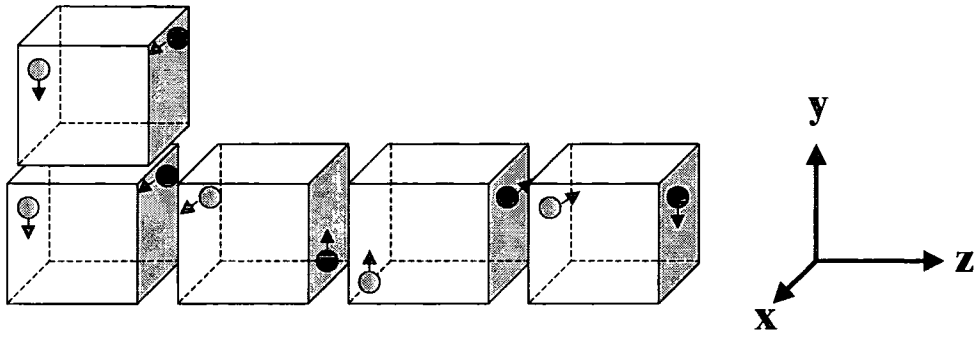

Figure 3.2: Twisted Periodic Boundary Conditions.

90 degrees about the z axis with respect to their co-ordinates and orientations in the original box, (and those in the neighbouring box in the opposite $(-z)$ direction are rotated through -90 degrees). In the case of hard ellipsoids an analytical expression can be obtained for the excess chemical potential of a dimer composed of two ellipsoids in contact [97]. This leads to an accurate value for $\Delta\mu$ in equation 3.7. For other model systems $\Delta\mu$ is equivalent to the *free energy change* in converting one mole of chiral solute into its mirror image in the presence of a twisted nematic solvent at infinite dilution. Consequently, a calculation of this free energy change combined with a calculation of the twist elastic constant will provide a simulation route to β.

3.2.3 Calculating free energy differences

The calculation of free energy differences has been described as the 'Holy Grail' of computational chemistry. Many of the physical properties a chemist wishes to determine, by calculation or experiment, depend upon the free energy of a system. Calculation of the absolute free energy of a system is virtually impossible. It is, however, often possible to calculate the difference in free energy between two (closely) related states.

For atomistic simulations there are three well know methods for calculating the free energy difference between two states [98–101]: thermodynamic perturbation theory (statistical perturbation theory), thermodynamic integration and slow growth. All three methods use a so called coupling parameter approach [102].

One approach is to make the Hamiltonian of the two states, A and B, a function of the coupling parameter, λ, which transforms the system from state A to state B, as the coupling parameter varies from 0 to 1 (see equation 3.8). There are, however, a number of other ways that state A can be transformed into state B.

$$E(\lambda) = \lambda E_B + (1 - \lambda)E_A \tag{3.8}$$

Thermodynamic perturbation

Thermodynamic perturbation treats the change from the initial to the final state as a series of discrete steps or *perturbations*. If one considers the two systems, A and B, then the free energy difference between them is given by

$$\Delta F_{BA} = -k_B T \ln \langle \exp[-(E_B - E_A)/k_B T] \rangle_A . \tag{3.9}$$

This expression is the key relationship in thermodynamic perturbation calculations [103]. Convergence of this expression is slow if the two systems are not similar, which is often the case. Consequently, a series of simulations are run in which state A is gradually mutated into state B by employing a coupling parameter, λ. This scales all the geometric and potential energy functions of state A to those of state B as λ changes from 0 to 1 in a series of small steps, λ_i. Each of these small free energy increments is referred to as a *window* and the overall procedure is termed *windowing*. At each λ_i the system is equilibrated and then an averaging period follows. The total free energy change is equal to the sum of all the incremental free energy changes from $\lambda = 0$ to 1. In practice two free energy increments are normally obtained from one simulation by perturbing the system from λ_i to λ_{i+1} and λ_{i-1}, this is termed *double wide sampling*. However, this should not be confused with *double ended sampling* which refers to performing both the forward (A to B) and the backward (B to A) calculations, which are used to check the convergence of the calculation [104]. Decisions do have to be made about the choices of λ_i and although uniform spacing is often used it is sometimes more advantageous to use smaller values of $\delta\lambda$ in regions where the energy is changing the most [105]. A final important point to make is that the

energy of the perturbed state (E_B in equation 3.9) must be obtained from both the potential parameters and the geometry corresponding to the B state. If the geometry is not changed to represent the intermediate states then no matter how small $\delta\lambda$ is, errors will arise.

Thermodynamic integration

If the change between the initial and final states is considered as a continuous process [99], the change in free energy can be written as

$$\Delta F_{BA} = \int_0^1 \left\langle \frac{\delta E_{BA}}{\delta \lambda} \right\rangle_\lambda \delta\lambda. \tag{3.10}$$

This is termed thermodynamic integration. In practice, the integrand in equation 3.10 is evaluated at a series of discrete points. The integral is approximated from these points using a numerical integration method, such as, the trapezoidal rule. As with the thermodynamic perturbation method the pathway between the physical end points is split into a series of λ intermediate states. Thermodynamic integration therefore, follows the same procedural protocol as thermodynamic perturbation. The main criterion for the thermodynamic integration method is that the λ pathway selected, contains enough λ points so that the numerical integration over these points is reasonably accurate.

Slow growth

This is a limiting case of both the thermodynamic perturbation and the thermodynamic integration method. The slow growth method only holds true when changes in λ are effected so slowly that the system essentially remains in equilibrium. In this case, it is assumed that no re-equilibration is necessary at each new window, and therefore, the ensemble average can be approximated by a single data collection point. Thus, equation 3.9 and equation 3.10 both reduce to,

$$\Delta F_{BA} = (E_B - E_A). \tag{3.11}$$

However, caution should be taken when applying and interpreting results [106–108] using this method as it is based on the unproven assumption that if λ

changes extremely slowly then the system remains at constant equilibrium and the ensemble can be approximated by a single point.

3.2.4 Choice of free energy technique

The best techniques for computing the free energy difference in a simulation are the thermodynamic perturbation and the thermodynamic integration methods. However, the convergence properties between the two approaches do differ markedly. Therefore, the most appropriate method is strongly dependent on the problem under investigation [109–117]. If the initial and final states closely overlap then the perturbation method is the most efficient. However, because the convergence of the ensemble average in equation 3.10 does not depend on the magnitude of the change in λ, the integration method is often preferred. In this work the thermodynamic perturbation method is employed to calculate the free energy difference between two enantiomers.

3.2.5 Relationship between microscopic and macroscopic HTP's

The microscopic helical twisting power, β, calculated using equation 3.7 can be related to the experimental macroscopic helical twisting power, β_M via the induced helical pitch P. Combining the expressions in equations 3.2 and 3.3 yields,

$$\beta_M = \frac{2\rho}{c_w}\beta. \tag{3.12}$$

3.3 The simulation model

This section describes in detail the simulation model used in the current investigation.

3.3.1 The solvent model

Atomistic modelling of liquid crystalline phases is computationally expensive at the present time. The simulation of a few hundred solvent molecules using a

fully atomistic potential (compared to a single solute molecule) is therefore, currently out of the question on a personal workstation. Thus, the solvent molecules employed in this work are represented by a well known, single site Gay-Berne potential, U_{ij}^{GB} [29]. The form of the Gay-Berne potential studied by de Miguel *et al* [43] is used. In this form of the Gay-Berne potential $\mu = 2$, $\nu = 1$, the length to breadth ratio $\sigma_{ee}/\sigma_{ss} = 3$ and the ratios of well-depths for end-to-end and side-to-side particles $\epsilon_{ee}/\epsilon_{ss} = 1/5$. For a Gay-Berne molecule with these dimensions a full phase diagram [118] is known (see figure 3.3). By setting $\sigma_0^{GB} = \sigma_{ss}$ to 5.7 Å and ϵ_0^{GB} to 3.32576 kJ/mol a nematic phase is achieved. The value of σ_0^{GB} is derived from simulation studies of the liquid crystal mesogen p-azoxyanisole (PAA) [46]. The value of ϵ_0^{GB} is deduced from the fact that this mesogen has a nematic-isotropic phase transition of 409.15 K, corresponding to a reduced temperature of $T^* = 1.0$, for a pure system of Gay-Berne particles at the chosen reduced density of $\rho^* = 0.32$.

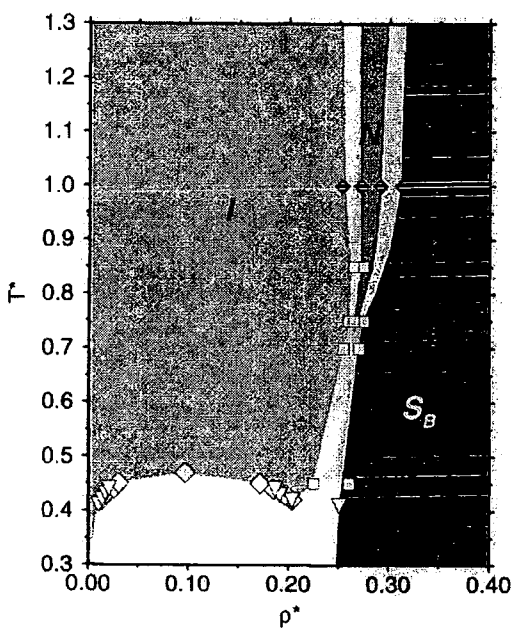

Figure 3.3: Phase diagram for Gay-Berne fluid (taken from Julian Brown's thesis, University of Bristol, October 1996).

3.3.2 The solute model

The liquid crystalline solute molecules are modelled using a fully atomistic potential energy function. The potential energy of the solute molecule, $U^{\mathrm{LJ}}_{\mathrm{solute}}$, is defined in terms of the energy of the solute molecule in an MM2 force field [74],

$$
\begin{aligned}
U^{\mathrm{LJ}}_{\mathrm{solute}} &= \sum_{angles}^{bending} \frac{k^b_\theta}{2}(\theta-\theta^0)^2_{ijk}(1+\mathrm{SF}.(\theta-\theta^0)^4_{\mathrm{ijk}}) \\
&+ \sum_{angles}^{stretch-bend} k^{sb}_\theta(\theta-\theta^0_{ijk})[(l-l^0)_{ij}+((l-l^0)_{jk})] \\
&+ \sum_{dihedrals}^{n=1,3} \frac{V_n}{2}(1-\cos n\phi) \\
&+ \sum_{non-bonded}^{vdW} \epsilon^* \left(2.9\times 10^5 \exp\left(\frac{-12.5}{P}-2.25P^6\right)\right) \\
&+ \sum_{non-bonded}^{elec} \frac{3\mu_i\mu_j(\cos X_{ij}-3\cos a_i\cos a_j)}{2r^3},
\end{aligned}
\tag{3.13}
$$

where k^b_θ is the angle bending constant, SF is the quartic bending term and θ_{ijk} and θ^0_{ijk} are the actual and natural bond angles respectively. k^{sb}_θ is the angle stretch-bend constant, and l and l^0 are the actual and natural bond lengths defining the bond angle θ_{ijk}. The dihedral angle, ϕ is defined by V_1, V_2, and V_3 which represent the first, second and third order torsional constants in the Fourier expansion. The van der Waals non-bonded part of the energy expression (fourth term in equation 3.13) is given by the Hill potential, which is only valid for $P \leq 3.311$. For $P > 3.311$ the van der Waals non-bonded part of the energy expression becomes

$$E^{vdW}_{non-bonded} = \epsilon^* 336.176 P^2. \tag{3.14}$$

In the above equation

$$P = r_m/r_{ij}, \tag{3.15}$$

where r_{ij} is the effective inter-nuclear distance, and $r_m = r_i + r_j$, where r_i and r_j are the van der Waals radii of the atoms i and j. $\epsilon^* = (\epsilon_i\epsilon_j)^{\frac{1}{2}}$, and ϵ_i and ϵ_j are the van der Waals well depths of the atoms, i and j. In the electrostatic

part of the non-bonded term (the fifth term in equation 3.13) μ_i and μ_j are the dipole moments of the two bonds, where X is the angle between the dipoles, and a_i a_j are the angles between the dipole axes and lines along which r (the distance between the midpoint of the bonds) is measured.

Prior to each of the Monte Carlo calculations the energy of the solute molecules was minimised with respect to the MM2 force field using the molecular modelling package CAChe [119]. Thereafter, the *minimum energy* structures of the solute molecules were considered as rigid entities. The energy minimisation calculations were carried out for each of the chiral dopant molecules shown in figure 3.4 [120, 121].

Material	Structure
A	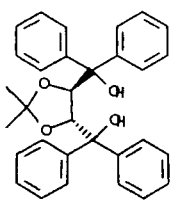
B	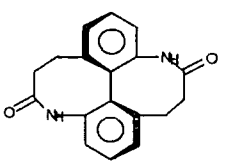
C	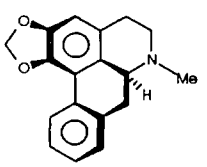
D	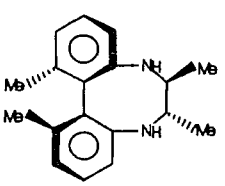
E	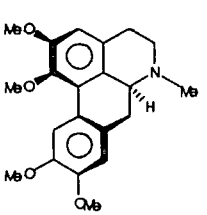

Material	Structure
BDH1281	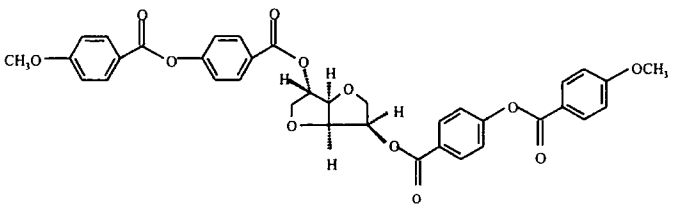
BDH1283	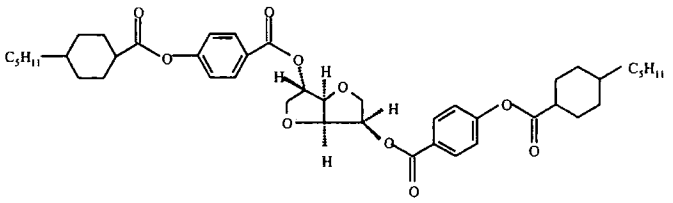
BDH1291	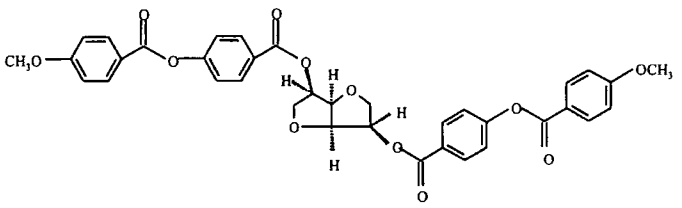
BDH1315	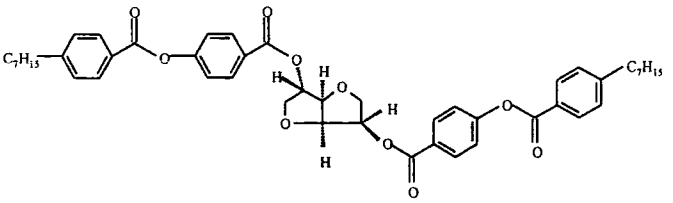
BDH1305	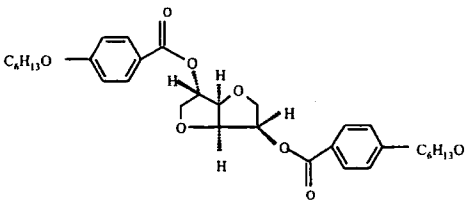
BDH1316	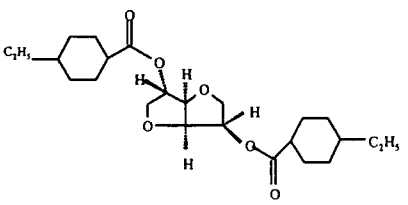

Material	Structure
BDH1321	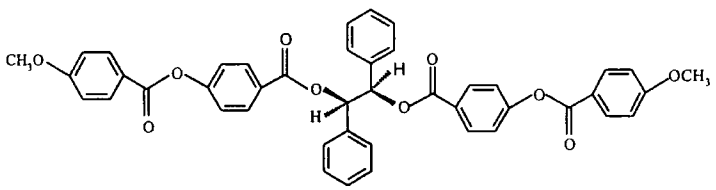
BDH1322	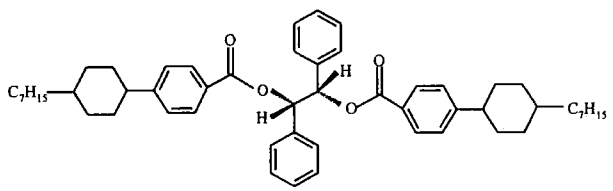
BDH1324	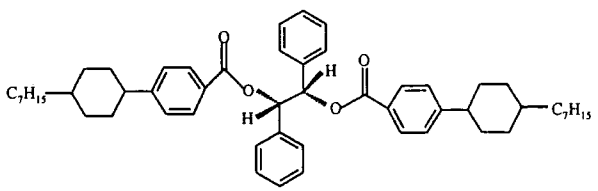
BDH1350	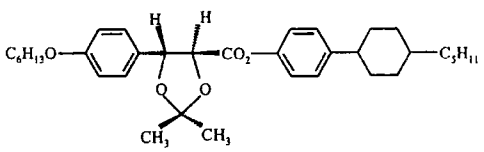
BDH1353	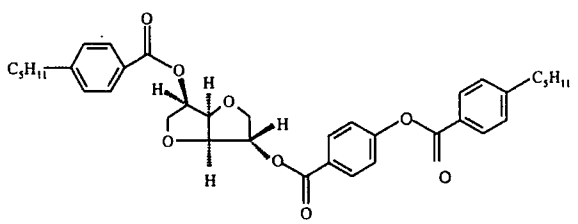
LF5	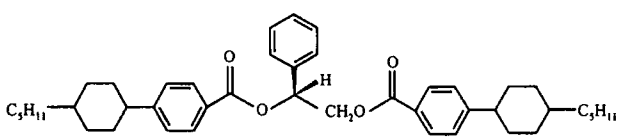

Figure 3.4: Structures of the chiral dopant molecules investigated.

3.3.3 The solvent-solute model

The solvent-solute interaction energy, $U_{ij}^{\mathrm{LJ/GB}}$, is summed over N_{GB} solvent molecules and N solute atoms. The form for the solvent-solute interaction energy is based on the work of Cleaver *et al.* [77]. They derived a generalized potential for two dissimilar Gay-Berne particles, see chapter 2 section 2.3.2.

$\epsilon_0^{\mathrm{LJ/GB}}$ is defined in equation 2.12, a value of ϵ_0^{LJ} is taken from ϵ^* in the MM2 Hill potential for each atom and ϵ_0^{GB} is taken as the well depth corresponding to the cross configuration of two Gay-Berne molecules. The value of ${\sigma_0}^{\mathrm{LJ/GB}}$ can be represented by the expression

$$ {\sigma_0}^{\mathrm{LJ/GB}} = \left[\left(\frac{{\sigma_0}^{\mathrm{LJ}}}{2^{1/2}} \right)^2 + \left(\frac{{\sigma_0}^{\mathrm{GB}}}{2^{1/2}} \right)^2 \right]^{\frac{1}{2}}, \tag{3.16} $$

However, an analytical form for ${\sigma_0}^{\mathrm{LJ}}$ is not available from the Hill potential, and this makes it difficult to obtain ${\sigma_0}^{\mathrm{LJ}}$ values from the van der Waals radii that are used in the MM2 force field. Instead, throughout this study equation 3.17 is employed. This was obtained from earlier fitting of the closest approach of a carbon atom to a phenyl ring.

$$ {\sigma_0}^{\mathrm{LJ/GB}} = ((r_m^{\mathrm{MM2}})^2 + (3.33825)^2)^{\frac{1}{2}}. \tag{3.17} $$

For a value of r_m^{MM2}(aliphatic carbon) = 1.94 Å, equation 3.17 provides a value of ${\sigma_0}^{\mathrm{LJ/GB}} = 3.86$ Å, which is in the expected range. In contrast, using equation 3.16 with ${\sigma_0}^{\mathrm{GB}} = 5.7$ Å and a value of ${\sigma_0}^{\mathrm{LJ}} \approx 3.43$ Å (obtained numerically from the Hill potential), a value of ${\sigma_0}^{\mathrm{LJ/GB}} = 4.7$ Å is obtained. The latter is too large to allow successful modelling of the shape of real molecules.

3.3.4 The complete molecular model

The complete functional form of the molecular model employed in this work, is written as a combination of the three individual potential energy functions, $U_{\mathrm{solute}}^{\mathrm{LJ}}$, U_{ij}^{GB} and $U_{ij}^{\mathrm{LJ/GB}}$ described previously in sections 3.3.1, 3.3.2, 3.3.3. Therefore, the total internal energy, U_{total}, of the combined solvent/solute model system is

written as,

$$U_{\text{total}} = U_{\text{solute}}^{\text{LJ}} + \sum_{i=i}^{N_{\text{GB}}} \sum_{j<i}^{N_{\text{GB}}} U_{ij}^{\text{GB}} + \sum_{i=i}^{N} \sum_{j=1}^{N_{\text{GB}}} U_{ij}^{\text{LJ/GB}}. \tag{3.18}$$

3.4 Simulation details

3.4.1 Monte Carlo free energy simulations

The computational model described in section 3.3 was employed in a series of Monte Carlo simulations in order to evaluate the free energy difference between a chiral dopant and its mirror image in a twisted nematic Gay-Berne solvent. The total free energy difference between the two systems is computed using the following equation

$$\Delta F_{BA} = -k_B T \ln \langle \exp(-\Delta E_{BA}/k_B T) \rangle_A , \tag{3.19}$$

where ΔE_{BA} is the energy difference between systems A and B and the angular brackets $\langle \rangle_A$ indicate an ensemble average for A. Equation 3.19 is only valid for two systems with similar Hamiltonians. Since real molecular systems are considered in this work then the Hamiltonians are, of course, very different. Consequently, the mutation of one enantiomer into its mirror image must be carried out in a series of small steps. In practice, two separate sets of simulations were employed. In set 1, the free energy change $\Delta F^{\text{solute/solvent}}$ was calculated for the growth of a single enantiomer into the solvent, and in set 2 the same quantity was obtained for the mirror image molecule. In each set of simulations a single rigid solute molecule was employed and a dimensionless control parameter $0 \leq \lambda \leq 1$ was used to scale the solvent/solute interactions $U_{ij}^{\text{LJ/GB}}$ (as described in section 3.3.3), such that

$$\begin{aligned} \Delta F^{\text{solute/solvent}} &= \sum_{i=1}^{n} F_{\lambda_{i+1}} - F_{\lambda_i} \\ &= \sum_{i=1}^{n} -k_B T \ln \left\langle \exp\left[-\left(E_{\lambda_{i+1}} - E_{\lambda_i} \right) / k_B T \right] \right\rangle_{\lambda_i} \end{aligned} \tag{3.20}$$

3.4.2 Methodology

Monte Carlo simulations were carried out using 504 Gay-Berne solvent molecules in a cuboidal cell of dimensions 1:1:2 at a Gay-Berne reduced density of $\rho^* = 0.32$, employing the twisted periodic boundary conditions of Allen and Master [96]. A random rotation/translation of the solute molecule and each of the solvent molecules was attempted during each Monte Carlo cycle. Molecular orientations were represented in terms of quaternions and a random rotation was carried out using the approach described in section 2.4.4 (references [122] and [123]), with move sizes adjusted to give Monte Carlo acceptance ratios in the range 35-55%. The simulations were carried out in the NVT ensemble at 400 K. (This corresponds to a nematic order parameter of $S_2 \approx 0.7$ for an untwisted Gay-Berne system.) Prior to each of the free energy calculations the solvent was well-equilibrated using 100000-200000 Monte Carlo cycles.

Initial free energy calculations employed 10 λ steps in the calculation of $\Delta F^{\text{solute/solvent}}$. However, these simulations gave un-reproducible values for the solute/solvent free energy. In order to improve the accuracy of the simulations, test runs were carried out on a $5\pi/2$ twisted simulation cell. On occasions this led to a relaxation of the twist back to the original value of $\pi/2$. A $5\pi/2$ twist also changed the clearing point from that of the untwisted nematic system. (The clearing point of the $\pi/2$ twisted system was found to be the same as the untwisted nematic.) Consequently all final simulations employed a $\pi/2$ twist, corresponding to a helical pitch of 4×105.829 Å, and 40 λ steps for $\Delta F^{\text{solute/solvent}}$ (80 λ steps per dopant) rather than the original 10 λ steps. All simulations employed 2000 Monte Carlo equilibration cycles and 50000 Monte Carlo production cycles at each value of λ using double-wide free energy sampling [124]. The initial point in the free energy calculation required a longer equilibration time (100000 cycles) and a longer production run (200000 cycles).

3.4.3 Computational results

The graph in figure 3.5 shows the total computed free energy change for the two enantiomers of dopant A as λ is varied between 0 and 1 in a sequence of simulations. This is a typical graph of the free energy change between two enantiomers

and similar graphs were seen for most of the dopant molecules studied in this work.

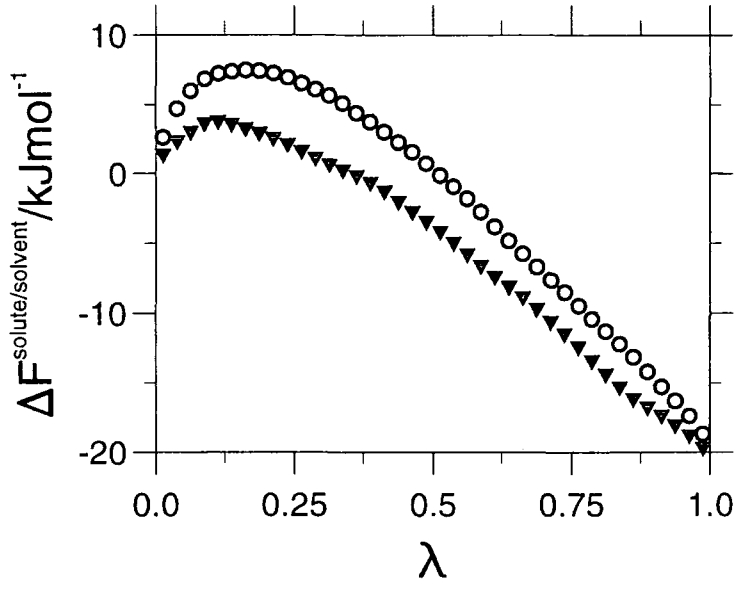

Figure 3.5: Graph showing the total change in the free energy for $0 \leq \lambda \leq 1$ for molecule A in figure 3.4. Triangles represent the enantiomer which produces a right-handed chiral nematic phase (same as the simulation box) and circles represent the mirror image molecule.

Each point on the graph represents a single simulation as indicated in section 3.4.1. The overall solvation free energy for both enantiomers is negative and is dominated by the increase in entropy associated with the addition of the solute. It should be noted, however, that at small values of λ (when $\lambda U_{ij}^{\mathrm{LJ/GB}}$ is small) the free energy change for both enantiomers is positive. This results from a disruption in the uniform twisted structure of the solvent due to the presence of the chiral dopant. This disruption is largest for the enantiomer that '*wants*' to induce a twist in the opposite direction to the imposed twist of the periodic box. It is this factor that is mainly responsible for the different behaviour of the two curves in figure 3.5.

The overall difference in free energy between the two enantiomers in the twisted nematic solvent is given by the difference in the curves at the end point ($\lambda = 1$). This value, $\Delta\mu$, is listed in table 3.1, for all the chiral liquid crystal materials investigated. These results are combined with the twist elastic constant

K_2 in order to obtain values of the microscopic helical twisting power, β (equation 3.7). The macroscopic helical twisting power, β_M, is calculated from the β values and the results obtained β_M(Comp.) are listed in table 3.1. Experimental values for β_M i.e.β_M(Exp.) are also included in table 3.1 for comparison purposes. For a Gay-Berne fluid, K_2, can be obtained by a careful fit of the wave-vector dependent fluctuations in the ordering tensor [47]. In this study the twist elastic constant of the Gay-Berne solvent was taken as, $K_2 \approx 6.96 \times 10^{-12}$ J m^{-1}.

Molecule	$\Delta\mu$/kJ mol^{-1}	β_M(Exp.)/μm^{-1}	β_M(Comp.)†/μm^{-1}
A	0.826	+104	+99.3
B	0.377	+58	+69.0
C	0.144	+24	+27.9
D	0.131	-21	-26.7
E	0.0	+8	0.0
BDH1281	0.885	+72	+73.4
BDH1283	0.474	+36	+39.0
BDH1291	0.874	+18.5	+19.9
BDH1315	0.818	+57	+61.9
BDH1305	0.620	+51	+60.8
BDH1316	0.236	+28	+30.4
BDH1321	0.342	+43	+44.8
BDH1322	0.701	+49	+46.4
BDH1324	0.701	+45	+46.4
BDH1350	0.319	+23	+32.7
BDH1353	0.874	+60	+68.3
LF5	0.400	+33	+31.4

† The molecular mass of the liquid crystal solvent used is taken as that of 4-n-pentyl-4′-cyanobiphenyl (5CB).

Table 3.1: Calculated values of $\Delta\mu$ and helical twisting powers for all the molecules studied. (The sign of β_M is specified for the enantiomer with the stereochemistry shown in figure 3.4. Estimated errors in $\Delta\mu$ are approximately ±15% in each case.)

The results presented in table 3.1 are encouraging. Within statistical errors the computed HTP values are in reasonable agreement with experimental data, and with the exception of dopant E (where $\beta_M = 0$) it is possible to successfully predict the direction of twist for each enantiomer. In order to try and detect the small free energy difference expected between the two enantiomers of material E additional (more extensive) calculations were carried out. Firstly, the number of perturbation steps was increased from 80 to 240. Secondly, the length of the equilibration steps at each point was increased to 1×10^7 Monte Carlo cycles and the length of the production run at each point was increased to 4×10^7 cycles for 80 perturbation steps. Neither of these techniques were able to detect a free energy difference between the two enantiomers within the statistical errors associated with the simulations.

Finally, in order to try and increase the overall free energy difference measured a further simulation was carried out on the liquid crystal chiral dopant B. In this simulation the value of the twist elastic constant of the solvent was increased by a factor of five, such that, $K_2 \approx 3.48 \times 10^{-11}$ J m^{-1}. However, in order to keep the density of the system constant, the values of σ_0^{GB} and ϵ_0^{GB} had to be altered. This required a new smaller σ_0^{GB} value of 3.8 Å. In order to achieve this the dimensions of the simulation box had to be reduced from 52.91 Å : 52.91 Å : 105.83 Å to 35.28 Å : 35.28 Å : 70.55 Å. Altering the value of ϵ_0^{GB} from 3.32576 kJ/mol to 11.08500 kJ/mol, had the most drastic effect, as it caused the temperature of the entire system to rise to $\approx$ 1000 K. The graph presented in figure 3.6, indicates that increasing the twist elastic constant of the solvent, K_2, does have the desired effect, in that, it increases the absolute value of the free energy difference. However, it also increases the size of the error associated with the free energy difference and so the results obtained are unreliable and hence the technique is unacceptable.

3.5 Discussion

The method presented provides a promising technique for the determination of HTP values, and may be of considerable use in the design of materials with high β_M. There are, however, a number of limitations and these are discussed here.

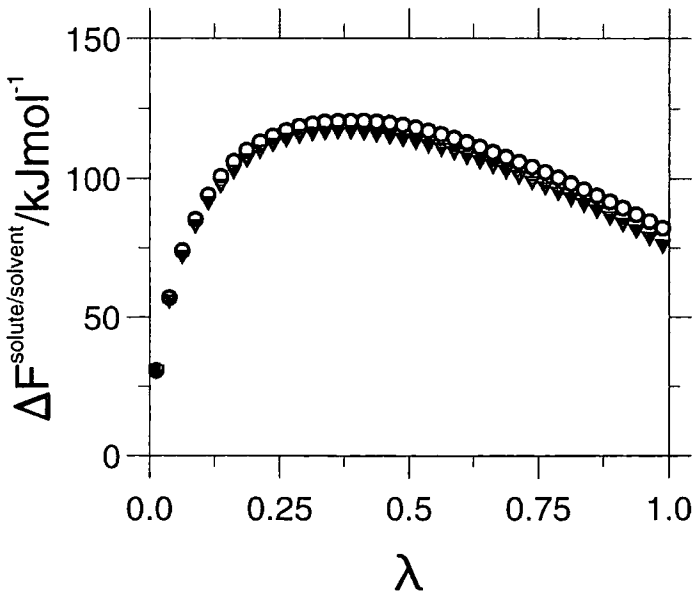

Figure 3.6: Graph showing the total change in the free energy for molecule B, in a solvent with an increased twist elastic constant K_2. Triangles represent the enantiomer which produces a right-handed chiral nematic phase (same as the simulation box) and circles represent the mirror image molecule.

The first drawback of this method is that all the calculations take place in a generic liquid crystal solvent, represented by the Gay-Berne potential. Although the potential employed in equation 3.18 is extremely sensitive to changes in molecular shape, it cannot take highly specific solute/solvent interactions into account. Consequently, one expects specific electrostatic or hydrogen bonding interactions between solute and solvent to lead to β_M values that vary considerably from the ones predicted by this technique. In the majority of experimental measurements the HTP values do not vary much between similar nematic solvents [93]. For this reason it is suggested that the main driving force involved in inducing a helical twist in a nematic phase is the excluded volume interactions arising from molecular shape. It should be noted, however, that some important studies have demonstrated how changes to certain nematic solvents can greatly effect the magnitude (and in some cases the sign) of β_M [94, 125]. Such cases are assumed to arise due to certain conformers being preferentially selected in certain solvents. Each conformer will have a different helical twisting power and this leads to different values of β_M being obtained in the different solvents. There is already some

evidence for this effect in the work of Ferrarini *et al.* [126]. The approach adopted in the current study could easily be adapted to test this factor by running rigid body simulations with different conformers. Flexible molecules could also be included in the current perturbation studies by adopting the internal co-ordinate Monte Carlo approach of reference [123], though longer runs would be required to ensure good sampling of conformational space in the presence of the solvent. Finally, the method used in this study can be extended to represent specific liquid crystals by using a fully atomistic treatment of the solvent. This opens up the possibility of an accurate treatment of all solute/solvent interactions. Atomistic simulations can be extremely expensive in terms of computer time, but they are becoming possible with the advances in computer speed [127].

A second limitation of the technique described is that the free energy differences computed are extremely small. This demands long simulations, with accurate Monte Carlo sampling and many steps in the perturbation calculation. It is however useful to note that there are a number of other ways in which $\Delta\mu$ of equation 3.7 can be calculated, which could provide speedier results with improved accuracy in the future. For example, both enantiomers can be included at the starting point of a simulation (one on top of each other), and then the perturbation calculation could involve the shrinking of one enantiomer inside the other until it disappears. This can be achieved by varying both the bond lengths and the values of the van der Waals radii, σ, for each of the atoms in the solute molecule (see figure 3.7). This technique could potentially provide greater accuracy in the calculation of β_M in fewer perturbation steps. Alternatively the speed of the calculation could be improved by using a cheaper solvent model, such as, the Kihara potential (repulsive spherocylinder) [128].

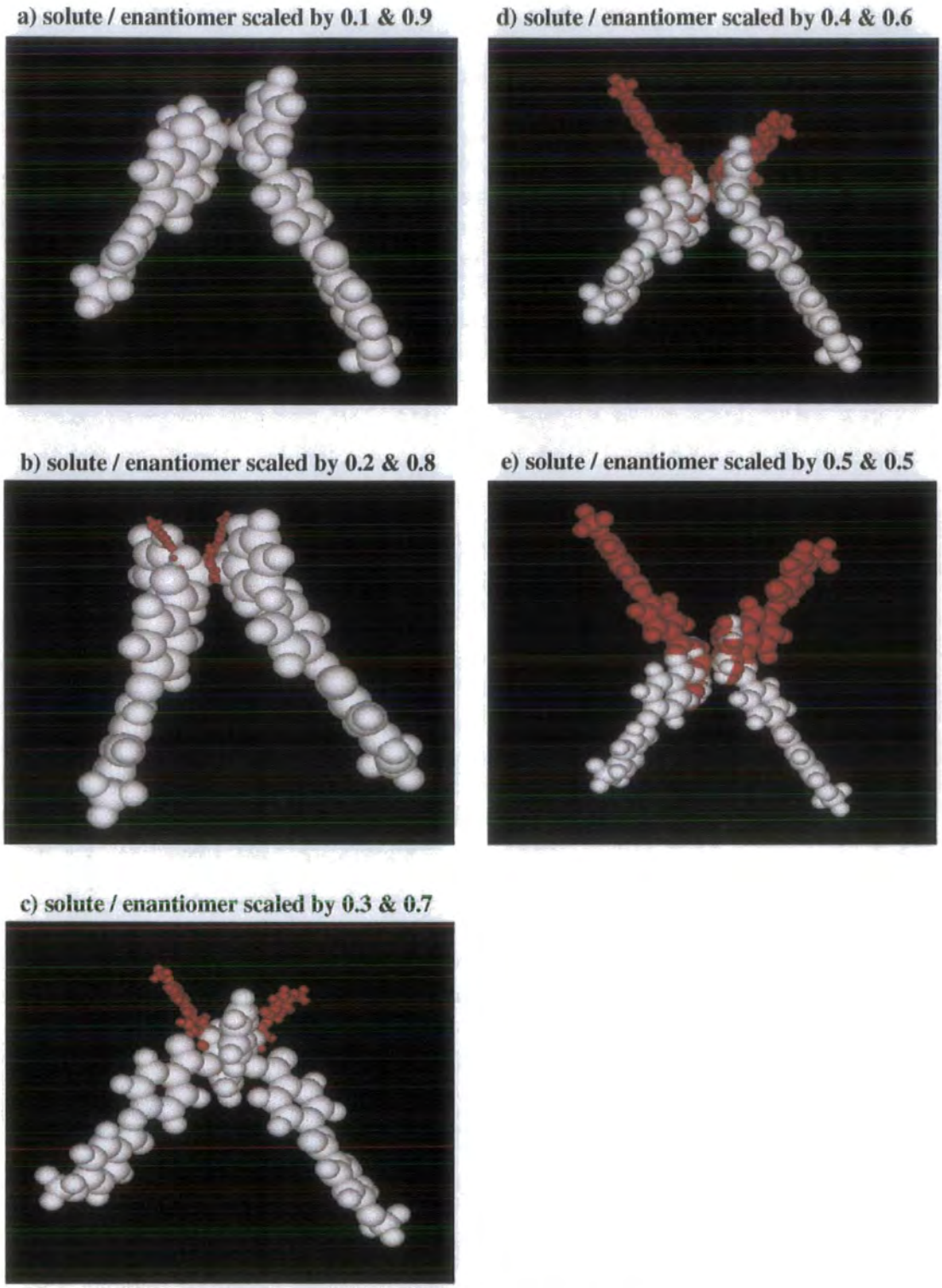

Figure 3.7: Schematic diagram showing how the perturbation calculation will look, starting with both enantiomer at the beginning and shrinking one enantiomer inside the other during the simulation by scaling both the bond lengths and the values of σ.

3.6 Different approaches to the calculation of the HTP

Ferrarini *et al.* have adopted a rather different approach to calculate the helical twisting power [129–132]. This approach is based on a single dopant molecule, and describes the interaction of the dopant with the solvent by molecular field theory. Here, the assumption is made that the surface of a chiral molecule in a nematic environment tends to orientate perpendicularly to the mesophase director. Ferrarini *et al.* derive an expression whereby the helical twisting power of the dopant molecules is first calculated by constructing two tensors, one describing the helicity of the dopant and the other describing the orientational order of the chiral dopant in the solvent mean field. These two tensors are then used to obtain a chirality order parameter [126, 130], Q, which is related to the helical twisting power, β, by;

$$\beta = \frac{RT\epsilon Q}{2\pi K_2 V} \tag{3.21}$$

where ϵ is the orientating strength of the solute in the solvent, K_2 is the twist elastic constant of the solvent, and V is the molar volume of the solvent.

In order to employ this theoretical model in computer simulations, a knowledge of the molecular structure of the chiral dopant is required, and from this, a definition of the molecular surface can be achieved. As an approximation the dopant molecules are generally considered to exist in a single rigid conformation. This theory, has been used, with reasonable success, to predict the helical twisting power of some real chiral dopants. However, in some cases the HTP predictions appear quite poor.

A direct comparison between the helical twisting power calculated using the Ferrarini *et al.* model and the approach adopted in this thesis (for the same molecular conformation of a chiral dopant) would be useful. In practice this is extremely difficult to achieve because, in Ferrarini's work, both the orientating strength of the nematic medium and the chirality order parameter contribute to the free energy term, $\Delta\mu$, in equation 3.7. However, calculations of the chirality order parameter could, in principle, be carried out in the future using the Monte

Carlo technique described in this thesis. This would aid the comparison of the two methods.

The HTP calculation method adopted in this thesis, is computationally more expensive than the approach employed by Ferrarini. This is largely due to the vast amount of time required to evaluate the expensive solvent-solvent interactions that contribute to the U_{ij}^{GB} energy term; these interactions are not required within molecular field theory. However, the technique presented here has some potential advantages over the molecular field theory approach. In particular, for flexible solute molecules, the Monte Carlo approach can allow for the substantial change in molecular shape that often occurs as a molecule enters a liquid crystal phase [127, 133]. In molecular field theory it is difficult to know the correct statistical weight for each conformer in a nematic phase without the aid of experimental order parameter data for each part of the molecule [134, 135].

CHAPTER

4

Development of a Liquid Crystal Force Field (LCFF)

4.1 Introduction

Recently, there has been considerable progress in the use of computer simulations to study bulk liquid crystal phases. These studies employ either, Monte Carlo or molecular dynamics simulation methods [136, 137] to sample the inter and intra-molecular degrees of freedom of a molecule [127, 138–145]. At the heart of these calculations is the molecular mechanics force field that describes the total energy of the molecules as a sum of the steric and non-bonded interactions present. The importance of the force field means that careful consideration must be given to its functional form and the parameters required in order to apply it to liquid crystal systems.

4.2 The molecular mechanics force field

The starting point for any calculation in theoretical chemistry is to decide which model to employ. Any model of *reality* must involve approximations, and the beauty of molecular mechanics is the simplicity of these approximations. The standard approach employed in molecular mechanics force fields is to consider a molecule as a collection of atoms joined together by elastic restoring forces. These forces are described by simple mathematical functions that characterize the distortion of each structural feature within the molecule, for example, bond stretches, angle bends, torsional angles, and non-bonded terms which incorporate both electrostatic and van der Waals interactions. Collectively, these potential energy functions make up the molecular mechanics force field, which is represented schematically in figure 4.1.

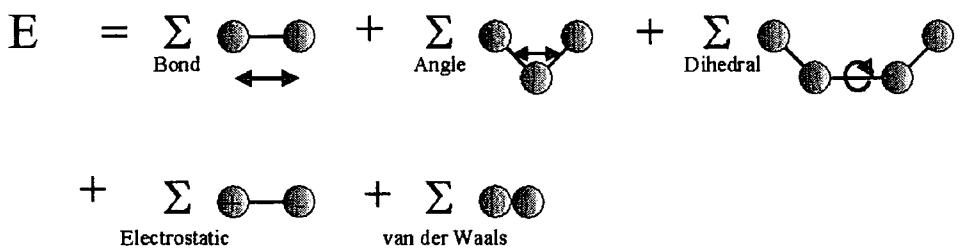

Figure 4.1: Schematic representation of the terms included in a molecular mechanics force field.

The total steric energy, E of the molecule of interest is defined with reference to the molecular mechanics force field. On its own the total steric energy has no physical significance. However, it can be thought of as a measure of how the energy of a particular molecular conformation varies from its hypothetical reference geometry (one where all the bonds, angles, etc take their natural values). Each molecular conformation has a different value of the steric energy. So although E has no direct physical significance by itself, the differences between the steric energies of any two conformations is equivalent to the energy difference between them. In general, the steric energy can be interpreted in terms of a relatively simple four-component picture of the inter and intra-molecular potential energy functions within the system involving bond stretches, angle bends,

torsional deformations and non-bonded parameters (as shown in equation 2.10 of section 2.3.2). However, more sophisticated force fields may include additional terms such as, hydrogen bonding or cross terms.

Once an appropriate force field has been chosen for the molecule of interest the aim of molecular mechanics is to optimize the molecular geometry by minimizing the total steric energy. This is achieved via a series of energy minimization routines, which result in the contributions to the steric energy being spread throughout the entire molecule.

4.2.1 General features of a molecular mechanics force field

In order to define a force field one must specify not only the functional form but also the potential parameters employed, as any two force fields may employ identical functional forms but undoubtably will use different potential parameters. Moreover, force fields which use the same functional form and different parameters may give comparable results to force fields which employ different functional forms. Therefore, a force field should be considered as a single entity. It is therefore, not strictly correct to divide the energy up into its individual components or even take some parameters from one force field and mix them with another. However, some terms in the force field are sufficiently independent of others to make this an acceptable approximation when parameterising the force field.

Development and parameterisation of a force field must consist of a compromise between the complex functional form employed, and the large number of different atom types. It is important to try and ensure, when developing a force field, that any associated errors are balanced. For example, it would be inappropriate to spend a large amount of time getting, say, the bond stretch terms correct, if the van der Waals parameters give rise to large errors. This problem is often overcome by using the same set of parameters for as wide a range of situations as possible. The non-bonded terms are particularly problematic and so in some simple molecular mechanics force fields it is common to use the same set of parameters for all atoms of the same element, for example, sp^3, sp^2 and sp-hybridised carbon atoms. An important feature of a molecular mechanics force field is its ability to transfer its functional form, and its parameters, from one mol-

ecule to another. This means that the same set of parameters can be employed to model a whole series of related molecules, rather than having to define a new set for each individual molecule. Without this feature, the task of parameterization would be impossible.

It is important to bear in mind as a deeper analysis of molecular mechanics force fields is undertaken that force fields are empirical and there is no *correct* form. Of course, if one functional form produces results that are closer to experiment than another then it is likely that this form will be favoured.

4.3 Functional form of a force field

4.3.1 Bond stretching interactions

The potential energy curve used to describe a typical bond stretching term has the form shown in figure 4.2. Of the many functional forms used to model this potential energy curve, the simplest and most popular is based on an harmonic potential, such as, Hooke's law

$$E_{bond} = \frac{K_r}{2}(r - r_0)^2. \tag{4.1}$$

Where E_{bond} is the energy of a bond stretch, K_r in the force constant for stretching a bond and r and r_0 are the actual and reference (natural) bond lengths respectively. The term *reference bond length*, is sometimes called the *equilibrium bond length*, but this is not strictly correct. The reason for this is that the reference bond length is the value that the bond adopts when all other terms in the force field are set to zero, whereas, the equilibrium bond length is the value that is adopted in a minimum energy structure, when all other terms in the force field contribute.

The forces between bonded atoms are extremely large and therefore require a considerable amount of energy in order to cause the bond to deviate significantly from its equilibrium value. This is reflected in the magnitude of K_r. As a result, it is quite common to keep the bond lengths fixed when performing fully atomistic calculations. These are normally carried out in a simulation using a SHAKE algorithm [146].

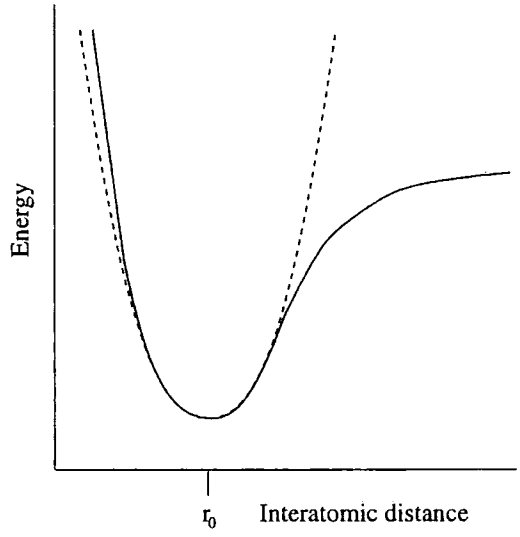

Figure 4.2: Variation of bond energy with interatomic distance (——), and harmonic potential (- - -).

For *real* molecules, an important point to recognize is that, the Hooke's law functional form is only a reasonable approximation to the shape of the potential energy curve at the bottom of the energy well. This is the case when the deviation from equilibrium is small. If the displacements from equilibrium are large, then the harmonic approximation does not hold true (see figure 4.2). Consequently, cubic and higher order terms are often added as corrections to the harmonic potential in more sophisticated force fields to improve the accuracy of the model.

4.3.2 Angle bending interactions

The deviation of the bond angles from their reference values is also commonly described using an harmonic potential

$$E_{angle} = \frac{K_\theta}{2}(\theta - \theta_0)^2. \tag{4.2}$$

where E_{angle} is the angle bending energy, K_θ is the force constant for the angle bending and θ and θ_0 are the actual and reference (natural) bond angles respectively. Rather less energy is required to distort an angle away from equilibrium than is needed to stretch a bond. Consequently, the values of the force constants are proportionately smaller for the angle bending terms, compared with the bond

stretching terms. As with the bond stretching potential, the accuracy of the force field can be improved by incorporating higher order terms. Such terms have been employed to treat certain pathological cases such as highly strained molecules.

4.3.3 Torsional angle interactions

Originally, it was thought that the torsional angle energy term could be omitted from the force field expression. However, the importance of torsional interactions to molecular structures cannot be underestimated. Most of the variation in structure and relative energies arise as a result of a complex interplay between torsional and non-bonded contributions. The existence of torsional energy barriers is, therefore, fundamental to understanding the structural properties of liquid crystal molecules.

The functional form of the torsional interactions is generally described by a cosine series expansion in the torsional angle ϕ. This expansion is normally truncated at the third order term, but for molecules containing flexible functional groups it is not uncommon to see higher order terms incorporated into the expression, in order to increase the accuracy of the model. Not all molecular mechanic force fields employ torsional potentials as it is sometimes possible to rely entirely on non-bonded interactions between 1, 4 atoms to achieve the desired energy profile. However, most force fields that are designed to study organic molecules do explicitly include a torsional potential energy term and a common functional form for this torsional potential is a Fourier series expansion

$$E_{dihedral} = \sum_{m=0}^{m=3} \frac{V_m}{2}[1 + \cos(m\phi - \delta)] \tag{4.3}$$

or,

$$E_{dihedral} = \sum_{m=0}^{m=3} \frac{V_m}{2}(1 + \cos m\phi) \tag{4.4}$$

where $E_{dihedral}$ is the total torsional energy, V_m are torsional force constants, ϕ is the torsional angle, and δ (in equation 4.3) is the phase angle. Figure 4.3 shows the typical variation in energy for the first three terms in the Fourier expansion.

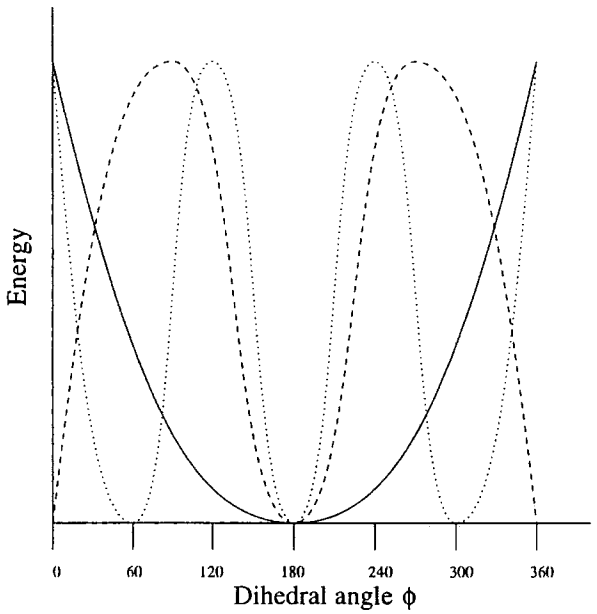

Figure 4.3: Variation of energy with torsional angle for one(——), two(- - -) and threefold(.....) barriers.

The force constant, V_m, is often referred to as the *rotational energy barrier height*, but to do so is misleading, obviously so, when more than one term is present in the Fourier expansion. Moreover, other terms in the force field equation contribute to the barrier height as a bond is rotated, especially the non-bonded interactions between the 1, 4 atoms. However, the values of the force constants do provide a qualitative indication of the relative barriers to rotation.

4.3.4 Non-bonded interactions

The interactions discussed so far are generally grouped together and termed *bonded interactions*, in the sense that they are defined by the connectivity of the molecule. Non-bonded interactions, on the other hand, do not depend upon a specific bonding relationship between atoms but are *through-space* interactions. There are two distinct groups of non-bonded terms: electrostatic and van der Waals interactions.

Electrostatic interactions

Electrostatic interactions provide a quantitative measure of the charge distribution within a molecule and can be represented in a number of ways. The most

common approach is an arrangement of fractional point charges throughout the molecule or *partial atomic charges*, if the charges are restricted to lie at the nuclear centres. These charges are designed to reproduce the electrostatic properties of the molecule. The electrostatic interaction between two molecules or different parts of the same molecule is calculated as a sum of the interactions between pairs of point charges, using a Coulomb potential

$$E_{electrostatic} = \sum_{i<j} \frac{q_i q_j}{4\pi\epsilon_0 r_{ij}}, \tag{4.5}$$

where q_i and q_j are the partial charges on atoms i and j, ϵ_0 is the dielectric constant in a vacuum and r_{ij} is the separation of the atoms i and j . The electrostatic properties of a molecule are a consequence of the distribution of the electrons and the nuclei and thus it is reasonable to assume that a set of partial charges could be obtained from quantum mechanical calculations. If sufficient point charges are used then all of the electric moments can be reproduced and the multipole interaction energy is exactly equal to that calculated from the Coulomb summation (equation 4.5).

An alternative to the point charge model is to assign dipoles to the bonds in the molecule. The electrostatic energy is then given as a sum of dipole-dipole interaction energies. This is the approach adopted in the MM(1-4) force fields, but can be inconvenient for molecules that have a formal charge and therefore require both charge-charge and charge-dipole terms in the energy expression.

An alternative approach to the calculation of electrostatic interactions is one which treats the molecule as a single entity. The *central multipole expansion*, and is based upon electric moments or *multipoles* (charge, dipole, quadrupole, etc), where each multipole can be represented by an appropriate distribution of charges. The main advantage of the multipole expansion is the efficiency of the calculation. Unfortunately, the multipole expansion is not applicable when molecules are separated by distances comparable to the molecular dimensions. Another problem with this method is that the multipole moments are properties of the entire molecule and so cannot be used to determine intra-molecular interactions. The multipole model tends to be restricted to calculations involving small molecules that are kept fixed in conformation during a calculation, and where the

interactions between molecules act at their centres of mass. For these reasons the point charge model is commonly used with charged species.

van der Waals interactions

The second component of the non-bonded interaction potential is the van der Waals term. A typical example of a van der Waals potential energy curve is shown in figure 4.4. The functional form of the curve is considered to arise due to a balance between the long range attractive forces and the short range repulsive forces. The attractive and repulsive interactions which occur between the atoms and the molecules can be obtained by fitting to experimental data or, in the case of small molecules, calculated using quantum mechanics. Such calculations are far from trivial, requiring electron correlation and large basis sets. In order to develop a successful force field, a means of accurately modelling the interatomic potential curve, using a simple empirical expression that can be calculated rapidly, is required. The need for the function to be evaluated rapidly is a consequence of the large number of van der Waals interactions that must be determined when modelling real molecular systems.

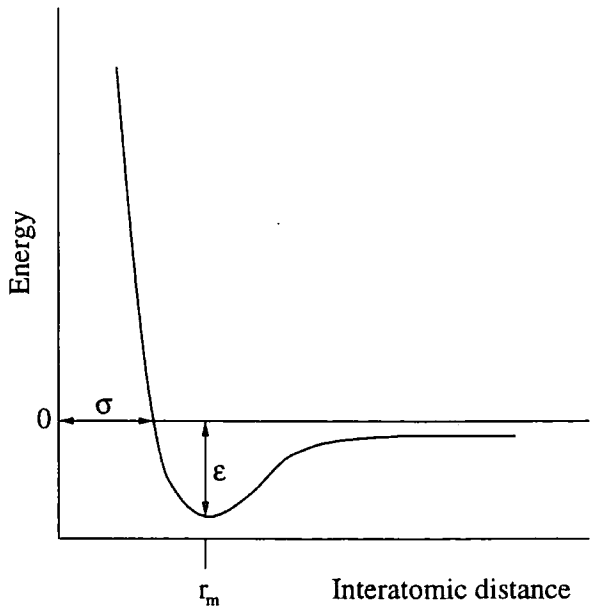

Figure 4.4: The Lennard-Jones potential.

Several different functional forms have been used to represent the van der

Waals interactions. The most popular, is the so called Lennard-Jones 12-6 potential, which takes the following form for the interaction between two sites,

$$E_{vdW}^{LJ} = 4\epsilon_{ij}\left[\left(\frac{\sigma_{ij}}{r_{ij}}\right)^{12} - \left(\frac{\sigma_{ij}}{r_{ij}}\right)^{6}\right]. \tag{4.6}$$

Here σ is the collision diameter (the separation for which the energy is zero) and ϵ is the well depth. These parameters are graphically illustrated in figure 4.4.

The Lennard-Jones equation may also be expressed in terms of the separation at which the energy passes through a minimum, r_m, where r_m=$2^{\frac{1}{6}}\sigma$. In this case the potential function is written as

$$E_{vdW}^{LJ} = \epsilon_{ij}\left[\left(\frac{r_m}{r_{ij}}\right)^{12} - 2\left(\frac{r_m}{r_{ij}}\right)^{6}\right], \tag{4.7}$$

or more commonly as

$$E_{vdW}^{LJ} = \left(\frac{A_{ij}}{r_{ij}^{12}}\right) - \left(\frac{C_{ij}}{r_{ij}^{6}}\right), \tag{4.8}$$

where $A_{ij} = 4\epsilon_{ij}\sigma_{ij}^{12}$ and $C_{ij} = 4\epsilon_{ij}\sigma_{ij}^{6}$

The Lennard-Jones 12-6 potential function is widely used, particularly for calculations on large systems where the r^{-12} term can be rapidly calculated by squaring the r^{-6} term. The r^{-6} term can also be calculated from the square of the distance without having to perform a computationally expensive square root calculation. Different powers (such as -9 or -10) have also been used for the repulsive (r^{-12}) part of the potential. These values, which produce a less steep curve are used in some force fields. Several formulations in which the repulsive term is replaced by a theoretically more realistic exponential term have also been proposed. These include the Buckingham potential, where A, B, and C are parameters which depend upon the types of atoms involved,

$$E_{vdW}^{Buckingham} = A\exp\left(\frac{B}{r_{ij}}\right) - \left(\frac{C}{r_{ij}{}^{6}}\right) \tag{4.9}$$

and the Hill potential [147],

$$E_{vdW}^{Hill} = -2.25\epsilon_{ij}\left(\frac{r_m}{r_{ij}}\right)^6 + 8.28 \times 10^5 \epsilon_{ij} \exp\left(\frac{-r_{ij}}{0.0736 r_m}\right) \tag{4.10}$$

The Hill potential (see chapter 3 section 3.3.2) was originally developed to enable the more realistic exponential term to be written in terms of Lennard-Jones parameters. The coefficients 2.25, 8.28×10^5 and 0.0736 were determined by fitting to data for the rare gases and were assumed to be applicable to other non polar gases.

When considering molecular systems, the non-bonded interaction energy depends not only upon the separation of the molecules but also on their relative orientations. It is usual to calculate the van der Waals interaction energy between two molecules using a site model in which the interaction is determined as the sum of the interactions between all pairs of sites on the molecules. Invariably, if the calculation of the van der Waals interactions is for a molecular system, then determination of the interaction parameters is extremely difficult and time consuming. It is, therefore, common in these cases to assume that the parameters for cross interactions can simply be obtained from the pure atom parameters using *mixing rules* [148].

The van der Waals and electrostatic interactions between atoms separated by three bonds (known as 1, 4 interactions) are often treated differently from other non-bonded interactions. This is because the interactions between such atoms contribute to the rotational barrier about the central bond. An empirical factor, f_{ij}, is often used to scale down the 1, 4 non-bonded interactions. This scaling factor is used for two main reasons. The first, is that the error associated with the use of an r^{12} repulsion term would be most significant for the 1, 4 atoms. The second reason is that when 1, 4 atoms come close together one sees a redistribution of the charges along the connecting bonds which would reduce the interaction. Such a redistribution would not be possible for two atoms which are the same distance apart but on different molecules.

4.3.5 Many body effects and effective pair potentials

The non-bonded interactions considered so far are calculated between pairs of interaction sites. The total non-bonded interaction energy is therefore determined

by adding together the interactions between all pairs of sites in the system (two body effects). The interaction between two molecules can however, be affected by the presence of a third (three body effects), fourth (four body effects) or more molecules. For very precise work, interactions involving more than three atoms may have to be taken into account, but they are usually small enough to be ignored. The computational effort is greatly increased if three body terms are included in the molecular model. Even with a simple pairwise model, the non-bonded interactions usually require by far the greatest amount of computational effort. The number of bond, angle and torsional terms increase approximately with N (the number of atoms in the system) but the number of non-bonded interactions increase with N^2. In general, there are N/3 times [31] more three body terms than two body terms and so it is clear why it is often considered preferable to avoid calculating them.

Fortunately, it is found that a significant proportion of the many body effects can be incorporated into a pairwise model if the latter is properly parameterized. The pair potentials most commonly used in molecular modelling are thus *effective* pairwise potentials; they do not represent the true interaction energy between two isolated particles, but are parameterized to include many body effects in the pairwise energy.

4.4 Force field parameterization

As already stated force fields contain a large number of parameters, even if they are intended for calculations on a relatively small set of molecules. Force field parameterization is therefore, a non trivial task, requiring a significant amount of effort in order to create an entirely new force field from scratch. Even the addition of a few parameters to an existing force field, in order to model a new class of molecules, is an extremely complicated and time consuming procedure. It is known, however, that the performance of a force field is often sensitive to just a few parameters and so it is sensible to spend time optimizing these parameters rather than changing the entire force field.

Molecular mechanics force fields may be used to determine a variety of structurally related properties. The initial step to parameterisation is to select the

data that is going to be used to guide this process. For example, bond lengths are determined from crystal structural data, whereas, non-bonded parameters are better derived by fitting to experimental thermodynamic data. In many cases, experimental data may be non existent or extremely difficult to obtain for a particular class of compounds. In such cases, quantum mechanical calculations are becoming increasingly popular. This is an important development because it greatly extends the range of chemical systems that can be investigated using the force field approach. Quantum mechanical calculations can be carried out on small representative systems in order to produce force field data. Clearly, a force field derived in such a way needs to be carefully validated by testing against real experimental data.

Once a functional form for the force field has been chosen and the parameterization data identified there are two basic methods that can be employed to obtain the potential parameters. The first method is simply *trial and error.* This method requires a gradual refinement of the force field parameters in order to achieve the best possible fit to experimental data. It is difficult to simultaneously modify a large number of parameters, so it usual to perform the parameterization in a series of steps. It is important to note that there is some coupling between all the degrees of freedom and so for much of the work none of the parameters can truly be taken in isolation. However, for some degrees of freedom the extent of the coupling is far more crucial to the parameterization process than for others. For example, parameters defining bond and angle parameters can often be treated separately from the other parameters and are therefore, easily transferred from one force field to another without any modification. By contrast, torsional and non-bonded interactions are extremely closely coupled and therefore have significant influence on each other. In such cases, it is normal to first determine the non-bonded interactions and then calculate the torsional potentials. Experimental data is often non existent for torsional angles, and so, it is common to use quantum mechanical calculations in order to determine the torsional potentials. The torsional potentials are then fitted to reproduce the energy curve obtained from the quantum mechanical calculations, in conjunction with the non-bonded parameters. Of course, it may be necessary at any stage to modify any of the parameters if the results are inadequate and so parameterization is invariably an

iterative process.

An alternative approach to parameterization is to use a *least squares fitting procedure.* This determines a set of parameters that give optimal fits to experimental data. Thermodynamic data, equilibrium conformations and vibrational frequencies are commonly used as the source of experimental data. The *error* for a given set of parameters equals the sum of squares of the differences between the observed and calculated values for the set of properties. The objective is to change the force field parameters to minimize the *error.* This is done by assuming that the properties can be related to a force field by a Taylor expansion. An iterative procedure is then used to minimize the sum of the squares of the differences.

4.5 A brief history of force fields

Over the years considerable work has been undertaken in order to develop new potentials that accurately model *real* systems. Force fields developed in this area are naturally divided into two main classes: united atom and all atom force fields. In the former, hydrogens attached to heavy atoms are removed and replaced by a single *united* atom potential. Such, united atom sites have the advantage of greatly reducing the the number of interaction sites in the molecule, but in certain cases seriously limit the accuracy of the force field. In the latter case, each atom is represented explicity by a potential energy function, which increases the accuracy of the force field but in turn also increases the computational expense.

In the early days molecular modelling was influenced strongly by the desire to model biological systems. Consequently, much of the initial work was centred around developing accurate parameters for biomolecules, particularly peptides and nuclei acids. The outcome of this work, was the development of force fields such as, CHARMM [55, 56] and AMBER [57–60]. These force fields have now been extended to contain many new parameters which cover a wider range of organic molecules. This is particularly true of the AMBER [61] all atom force field.

A different strand of force field development stems from the work of Allinger and co-workers with their development of the MM1 [73], and MM2 [74] force

fields. These have now been largely superseded by the newer MM3 [75], and most recently MM4 [149–152] force fields. The potential parameters employed in these MM force fields have been developed over many years, with their emphasis being on the prediction of structural and conformational energies of small isolated organic molecules. These force fields are now extremely accurate in predicting molecular structures in the gas phase. However, their main draw back is that they are extremely complicated in terms of the number functions that are used for individual molecules.

Recent years have also seen the development of Jorgensen's OPLS (Optimised Potentials for liquid simulations) united atom and all atom force fields [67–70, 153]. These force fields are different from all the others in that they have been specifically designed to improve the intermolecular non-bonded potential energy functions. The Lennard-Jones potentials are not based on crystal data, like many of their predecessors, but on accurate predictions of thermodynamic properties of liquids. Jorgensen's approach to developing accurate non-bonded parameters has involved numerous liquid simulations, in order to fit the intermolecular potential energy functions to thermodynamic and structural data. The principle points for comparison with experiment are the liquid phase densities and heats of vapourisation. Due to the accuracy of the non-bonded potentials in the OPLS-AA force field it is becoming the most widely used force field in atomistic simulations at the present time, and with its continued development it is likely to become even more popular in the future.

None of the force fields, to date,have been designed specifically to model mesogenic molecules. This is partly because liquid crystal molecules are not confined to any particular class of compound. They contain readily identifiable subunits that occur in a wide range of systems, from simple organic molecules to polymers. In view of this, it has only been possible, to date, to represent accurately simple liquid crystal molecules containing common structural features, such as alkyl chains and saturated ring structures. Force field calculations involving functional groups such as, -N=N-, F, CN, -O-C=O, which are also common to liquid crystals, yield less accurate structures and energies. The reason for this is that these functional groups are not represented in the force field control set.

4.6 Development of a force field for liquid crystals (LCFF)

A number of elements must come into consideration when choosing a functional form for a liquid crystal force field. The most accurate single molecule force fields to date are the MM4 [149–152] and the Merck Molecular Force Field (MMFF94) [62–66]. The main difference between these two force fields and the AMBER force field is in the number and type of terms used to describe the intramolecular degrees of freedom. The MM4 and MMFF94 use more sophisticated potentials with many more terms (including cross-terms such as bend-stretch interactions) whereas AMBER employs the simple harmonic potential functions (as described in sections 4.3.1 and 4.3.2). The AMBER approach, which uses an harmonic force field, was followed in the work described in this thesis. In simulating bulk phases it is rarely necessary to describe bond lengths or angles to the same degree of accuracy as is required in predicting the minimum energy of a molecule in the gas phase. Indeed it is often useful to fix the bond lengths (as discussed in section 4.3.1) using the SHAKE algorithm [85] in order to increase the time-step within a molecular dynamics simulation. The main problem in simulating mesogens arises in determining good torsional potentials (see section 4.3.3). Rotation about a chemical bond requires a relatively small change to the internal energy, but can lead to a large change in structure for rod-shaped molecules. Consequently, the internal rotations are strongly coupled to the molecular packing in a fluid [127,133] and hence have a major influence on the transition temperatures.

Both the MM4 and the MMFF94 force fields use an exponential form to model the repulsive part of the non-bonded van der Waals interactions. While this is certainly more accurate than a $1/r^{12}$ form, at short intermolecular separations, it is extremely expensive for bulk simulations of mesogens where thousands of non-bonded interactions must be computed in a single molecular dynamics step or in a Monte Carlo trial move. Consequently, in this current investigation the OPLS and AMBER force fields have been utilized and a Lennard-Jones 12:6 form has been adopted to describe the non-bonded van der Waals parameters. At the temperature and pressure ranges normally associated with liquid crystal mesophases (250-450 K, 1 atmosphere) one would expect the sampling of the high

energy region of the repulsive part of the potential to be a relatively rare event. Moreover, in fluid states of matter, groups are constantly in motion, so modelling the closest approach of atoms to the highest level of accuracy is less important than it would be in a crystal. Consequently, the choice of a $1/r^{12}$ repulsive term is the optimum one for liquid crystal work. The importance of using *effective two-body potentials* to describe the non-bonded interactions is also noted. For reasons of computational expense, the use of *three body potentials* for mesogen simulation is currently out of the question. However, in a normal fluid a sizeable contribution to the non-bonded interactions arises from the *three body* terms. For practical purposes these contributions must currently be consumed into the *two body terms.* Consequently, the best *effective two body potentials* are those that arise from fitting to the thermodynamic properties of real liquids, rather than those found by fitting to pair-interaction structures/energies in the gas phase. Jorgensen has taken this approach in designing the OPLS force field, relying on Monte Carlo simulations of small molecules to allow fitting to liquid state properties to obtain the *two body* potentials. A recent comparison of MMFF94 and OPLS-AA [154] in simulating liquid butane, methanol, and N-methylacetamide testifies to the usefulness of this approach.

The final key consideration in designing a LCFF is the choice of either an *all atom* or a *united atom* form. The latter replaces hydrogens on attached carbons by a single *united atom* potential. This is advantageous with respect to savings in computer time and has been used in most previous liquid crystalline simulations [136]. However, recent work on PCH5, described in chapter 5 of this thesis [155], indicates that hydrogens attached to carbons in a phenyl ring fulfill a vital role. Inclusion of partial charges on both the hydrogens and the carbons in an aromatic ring allows the ring quadrupole to be mimicked; quadrupolar interactions have a significant influence on short range packing of mesogenic molecules [156]. The hydrogen atoms are included explicitly in this liquid crystal force field, as the aim of this work is to study the dipole correlation in me5NF and GGP5Cl, both of which have aromatic rings as shown in figure 4.5. Garcia *et al* [157] have recently described a hybrid force field for a group of liquid crystal molecules where phenyl hydrogens are included explicitly but aliphatic hydrogens are excluded. Their approach seems a useful compromise, between keeping vital interactions

and minimizing computer time.

Considering all the principles described above we write the functional form of the liquid crystal force field (LCFF) in the AMBER/OPLS form

$$E_{total} = \sum_{\text{angle}} K_\theta(\theta - \theta_{eq})^2 + \sum_{\text{dihedral}} \left(\sum_{m=1}^{6} \frac{V_m}{2} [1 + cos(m\phi)] \right) + \sum_{\text{non-bonded}} \sum_{i<j} \left(\frac{q_i q_j}{4\pi\epsilon_0 r_{ij}} + \frac{A_{ij}}{r_{ij}^{12}} - \frac{C_{ij}}{r_{ij}^{6}} \right) f_{ij}, \quad (4.11)$$

where K_θ and V_m are force constants representing angle bending and torsional motion respectively; the non-bonded energy between atoms i and j at a distance r_{ij} is represented by a Coulomb plus a Lennard-Jones potential, where A_{ij} and C_{ij} can be expressed in terms of the well depth and collision parameters, ϵ_{ij} and σ_{ij} respectively: $A_{ij} = 4\epsilon_{ij}\sigma_{ij}^{12}$, $C_{ij} = 4\epsilon_{ij}\sigma_{ij}^{6}$. ($f_{ij} = 0.5$ for 1, 4 12:6 non-bonded terms, $f_{ij} = 0.125$ for 1, 4 electrostatic terms and $f_{ij} = 1$ for all other non-bonded interactions.)

4.7 Determination of the force field parameters

Many scientists have spent their entire life dedicated to the study of force field development. This has usually proved to be an extremely difficult and time consuming process. Therefore, in this work the well known AMBER and OPLS-AA (all-atom) force fields [69, 158, 159], have been adapted and modified for the typical liquid crystal mesogens me5NF and GGP5Cl (figure 4.5).
Between them, these two molecules contain common structural features that are present in many liquid crystal mesogens: conjugated phenyl rings, lateral fluorination, ester group, alkyl chains, terminal dipolar groups (chloro and cyano groups).

Ultimately, the aim of this liquid crystal force field is to accurately treat both the intermolecular and intra-molecular non-bonded interactions as well as intra-molecular bond stretches, angle bends, and dihedral angles. The latter two components were the most difficult to determine for the mesogens me5NF and GGP5Cl, and therefore, were the main focus of the parameterization process.

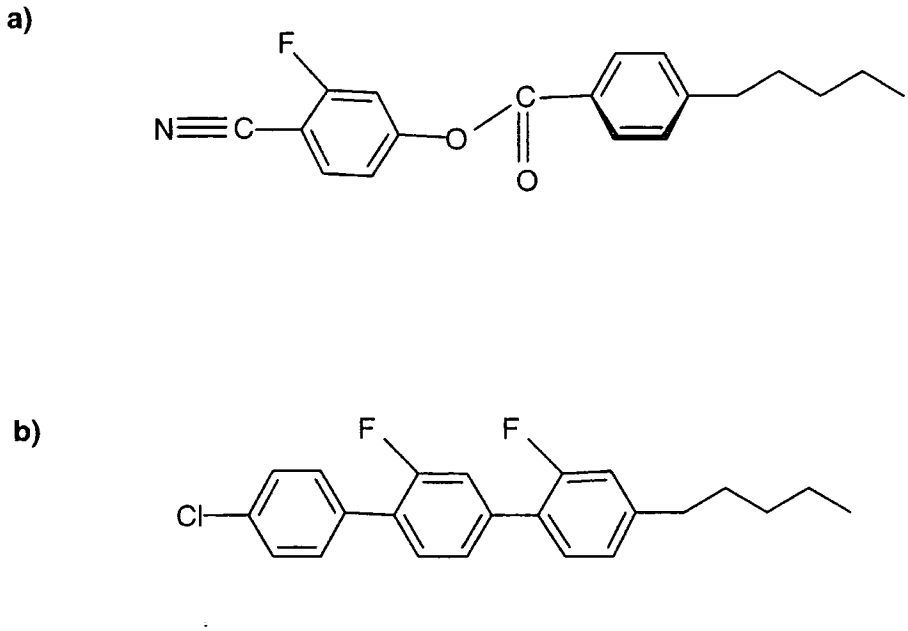

Figure 4.5: Structures of a) me5NF and b) GGP5Cl.

In order to parameterize any unknown bond angle and torsional parameters one needs to optimize them against some kind of data that represents *reality*. Experimentally determined molecular geometries, which can be obtained from microwave, NMR, or X-ray diffraction techniques can be used as a source of such data. However, experimental data depends upon the molecular environment within the material. Thus, the equilibrium geometries of a molecule in a crystal, solution or gas phase will be different from each other. So, in order to obtain molecular parameters that are independent of the medium, gas phase experiments or *ab initio* calculations must be employed. In this work the latter method was chosen to produce *reality* data.

4.7.1 Atom types

The basis of a force field is the choice of atom types. An atom type is a selection of atoms that are similar enough, both chemically and physically, to be treated identically in a molecular mechanics calculation. The molecules me5NF and GGP5Cl require 10 different atom types, which are described in table 4.1.

Atom	mass/ amu	Type
C	12.01	C in carbonyl carbon
CA	12.01	C in Benzene
CT	12.01	C alkanes
CZ	12.01	C in cyano
F	19.00	Fluorine
HA	1.008	H in Benzene
HC	1.008	H alkanes
NZ	14.01	N in cyano
O	16.00	O in carbonyl
OS	16.00	O in ester

Table 4.1: Atom Types used in LCFF for me5NF and GGP5Cl.

4.7.2 Bond stretching and angle bending parameters

Suitable values for all the reference bond length parameters, r_0 and the force constants, K_r were taken from the AMBER/OPLS force fields along with the majority of the bond angle parameters, θ_0 and K_θ (see table 4.4 and table 4.5). Good force field data was unavailable for the ester group in me5NF. Consequently, a full *ab initio* energy minimization calculation for the mesogenic fragment phenyl benzoate was initially carried out using Gaussian94 [160] (figure 4.6). The use of the small phenyl benzoate fragment instead of the mesogen me5NF is purely because, at the present time, good quality *ab initio* calculations can only be performed for fairly small molecules (approximately 15 heavy atoms) on a personal workstation.

Finally, bond angle distortions from the equilibrium geometry were determined, using *ab initio* calculations, in order to determine the harmonic force constants, K_θ, for the angles θ_1-θ_4 shown in figure 4.6. The results for the *ab initio* angles and force constants are given in table 4.2. Included in this table are the single crystal X-ray diffraction data for this molecule [161] together with the parameter values used in three other force fields. The results for the *ab initio* angles are in good agreement with the X-ray diffraction data. The *ab initio* force constants are in good agreement with the values used in the MM3 and MMFF94

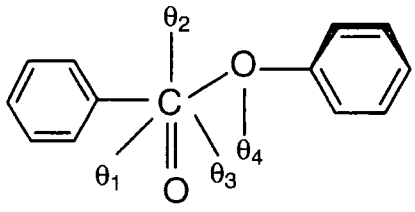

Figure 4.6: Structure of the molecule phenyl benzoate which is used to calculate the bond angles θ_1, θ_2, θ_3, and θ_4.

No	crystal	*ab initio*		MM3		MMFF94		OPLS-AA	
	θ /^{o}	θ /^{o}	K_θ	θ /^{o}	K_θ	θ /^{o}	K_θ	θ /^{o}	K_θ
1	126.0	125.4	334.72	124.5	301.00	120.0	439.46	120.4	334.72
2	110.9	111.4	338.90	110.1	391.30	102.8	487.62	111.4	338.90
3	118.2	118.1	345.60	111.8	463.54	95.3	367.22	no data	
4	123.1	123.0	347.27	122.0	481.60	124.4	698.31	123.4	347.27

† force constants, K_θ, in kJ mol^{-1} rad^{-2}

Table 4.2: Comparison of angle parameters for an ester group†.

force fields, although it should be stressed that these force fields also use higher order terms to describe deviations from harmonicity.

4.7.3 Torsional parameters

Torsional parameters are the most critical geometrical characteristic for flexible liquid crystal molecules, as changes in dihedral angles profoundly affect the average molecular shape. Some dihedral angle data for the mesogens me5NF and GGP5Cl is already available from the AMBER all-atom force field. The exception to this is the three dihedral angles in the linking ester group of me5NF and two inter-ring dihedrals for GGP5Cl. In order to determine the unknown parameters for these five dihedral angles ($\phi_1 - \phi_5$), restricted Hartree-Fock calculations at the RHF/6-31G* level were performed on the smaller mesogenic fragments, methyl benzoate, phenyl benzoate, phenyl acetate, 2-fluorobiphenyl and 2,2'-difluorobiphenyl shown in figure 4.7.

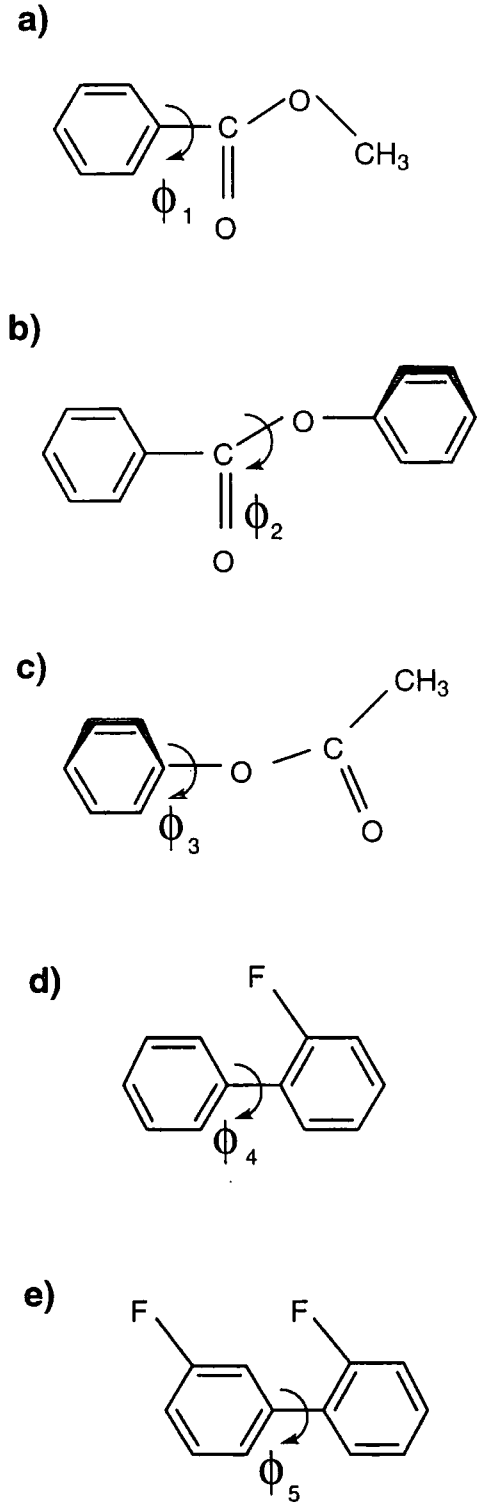

Figure 4.7: Structure of a) methyl benzoate ϕ_1, b) phenyl benzoate ϕ_2, c) phenyl acetate ϕ_3, d) 2-fluorobiphenyl ϕ_4 and e) 2,2'-difluorobiphenyl ϕ_5.

Fitting the torsional parameters

Using quantum mechanical data to obtain a set of torsional coefficients $\{V_i\}$ for each ϕ requires careful fitting. To do this a least squares fit to the *ab initio* data was carried out using the full molecular force field, with the set of torsional coefficients $\{V_i\}$ used as variable parameters in the fit. At each step in the least squares minimization the following procedure was used:

i) start with the initial (approximate) values for $\{V_i\}$,
ii) minimize the energy of the molecule in the force field for a set of values of the dihedral angle ϕ (with ϕ constrained at each point),
iii) calculate the sum of the squares of the differences between the *ab initio* data and the data obtained from the energy minimizations.

In practice this procedure requires thousands of separate energy minimization calculations to obtained converged values for $\{V_i\}$. However, it does ensure that all other force field contributions to the torsional angle energy (including the important contributions from non-bonded interactions) are taken properly into account in the fitting of $\{V_i\}$. All energy and least squares minimizations used Powell minimization routines [162], and the final root mean square errors between fitted and *ab initio* data points were 0.47, 0.48, 1.37, 0.83 and 0.96 kJ mol^{-1} for ϕ_1-ϕ_5 respectively.

Results from the fitting procedure are shown in figures 4.8 and 4.9 for the individual groups in the mesogens me5NF and GGP5Cl respectively. The dihedral angle energy profiles for ϕ_1 and ϕ_3 in the molecule me5NF are symmetrical about 180° and were straight forward to fit requiring only a single V_2 term in the Fourier expansion of equation 4.4. The minimum in the potential energy occurs at different dihedral angles: 180° (and 0°) for ϕ_1 and 90° for ϕ_3. This is in fairly good agreement with the X-ray single crystal structures for this molecule which gives ϕ_1 at 171.32° and ϕ_3 at 116.7°. However, it should be stressed that when the barriers to rotation are small, gas phase energy minima for the dihedral angles often change slightly in the crystal in order to accommodate packing constraints. The barriers to rotation are given in table 4.3. For comparison the

trans-gauche conversion barriers in an alkyl chain are approximately 13.6 kJ /mol for a typical liquid crystal in the gas phase; this is calculated from plane-wave GGA DFT [27]. For ϕ_1, at room temperature ($RT \approx 2.5$ kJ/mol at 298 K) a severely restricted rotation between two equally populated states is expected but almost free rotation for ϕ_3. The *ab initio* calculations for ϕ_2 (in phenyl benzoate) were significantly more expensive than for ϕ_1 and ϕ_3, as more than one Fourier coefficient was required. Therefore, the fitting of ϕ_2 could only take place once values of $E(\phi_1)$ and $E(\phi_3)$ had been obtained. A good fit, with V_1, V_2 and V_3 terms is obtained. However it is noted that the barrier to rotation about ϕ_2 is extremely high (table 4.3) and that most of this contribution arises from the steric repulsions between the two phenyl groups. Finally, it should be noted that the phenyl-ester-phenyl structure in phenyl benzoate is easy to prepare synthetically and so is commonly used as a linking group in calamitic liquid crystals. It is often assumed to be coplanar in its minimum energy conformation. This is not the case in the crystal structure or in this work. However, the coplanar configuration is only 4.6 kJ/mol higher in energy than the minimum energy configuration and so is easily accessible. The effective torsional barrier measured in a liquid crystal phase will always contain a contribution that arises from the preferred packing arrangement of molecules in the bulk. Depending on the phase, this has been seen to influence conformational energies by 2-3 kJ/mol [133]. ϕ_4 was fitted with three Fourier terms V_1, V_2 and V_3, but the torsional angle ϕ_5 required a minimum of five Fourier coefficients V_1, V_2, V_3, V_4, and V_6 for the same quality of fit.

dihedral angle	*ab initio* energy barriers	LCFF energy barriers	MM3 energy barriers
ϕ_1	31.76	32.76	106.10
ϕ_2	49.66	50.17	68.90
ϕ_3	4.56	4.31	8.40
ϕ_4	14.21, 5.89	15.05, 6.09	37.00, 1.20
ϕ_5	18.88, 5.56	19.36, 5.71	37.00, 0.80

Table 4.3: Comparison of *ab initio* and LCFF torsional energy barriers. Values given are in kJ mol^{-1}.

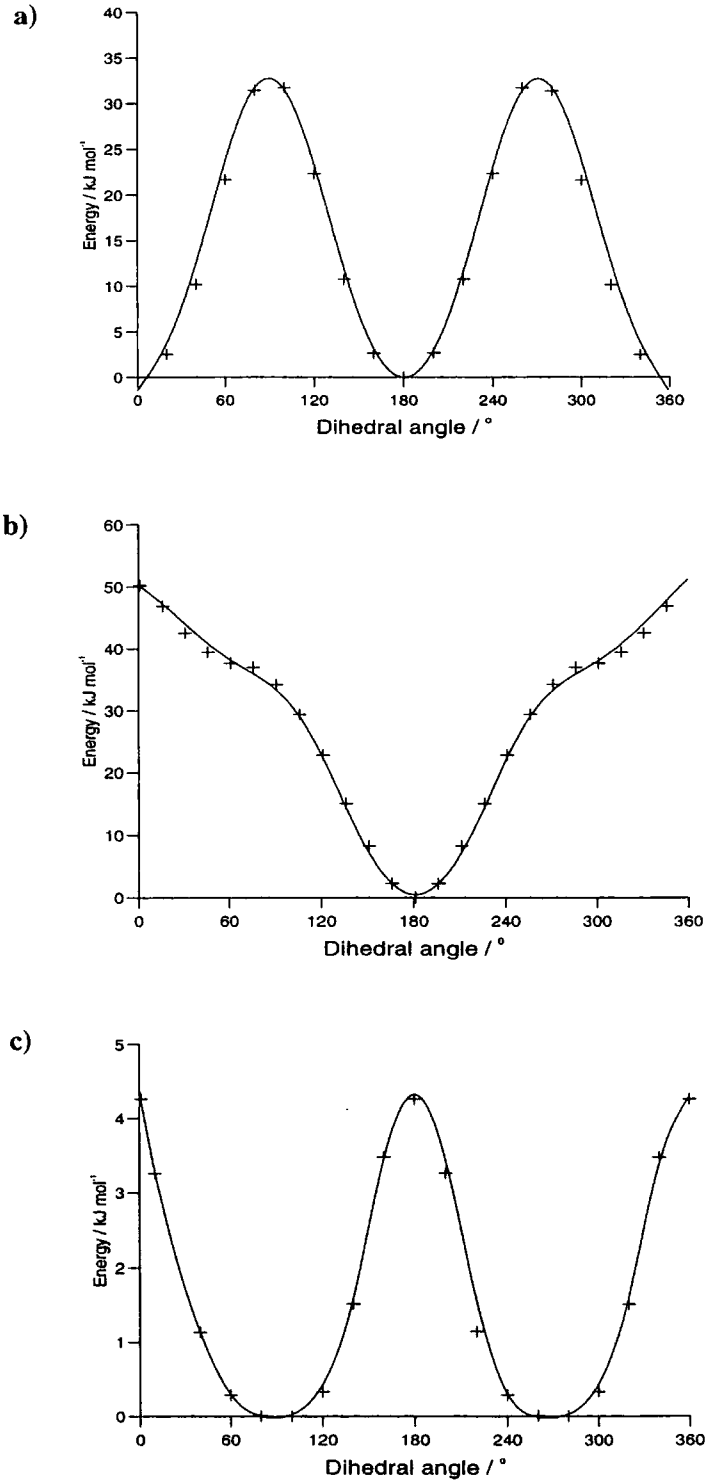

Figure 4.8: Graphs showing the *ab initio* (+ + +) and fitted data (—) for the torsional angles, a) ϕ_1, b) ϕ_2, and c) ϕ_3, defined in figure 4.7.

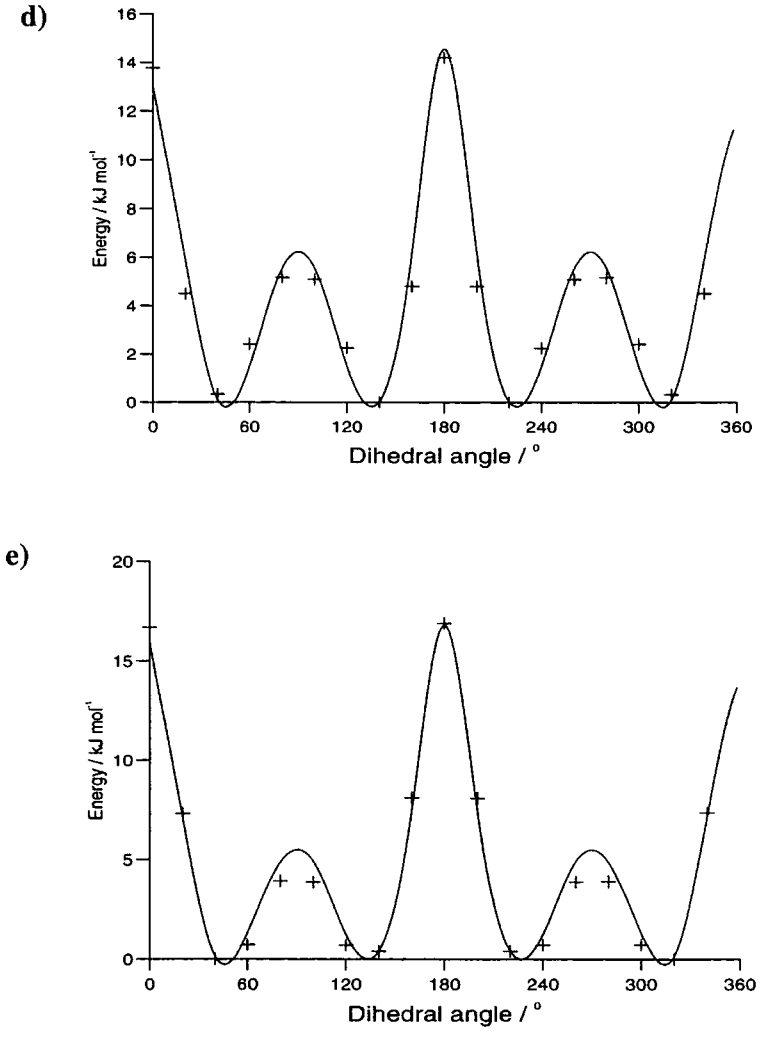

Figure 4.9: Graphs showing the *ab initio* (+ + +) and fitted data (—) for the torsional angles a) ϕ_4, and b) ϕ_5 defined in figure 4.7.

The values of the Fourier coefficients obtained for each dihedral are given in table 4.6 and comparison between *ab initio* and LCFF energy barriers are given in table 4.3[1]. Included in table 4.3 are the molecular mechanics dihedral barrier results using the augmented form of the MM3 force field available in the

[1]Since this work was carried out, there has been some dynamic NMR spectroscopy work published (in June 2000) for the *free energy barrier* of methyl benzoate [163]. The results obtained indicate that the barrier to rotation is 4.92 ± 0.2 kcal mol^{-1}, which is considerably lower than the value calculated in this work. They also carried out *ab initio* calculations using an improved basis set of MP2/6-31G*. The results from this calculation produced a value of 6.94 kcal mol^{-1} which overestimates the experimental rotational barrier.

CACHe modelling suite [119] to calculate energy barriers. The MM3/CACHe results consistently over-estimate the *ab initio* energy barriers. In some cases, for example, ϕ_1 and ϕ_2, the MM3/CACHe results are extremely poor. While the energy barriers may not be significant for minimum energy configurations, they are of major importance in a molecular dynamics calculation.

4.7.4 Non-bonded parameters

Both the van der Waal parameters and the electrostatic non-bonded parameters were adopted from the OPLS-AA all-atom force field of Jorgensen and co-workers [69,158,159]. The non-bonded parameters in the OPLS-AA force field have been optimized to reproduce the correct densities and heats of vaporization for a series of small organic molecules.

It is important to note that the functional form of the bond stretching, angle bending and the torsional potential terms have been adopted from the AMBER force field, whilst, the non-bonded interactions have been derived from OPLS-AA force field. Therefore, the 1, 4 non-bonded interactions need to be scaled appropriately. Merger of the OPLS-AA non-bonded potential functions and the intra-molecular AMBER force field parameters has already been considered [69, 71]. The convention used in these references is followed in this work; the 1-4 Lennard-Jones interactions are scaled by a factor of 2 (compared to intermolecular interactions) and electrostatic interactions are scaled by a factor of 8. A summary of all the non-bonded parameters used in this current work are presented in table 4.7. It is interesting to note that the partial charges in table 4.7 are significantly higher than those obtained from *ab initio* molecular orbital calculations using Mullikan charge distributions. The latter gave inadequate results when used to verify properties of pure liquids, and are unable to properly represent the molecular quadrupole that arises from charge separation in the phenyl ring.

4.8 The complete LCFF for me5NF and GGP5Cl

The following section presents the complete set of potential energy parameters employed in the LCFF in order to successfully model the mesogens me5NF and GGP5Cl.

Bond parameters

bond	bond length/Å
C - CA	1.490
C - O	1.229
CA - OS	1.364
C - OS	1.327
CA - CA	1.400
CA - CT	1.510
CA - NZ	1.261
CA - CZ	1.451
CZ - NZ	1.157
CT - CT	1.529
CT - HC	1.090
CA - F	1.354
CA - HA	1.080
CA - O	1.380
CT - OS	1.410
C - CT	1.522

Table 4.4: Bond Parameters.

Angle parameters

Angle	K_θ /kJ mol^{-1} rad^{-2}	Angle /^{o}
CA - CA - CZ	292.880	120.0
CA - CZ - NZ	711.280	180.0
CA - CA - OS	292.880	120.0
CA - CA - F	334.720	113.0
C - CA - CA	355.640	120.0
C - CA - HA	146.440	120.0
CA - CA - CA	263.590	120.0
CA - CA - CT	292.880	120.0
CA - CA - HA	146.440	120.0
CA - CT - CT	263.590	114.0
CA - CT - HC	146.440	109.5
CT - CT - CT	244.350	112.7
CT - CT - HC	156.900	110.7
HC - CT - HC	138.070	107.8
OS - C - CA	338.900	111.4
C - OS - CT	347.270	116.9
HC - CT - OS	146.440	109.5
CT - C - O	334.720	120.4
C - CT - HC	146.440	109.5
OS - C - CT	338.900	111.4
O - C - CA	334.720	125.4
CA - OS - C	345.600	118.1
O - C - OS	347.270	123.4

Table 4.5: Angle Parameters.

Torsional parameters

dihedral angle	V_1	V_2	V_3	V_4	V_6
HC - CT - CT - HC	0.000	0.000	1.331	0.000	0.000
HC - CT - CT - CT	0.000	0.000	1.531	0.000	0.000
CT - CT - CT - CT	7.280	-0.657	1.167	0.000	0.000
HC - CT - CA - CA	0.000	0.000	0.000	0.000	0.000
CT - CT - CA - CA	0.000	0.000	0.000	0.000	0.000
HC - CT - CT - CA	0.000	0.000	1.933	0.000	0.000
CA - CA - CA - CA	0.000	39.748	0.000	0.000	0.000
CA - CA - CA - HA	0.000	39.748	0.000	0.000	0.000
HA - CA - CA - HA	0.000	39.748	0.000	0.000	0.000
OS - C - CA - CA	0.000	11.171	0.000	0.000	0.000
CA - C - OS - CA	10.862	17.016	0.916	0.000	0.000
O - C - OS - CA	10.862	17.016	0.916	0.000	0.000
C - OS - CA - CA	0.000	7.950	0.000	0.000	0.000
O - C - CA - CA	0.0 00	8.996	0.000	0.000	0.000
CA - CA - CA - CA(F)	-0.142	6.284	-0.201	0.000	0.000
CA(F) - CA - CA - CA(F)	0.791	9.305	0.000	4.322	2.594

Table 4.6: Torsional Parameters in kJ mol^{-1}.

Non-bonded parameters

atom	charge/e^{-1}	σ/Å	ϵ /kJ mol^{-1}
CT	-0.000	3.500	0.276
HC	0.060	2.500	0.126
CA	-0.115	3.550	0.293
HA	0.115	2.420	0.126
F	-0.246	2.940	0.255
CZ	0.395	3.650	0.628
NZ	-0.430	3.200	0.711
C	0.700	3.750	0.439
O	-0.800	2.960	0.879
OS	-0.400	3.000	0.711

Table 4.7: Non-bonded Parameters.

4.9 Testing the LCFF force field

4.9.1 Methodology

The LCFF was developed and tested by computing the structures and thermodynamic properties of the fragment molecules phenyl acetate, methyl benzoate, and the mesogens me5NF and GGP5Cl. In each case an initial molecular configuration was generated from a *bcc* lattice in which 216 molecules were given a small random displacement from their lattice positions and randomly orientated inside a cuboidal simulation box at gas phase densities. Initially, the isothermal-isobaric algorithm of Berendsen was employed to relax the molecular configuration. A nominal pressure of 10^5 Pa was used until the desired density of approximately 1 g cm^{-3} was achieved. Thereafter the system was equilibrated using a Nosé-Hoover thermostat and a Hoover barostat at a pressure of 1 atmosphere, employing relaxation times of 1 ps and 4 ps respectively. The simulations retained cubic periodic boundary conditions throughout, and employed the leap frog algorithm with a time-step of 2 fs and made use of the SHAKE procedure to constrain bond

lengths. However, other than this the molecules were treated as fully flexible, allowing for angle bending and dihedral angle changes. The *long-range* electrostatic interactions were handled by a Ewald sum with the convergence parameter α set at 0.48 $Å^{-1}$ and 6 k-vectors were used for each of the directions (x,y,z) in the periodic box. A cut-off of 9 Å was used for the *short range* 12:6 interactions. All calculations used the molecular dynamics package DL_POLY_2.11 [164]. A typical run consisted of a equilibration period of (in total) 1000 ps, followed by a production run of 500 ps.

The heats of vaporization for the molecules phenyl acetate and methyl benzoate were computed using gas phase Monte Carlo simulations at 298 K. Molecular dynamics simulations can be quite problematic for isolated molecules; poor sampling of configurational space often arises when molecules get stuck in particular vibrational modes, and there are no molecular collisions to allow molecules to exchange energy and transverse torsional energy barriers. The gas phase Monte Carlo simulations were performed using the program DUMMP (Durham University Molecular Modelling Package), these provide excellent sampling of configurational space for isolated molecules. Typical run lengths consisted of 1×10^6 attempted Monte Carlo moves for equilibration and 2×10^6 attempted Monte Carlo moves to calculate thermodynamic averages.

4.9.2 Computational results

The simulation runs for the molecules phenyl acetate, methyl benzoate, me5NF and GGP5Cl yielded key thermodynamic properties such as the heat of vaporization $\Delta_{vap}H$, and the densities $\langle\rho\rangle$ [69, 72]. Values of the mean density $\langle\rho\rangle$ at equilibrium are given in table 4.8. $\langle\rho\rangle$ values are in excellent agreement with experiment (better than 1%) for the three systems with available experimental data at the corresponding simulation temperatures. For GGP5Cl experimental density data is not available in the isotropic phase. However, a value of $\rho = 1.158$ g cm^{-3} is available in the nematic phase at 338 K. This temperature is 55 K below the simulation temperature used in this study and so the computed density for GGP5Cl is in the range that one would predict based on typical density changes across the nematic/isotropic temperature range. Small errors in Lennard-Jones

ϵ or σ parameters can lead to large variations in the density, so the results obtained give a high degree of confidence in the non-bonded parameters employed in the force field. Moreover, significant deviations from the correct liquid state torsional potentials influence the local packing arrangements of the molecules, again leading to poor predictions for the density.

liquid	T / K	$\langle\rho\rangle$/gcm^{-3}	ρ (exp)/gcm^{-3}
me5NF	303	1.1126	1.1300
GGP5Cl	393	1.0680	1.1580 (338 K)
phenyl acetate	298	1.0818	1.0780
methyl benzoate	298	1.0911	1.0838

Table 4.8: Computed densities from simulations of me5NF, GGP5Cl, phenyl acetate and methyl benzoate.

Following Jorgensen and co-workers [153], the heat of vaporization has been calculated from the following equations,

$$\Delta_{\text{vap}}H = H_{\text{gas}} - H_{\text{liquid}} \tag{4.12}$$

where,

$$H_{\text{gas}} = E_{\text{intra}} + pV \tag{4.13}$$

and,

$$H_{\text{liquid}} = E_{\text{intra}} + E_{\text{inter}} + pV. \tag{4.14}$$

Assuming ideality, the pV term for the gas phase is equal to RT, and the pV term in the liquid is negligible. Therefore, equation 4.12 becomes,

$$\Delta_{\text{vap}}H = E_{\text{intra}}(g) - (E_{\text{intra}}(l) + E_{\text{inter}}(l)) + RT(g). \tag{4.15}$$

$E_{\text{intra}}(g)$ is obtained from the gas phase Monte Carlo simulations and $E_{\text{intra}}(l) + E_{\text{inter}}(l)$ is the total potential energy of the liquid, obtained from the liquid phase

molecular dynamics simulations. The results for the molecules butane, benzene, phenyl acetate and methyl benzoate are listed in table 4.9 along with the experimental data for these molecules[2]. There is excellent agreement between experimental and calculated values, which again points to an accurate representation of the non-bonded interactions.

liquid	T / K	$E_{intra+inter}(l)$	$E_{intra}(g)$	$\Delta_{vap}H$	$\Delta_{vap}H$ (exp)
butane	298	-2.070	7.110	5.590*	5.350†
benzene	298	-8.330	0.000	7.768*	8.090††
phenyl acetate	298	3.420	13.430	10.600	10.320†††
methyl benzoate	298	-26.060	-13.350	13.310	13.200††††

* For comparison, values of 5.44 kcal mol^{-1} and 8.05 kcal mol^{-1} were calculated for butane and benzene respectively by Jorgensen using a MC technique [69,165]. † ref [69], †† ref [165], ††† ref [166], †††† ref [167].

Table 4.9: Heats of Vapourisation in kcal mol^{-1}.

4.10 Conclusions

Accurate representation of conformational energy profiles is necessary for good quality atomistic simulations of liquid crystal molecules. Most experience to date indicates that commercial force fields cannot be trusted for this purpose. Reliable predictions using molecular simulations are only possible if reliable force fields are employed. This is especially true in atomistic simulations of fully flexible mesogens, where the molecular properties reflect a subtle interplay of intermolecular and intra-molecular forces.

This current study describes preliminary work in the development and testing of a new force field designed specifically for liquid crystal molecules. So far a set of force field parameters for the mesogens me5NF and GGP5Cl have been developed, however, these molecules contain many of the key structural elements found in many calamitic liquid crystals: conjugated phenyl rings, lateral fluorination,

[2]butane and benzene were chosen to check the reliability of the method used to calculate the heats of vapourisation

an ester group, alkyl chains, terminal chloro and cyano groups. The liquid crystal force field builds upon the existing all-atom AMBER and OPLS force fields, with new angle and torsional energy parameters derived from fitting to *ab initio* RHF/6-31G* molecular orbital calculations. The force fields have been tested on liquid state simulations of the molecules phenyl acetate and methyl benzoate and the mesogens me5NF and GGP5Cl. Good agreement is found between the simulation and experimental results for densities and heats of vaporization. The availability of more structural and thermodynamic data for liquid crystal molecules, coupled with the considerable increase in computer power, will undoubtedly see the continued evolution of new force fields with added complexity and greater accuracy.

CHAPTER

5

Calculation of the Kirkwood correlation factor, g_1

5.1 Introduction

The Kirkwood-Frohlich equation [168]

$$\frac{(\epsilon - n^2)(2\epsilon + n^2)}{\epsilon (n^2 + 2)^2} = \frac{N\mu_{\text{eff}}^2}{9\epsilon_0 k_B T}, \tag{5.1}$$

is commonly used in dielectric studies of isotropic liquids. It allows a value for the mean square dipole moment μ_{eff}^2 to be determined from measurements of the electric permittivity ϵ (static dielectric constant) and the refractive index n for a molecular number density N. Local dipole-dipole interactions occur in most polar molecules and in these cases μ_{eff}^2 differs from the mean square dipole moment μ^2,

$$\mu_{\text{eff}}^2 = g_1 \mu^2, \tag{5.2}$$

where g_1 is the Kirkwood correlation factor.

Calamitic liquid crystal molecules with longitudinal dipole moments often exhibit a preferred anti-parallel dipole-correlation leading to values of $g_1 < 1$ in the isotropic phase. This is undesirable in mesogens designed for twisted nematic displays. A tendency for anti-parallel dipole association will reduce the value of the effective dipole moment parallel to the long-molecular axis in the nematic phase, and therefore reduce the dielectric anisotropy $\Delta\epsilon = \epsilon_{\|} - \epsilon_{\perp}$, thus raising the threshold voltage for electro-optic switching.

Small changes in molecular structure often give rise to significant changes in the molecular properties of liquid crystals. For example, the two molecules 4-(*trans*-4-n-pentylcyclohexyl)benzonitrile (PCH5) and 4-(*trans*-4-n-pentylcyclohexyl)chlorobenzene (PCH5-Cl), shown in figure 5.1, vary only in the dipolar functional group attached to the phenyl ring.

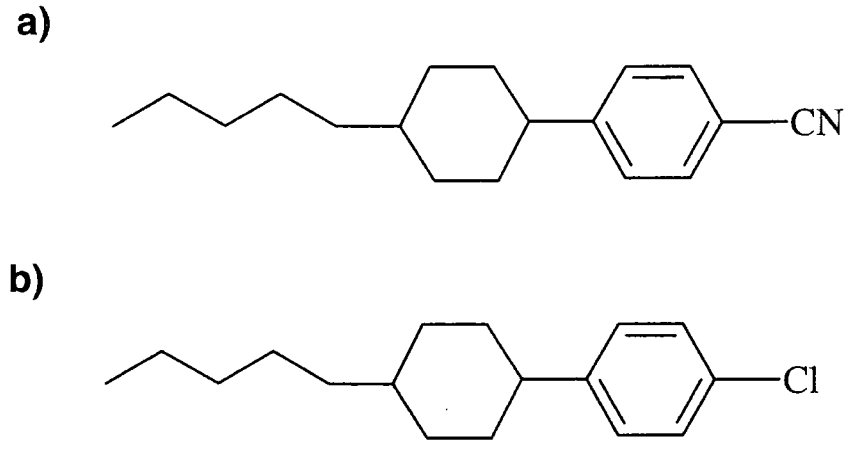

Figure 5.1: The molecular structures of a) PCH5 and b) PCH5-Cl.

However, PCH5 exhibits a nematic phase with a clearing point at 328 K, while PCH5-Cl has a crystal to isotropic liquid transition at 305 K and a virtual nematic-isotropic transition at 277 K. The two materials also differ in their dipole correlation. Experiment shows that in the isotropic phase PCH5 prefers anti-parallel dipole association ($g_1 = 0.88$, measured at 343 K) and PCH5-Cl favours parallel dipole association ($g_1 = 1.20$, measured at 309 K).

5.2 The simulation model

In recent work,Yakovenko and co-workers [169–171] have developed a united atom model of PCH5, with the aim of studying the properties of the isotropic and nematic phases via computer simulations. However, calculations of properties in the bulk, such as dipole correlation, require a far more sophisticated model, in particular, one which provides a full treatment of the long range electrostatic interactions. Consequently, in this current study, the liquid crystal mesogens are represented as fully flexible entities composed of a series of atom based potential energy functions, whose functional form is represented by a variant of the AMBER/OPLS all atom force field developed in chapter 4.

As explained in chapter 4 the OPLS-AA force field of Jorgensen and co-workers was chosen for the non-bonded parameters. The reason for this is that the non-bonded terms in the OPLS-AA force field have been designed with the aim of predicting the correct densities and heats of vaporisations for a series of small molecules. This is important for work of this type where errors in the predicted density will influence significantly the temperature of the clearing point/melting point of the molecule, and hence the calculated properties in the pre-transitional region of the isotropic phase. The non-bonded parameters and the numerous force field parameters for the internal molecular geometry used in this force field for the two mesogens, PCH5 and PCH5-Cl, are derived from the AMBER force field, whose potential parameters are summarised in tables 4.4, 4.5, 4.6 and 4.7 in chapter 4.

It should be noted that the partial charges presented in table 4.7 are significantly higher than those calculated from Mullikan charge distributions obtained from standard basis set *ab initio* molecular orbital calculations. The reason for this is that the latter are unable to properly represent the molecular quadrupole that arises from charge separations in the phenyl rings.

5.3 Methodology for PCH5 and PCH5-Cl

All calculations used the molecular dynamics simulation program, DL_POLY_2.11 [164]. For each system, an initial molecular configuration was generated from a

bcc lattice in which 125 molecules were given small random displacements from their lattice positions and randomly orientated inside a cuboidal simulation box at gas phase densities. Initially, the isothermal-isobaric algorithm of Berendsen was employed (section 2.5.3) to relax the molecular configuration. A nominal pressure of 10^5 Pa was used until the desired volume of approximately 6.4×10^4 Å^3 had been achieved. Thereafter the system was equilibrated using a Nosé-Hoover thermostat and a Hoover barostat (section 2.5.3) at a pressure of 1 atmosphere, employing relaxation times of 1 ps and 4 ps respectively. The simulations retained cubic periodic boundary conditions throughout employing the leap frog algorithm (described in section 2.4.7) with a time-step of 2 fs. The *long-range* electrostatic interactions were handled by a Ewald sum with the convergence parameter α set at 0.48 Å^{-1} and 6 k-vectors were used for each of the directions (x,y,z) in the periodic box. A cut-off of 9 Å was used for the *short range* 12:6 interactions.

Initial simulations of PCH5 were carried out in the pre-transitional region of the isotropic phase at 343 K. Full equilibration of the system density required approximately 200 ps. During this time densities were low and molecular reorientation was rapid and single particle properties (including g_1 and g_2, see section 5.4.4) were seen to fluctuate rapidly. After the equilibrated density was reached a further period of 100 ps was allowed for these quantities to converge to their equilibrium values. Finally, results were calculated over a further simulation production run of 600 ps. Further shorter simulations were performed at the higher temperature of 377 K to assess the temperature dependence of the results. Here, a 300 ps equilibration time was allowed, starting from the end point of the lower temperature simulations, and a further 200 ps production run to compute simulation data. For PCH5-Cl initial simulations were carried out at 343 K. Here, the density required 200 ps to equilibrate, and a further 400 ps were allowed for the equilibration of g_1 and g_2. The production run was carried out over a further 300 ps. Finally, the temperature was dropped to 309 K and a further 300 ps was allowed for equilibration at this temperature. This was followed by a 300 ps production run.

5.4 Results for PCH5 and PCH5-Cl

5.4.1 Density

Values of the system density, ρ, were monitored throughout the simulations. The final computed values of the system density $\langle\rho\rangle$ for PCH5 and PCH5-Cl are given in table 5.1. These values are in excellent agreement with experimental values, for both systems (better than 1%), and are a good indication of the accuracy of the intermolecular force field used.

molecule	simulation T/K	$\langle$boxsize$\rangle$ / Å	$\langle\rho\rangle$ / kg m^{-3}	ρ(exp) / kg m^{-3}
PCH5	343	38.50	928.7±3.6	926
PCH5	377	38.54	926.0±4.5	–
PCH5-Cl	309	38.28	978.6±3.7	986
PCH5-Cl	343	38.43	967.3±3.6	–

Table 5.1: Box lengths and computed densities from simulations of the mesogens PCH5 and PCH5-Cl.

The value of the system density turns out to be quite sensitive to the intermolecular parameters. Small changes to these values can lead to significant changes in the density. In this work the Jorgensen non-bonded parameters have been used in the force field, and it is encouraging that the same parameters that predict the correct density for small molecules seem to be directly transferable to these larger mesogens. One should note the importance of correctly treating the long-range part of the electrostatic interactions because this can also have a significant influence on the system density.

5.4.2 Dipolar and orientational correlation functions

In the isotropic liquid phase the dipolar and orientational correlation is expected to be short range, and therefore, should decay to zero within the simulation box. To confirm this the distance dependent correlation functions, $g_1(r)$ and $g_2(r)$, were

calculated using equation 5.3.

$$g_l(r) = \langle P_l \cos(\theta_{ij}) \rangle_{\text{shell}}, \qquad l = 1, 2 \tag{5.3}$$

where $\langle\rangle_{\text{shell}}$ indicates an ensemble average over molecules j in a spherical shell of width dr at a distance r between the centres of the dipolar groups of molecules i and j, and θ_{ij} is the angle between the dipole vectors in molecules i and j. The mesogens PCH5 and PCH5-Cl have only a single polar group, and hence, the dipole vector is defined by the the bond vector along the C-CN and C-Cl bonds respectively.

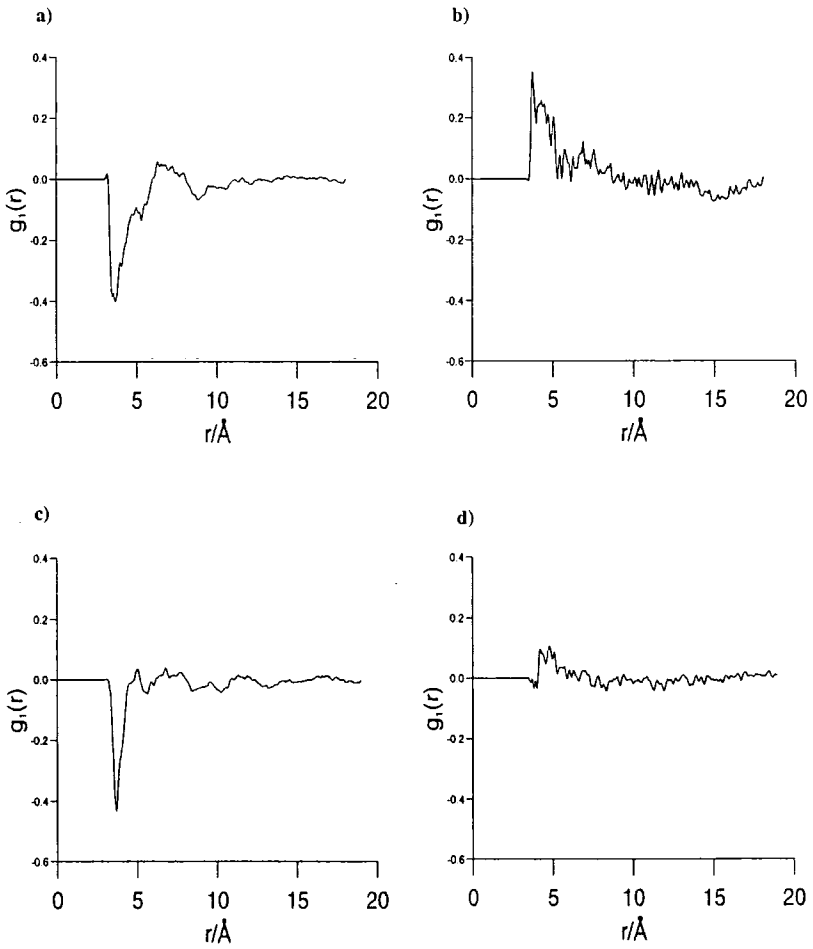

Figure 5.2: Pair correlation functions $g_1(r)$ for PCH5 and PCH5-Cl. (a) PCH5 at T=343 K, (b) PCH5-Cl at T=309 K, (c) PCH5 at T=377 K, (d) PCH5-Cl at T=343 K.

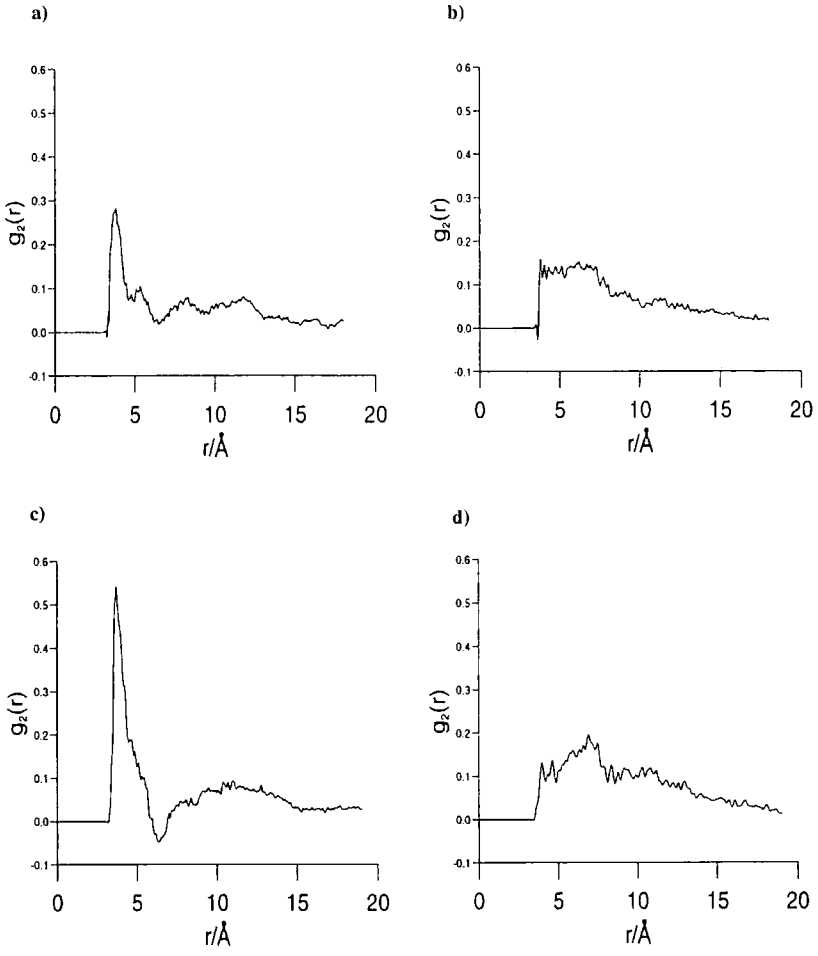

Figure 5.3: Pair correlation functions $g_2(r)$ for PCH5 and PCH5-Cl. (a) PCH5 at T=343 K, (b) PCH5-Cl at T=309 K, (c) PCH5 at T=377 K, (d) PCH5-Cl at T=343 K.

Graphs of $g_1(r)$ and $g_2(r)$ for PCH5 and PCH5-Cl are plotted in figures 5.2 and 5.3 respectively. For $g_1(r)$, positive values indicate a preferred parallel alignment of dipoles at a distance r[1] and negative values indicate a preferred anti-parallel alignment. A clear distinction between the behaviour of the two similar mesogens, PCH5 and PCH5-Cl at small distances, r, is seen from the $g_1(r)$ graphs. For example, PCH5 exhibits a strong preference for anti-parallel association with a pronounced trough in $g_1(r)$ for $r \approx 4.0-5.5$ Å and PCH5-Cl exhibits a preference for parallel association through a small peak in $g_1(r)$ for $r \approx 4.0-5.0$ Å at 309 K. For the higher temperature PCH5 simulation, the position of the trough sharpens

[1] r is taken as the central atom for the molecules PCH5 and PCH5-Cl.

somewhat but the area under it drops significantly. The broad trough at 343 K is indicative of a series of preferred anti-parallel configurations of varying energy. At higher temperatures molecules have more energy and some of the higher energy anti-parallel configurations become less favoured at 377 K. The peak in $g_1(r)$ for PCH5-Cl reduces considerably as temperature is raised and further from the phase transition at 343 K the preference for parallel dipole association has almost disappeared completely.

5.4.3 Order parameter

Although, both the $g_1(r)$ (in figure 5.2) and the $g_2(r)$ (in figure 5.3) curves tend toward zero as r increases, small fluctuations in order remain even at long distances. This is typical for simulations of relatively small systems. Short-range orientational fluctuations are propagated across the system by the periodic boundary conditions and the average value of the systems order parameter $S_2 = \langle P_2(\cos\theta)\rangle$ is therefore non-zero (usually $0.1 < S_2 < 0.2$). To check this $\langle S_2\rangle$ was calculated from the largest eigenvalue λ_+ obtained through the standard method of diagonalising the ordering tensor

$$Q_{\alpha\beta} = \frac{1}{N}\sum_{j=1}^{N}\frac{3}{2}\mathbf{u}_{j\alpha}\mathbf{u}_{j\beta} - \frac{1}{2}\delta_{\alpha\beta}, \qquad \alpha,\beta = x,y,z. \tag{5.4}$$

The vector $\mathbf{u}_j$ in equation 5.4 is defined as the long molecular axis obtained through diagonalisation of the moment of inertia tensor [139]

$$I_{\alpha\beta} = \sum_i m_i(\mathbf{s}_i^2\delta_{\alpha\beta} - \mathbf{s}_{i\alpha}\mathbf{s}_{i\beta}), \tag{5.5}$$

where the atomic distance vectors $\mathbf{s}_i$ were measured relative to the molecular centre of mass. For relatively small systems, this standard approach to calculate $\langle S_2\rangle$ often exaggerates the order in the system, because λ_+ is always greater than zero. An alternative (and often better) approach for the isotropic phase is to follow Eppenga and Frenkel [24] and to calculate S_2 from $-2\times$ the middle eigenvalue λ_- of the ordering tensor. The calculated order parameters for each simulation are given in table 5.2.

molecule	simulation T/K	⟨boxsize⟩ / Å	$\langle S_2 \rangle$ (from λ_-)	$\langle S_2 \rangle$ (from λ_+)
PCH5	343	38.50	0.05	0.15
PCH5	377	38.54	0.08	0.19
PCH5-Cl	309	38.28	-0.05	0.08
PCH5-Cl	343	38.43	0.00	0.19

Table 5.2: Box lengths and order parameters from simulations of the mesogens PCH5 and PCH5-Cl.

The values are typical of those calculated in the pre-transitional region of the isotropic phase for similar sized systems of single-site potentials (hard-spherocylinders and Gay-Berne fluids). Unexpectedly, in both systems the values of $\langle S_2 \rangle$ are slightly larger for the higher temperature system. This is simply an indication of the errors associated with simulations of relatively small systems such as this. Simulations of larger numbers of molecules using single-site potentials indicate that such *system size effects* diminish as the number of molecules increases above 1000 (see section 5.4.5).

5.4.4 Kirkwood correlation factor

So far the preferred parallel or antiparallel dipole association in the bulk isotropic phase has been quantitatively determined by calculating the dipolar correlation function, $g_1(r)$. It is possible to obtain a quantitative value for the overall degree of parallel or anti-parallel alignment exhibited by the molecular dipoles, by calculating the Kirkwood correlation factor, g_1.

$$g_1 = 1 + \frac{1}{N} \left\langle \sum_i^N \sum_{j \neq i}^N \cos\theta_{ij} \right\rangle . \tag{5.6}$$

The angle between the dipole vectors in molecules i and j is given by θ_{ij}, and $\langle\rangle$ indicates an ensemble average. The value of the Kirkwood factor reflects the degree of correlation between orientations of neighbouring molecules. For example, when molecules tend to orientate with their molecular dipoles parallel

to one another, then $g_1 > 1$. However, when they align with their molecular dipoles anti-parallel then $g_1 < 1$.

A similar relationship exists for the orientational correlation factor, g_2.

$$\begin{aligned} g_2 &= 1 + \frac{1}{N}\left\langle \sum_i^N \sum_{j\neq i}^N P_2\left(\cos\theta_{ij}\right)\right\rangle \\ &= 1 + \frac{1}{N}\left\langle \sum_i^N \sum_{j\neq i}^N \frac{3}{2}\cos\theta_{ij} - \frac{1}{2}\right\rangle. \end{aligned} \tag{5.7}$$

Values of g_1 and g_2 are calculated using equations 5.6 and 5.7 and the results are presented in table 5.3. Overall, the results presented in table 5.3 show reasonably good agreement with the values obtained from experimental dielectric and index of refraction measurements for the two mesogens PCH5 and PCH5-Cl. This confirms the individual preferences for anti-parallel (PCH5) and parallel (PCH5-Cl) dipole association in the isotropic phase.

molecule	T/K	g_1	g_2	g_1(exp)
PCH5	343	0.66±0.04	3.63± 0.03	0.88
PCH5	377	0.95±0.07	4.41± 0.03	-
PCH5-Cl	309	1.06±0.02	4.81± 0.05	1.20
PCH5-Cl	343	1.22±0.02	4.08± 0.02	-

Table 5.3: Computed pairwise correlation factors g_1 and g_2.

However, it should be emphasised that there are large error bars associated with these quantities and it should be noted that the g_1 and (to a greater extent) g_2 values will be influenced by the fact that the distance dependent correlation functions do not fully decay to zero within the simulation box. One therefore expects the calculated g_1 and (in particular) g_2 values to be dependent on the system size. More reliable values can only be achieved by simulations with a larger number of molecules (see section 5.4.5). The values obtained for g_2 for both materials are similar to those seen in simulation studies of $(L/D = 3)$ hard ellipsoids in the pre-transitional region. Values of g_2 usually increase as the

isotropic-nematic is approached, and can reach values of $g_2 \approx 100$ at temperatures very close to the isotropic-nematic phase transition [172]. One would therefore expect the lower temperature simulations to exhibit slightly higher values of g_2. This is seen for PCH5-Cl but not for PCH5. It should be noted, however, that the error bars for g_2 are rather large. In addition, local fluctuations in orientational order are exaggerated in importance within a relatively small simulation box and the g_2 results obtained in this study reflect these *system size induced* errors.

5.4.5 Sources of error

A number of results obtained so far in this investigation have significant error bars associated with them. There are several potential sources within the simulations for theses errors, such as, molecular re-orientation of the molecules, diffusion of the molecules and system size effects. In this section these properties are now discussed in more detail.

Molecular re-orientation

In order to calculate the correlation of the molecular dipoles via computer simulation, one must ensure that the molecules are rotating sufficiently in the isotropic fluid. This is investigated by characterising the rotational dynamics of the mesogens using a re-orientational time-correlation function

$$C_l(t) = \sum_{i,j} \sum_{j \neq i} < P_l[\mathbf{u}_i(t) \cdot \mathbf{u}_i(0)] >, \tag{5.8}$$

where P_l is a Legendre polynomial and $\mathbf{u}_i$ is a unit vector defining the molecular axis for each molecule i. For the mesogens PCH5 and PCH5-Cl the molecular axis is defined by the dipole vector along the C-CN and C-Cl bonds respectively.

In an isotropic liquid the rotational motion of a molecule is influenced by its neighbouring molecules and therefore over time, the correlation should decay to zero. For the two molecular systems, PCH5 and PCH5-Cl the decay of C_l, for l= 1, 4 is plotted in figure 5.4. It is evident from these graphs that the decay of the re-orientational correlation function is *extremely slow* for both molecular systems. However, in the initial equilibration period, starting from a low density for both systems, the re-orientational motion is rapid.

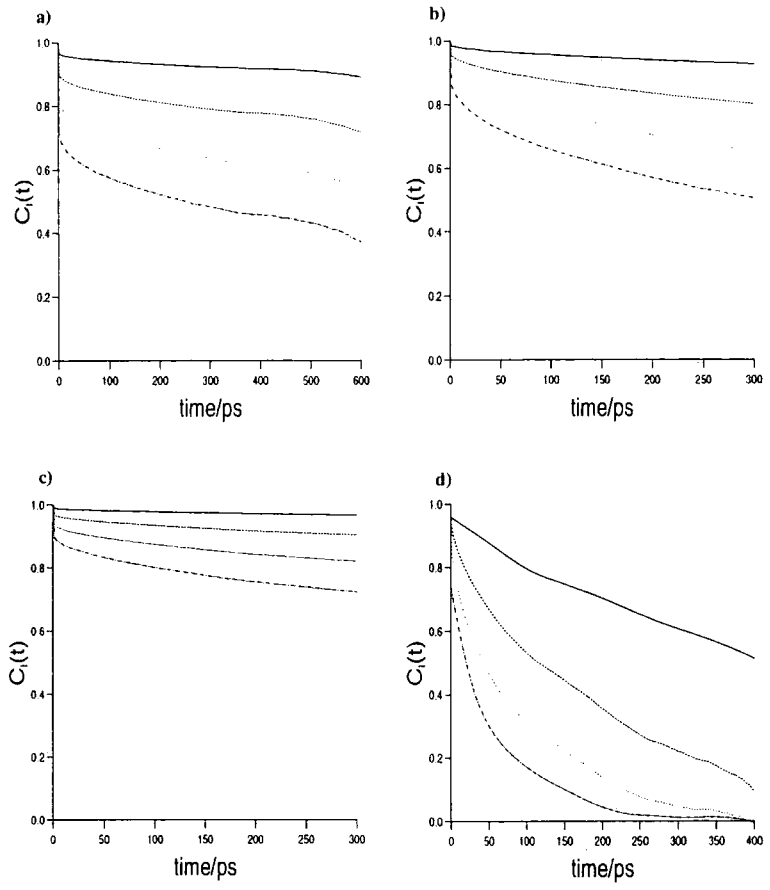

Figure 5.4: Re-orientational correlation functions: P_1, bold line; P_2, dashed line; P_3, dotted line; P_4, dashed/dotted line (a)PCH5 at 343 K; (b)PCH5-Cl at 309 K; (c)PCH5 at 377 K; and (d)PCH5-Cl at 343 K.

Diffusion

The diffusion coefficient was also calculated from the Einstein relation

$$2tD = \frac{1}{3} \lim_{t \to \infty} \left\langle |\mathbf{r}_i(t) - \mathbf{r}_i(0)|^2 \right\rangle , \tag{5.9}$$

where $\mathbf{r_i}(t)$ is the molecular position vector.

The overall diffusion coefficient for the two molecular systems and the diffusion coefficients along each of the three main axes of the simulation box, D_x, D_y, and D_z were determined. This ensures that the system does not become frozen in any one direction. All the computed diffusion results are presented in table 5.4. Experimentally the value of the diffusion coefficient for PCH5 at 333 K, is found

to be $\approx 1.0 \times 10^{-10}\mathrm{m}^2/\mathrm{s}$, which compares well to our computed value, for the mesogen PCH5 at 343 K (given in table 5.4).

molecule	T/K	$D/10^{-10}\mathrm{m}^2/\mathrm{s}$	$D_x/10^{-10}\mathrm{m}^2/\mathrm{s}$	$D_y/10^{-10}\mathrm{m}^2/\mathrm{s}$	$D_z/10^{-10}\mathrm{m}^2/\mathrm{s}$
PCH5	343	0.57	0.65	0.52	0.54
PCH5	377	4.00	3.21	4.52	4.30
PCH5-Cl	309	3.84	3.36	3.78	4.23
PCH5-Cl	343	10.05	7.27	12.39	10.51

Table 5.4: Diffusion coefficients for the mesogens PCH5 and PCH5-Cl.

System size effects

An investigation into the true dependency of the Kirkwood correlation factor on the system size was carried out. State of the art molecular dynamics simulations described in section 5.3 were employed, except the system size was increased from 125 to 1000 PCH5 molecules. A schematic representation of the two molecular systems simulated, is shown in figure 5.5.

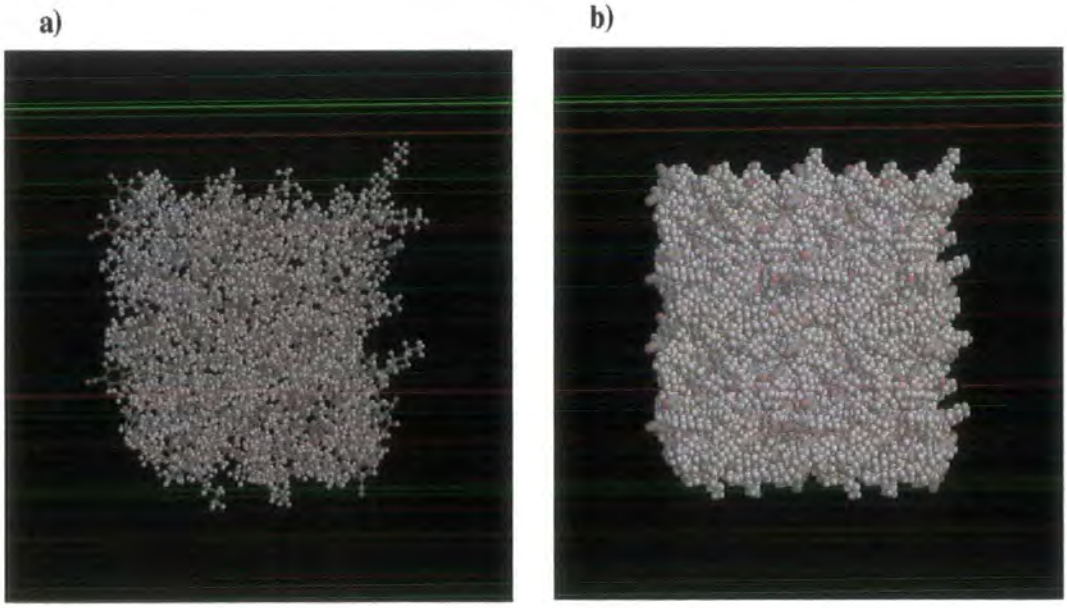

Figure 5.5: Schematic representation of the two systems containing a) 125 PCH5 molecules, and b) 1000 PCH5 molecules.

The initial molecular configuration of the large (1000 PCH5) system was generated by taking the final configuration of the original (125 molecules) system and doubled up the coordinates in all directions until a desired system volume of 4.6 x 10^5Å^3 was achieved. Exactly the same simulation procedure and parameters were employed in this calculation, as in the initial work (see section 5.3). However, unlike the original simulation, this calculation could not be executed on a personal workstation. Instead, it was executed on the Cray T3E super-computer using a parallel version of the DL_POLY_2.11 program, on 128 processors [164]. Even on a super-computer full equilibration of the system was much longer and required approximately 500 ps in order to remove the strong correlation that was initially present between molecules separated by one box length. This problem occurred purely as a consequence of the method used to generate the large molecular configuration. After equilibration a further 250 ps production run was carried out in order to evaluate the correlation functions, g_1 and g_2. A comparison of the computational details for the two simulations on PCH5 are presented in table 5.5.

molecule	T /K	number of molecules	equilibrium time /ps	production time /ps	CPU time /hours
PCH5	343	125	300	600	800 Dec alpha
PCH5	343	1000	500	250	128 Cray T3E

Table 5.5: Simulation details for PCH5.

The distance dependent correlation functions, $g_1(r)$ and $g_2(r)$, were calculated for the two systems, using equation 5.3. For the small system, containing 125 PCH5 molecules, it has already been seen that although $g_1(r)$ and $g_2(r)$ tend towards zero as r increases, small fluctuations in order remain even at long distances. However, simulations of the larger system, using the same single site potential, indicate that such *system size effects* diminish when 1000 molecules are reached. This is seen clearly, by comparing the $g_1(r)$ and $g_2(r)$ graphs for the two systems, presented in figure 5.6. For the large system the fluctuations in order at large distances are rapidly reduced, producing graphs that decay smoothly to zero. Therefore, one expects the statistics for the dipolar and orientational

correlation functions, $g_1(r)$ and $g_2(r)$, to be much better for the larger system.

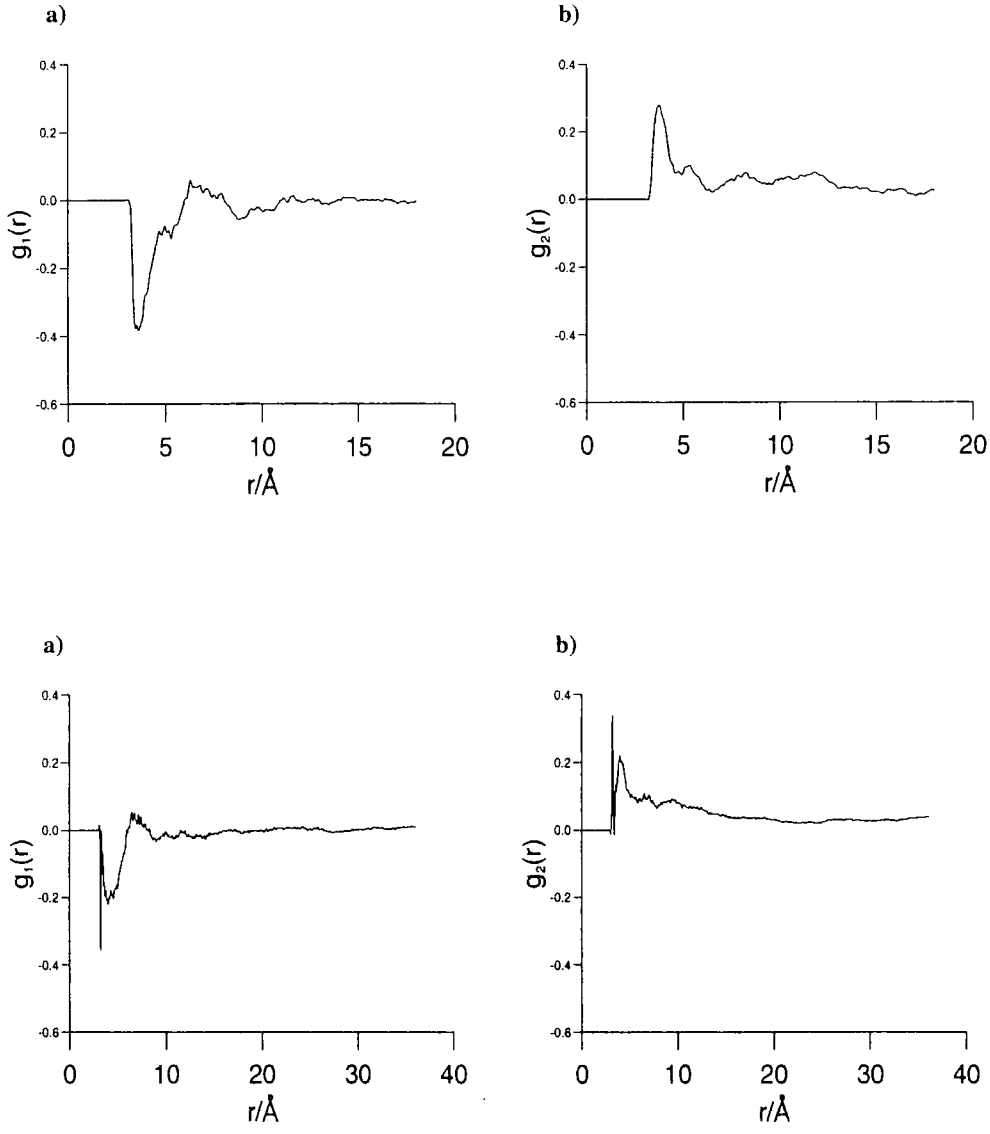

Figure 5.6: Pair correlation functions a) $g_1(r)$ and b) $g_2(r)$ for 125 PCH5 molecules and 1000 PCH5 molecules at 343 K respectively.

The Kirkwood correlation factor, g_1, and the orientational correlation factor, g_2, were calculated for the large PCH5 system using equations 5.6 and 5.7 respectively. The results from these calculations are presented in table 5.6 along with the results from the original PCH5 system. As predicted, the accuracy of the Kirkwood correlation factor for this large system has dramatically improved, and now compares extremely well to the experimentally measured value.

molecule	T/K	no. of molecules	g_1	g_2	g_1(exp)
PCH5	343	125	0.66 ± 0.04	3.63 ± 0.03	0.88
PCH5	343	1000	0.89 ± 0.02	12.90± 0.05	0.88

Table 5.6: Comparison of experimental and computed Kirkwood correlation factors g_1.

5.4.6 Correlation between molecular groups

Following the calculation of the Kirkwood correlation factor it is interesting to consider which interactions are responsible for the difference in dipole correlation of the two molecules. In the liquid phase the molecules are expected to be continually moving with respect to each other. However, the local structure of the fluid is expected to be influenced by configurations where molecules experience strong local interactions. Such interactions momentarily cause the molecules to stay in those configurations longer than they would do in the absence of strong group-group interactions. A detailed insight into the local molecular alignment of the molecules is achieved by plotting the distribution functions $g(r)$ (figures 5.8 and 5.9) and $g_1(r)$ (figures 5.10 and 5.11) for all the different possible combinations of the individual molecular groups (i.e. phenyl ring, cyclohexyl group, polarisable group), within the mesogens. These graphs can then be interpreted by reference to figure 5.7 which shows the molecular dimensions.

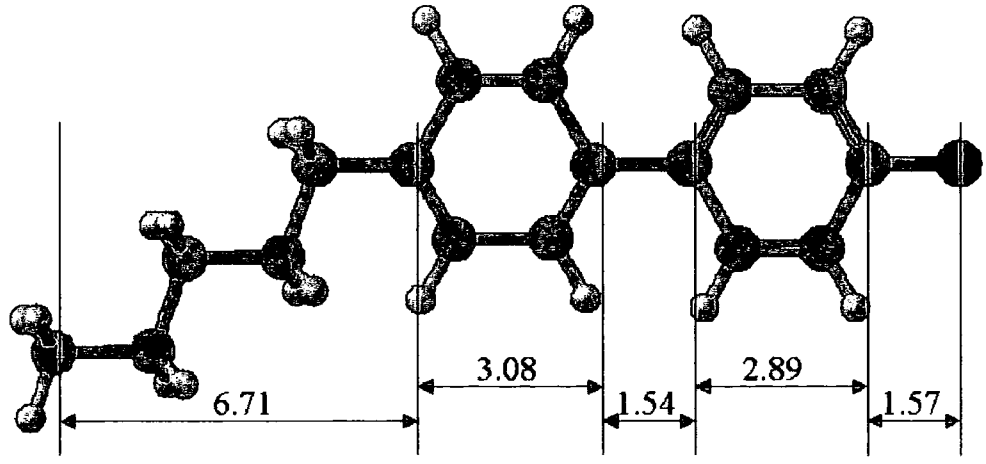

Figure 5.7: Schematic diagram indicating the dimensions of PCH5 and PCH5-Cl.

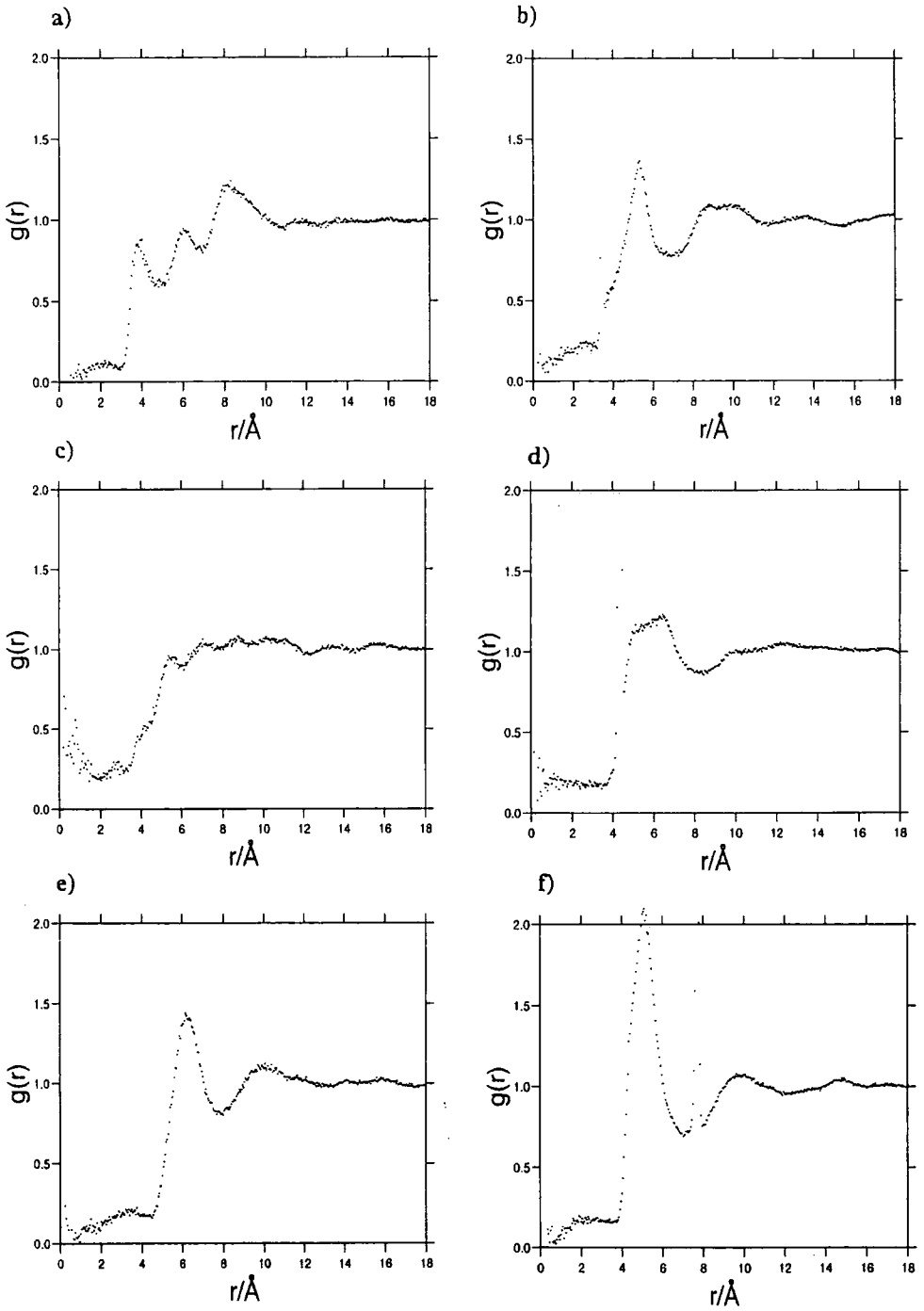

Figure 5.8: Pair correlation functions g(r) for individual groups in molecule PCH5 at T=343 K (a) CN-CN, (b) CN-phenyl, (c) phenyl-phenyl, (d) phenyl-cyclohexane, (e) cyclohexane-cyclohexane, (f) CN-cyclohexane.

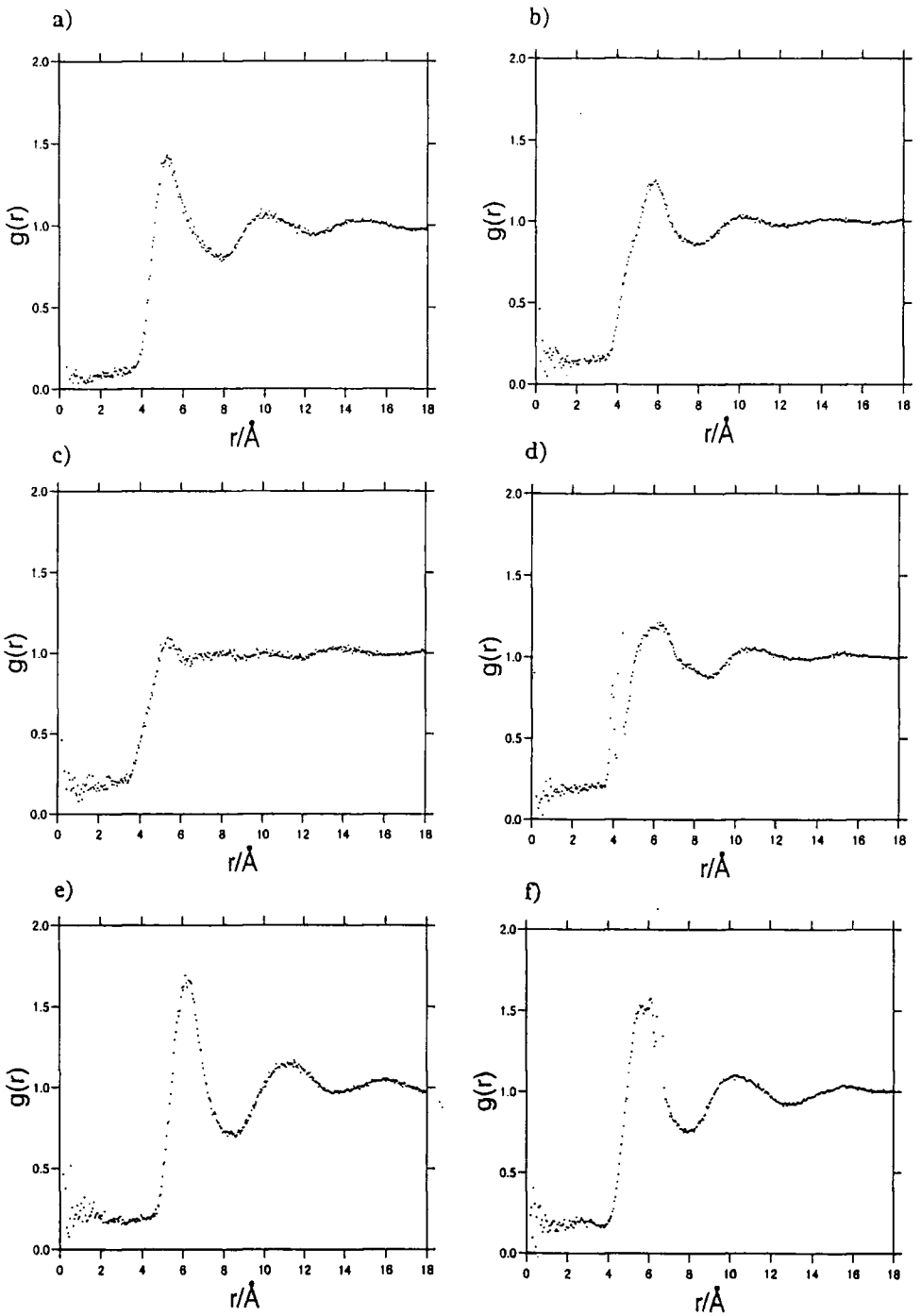

Figure 5.9: Pair correlation functions g(r) for individual groups in molecule PCH5-Cl at T=309 K (a) Cl-Cl, (b) Cl-phenyl, (c) phenyl-phenyl, (d) phenyl-cyclohexane, (e) cyclohexane-cyclohexane, (f) Cl-cyclohexane.

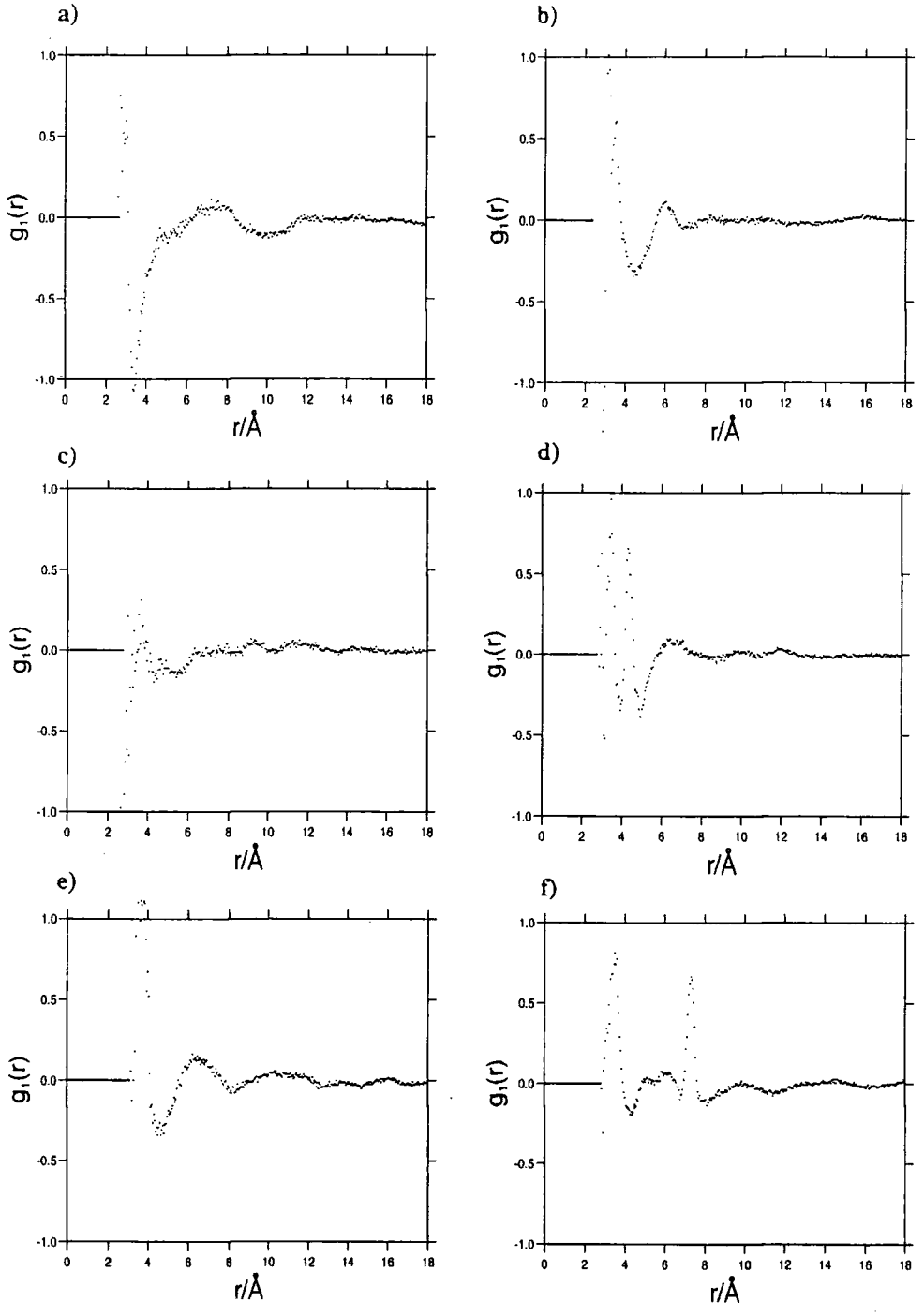

Figure 5.10: Pair correlation functions $g_1(r)$ for individual groups in molecule PCH5 at T=343 K (a) CN-CN, (b) CN-phenyl, (c) phenyl-phenyl, (d) phenyl-cyclohexane, (e) cyclohexane-cyclohexane, (f) CN-cyclohexane.

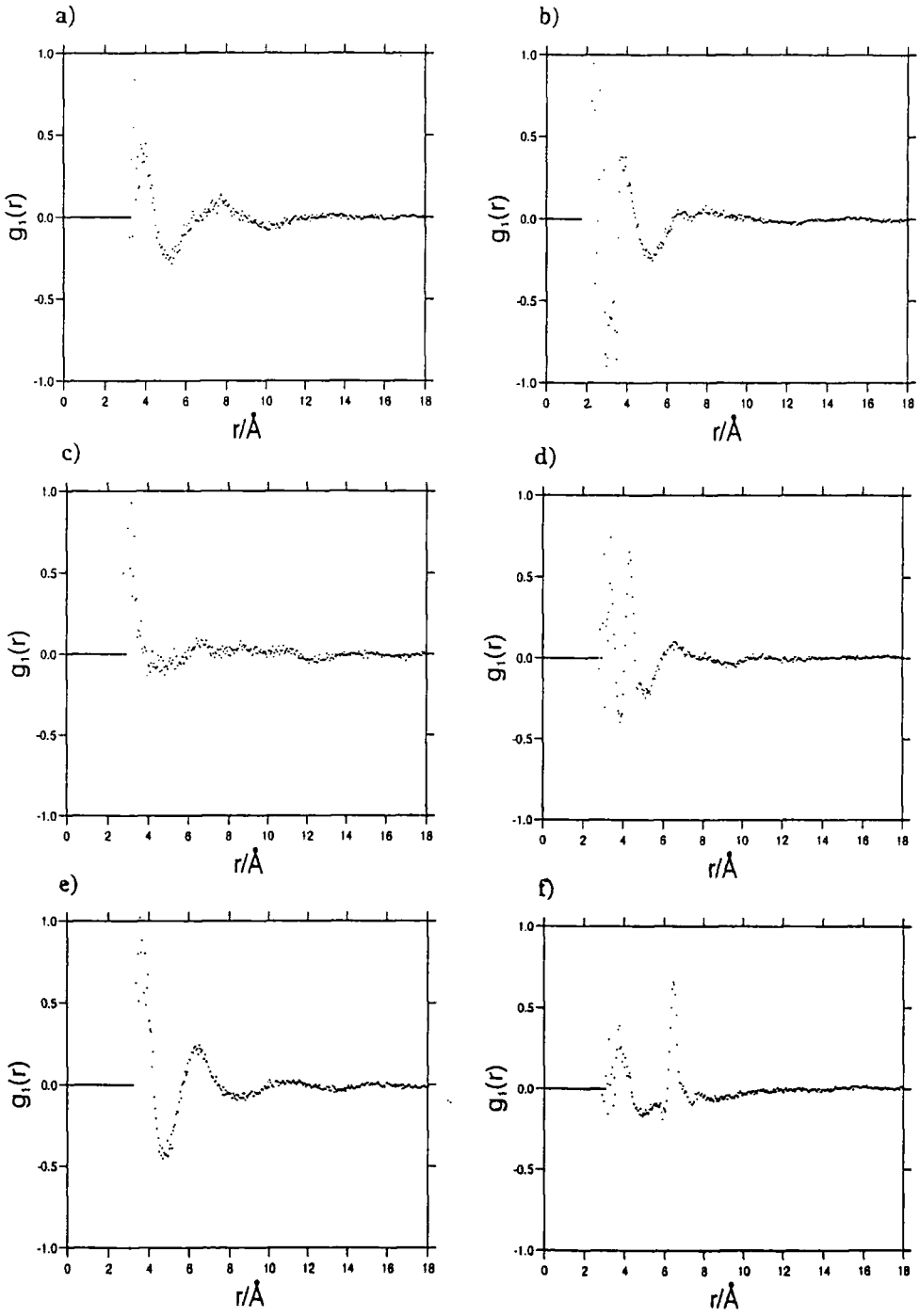

Figure 5.11: Pair correlation functions $g_1(r)$ for individual groups in molecule PCH5-Cl at T=309 K (a) Cl-Cl, (b) Cl-phenyl, (c) phenyl-phenyl, (d) phenyl-cyclohexane, (e) cyclohexane-cyclohexane, (f) Cl-cyclohexane.

The presence of positive and negative peaks in the $g_1(r)$ graphs indicates the formation of parallel and anti-parallel dipole dimers respectively. Collectively, the information displayed, by the peak heights, positions, and orientations in the two distribution functions enables a comprehensive picture to be drawn describing the preferred molecular arrangements of the molecules in the bulk. However, this methodology is extremely time consuming and a more efficient technique, is to define a two dimensional distribution function $g(r, \pm|z|)$,

$$\text{for} \quad \mathbf{r}_i \cdot \mathbf{r}_j \geq 0, \qquad g(r, +|z|) = \frac{V}{N^2} \left\langle \sum_i \sum_{j \neq i} \delta(\mathbf{r} - \mathbf{r}_{ij}) \delta(z - |z_{ij}|) \right\rangle, \quad (5.10)$$

$$\text{for} \quad \mathbf{r}_i \cdot \mathbf{r}_j \leq 0, \qquad g(r, -|z|) = \frac{V}{N^2} \left\langle \sum_i \sum_{j \neq i} \delta(\mathbf{r} - \mathbf{r}_{ij}) \delta(z + |z_{ij}|) \right\rangle.$$

Here, $\mathbf{r}_i$, $\mathbf{r}_j$ are the axis vectors of the groups used in each molecule, $r_{ij} = |\mathbf{r}_i - \mathbf{r}_j|$ is the distance of separation between the centres of the two groups and the distances $|z_{ij}|$ are the absolute values of the projection of $\mathbf{r}_{ij}$ onto the axis vector of each molecular group (as shown in figure 5.12).

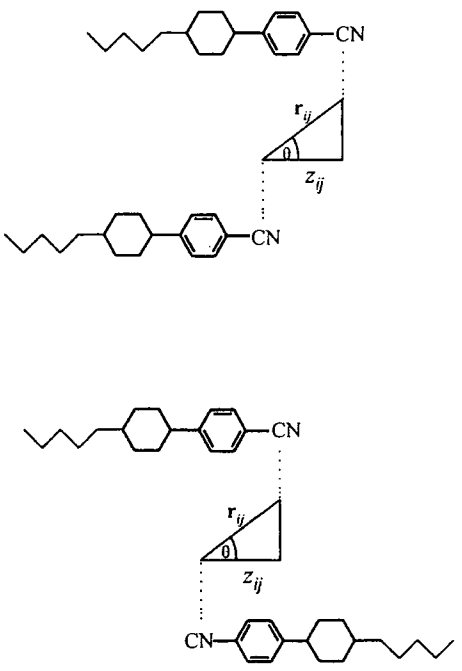

Figure 5.12: Schematic diagram showing the definition of the inter-group distances for the two dimensional pair correlation functions.

In equation 5.10 two separate functions, $g(r, \pm|z|)$, are compiled, which depend on the angles between the axis vectors of molecules i and j. However, these can be represented on a single plot by using positive values $(+|z|)$ to represent parallel alignment (at $\mathbf{r}_i \cdot \mathbf{r}_j \geq 0$) and negative values $(-|z|)$ to represent anti-parallel alignment (at $\mathbf{r}_i \cdot \mathbf{r}_j \leq 0$). In compiling $g(r, \pm z)$ histograms one considers the positional correlation between phenyl, cyclohexyl, and dipolar groups (C-CN, C-Cl). This generates the six two dimensional functions shown in figures 5.13 (for PCH5) and 5.14 (for PCH5-Cl).

It is clear from figures 5.13 and 5.14 that the correlation of individual groups is different in the two systems. Detailed analysis of the distribution functions concludes that in both cases a number of parallel and anti-parallel dipole dimers exist. To see this one catalogues the individual peaks in $g(r, \pm|z|)$ and then assigns these peaks to specific molecular pair configurations. The results are given in in tables 5.7 and 5.8. The main pair configurations that one expects to see are sketched in figure 5.15 and the assignment of pair configurations to specific peaks is indicated in column four of the tables.

Figures 5.13 and 5.14 show that the pair configurations that are energetically favoured change in going from PCH5 to PCH5-Cl. In PCH5 the most favoured pair configurations are G, E and A. In PCH5-Cl these change to A and B. The regions of high probability density for PCH5 result mainly from strong dipolar interactions involving the cyano groups and the phenyl rings. Such interactions favour anti-parallel arrangements of dipoles. However, PCH5-Cl has a much weaker dipole, and consequently dipolar interactions are less important relative to the favoured van der Waals interactions between the phenyl and cyclohexyl rings. It should be noted that the smaller dipole in PCH5-Cl means that interconversion between configurations such as A and B occurs far more easily than in PCH5. This is shown by the broad arc of probability density between $r = 5, z = 0$ and $r = 7, z = 5$ seen in the plot of $g(r, \pm|z|)$ for the C-Cl—C-Cl interactions (figure 5.14a).

The results obtained are in agreement with experimental dielectric measurements of liquid crystal molecules in solutions in isotropic solvents [173,174]. They also indicate the presence of parallel and anti-parallel dipole dimers. The latter can be interpreted in terms of the Dunmur/Toriyama model for molecular as-

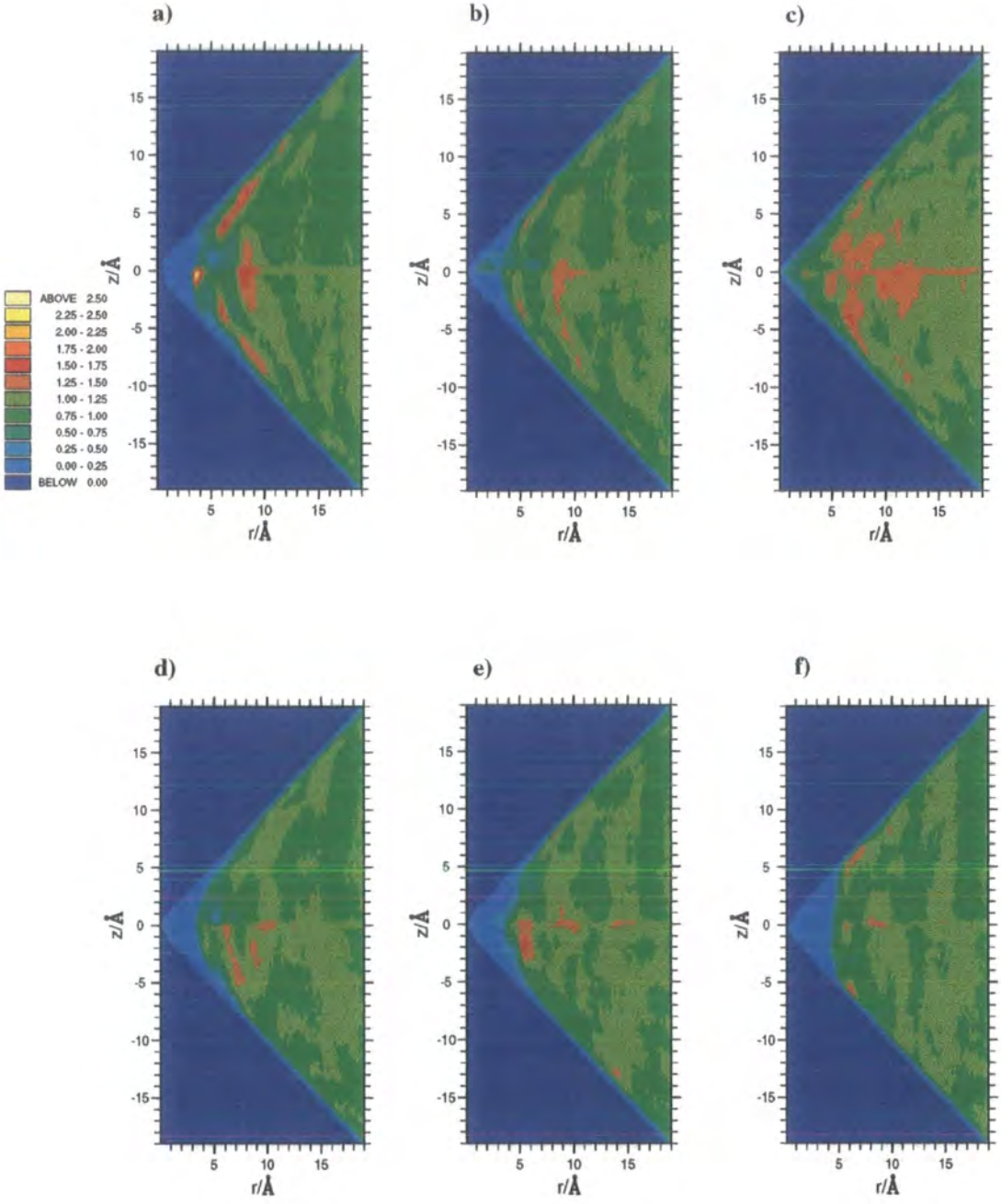

Figure 5.13: Two-dimensional correlation functions for individual groups in molecule PCH5 at T=343 K. (a) C-CN—C-CN, (b) C-CN—phenyl, (c) C-CN—cyclohexyl, (d) phenyl—phenyl, (e) phenyl—cyclohexyl, (f) cyclohexyl—cyclohexyl.

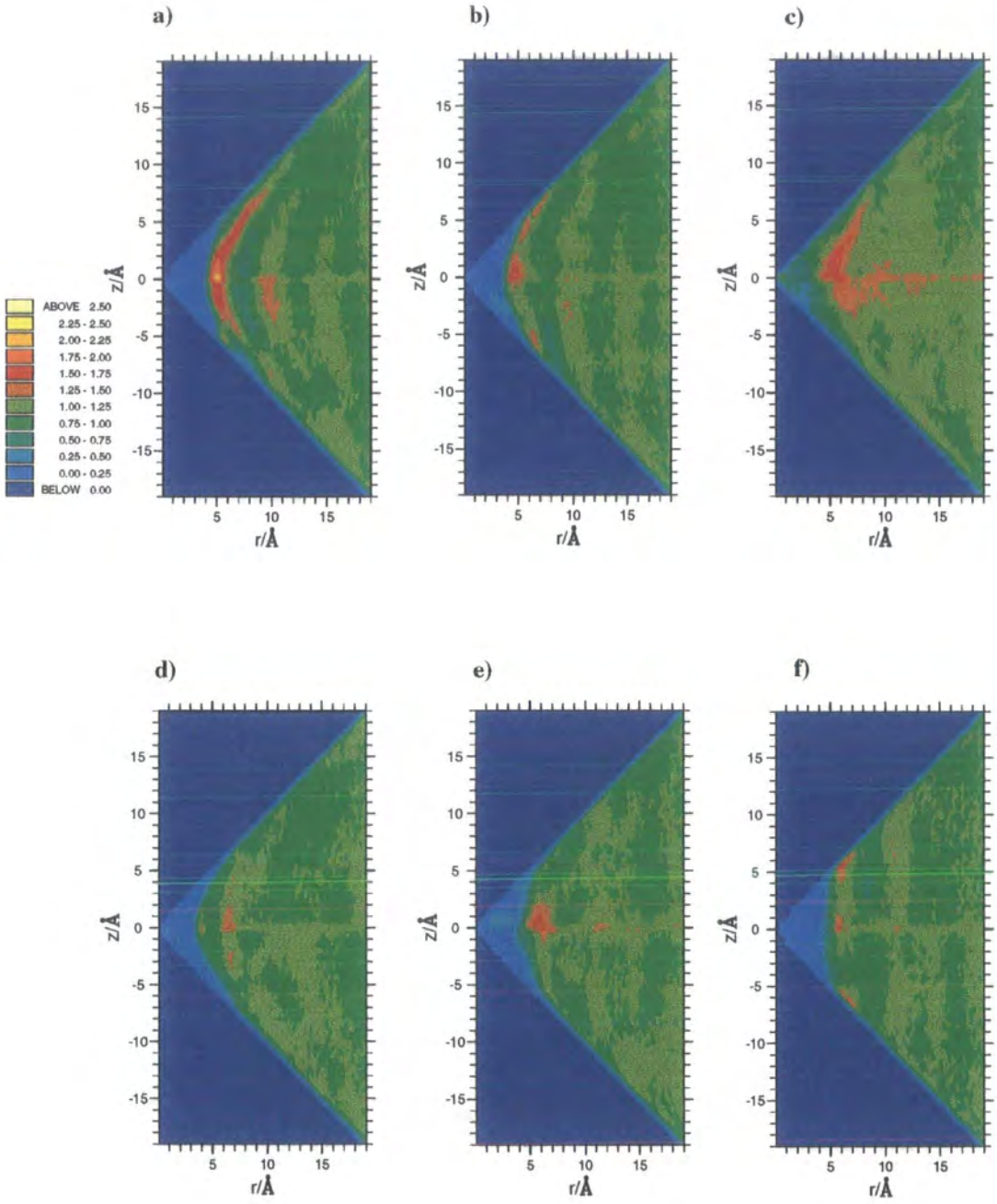

Figure 5.14: Two-dimensional correlation functions for individual groups in molecule PCH5-Cl at T=309 K. (a) C-Cl—C-Cl, (b) C-Cl—phenyl, (c) C-Cl—cyclohexyl, (d) phenyl—phenyl, (e) phenyl—cyclohexyl, (f) cyclohexyl—cyclohexyl.

group interactions	r/Å	z/Å	configurations
C-CN—C-CN	4	0	A (strong correlation)
	8	0	A (strong, secondary)
	6	-4	G
	9	-8	E
	6	4	B
	8	6–7	C
C-CN—phenyl	9–10	0	G
	5	-3	F
	9	-5	F,E
	11	-8	E
C-CN—ring	7	0	C,F
	11	0	C (secondary)
	9	-2	G
	6	-4	E
phenyl—phenyl	6	0– -2	F
	7	-5	E
	9	-3	G
	11	0	F (secondary)
phenyl—cyclohexyl	6	0- -2	E
	9	0	E (secondary)
cyclohexyl—cyclohexyl	6	0	A,D
	9	0	A,D (secondary)
	6	-6	F
	7	6	C

Table 5.7: Approximate positions of the main peaks in the two dimensional translational correlation function $g(r, \pm|z|)$ for PCH5 at 343 K. Positive values of z indicate parallel association and negative values of z indicate anti-parallel association. Column four indicates the pair configuration(s) from figure 5.15 which are responsible for each peak. ("Secondary" indicates a peak that arises from next nearest neighbour interactions.)

group interactions	r/Å	z/Å	configurations
C-Cl—C-Cl	5	0	A (strong)
	7	5	B (strong)
C-Cl—phenyl	5	1	A
	6	4	B,C
	7	6	C
	7	-6	F
C-Cl—ring	6	0-3	A,B
phenyl—phenyl	7	0-1	A
phenyl—cyclohexyl	6	0–1	B
	11	0	A (secondary)
cyclohexyl—cyclohexyl	6	0–1	A
	6	5	B

Table 5.8: Approximate positions of the main peaks in the two dimensional translational correlation function $g(r, \pm|z|)$ for PCH5-Cl at 309 K. Positive values of z indicate parallel association and negative values of z indicate anti-parallel association. Column four indicates the pair configuration(s) from figure 5.15 which are responsible for each peak. ("Secondary" indicates a peak that arises from next nearest neighbour interactions.)

sociation [173] which considers an equilibrium between parallel and anti-parallel dipole species. However, it must be stressed that the Dunmur/Toriyama pairwise association model is too simple to directly translate to the liquid phase. Here, several preferred configurations are found for both parallel and anti-parallel association, and this would translate to several equilibrium constants of different magnitude within the Dunmur/Toriyama model. In an early simulation study of liquid crystal systems [175], Wilson and Dunmur considered the interactions of pairs of PCH5 molecules in the gas phase and also reported a preference for anti-parallel dipole association. However, in the current work it is observed that the preferred liquid state dimers are rather different in structure to those predicted for the gas phase (figure 4 of reference [175]). The gas phase calculations indi-

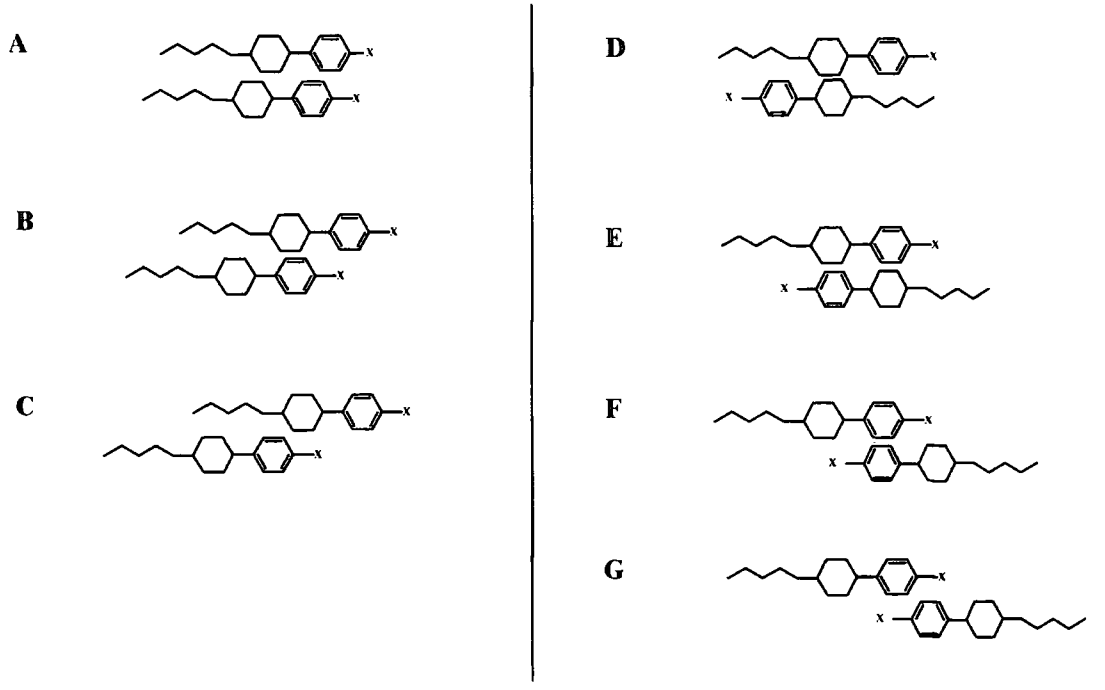

Figure 5.15: Schematic diagram showing molecular pair configurations.

cated a preference for configuration D. This is not altogether surprising because this configuration allows for the strongest van der Waals attractions between a molecular pair. Maximising van der Waals interactions between a molecular pair is less important in the liquid phase (or in a liquid crystal phase) because any pair of molecules is surrounded by a "swarm" of neighbours with which it interacts. Analysis of the $g(r, \pm|z|)$ trajectories illustrates the large effects that small changes in molecular structure can produce in terms of intermolecular interactions. It also points to the way in which careful molecular design can preferentially select favourable molecular interactions within liquid crystals in order to produce the desired effect in terms of molecular ordering. In the case of strongly dipolar molecules, dipole interactions usually favour anti-parallel dipole alignment. However, it is believed that appropriate arrangements of functional groups within a molecule can combat this trend generating preferred parallel dipole association and increasing μ_{eff}^2 in the bulk phase. Indeed, the combination of aliphatic, aromatic and fluorinated alkyl groups within the same molecule has been utilized by Tournilhac and co-workers [176–178] to design molecules with preffered parallel alignment in smectic A and smectic C phases. The $g(r, \pm|z|)$ analysis (above)

provides a useful way to study the effects of individual functional groups via simulation. In the future these types of calculations may prove extremely valuable in terms of *molecular engineering* applications.

5.5 Conclusions for PCH5 and PCH5-Cl

The different dipole correlation behaviour of PCH5 and PCH5-Cl has been successfully modelled. This is best seen through the distance dependent correlation functions, $g_1(r)$, that show preferred anti-parallel association for PCH5 and preferred parallel association for PCH5-Cl at short distances. Kirkwood correlation values have also been determined and these are in qualitative agreement with experimental data. Eliminating any system size effects has enabled not only the prediction of g_1 values that are in qualitative agreement with experiment but also g_1 values that are in excellent quantitative agreement. Excellent agreement has also been obtained between experimental and computed densities for both systems.

Extensive analysis of the equilibrium molecular dynamics trajectories has allowed the determination of which groups influence molecular association in the isotropic phase. It should be noted that the picture of dipole correlation in the bulk is a complicated one. In the case of both molecules several parallel and anti-parallel dimers can be detected and it is the subtle differences in preference for individual molecular pair configurations that give rise to the different values of g_1.

This work shows that it now possible to use atomistic simulations to predict bulk phase properties for mesogenic systems. The results obtained are encouraging and provide motivation for using techniques such as this in molecular engineering applications to determine molecular properties prior to synthesis. In the case of g_1 calculations it should be possible in the near future for molecular simulations to determine which of a series of similar structures will give rise to the largest effective dipole moment in the condensed state. This is something which may currently only be hypothesised with the aid of considerable chemical intuition.

Finally, one should note the importance of modelling intermolecular interac-

tions as accurately as possible in order to account for the behaviour that results from changes in molecular structure. Proper handling of long range forces is essential, resulting in a heavy computational load arising from an Ewald summation. The calculations described here required the equivalent of 800 CPU hours on a state-of-the-art processor. However, it is expected that rapid advances in computer speed will greatly increase the accessibility of such calculations within the next few years.

5.6 Simulation studies of me5NF and GGP5Cl

It has already been shown that molecular simulations are becoming a powerful tool for studying the behaviour of liquid crystal molecules [127, 138, 139, 144, 145, 169, 171, 179]. Previous simulations of the mesogens PCH5 and PCH5-Cl (described earlier in this chapter and in [156]), have indicated that it is possible to successfully predict the different dipole association behaviour which occurs in the bulk phase. It has been shown that it is also possible to determine which interactions are responsible for stabilising individual pair configurations that give rise to the different dipole correlations observed experimentally.

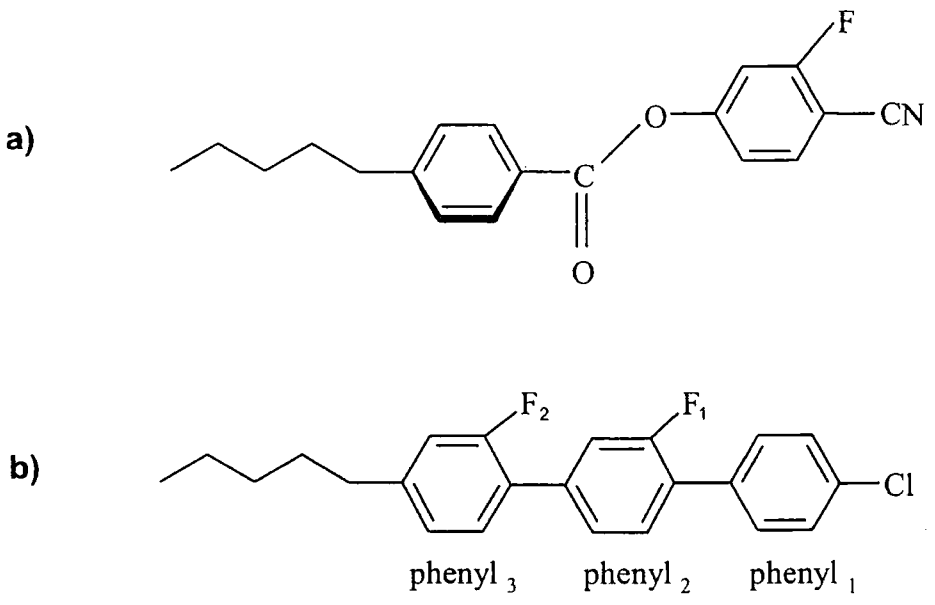

Figure 5.16: The molecular structures for the two molecules used in this study, a) me5NF and b) GGP5Cl.

Two additional mesogens me5NF and GGP5Cl (figure 5.16) have been studied using the same methodology as previously described for the mesogens PCH5 and PCH5-Cl. These molecules are chemically more complex than PCH5 and PCH5-Cl (which differ only in the dipolar functional group that is attached to the phenyl ring). They contain several polarisable groups, and therefore, are more challenging to study.

5.7 Methodology for me5NF and GGP5Cl

Simulations of the mesogens me5NF and GGP5Cl were carried out for 216 molecules rather than 125 molecules previously used to study PCH5 and PCH5-Cl. This is due to the increased molecular length of the molecules[2]. Experimental dielectric and index of refraction measurements have already yielded data for g_1 in the pre-transitional region at 303 K for me5NF and 393 K for GGP5Cl. (For GGP5Cl the nematic-isotropic clearing point is at 386.8 K and me5NF undergoes a monotropic transition to a nematic state at 296.8 K.) Simulations of the mesogens me5NF and GGP5Cl were therefore carried out at 303 K and 393 K respectively. Full equilibration of the system density required approximately 200 ps for each system. During this time single particle properties such as g_1 and g_2 were seen to fluctuate rapidly. After the equilibrated density was reached a further period of 500 ps was allowed for these quantities to converge to their equilibrium values. Finally, results were calculated over a further 300 ps production run.

5.8 Results for me5NF and GGP5Cl

5.8.1 Density

Computed values of the system density, $\langle\rho\rangle$, for the mesogens me5NF and GGP5Cl are presented in table 5.9. These results again confirm that the computed density values are in excellent agreement with experimentally measured values (better

[2]In a computer simulation the minimum dimension of the simulation box must be greater than twice the molecular length.

than 1%).

molecule	simulation T/K	$\langle\rho\rangle$/gcm^{-3}	ρ(exp)/gcm^{-3}
me5NF	303	1.126	1.130
GGP5Cl	393	1.068	1.158(338 K)

Table 5.9: Computed densities and order parameters of me5NF and GGP5Cl.

5.8.2 Dipole and orientational correlation

A useful monitor of how the dipolar and orientational correlation varies as a function of molecular separation is provided by the distance dependent correlation functions in equation 5.3. The mesogens me5NF and GGP5Cl contain many polar groups and therefore it is necessary to calculate the overall dipole vector using the classical definition of μ. This is obtained from the molecular partial charges in the force field

$$\mu = \sum_i q_i \mathbf{r}_i, \tag{5.11}$$

and gives the direction of the dipole vector as $\hat{\mu} = \mu/|\mu|$.

Graphs of $g_1(r)$ are plotted in figure 5.18 for me5NF and GGP5Cl. Positive values indicate a preferred parallel alignment of dipoles at a distance r[3] and negative values indicate a preferred anti-parallel alignment. me5NF exhibits a strong preference for anti-parallel association, as seen by the large trough in $g_1(r)$ at 3.3 Å. This trough arises from nearest neighbour interactions and has an onset of 3 Å (corresponding to the closest separation expected for two side-by-side mesogens) and extends to approximately 6 Å. It is possible, however, that the interactions observed at 6 Å are from shifted molecules, rather than trimers. Beyond 6 Å a small positive peak in $g_1(r)$ is seen; this arises from next nearest neighbour interactions. However, this is much smaller than the trough (at 3.3

[3] r is taken as the central carbonyl carbon for the molecule me5NF and the aromatic carbon atom on phenyl$_2$ ring (the connecting phenyl$_2$-phenyl$_3$ carbon) for the molecule GG5Cl respectively.

Å) and indicates that in addition to transient dimers of aligned molecules within the liquid, one would expect to see some head-to-tail paired trimers as indicated schematically in figure 5.17.

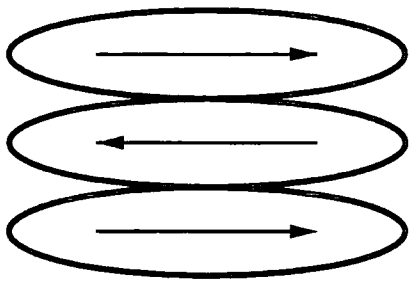

Figure 5.17: Schematic diagram showing local packing in the pre-transitional region for me5NF.

This is entirely consistent with the expected picture for a mesogen in the pre-transitional region of the isotropic phase, where depolarised light scattering measurements indicate substantial short range orientational correlation [180]. In contrast, for GGP5Cl the $g_1(r)$ signal arising from first nearest neighbour interactions is small and positive in sign indicating a preference for local parallel dipole association. The onset of this peak is 3.5 Å and it extends to 3.8 Å. A small trough from 3.8 Å to 5.9 Å is also seen, which could indicate second nearest neighbour molecules, but is more likely (as will be discussed in section 5.8.5) to arise from nearest neighbour molecules with anti-parallel dipoles which dominate at these slightly longer distances. Finally, a small peak in $g_1(r)$ can be seen beyond 5.9 Å that most probably arises from second nearest neighbour molecules. This is indicative of the presence of small transient clusters of three aligned molecules as seen in me5NF, but in this case there is a slight preference for parallel alignment of dipoles within these clusters.

$g_2(r)$ graphs for me5NF and GGP5Cl are plotted in figure 5.19. The peaks centred at 3.5-3.6 Å and 5.8-5.9 Å correspond to pair and triplet interactions for aligned particles, as already indicated in the analysis of the $g_1(r)$ results. The triplet peak for GGP5Cl is rather larger than that seen for me5NF indicating that there are likely to be more transient trimers for this material. However, it should

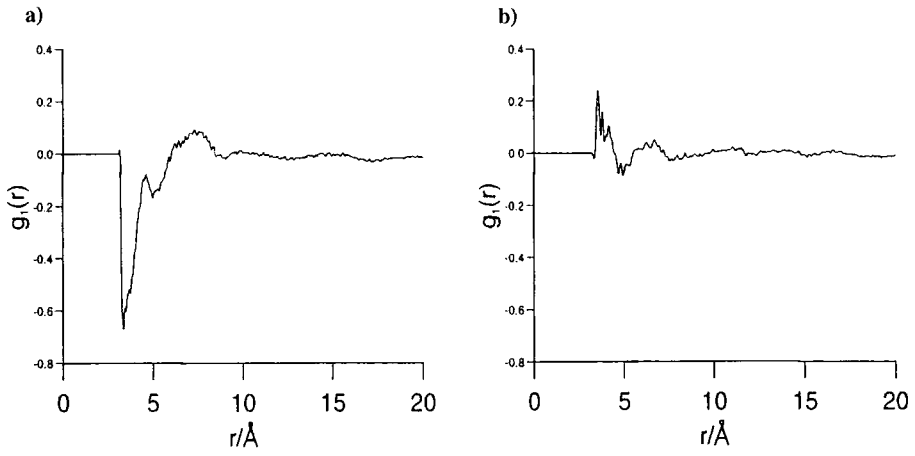

Figure 5.18: Pair correlation functions $g_1(r)$ a) me5NF at 303 K and b) GGP5Cl at 393 K.

be noted that the corresponding peak in $g_1(r)$ at this distance is smaller. It is already known from figure 5.18 that me5NF shows extremely strong anti-parallel association and because of this most of the trimers will be of the form shown in figure 5.17. Consequently, this suggests that many of the transient trimers for GGP5Cl are likely to contain a mixture of anti-parallel and parallel associated molecules. A preference for purely parallel associated trimers would have resulted in the secondary peak in $g_1(r)$ at 5.9 Å being larger than the corresponding peak for me5NF.

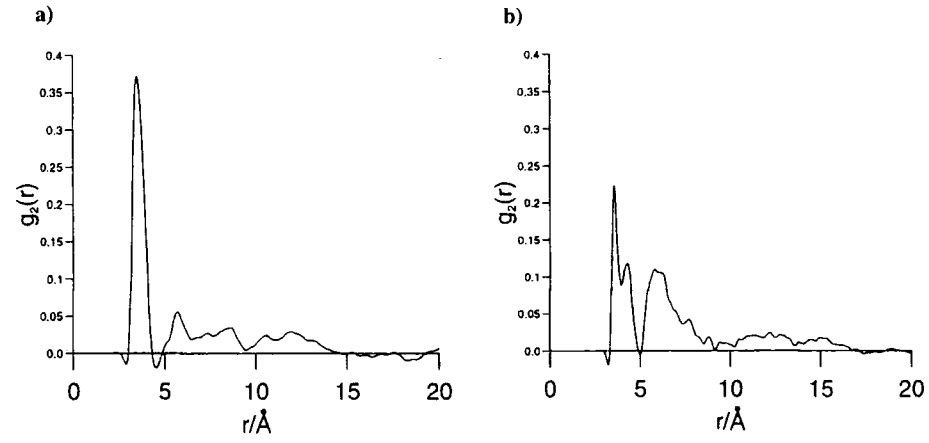

Figure 5.19: Pair correlation functions $g_2(r)$ a) me5NF at 303 K and b) GGP5Cl at 393 K.

5.8.3 Order parameter

For PCH5 and PCH5-Cl [156], fluctuations in the orientational order remained for distances equivalent to half the box length. It should be noted that for the mesogens, me5NF and GGP5Cl, the larger system size of 216 molecules (compared to 125 for the cyano materials of reference [156]), seems to be sufficient for these fluctuations to die out well within half the simulation box dimensions. To check this the system order parameter was calculated using the the same two methods previously described in section 5.4.3. The calculated order parameters for each simulation are given in table 5.10, and are typical of those usually obtained in the pre-transitional region for similar sized systems of single-site potentials.

molecule	simulation T/K	$\langle$boxsize$\rangle$ / Å	$\langle S_2 \rangle$ (from λ_-)	$\langle S_2 \rangle$ (from λ_+)
me5NF	303	45.99	0.04	0.09
GGP5Cl	393	49.37	-0.03	0.11

Table 5.10: Box lengths and order parameters from simulations of the mesogens me5NF and GGP5Cl.

5.8.4 Kirkwood correlation factor

The values of g_1 and g_2 were calculated from equations 5.6 and 5.7 and the results are given in table 5.11. The g_1 result for the mesogen me5NF is in excellent agreement with the value obtained from experimental dielectric measurements [181] and confirms that individual molecules have a preference for anti-parallel dipole association in the isotropic phase. However, for GGP5Cl the experimental result is not reproduced. Part of the discrepancy between the experimental and calculated results may be caused by errors induced by the relatively small system size. However, the main source of error appears to arise from a subtle failure in the force field used. A detailed analysis of pair configurations (presented in section 5.8.5) indicates that a series of both parallel and anti-parallel dipole pair configurations arise for GGP5Cl, and that the structure of these preferred configurations are dominated by the charge distribution of the molecule. The force field used in

this study does not correctly favour the anti-parallel configurations sufficiently. The likely problem is caused by the combination of both highly polar groups and highly polarizable groups in GGP5Cl. In such circumstances one would expect polarization effects to be important. The neglect of such interactions in the force field used (and the majority of standard molecular mechanics force fields) makes it difficult to correctly model the relative stability of pairwise associated molecules in GGP5Cl.

The g_2 values obtained for both materials are typical of those seen in the pre-transitional region and (for example) are similar to those obtained in simulation studies of $(L/D = 3)$ hard ellipsoids in the pre-transitional region. Values of g_2 usually increase as the isotropic-nematic is approached, and can reach values of $g_2 \approx 100$ at temperatures very close to the isotropic-nematic phase transition.

molecule	T/K	g_1	g_2	g_1(exp)
me5NF	303	0.79±0.005	1.55±0.017	0.78
GGP5Cl	393	1.04±0.014	1.62±0.010	0.79 (343 K)

Table 5.11: Computed pairwise correlation factors g_1 and g_2.

5.8.5 Correlation between molecular groups

As with the mesogens PCH5 and PCH5-Cl (described earlier in this chapter and in [156]), it is possible to look in detail at the correlation between individual molecular groups within the fluid by defining a two dimensional distribution function $g(r, \pm|z|)$ (equation 5.10). By considering the positional correlation between all the main structural groups in the mesogen me5NF including the dipolar groups, 15 two dimensional distribution functions are generated. These are shown in figure 5.22. In a similar manner 21 two dimensional distribution functions are generated for the molecule GGP5Cl and these are shown in figure 5.23.

A number of features are immediately clear from figures 5.22 and 5.23. The series of peaks seen in the functions $g(r, +|z|)$ and $g(r, -|z|)$ can only be explained by the presence of both anti-parallel and parallel dipole dimers for the two molecules. There are also secondary peaks in $g(r, \pm|z|)$ that arise at large values of r and can only be explained by the presence of trimers (as indicated

earlier in the behaviour of $g_1(r)$ and $g_2(r)$). The position of the main peaks in $g(r, \pm|z|)$ from figures 5.22 and 5.23 are classified in tables 5.12 and 5.13. From the known molecular dimensions (figures 5.20 and 5.21), the peaks in $g(r, \pm|z|)$ can be assigned to approximate pair configurations.

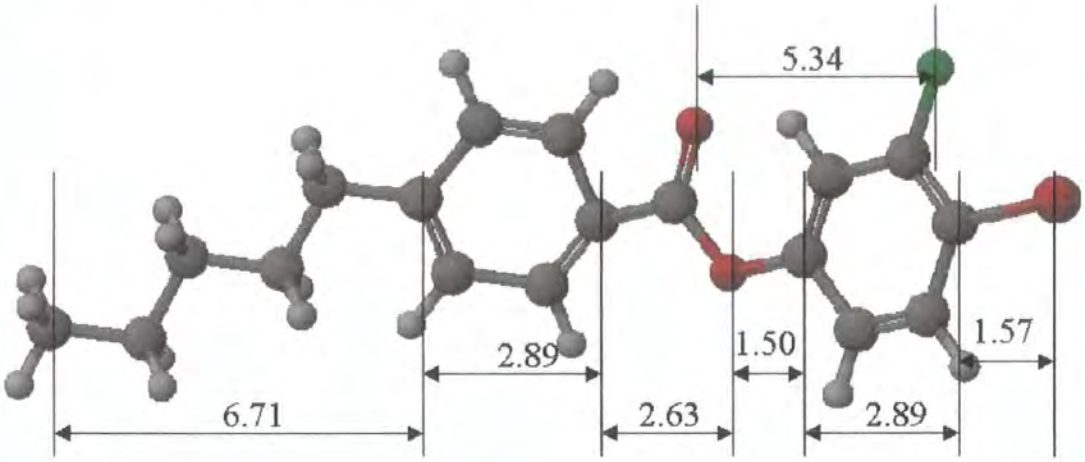

Figure 5.20: Schematic diagram indicating the molecular dimensions with the mesogen me5NF.

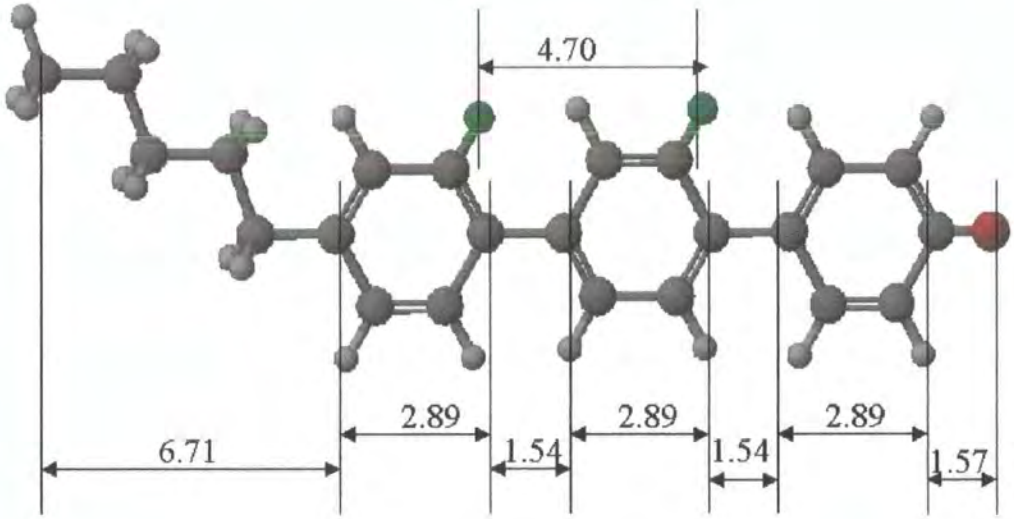

Figure 5.21: Schematic diagram indicating the molecular dimensions with the mesogen GGP5Cl.

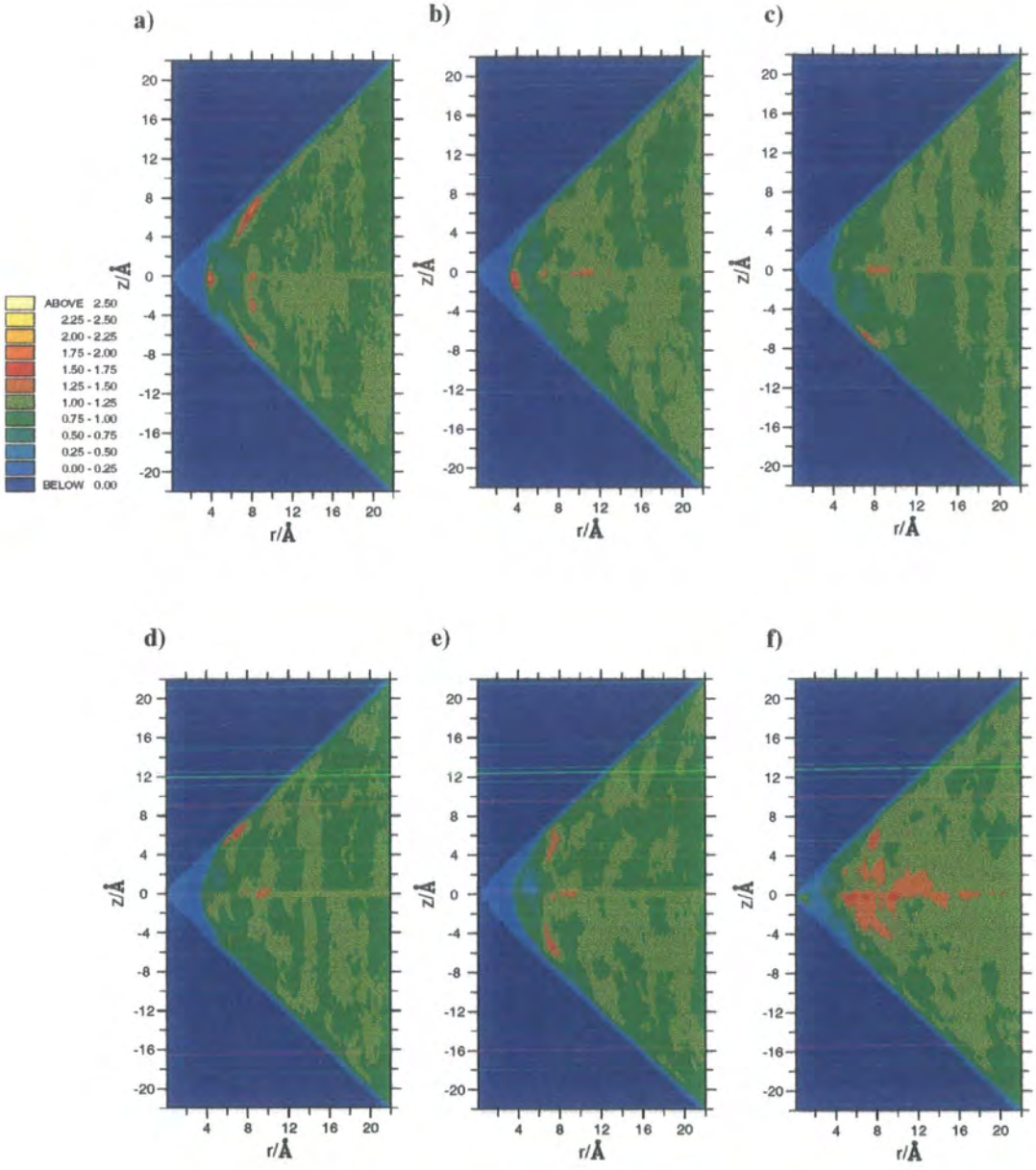
a)
b)
c)
d)
e)
f)
ABOVE 2.50
2.25 - 2.50
2.00 - 2.25
1.75 - 2.00
1.50 - 1.75
1.25 - 1.50
1.00 - 1.25
0.75 - 1.00
0.50 - 0.75
0.25 - 0.50
0.00 - 0.25
BELOW 0.00
z/Å
r/Å

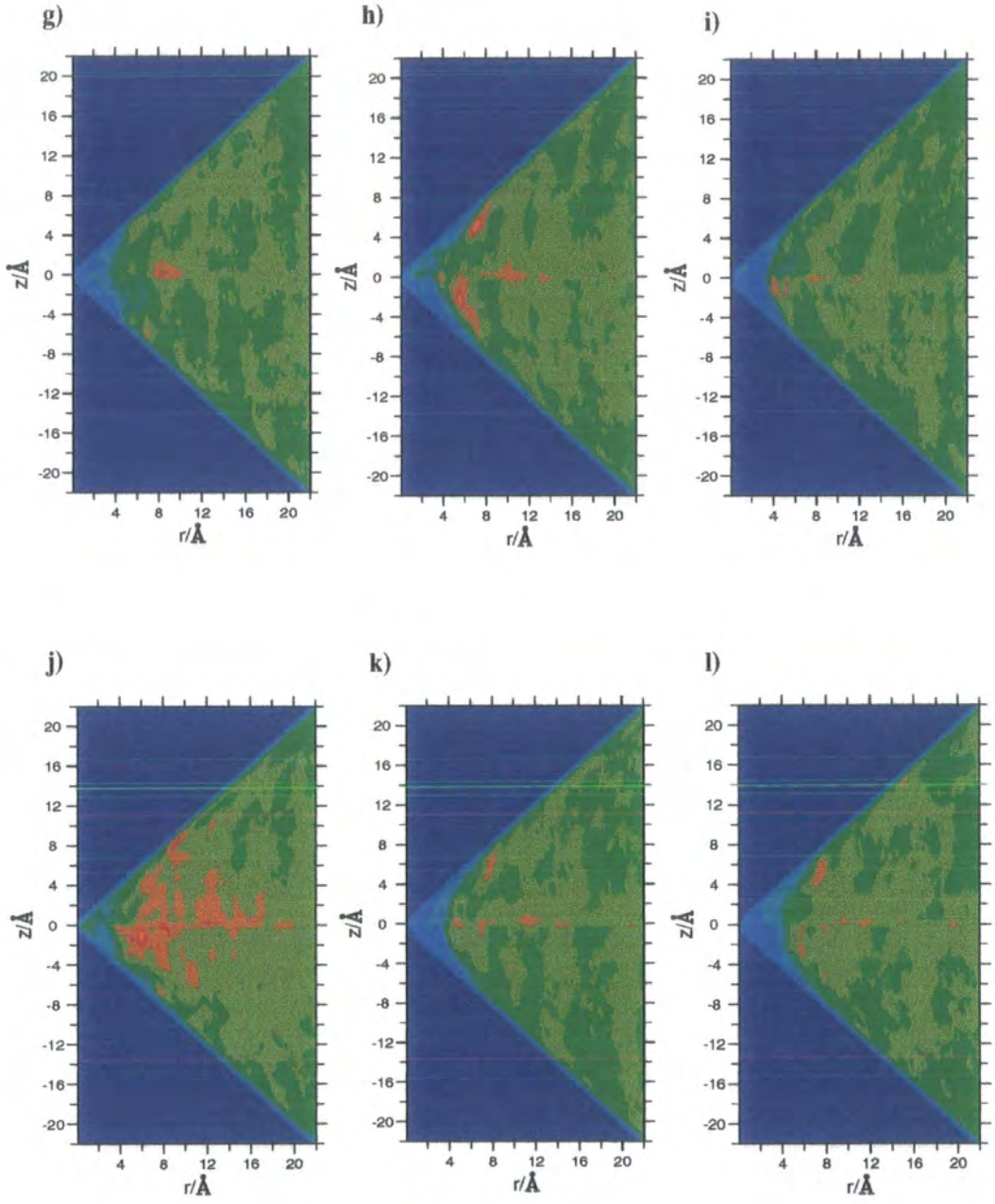
g)
h)
i)
j)
k)
l)
z/Å
r/Å
20
16
12
8
4
0
-4
-8
-12
-16
-20
4
8
12
16
20

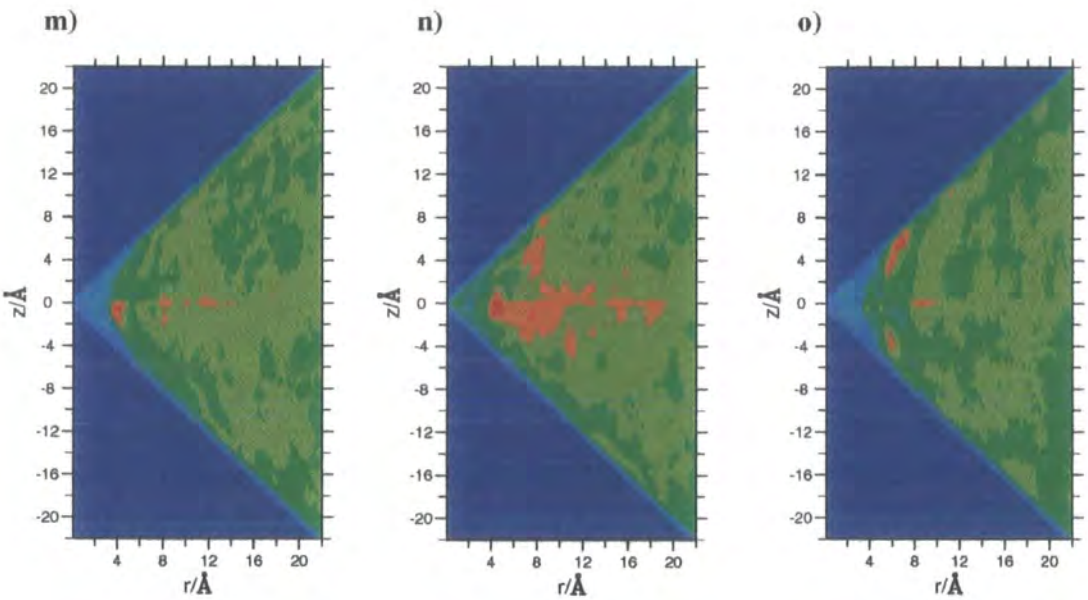

Figure 5.22: Two-dimensional correlation functions for individual groups in molecule me5NF at T=303 K. (a) C-CN—C-CN, (b) C-F—C-F, (c) ester—ester, (d) $phenyl_1$—$phenyl_1$, (e) $phenyl_2$—$phenyl_2$, (f) $phenyl_1$—$phenyl_2$, (g) C-CN—C-F, (h) C-CN—ester, (i) C-CN—$phenyl_1$, (j) C-CN—$phenyl_2$, (k) ester—$phenyl_1$, (l) ester—$phenyl_2$, (m) C-F—ester, (n) C-F—$phenyl_1$, (o) C-F—$phenyl_2$.

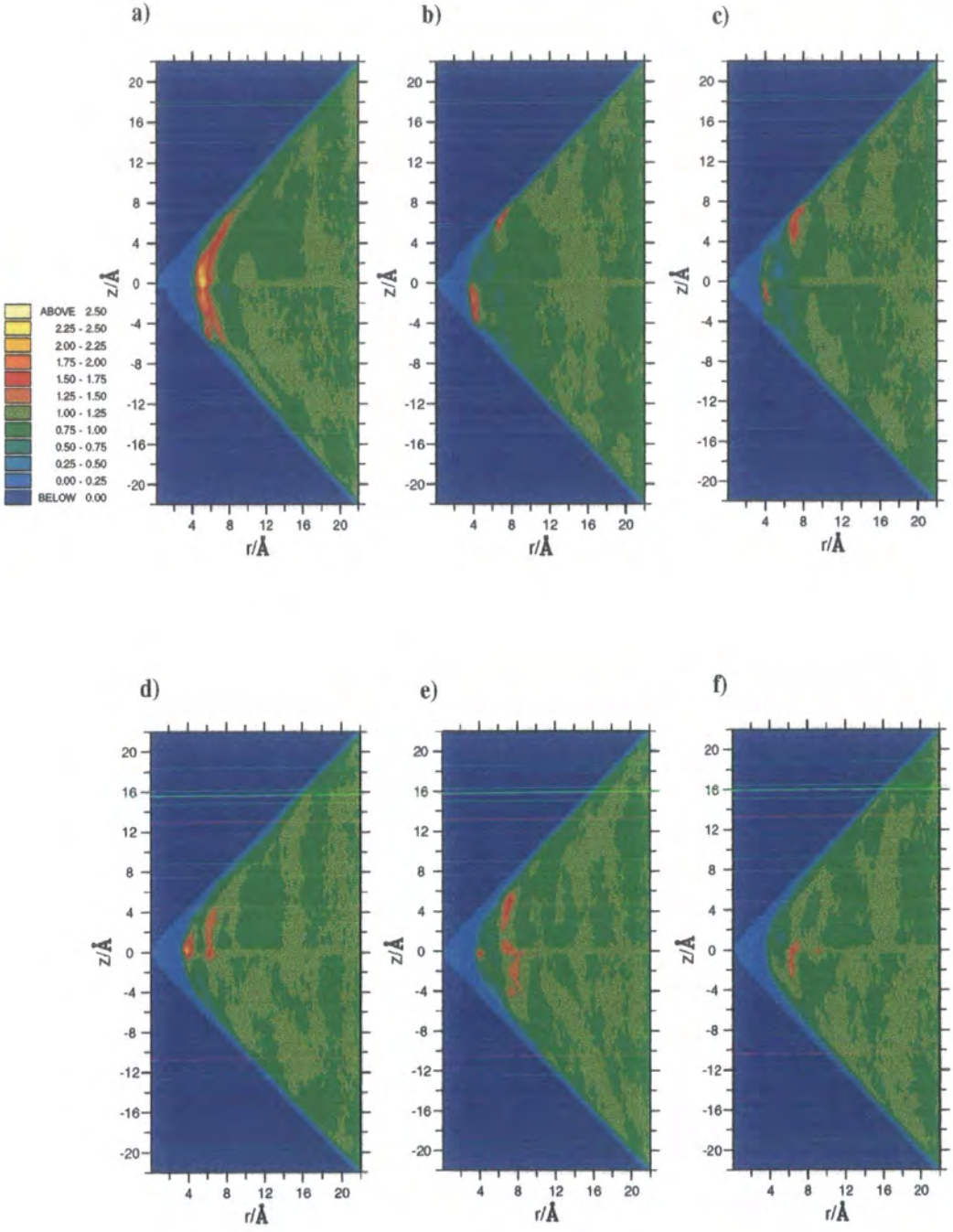
a)
b)
c)
d)
e)
f)
ABOVE 2.50
2.25 - 2.50
2.00 - 2.25
1.75 - 2.00
1.50 - 1.75
1.25 - 1.50
1.00 - 1.25
0.75 - 1.00
0.50 - 0.75
0.25 - 0.50
0.00 - 0.25
BELOW 0.00
z/Å
r/Å

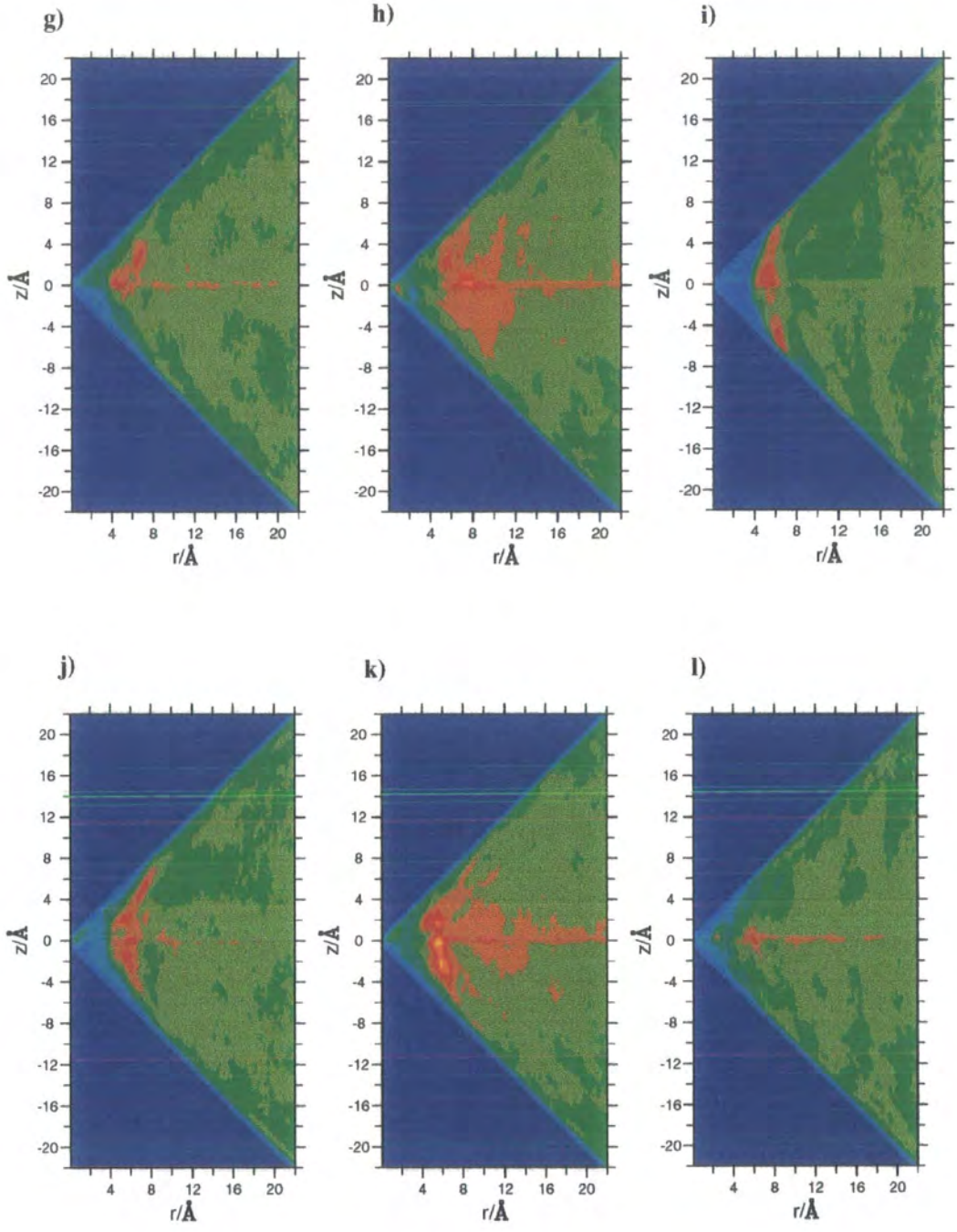
g)
h)
i)
j)
k)
l)
z/Å
r/Å
20
16
12
8
4
0
-4
-8
-12
-16
-20
4
8
12
16
20

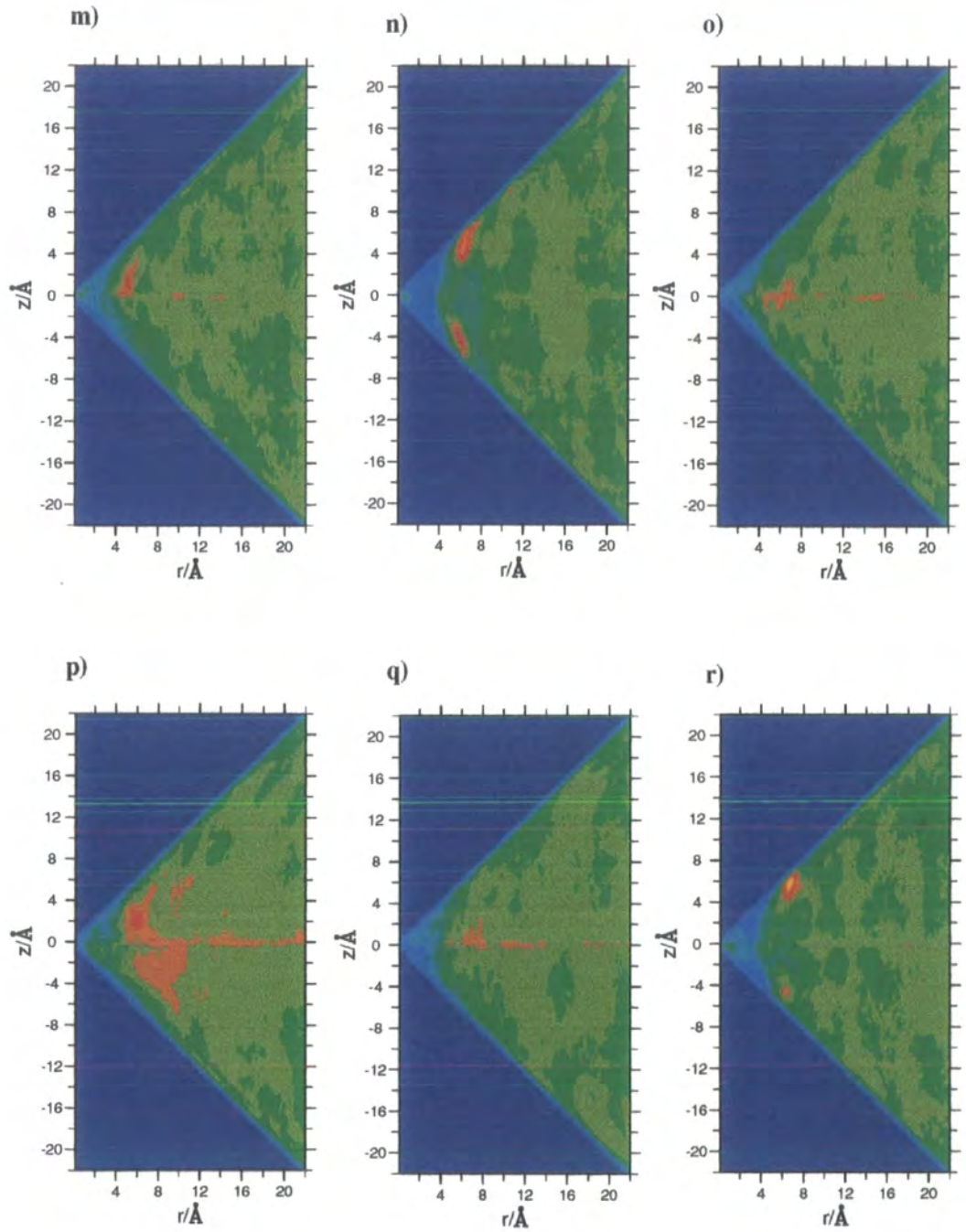
m)
n)
o)
p)
q)
r)
z/Å
r/Å
20
16
12
8
4
0
-4
-8
-12
-16
-20
4
8
12
16
20

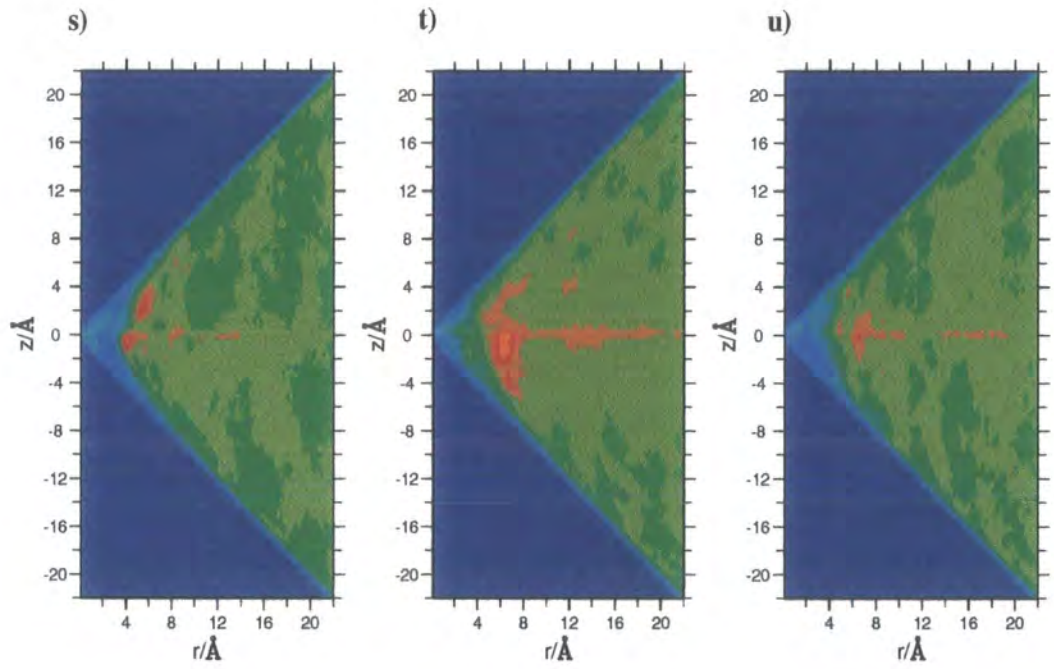

Figure 5.23: Two-dimensional correlation functions for individual groups in molecule GGP5Cl at T=393 K. (a) C-Cl—C-Cl, (b) C-F_1—C-F_1, (c) C-F_2—C-F_2, (d) phenyl$_1$—phenyl$_1$, (e) phenyl$_2$—phenyl$_2$, (f) phenyl$_3$—phenyl$_3$, (g) C-Cl—C-F_1, (h) C-Cl—C-F_2, (i) C-Cl—phenyl$_1$, (j) C-Cl—phenyl$_2$, (k) C-Cl—phenyl$_3$, (l) C-F_1—C-F_2, (m) C-F_1—phenyl$_1$, (n) C-F_1—phenyl$_2$, (o) C-F_1—phenyl$_3$, (p) C-F_2—phenyl$_1$, (q) C-F_2—phenyl$_2$, (r) C-F_2—phenyl$_3$, (s) phenyl$_1$—phenyl$_2$, (t) phenyl$_1$—phenyl$_3$, (u) phenyl$_2$—phenyl$_3$.

group interactions	r/Å	z/Å	configurations
C-CN—C-CN	4	0	A (strong correlation)
	8	0	A (secondary, weak)
	8	7	B (strong correlation)
C-F—C-F	4	0	A (strong correlation)
	6.5	0	A (secondary, weak)
ester—ester	7–10	0	A (secondary, weak)
	8	-7	E
$phenyl_1$—$phenyl_1$	7	6.5	B (strong correlation)
$phenyl_2$—$phenyl_2$	8.5	0	A (secondary, weak)
	7	5–6	B (weak)
	7	-6	D
$phenyl_1$—$phenyl_2$	5–6	0	B, D
	9.5	0	B, D (secondary)
	8	6	A
C-CN—C-F	9	0	A (secondary)
C-CN—ester	4	-2	E (strong correlation)
	9–12	0	B, C(secondary, weak)
	7–8	5–6.5	B (strong correlation)
C-CN—$phenyl_1$	4	-1	E (weak)
	8	0	B (secondary, weak))
C-CN—$phenyl_2$	4	-1	D (strong correlation)
	8	0	D (secondary)
	12	0	D (secondary)
ester—$phenyl_1$	5	0	C (weak)
	7	0	C (secondary, weak)
	11	0	C (secondary, weak)
	8	5	A (weak)
ester—$phenyl_2$	5	-3	D (weak)
	7.5	6.5	B
C-F—ester	4	-1	C (strong correlation)
	9	0	B, C (secondary, weak)
	12	0	B, C (secondary weak)
C-F—$phenyl_1$	8–10	0	A (secondary, weak)
	8	4–6	B
	8	-2	C
	4.5	-0.5	E
C-F—$phenyl_2$	7	5.5	B
	6	-4	C (weak)
	8.5	0	B (secondary, weak)

Table 5.12: Approximate positions of the main peaks in the two dimensional translational correlation function $g(r, \pm|z|)$ for me5NF at 303 K. Positive values of z indicate parallel association and negative values of z indicate anti-parallel association. Column four indicates the pair configuration(s) from figure 5.22 which are responsible for each peak. ("Secondary" indicates a peak that arises from next nearest neighbour interactions.)

group interactions	r/Å	z/Å	configurations
C-Cl—C-Cl	5	-2–2	C, H (strong correlation)
$C\text{-}F_1$—$C\text{-}F_1$	4.5	-2	F
	7	6	A
$C\text{-}F_2$—$C\text{-}F_2$	4.5	-2	I
	7	6	A
$phenyl_1$—$phenyl_1$	4	0	C, E (strong correlation)
	7	0	C, E (secondary)
$phenyl_2$—$phenyl_2$	4	0	C
	8	0	C (secondary)
	7	5	A
$phenyl_3$—$phenyl_3$	7	-2–0	I
C-Cl—$C\text{-}F_1$	5	0	A, E
	6	3	B
C-Cl—$C\text{-}F_2$	6-10	0	(secondary)
	5.5	2	D
C-Cl —$phenyl_1$	6	0–2	C
	7	-6	E
C-Cl—$phenyl_2$	6	-3–0	H
	6	2	B
	7.5	5.5	A
C-Cl—$phenyl_3$	5.5	0	F (strong correlation)
	10	0	(secondary)
	6	-3	G (strong correlation)
	5.5	2	D
$C\text{-}F_1$—$C\text{-}F_2$	5.5	0	B
$C\text{-}F_1$—$phenyl_1$	4.5	1	A
	10	0	(secondary, weak)
$C\text{-}F_1$—$phenyl_2$	7	5	A
	7	-4	E
$C\text{-}F_1$—$phenyl_3$	4.5–7.5	0	B (weak)
$C\text{-}F_2$—$phenyl_1$	6	2	D
$C\text{-}F_2$—$phenyl_2$	7	0	(secondary)
$C\text{-}F_2$—$phenyl_3$	7	6	A (strong correlation)
	6.5	-5	G (weak)
$phenyl_1$—$phenyl_2$	4	-1	F
	8.5	0	(secondary, weak)
	6	2	A
$phenyl_1$—$phenyl_3$	6.5	-2–0	F, G
$phenyl_2$—$phenyl_3$	7	0	(secondary)

Table 5.13: Approximate positions of the main peaks in the two dimensional translational correlation function $g(r, \pm|z|)$ for GGP5Cl at 393 K. Positive values of z indicate parallel association and negative values of z indicate anti-parallel association. Column four indicates the pair configuration(s) from figure 5.23 which are responsible for each peak. ("Secondary" indicates a peak that arises from next nearest neighbour interactions.)

The major configurations are sketched in figure 5.24 for the me5NF and in figure 5.25 for the mesogen GGP5Cl and the assignment of peaks is carried out in column four of tables 5.12 and 5.13. (In figure 5.25 the fluorines have been drawn on opposite sides of the GGP5Cl molecule. However, it is known that there is a mixture of the two fluorine conformations that arise from rotation about the $phenyl_2$-$phenyl_3$ dihedral angle. This is considered in detail in section 5.8.6.)

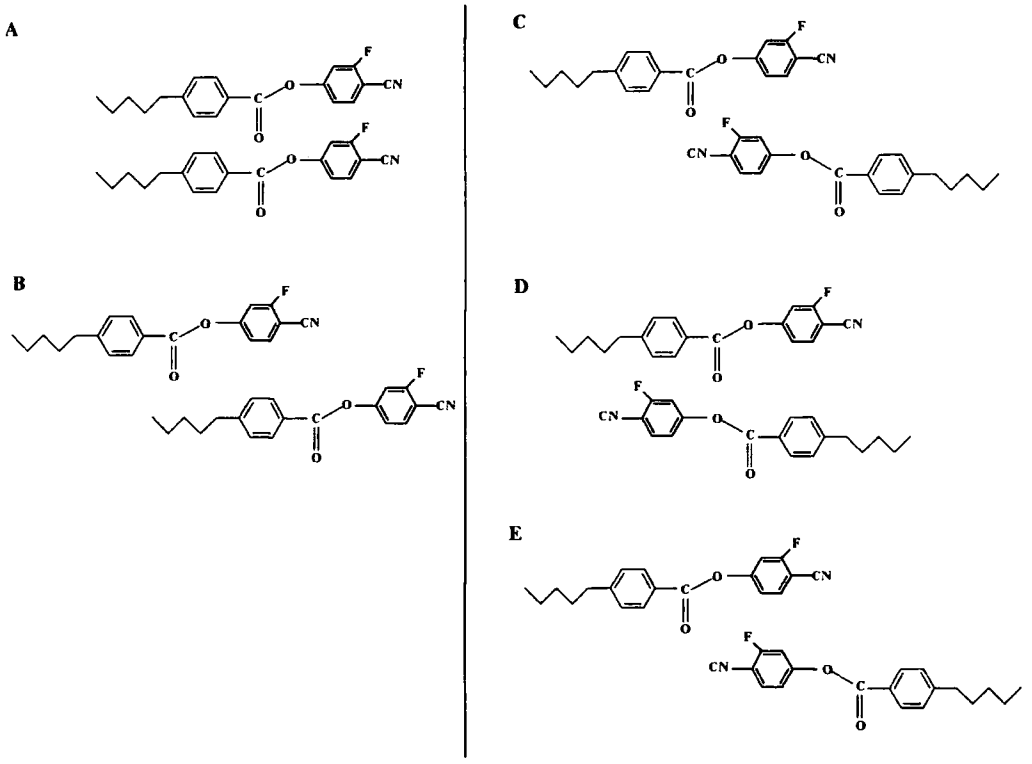

Figure 5.24: Schematic diagram showing molecular pair configurations for mesogen me5NF.

In me5NF the most favoured pair configurations are B and D indicating both parallel and anti-parallel dipole dimers. The regions of high probability density for me5NF result mainly from strong electrostatic interactions involving the cyano groups and the phenyl rings. In configurations B and D one should note the favourable quadrupolar interactions that arise from having $phenyl_1$ directly above $phenyl_2$. For a bare phenyl ring the component of the quadrupole moment perpendicular to the plane of the rings has a negative sign and consequently the centres of two parallel phenyl rings prefer to be shifted with respect to each other, rather than to be stacked directly on top of each other. (Alternatively, they pre-

fer a herringbone packing, as in the crystal structure of benzene.) However, the attachment of a fluorine and a cyano group to a phenyl ring changes the sign of the quadrupole moment perpendicular to the plane of the rings. Consequently, the quadrupolar interactions favour the parallel stacking of phenyl_1 and phenyl_2 directly above each other.

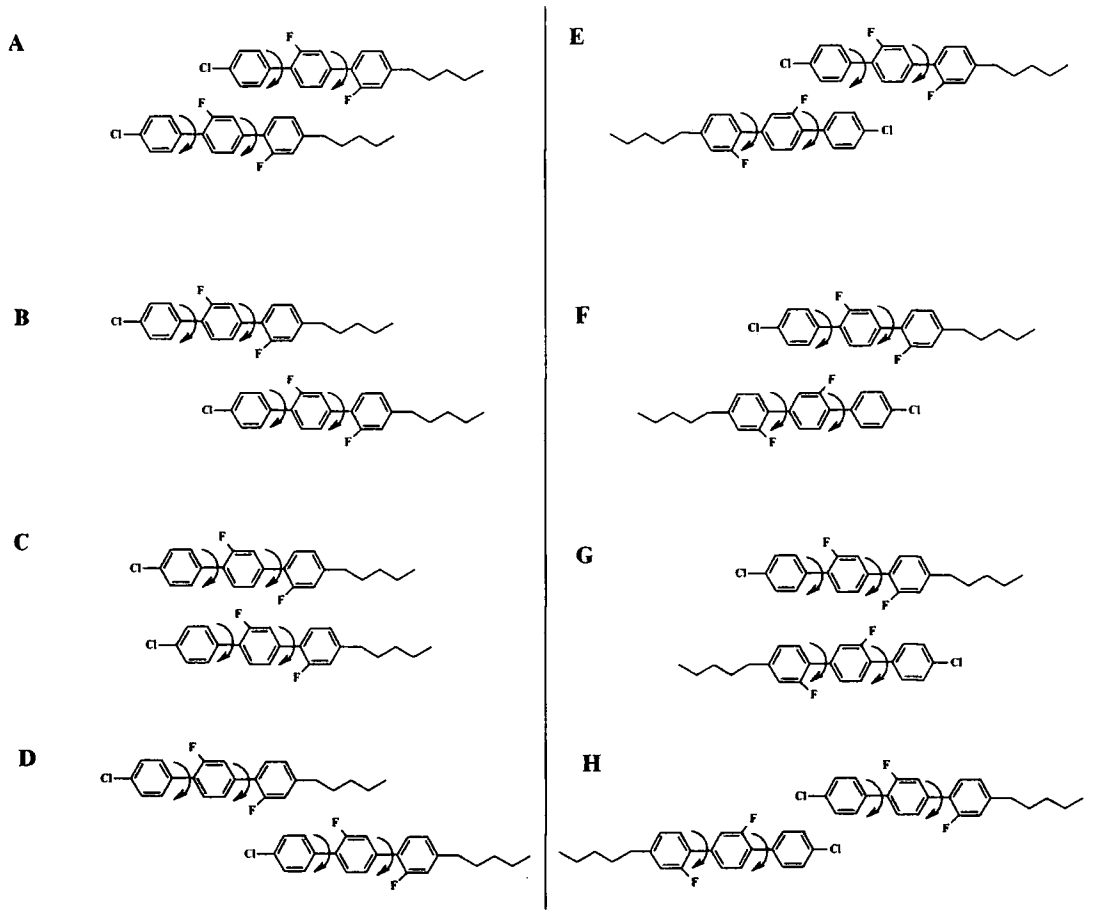

Figure 5.25: Schematic diagram showing molecular pair configurations for mesogen GGP5Cl.

In GGP5Cl, none of the favoured pair configurations shown in figure 5.25 are particularly dominant. This is most probably due to the absence of a single dominant electrostatic interaction (such as the phenyl_1-phenyl_2 quadrupole interaction in me5NF). Instead, a range of electrostatically favoured configurations are possible: parallel stacked fluorinated rings with the centre of one ring shifted slightly relative to the centre of the other ring, or stacked rings with the fluorines on opposite sides.

It should be noted that the picture of dipole correlation presented in this work is consistent with the theory of pairwise association of Dunmur and Toriyama [173]. The latter considers an equilibrium between parallel and anti-parallel dipole species and works well for dilute solutions of mesogens where there is molecular association to form transient dimers. However, in the liquid phase the situation is rather more complicated with evidence for several transient parallel and anti-parallel dimers, as well as some transient trimer species. Experimental dielectric measurements also provide strong evidence for coincident parallel and anti-parallel dipole association. Dunmur and Toriyama have presented experimental measurements for mesogens in solutions of isotropic [173, 174] or liquid crystalline solvents [182] that can be interpreted in terms of the pairwise association model.

5.8.6 Arrangement of Fluorines in GGP5Cl

It is interesting to consider how the fluorines in the core of GGP5Cl are arranged with respect to each other and to other fluorines on neighbouring molecules in the fluid. To this end the distribution function for the phenyl$_2$-phenyl$_3$ inter-ring torsional angle (as shown in figure 5.26) has been calculated.

In gas phase *ab initio* calculations [183] a four-fold torsional potential with no preference for the fluorines being on either side of the molecule is observed. However, in the liquid phase (figure 5.26) the peaks at 138° and 222°, which correspond to the fluorines on opposite sides of the molecule, are larger than those at 39° and 320°, which correspond to the fluorines on the same side of the molecule. An intramolecular preference for an anti-parallel arrangement of the transverse components of the dipole moment is therefore seen. To examine how fluorines on neighbouring molecules are oriented relative to each other, the distance dependent dipole correlation functions $g_1(r)$ (as defined by equation 5.6)were calculated for the C-F$_1$ and C-F$_2$ bonds and the cross correlation function involving the angle between C-F$_1$ and C-F$_2$ bonds, as plotted in figure 5.27. For all three functions one sees a sharp positive peak at short distances ($\approx$ 3 Å), a trough at slightly longer distances ($\approx$ 3.5 Å (C-F$_1$), 4 Å (C-F$_2$, C-F$_1$/C-F$_2$)) and a diffuse positive peak at $\approx$ 6.5 Å. The short distance peak is likely to correspond to configurations C, F and G for C-F$_1$ where two rings lie on top

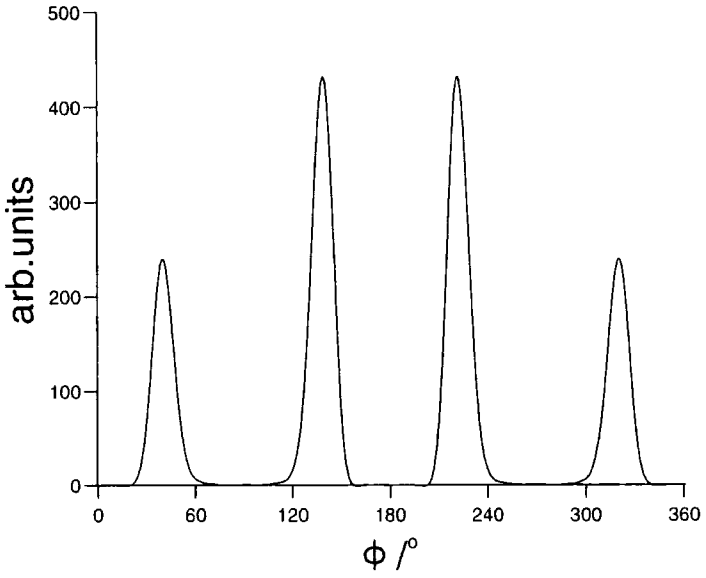

Figure 5.26: The phenyl$_2$–phenyl$_3$ inter-ring torsional angle in the pre-transitional isotropic/nematic region of GGP5Cl. (The zero of the torsional angle is defined when two coplanar fluorines are on the same side of the molecule.)

of each other, apart from a small offset in their positions. This is the lowest energy arrangement for two quadrupoles that are constrained parallel to each other. However, the trough and the diffuse positive peak arise from contributions involving a number of the configurations shown in figure 5.25.

5.9 Conclusions for me5NF and GGP5Cl

The calculations for me5NF and GGP5Cl, together with those given previously for PCH5 and PCH5-Cl, represent the most accurate all atom study of mesogenic molecules carried out to date. The different dipole-correlation behavior of me5NF and GGP5Cl has been successfully modelled. Excellent agreement between experimental and computed densities has been obtained for both mesogens. The computed g_1 value for me5NF is in excellent agreement with the experimentally determined value. The picture of dipole correlation in the bulk is seen to be extremely complicated. me5NF exhibits a preference for anti-parallel dipole association as seen through the distance dependent correlation function, $g_1(r)$. However, GGP5Cl shows no marked preference for parallel or anti-parallel dipole association. However, for both molecules, several parallel and anti-parallel dipole

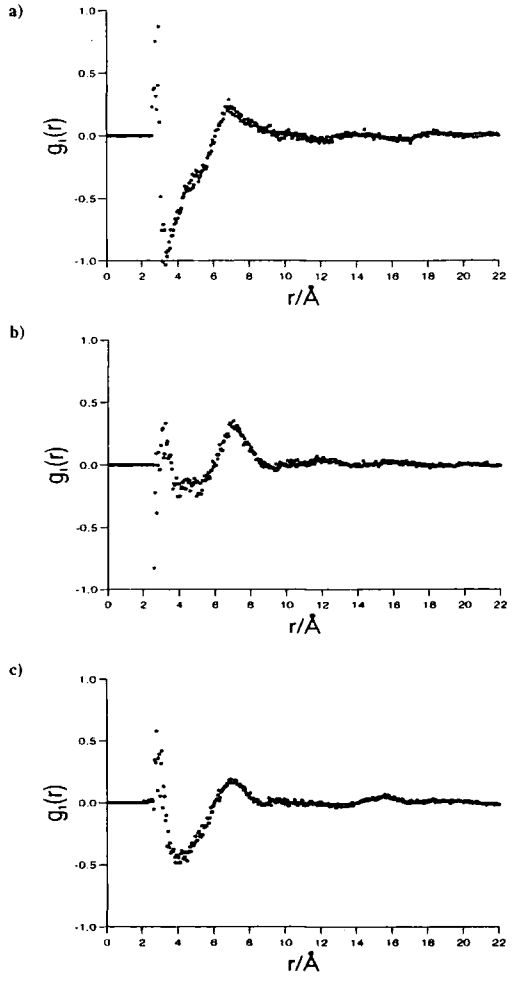

Figure 5.27: Distance dependent dipole correlation functions. a) C-F_1 bond, b) C-F_2 bond, c) cross correlation function for the C-F_1 and C-F_2 bonds.

dimers can be detected in addition to some trimers. Extensive analysis of equilibrium molecular dynamics trajectories has also allowed the identification of the groups that were responsible for the stabilisation of these interactions. Interactions between quadrupoles on aromatic rings appear to be extremely important in stabilising particular pair configurations. However, it is evident that small changes in molecular structure could easily influence the balance of which pair configurations are most favoured. It is therefore, difficult to use these calculations directly in molecular engineering applications to suggest ways of stabilizing pair configurations that would lead to large effective dipole moments in the bulk.

The current study has also examined the relative orientations of the two fluorines on separate phenyl rings, and in the case of GGP5Cl an intra-molecular

preference for an anti-parallel arrangement of the dipoles is seen. The intermolecular correlation between C-F bond orientations is a complicated one and evidence is seen for both parallel and anti-parallel dipole correlation at different distances.

Finally, as discussed in section 5.5 for PCH5 and PCH5-Cl proper handling of long range contributions to the forces and potential using an Ewald sum (or method of equivalent accuracy) is essential to ensure that these interactions are correctly handled in simulations of this type. In addition, it is likely that the absence of any force field terms that are capable of modelling polarization effects in GGP5Cl, leads to inaccuracies in determining the correct balance of anti-parallel and parallel dipole dimers in this highly polarizable material. The absence of these terms is likely to be responsible for the discrepancy between calculated and experimental values of g_1.

Due to the molecules increased length the calculations described here required larger system sizes compared to the earlier work on the molecules PCH5 and PCH5-Cl. Therefore these calculations are slower and require the equivalent of 2200 CPU hours on state-of-the-art processors. However, we expect rapid advances in computer speed to greatly increase the accessibility of such calculations within the next few years.

CHAPTER

6

Calculation of the rotational viscosity γ_1 of nematic liquid crystals

6.1 Introduction to viscosity in liquid crystals

From its definition a liquid crystal mesogen would be expected to have a higher viscosity than an isotropic fluid. Indeed, this is the case, because in a nematic liquid crystal the translational motion of the fluid is coupled with the orientational motion of the director. Therefore, the flow properties exhibited by a nematic liquid crystal are remarkably different from those of an ordinary fluid [184].

Most of the hydrodynamic effects observed in nematic liquid crystals are explained by the Leslie-Ericksen (LE) theory [185–188], which has more recently been renamed the Leslie-Ericksen-Parodi (LEP) theory. According to this theory the viscosity coefficients of a uniaxial nematic liquid crystal can be calculated from a correlation function of the stress tensor, σ_{ij} and the director, $\mathbf{n}$. The vis-

cous part of the stress tensor is given by [189]

$$\sigma_{ij} = \alpha_1 n_i n_j V_{kp} + \alpha_2 n_j N_i + \alpha_3 n_i N_j + \alpha_4 V_{ij} + \alpha_5 n_j V_{ik} n_k + \alpha_6 n_i V_{jk} n_k, \quad (6.1)$$

where n_i, n_j, and n_k are components of the director, α_{1-6} are the Leslie coefficients and V_{kp}, V_{kp}, V_{ij}, V_{ik} and V_{jk} are vector components of the velocity gradient tensor, $\boldsymbol{V}$. The symmetric component of the velocity gradient tensor is defined in equation 6.2

$$V_{ij} = \frac{1}{2}(v_{i,j} + v_{j,i}). \quad (6.2)$$

$\boldsymbol{N}$ is the rotation of the director relative to the fluid

$$N = \dot{n}_i - \frac{1}{2}(v_{i,j} + v_{j,i})n_j, \quad (6.3)$$

where $\dot{n}_i$ is the first derivative of the ith component of the director and $v_{i,j}$ and $v_{j,i}$ are components of the vector, V_{ij}, (in equation 6.2) defining the velocity gradient tensor.

In the Leslie-Ericksen theory there are 6 Leslie coefficients, α_1 to α_6. These Leslie coefficients are considered as material constants of the stress tensor, and are assumed to be independent of the velocity gradient and time; they do, however, depend on the pressure and temperature. All the Leslie coefficients must be known if the Leslie-Ericksen equations are to be used to calculate the director rotations and the flow phenomena of liquid crystals.

More recently it has been shown that four of the Leslie coefficients can be related to one another via the Parodi equation [190] (equation 6.4), hence the new name Leslie-Ericksen-Parodi theory.

$$\alpha_2 + \alpha_3 = \alpha_6 - \alpha_5. \quad (6.4)$$

Therefore, experimentally the viscous properties of a nematic liquid crystal can be described by five independent coefficients.

6.1.1 Shear viscosity coefficients

Figure 6.1 shows a schematic diagram which indicates how the director orientates with respect to the flow velocity and the velocity gradient, under shear flow. In the following discussion figure 6.1 will be used to indicate how the shear viscosity coefficients of a nematic liquid crystal are calculated.

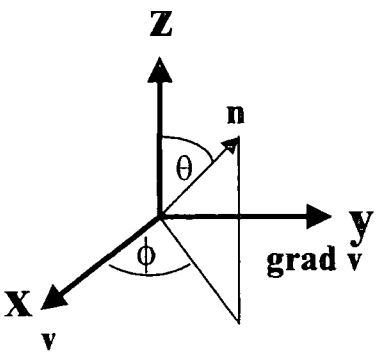

Figure 6.1: Director orientation with respect to the flow velocity **v**, and the velocity gradient.

If a nematic liquid crystal flows parallel to the x-axis, and the velocity gradient is parallel to the y-axis, then the orientation of the director, **n**, is described in terms of the polar angles θ and ϕ.

$$\mathbf{n} = (\sin\theta\cos\phi, \sin\theta\sin\phi, cos\theta) \tag{6.5}$$

Assuming the velocity is only a function of y, then the only non-vanishing parts of the velocity gradient tensor (equation 6.2) are

$$V_{xy} = V_{yx} = \frac{1}{2}v_{x,y}. \tag{6.6}$$

If the orientation of the director is fixed by the application of an electric or magnetic field then the rotation of the director given by equation 6.3 is reduced to

$$\boldsymbol{N} = \frac{1}{2}(-\sin\theta\sin\phi, \sin\theta\cos\phi, 0)v_{x,y}. \tag{6.7}$$

However, if the nematic liquid crystal is then sheared between two infinite parallel plates in the xz-plane, a constant velocity gradient parallel to the y-axis results. Assuming stationary flow, the σ_{xy} component of the stress tensor can be calculated using equations 6.1, 6.3, 6.6 and 6.7. By collecting all the terms with the same dependence on the director orientation together one derives a viscosity, η,

$$\begin{aligned}\eta(\theta,\phi) &= \frac{1}{2}(\alpha_4+\alpha_5-\alpha_2)\sin^2\theta\sin^2\phi \\ &+ \frac{1}{2}(\alpha_4+\alpha_6+\alpha_3)\sin^2\theta\cos^2\phi \\ &+ \frac{\alpha_3}{2}\sin^2\theta\cos^2\phi \\ &+ \frac{\alpha_4}{2}\cos^2\theta \\ &+ \alpha_1\sin^4\theta\cos^2\phi\sin^2\phi.\end{aligned} \tag{6.8}$$

On examining equation 6.8, it makes sense to introduce a new set of viscosity coefficients, η_1, η_2, η_3 and η_{12}, which will replace the Leslie coefficients α_1 to α_6, to describe the shear viscosity of an incompressible nematic liquid crystal.

$$\begin{aligned}\eta_1 &= \frac{1}{2}(\alpha_4+\alpha_5-\alpha_2) \\ \eta_2 &= \frac{1}{2}(\alpha_4+\alpha_6+\alpha_3) \\ \eta_3 &= \frac{1}{2}\alpha_4 \\ \eta_{12} &= \alpha_1\end{aligned} \tag{6.9}$$

The anisotropic shear viscosities are schematically illustrated for a nematic liquid crystal phase, with a velocity gradient, in figure 6.2. Each molecule is representative of a specific orientation. The director can be aligned along any axis of the co-ordinate system, depending on the packing density of the system and other parameters of the molecule. Generally three different shear viscosities, η_1, η_2 and η_3 result for the three axes. Their magnitude depends on the relative orientation of the flow pattern to the director orientation. These three shear viscosity coefficients can be determined separately from shear flow experiments with adequate director orientations. However, a further viscosity coefficient, η_{12}, has to be

taken into account if the director lies in the shear plane and is neither parallel to the flow velocity nor parallel to its gradient. The coefficient η_{12} is usually small in comparison with η_1 and η_2, but determination of η_{12} is more complicated as it requires at least three experiments. Two for the determination of η_1 and η_2 and one experiment with a director orientation where the influence of η_{12} on the shear viscosity is maximal ($\theta = 90^0$ or $\theta = 45^0$). Several notations for the shear viscosity coefficients have been suggested. The notation used here stems from Helfrich [191]. However, a different notation was proposed by Miesowicz [192].

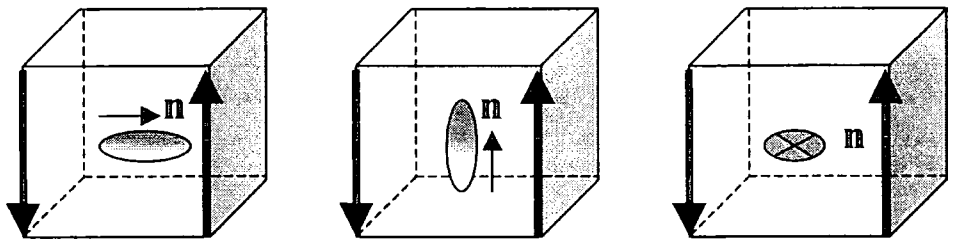

Figure 6.2: Schematic representation of the shear viscosities, η_1, η_2 and η_3. Where the director is: a) perpendicular to the flow pattern but parallel to the velocity gradient, b) parallel to the flow pattern but perpendicular to the velocity gradient, and c) both perpendicular to the flow and the gradient.

6.1.2 Rotational viscosity coefficient

In addition to the shear flow viscosities there is also another viscosity coefficient termed the rotational viscosity, γ_1. This arises due to viscous torques, M, being exerted on the director of a liquid crystal sample during a rotation of the director at an angular velocity, $\dot{\phi}$, and is given by equation 6.10,

$$M = \gamma_1 \dot{\phi} V. \tag{6.10}$$

The rotational viscosity is an extremely important quantity for the dynamical switching behaviour required in display devices. A large number of nematic liquid crystal display devices are currently in production and hence the measurement of the rotational viscosity coefficient is of great practical importance in establishing

efficient device design. The characteristic property of a nematic liquid crystal phase that is most important for display devices is the materials switching time. This is the time taken for the liquid crystal to relax after the applied voltage is removed (t_{off}) or likewise, the time taken to switch on the liquid crystal display when a voltage is applied (t_{on}). The switching times, for example, of a twisted nematic display are given by the expressions in equations 6.11 and 6.12.

$$t_{on} = \frac{\gamma_1 d^2}{\epsilon_0 \Delta\epsilon}(U^2 - U_0^2)^{-1} \tag{6.11}$$

$$t_{off} = \frac{\gamma_1 d^2}{k\pi^2}. \tag{6.12}$$

Here, k is a function dependent on the elastic constants of the material, U is the applied voltage, U_0 is the threshold voltage, ϵ_0 is the vacuum dielectric permittivity, $\Delta\epsilon$ is the dielectric anisotropy and d is the spacing of the electrodes.

Although other nematic liquid crystal displays have different expressions for the switching times [193], t_{on} in equation 6.11 and t_{off} in equation 6.12, they are all dominated by the rotational viscosity coefficient. Hence, the rotational viscosity coefficient is one of the most important material properties of liquid crystals for electro optical applications.

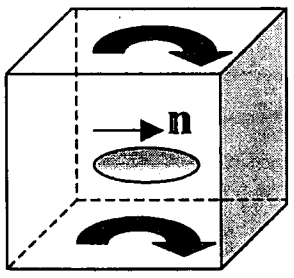

Figure 6.3: Schematic representation of the rotational viscosity γ_1.

A schematic representation of the rotational viscosity is given in figure 6.3, and it can be visualised as the rotation around an axis perpendicular to the director. In display devices this particular type of motion takes place when the orientation

of the liquid crystal molecules is changed from planer (with the director parallel to the boundary surface) to the corresponding homeotropic configuration due to a voltage being applied or removed.

6.2 Determination of the rotational viscosity of nematic liquid crystals

Unlike the shear viscosity coefficients, where several experimental methods are now well established [194], the rotational viscosity coefficient of even the most simple liquid crystal molecules are difficult to obtain experimentally. A number of experimental techniques are discussed briefly in section 6.2.1 whilst some computational techniques for calculating γ_1 are considered in section 6.2.2. Despite the availability of a number of experimental and computational techniques for determining γ_1 there is still a desire to develop new, simple and more accurate techniques for nematic liquid crystals.

6.2.1 Experimental methods of calculating γ_1

Several experimental methods have been proposed for measuring the rotational viscosity of liquid crystals. One simple method, that does not require expensive experimental setups, is the transient displacement current method [195–199], which involves the application of a dc voltage to a nematic liquid crystal cell. The rotational viscosity is evaluated from the displacement current by a simple analysis technique which employs a torque-balance equation approach. However, this method is not applicable to cells with low resistivity as the conduction current is negligable.

Alternatively, mechanical methods can be used to obtain γ_1. Such methods involve applying a rotating electrical [200] or magnetic field, H, [201] to a suspended nematic liquid crystal sample. The torque, M, exerted on the director by the field is

$$M = \frac{1}{2}\mu_0 \chi_a H^2 V \sin 2(\psi - \phi), \tag{6.13}$$

where χ_a is the anisotropy of the magnetic susceptibility. (This method is only suitable for nematic liquid crystals which have a positive magnetic anisotropy because the director will finally evade to the direction of the rotation axis in materials that possess a negative magnetic anisotropy.) Under stationary conditions and small angular velocities of the field, the director will follow the rotation of the field with a constant phase lag $(\psi - \phi)$. However, eventually the viscous and magnetic torque become equal giving

$$\gamma_1 \dot{\phi} = \frac{1}{2}\mu_0 \chi_a H^2 V \sin 2(\psi - \phi). \tag{6.14}$$

Increasing the angular velocity of the rotating field increases the phase lag between the field and the director, until the maximum torque is exerted at a phase lag of $\pi/4$. The corresponding angular velocity is termed the *critical angular velocity*, $\dot{\phi}_c$,

$$\dot{\phi}_c = \frac{\mu_0 \chi_a H^2}{2\gamma_1}. \tag{6.15}$$

Measuring the torque (via the twisting of the suspension wire) on a sample of a nematic liquid crystal in a field rotating with an angular velocity smaller than the critical one represents a relatively simple method for the determination of the rotational viscosity coefficient [202].

Rotational viscosities can also be measured experimentally using director relaxation methods. Here, a non-equilibrium orientation of the director is produced and the time constant for the relaxation to equilibrium is determined. A director deformation can be induced by the application of a magnetic [203] or electric field [204], and the relaxation process can be followed using optical methods or by dielectric constant measurements. In these methods the director is usually orientated at the beginning of the experiment by a magnetic or electric field. After switching off the field the relaxation time, τ, of the director back to equilibrium is monitored [205–208]. A measurement of τ gives the rotational viscosity

$$\tau = \frac{2\gamma_1}{\mu_0 \chi_a H^2}. \tag{6.16}$$

6.2.2 Computational methods of determining γ_1

Recently, with the development of high powered super computers, the doors have opened to simulation studies of transport properties of complex molecular fluids. Such studies have provided a greater understanding of the influence that molecular architecture has upon the transport properties in materials such as nematic liquid crystals.

In nematic liquid crystals there are basically two known methods of obtaining numerical estimates of the rotational viscosity for molecular model systems, both of which require molecular dynamics simulations. The first group of methods are based upon real experimental setups, which are described in section 6.2.1. Atsutaka Manabe [209] has measured γ_1 for a model system of the mesogen PCH5. The technique employed involves coupling an external field to the liquid crystal and allowing the director to relax back to equilibrium in a technique that is analogous to the director relaxation experiment described in section 6.2.1. This method is promising, although there is one major problem, in that the external field influences the order parameter and this in turn affects the value of γ_1.

A different approach is to employ a non-equilibrium molecular dynamics simulation (NEMD) technique, which has been proposed by Sarman and Evans [49–52, 210–213]. Here, the director is constrained using a Gaussian constraint algorithm at an angle to the flow field, and the rotational viscosity is calculated directly by evaluating the Green-Kubo relations. Whilst this method is relatively inexpensive it has two major drawbacks. Both the confining of the director using a director constraint algorithm and the application of Lees-Edwards boundary conditions [214] are extremely difficult to implement, particularly for flexible molecules.

Alternatively, standard equilibrium molecular dynamics simulations (EMD) can be performed. With this technique the rotational viscosity is still calculated by evaluating the Green-Kubo relations. In this method, however, there is no need to confine the director using a constraint algorithm or implement complex boundary conditions as γ_1 is not calculated directly from the Green-Kubo relations but instead is evaluated by analysing the fluctuations of the director trajectories during the course of the simulation. Two methods are suggested by Sarman and

Evans for calculating γ_1 using equilibrium molecular dynamics. The first method involves calculating the director angular velocity autocorrelation function, which is given by equation 6.17

$$\frac{1}{\gamma_1} = \frac{V}{2k_BT}\int_0^\infty \langle \Omega(t) \cdot \Omega(0) \rangle \, dt. \tag{6.17}$$

where V is the volume of the system, k_B is the Boltzmann constant, T is the temperature, $\Omega(t)$ is the angular velocity of the director at a time t and $\Omega(0)$ is the angular velocity of the director at a time zero.

The second and the simplest method involves calculating the mean square displacement of the director using equation 6.18

$$\frac{1}{\gamma_1} = \frac{V}{k_BT}\mathrm{lim_{t\to\infty}lim_{v\to\infty}}\frac{(\mathbf{n(t)} - \mathbf{n}(0))^2}{4\mathrm{t}}. \tag{6.18}$$

where V is the volume of the system, k_B is the Boltzmann constant, T is the temperature, $\mathbf{n}(t)$ is the director orientation at a time t and $\mathbf{n}(0)$ is the director orientation at a time zero.

6.3 Simulation details

In this work a simple liquid crystalline simulation model is employed, which is based on the well-known Gay-Berne potential [29]. The use of axially symmetrical particles described by a simple potential means that the number of pair interaction is small and thereby the computation time required is decreased compared to fully atomistic systems. The form of the Gay-Berne pair potential employed, is that studied by de Miguel *et al.* [43] (see chapter 3 section 3.3.1). Quantitative values of γ_1 are obtained using the two different equilibrium molecular dynamics simulation techniques described in section 6.2.2. Both methods rely purely, on monitoring the director fluctuations over a period of time. Equilibrium molecular dynamics simulations were carried out on two Gay-Berne systems of differing size, in order to assess the system size dependency of the rotational viscosity. Results for both systems, employing the two different methods, are presented in section 6.3.2.

6.3.1 Methodology

An initial nematic molecular configuration was generated from a *bcc* lattice in which 256 Gay-Berne molecules were given a small random displacement from their lattice positions and randomly orientated inside a cuboidal simulation box at a Gay-Berne reduced density of $\rho^* = 0.32$. After a period of equilibration, initial simulations were carried out in the NVE ensemble at a temperature of 400 K. These conditions ensured that the system was well inside the nematic phase (see phase diagram in section 3.3.1), and this was confirmed by measuring the nematic order parameter which had a value of approximately 0.64. The simulation retained cubic periodic boundary conditions throughout and the equations of motion were solved using the leap frog algorithm [79] with an integration time-step of 1 fs. Two production runs were executed, one for each of the two methods used for calculating the rotational viscosity. For the rotational viscosity calculated from the mean square displacement of the director the production run required 10000000 steps with a collection of the co-ordinate data every 1000 steps. However, the calculation of the rotational viscosity via the director angular velocity autocorrelation function required a production run of 100000 steps with the co-ordinate data collected every step. Following these initial simulations the 256 Gay-Berne system was doubled up in the x, y and z direction in order to create a new configuration of 2048 Gay-Berne particles. After a period of equilibration, two production runs were performed under the same simulation conditions. The latter calculation was carried out in order to investigate the system size dependency of the rotational viscosity calculated by both methods. All calculations used the molecular dynamics program, GBMOL [215].

The angular velocity autocorrelation function

In order to calculate the rotational viscosity coefficient via the angular velocity autocorrelation function technique the following steps must be taken;

- Calculate the director $\mathbf{n}$. In a nematic liquid crystal the unit eigenvector corresponding to the largest eigenvalue of the order tensor, $\mathbf{Q}_{\alpha\beta}$ (chapter 5 section 5.4.3) is termed the director.

- Make sure the director does not flip during the course of the simulation.
- Calculate the first derivative of the director $\dot{\mathbf{n}}$.
- Calculate the angular velocity, $\boldsymbol{\Omega}$, where $\boldsymbol{\Omega} = \mathbf{n} \times \dot{\mathbf{n}}$.
- Ensure that the calculation is performed in the director fixed frame. This is carried out by multiplying $\boldsymbol{\Omega}$ by an eigenvector rotation matrix which transforms it to the director fixed frame.

The three eigenvectors defining the position of the director in the director fixed frame are;

$$\begin{aligned} \mathrm{u}_1 &= (\mathrm{u}_{1x}, \mathrm{u}_{1y}, \mathrm{u}_{1z}) \\ \mathrm{u}_2 &= (\mathrm{u}_{2x}, \mathrm{u}_{2y}, \mathrm{u}_{2z}) \\ \mathrm{u}_3 &= (\mathrm{u}_{3x}, \mathrm{u}_{3y}, \mathrm{u}_{3z}) \end{aligned} \tag{6.19}$$

Therefore, the angular velocity relative to the director fixed frame is given by the transformation,

$$\begin{pmatrix} \mathrm{u}_{1x}, \mathrm{u}_{1y}, \mathrm{u}_{1z} \\ \mathrm{u}_{2x}, \mathrm{u}_{2y}, \mathrm{u}_{2z} \\ \mathrm{u}_{3x}, \mathrm{u}_{3y}, \mathrm{u}_{3z} \end{pmatrix} \begin{pmatrix} \Omega_x \\ \Omega_y \\ \Omega_z \end{pmatrix} = \begin{pmatrix} \Omega'_x \\ \Omega'_y \\ \Omega'_z \end{pmatrix} = \begin{pmatrix} \Omega_1 \\ \Omega_2 \\ \Omega_3 \end{pmatrix} \tag{6.20}$$

- As a check $\Omega_3 = 0$.
- Make sure the new director, in director fixed frame has not flipped during the transformation.

The mean square displacement of the director

In this method the following steps must be taken:

- Calculate the director $\mathbf{n}$.
- Make sure the director does not flip during the course of the simulation.
- Calculate the displacement of the director in time $[\mathbf{n}(\mathrm{t}) - \mathbf{n}(0)]$.
- Calculate the mean squared displacement of the director in time $[\mathbf{n}(\mathrm{t}) - \mathbf{n}(0)]^2/2\mathrm{t}$.

6.3.2 Computational results

The graphs in figures 6.4a and 6.4b show plots of the director angular velocity autocorrelation function versus time for the two Gay-Berne systems containing 256 and 2048 molecules respectively. From equation 6.17 it is clear that a quantitative value of γ_1 can be obtained from the graphs presented in figure 6.4 by simply integrating the curve between times $t = 0$ and $t = \infty$. This yields a value which when multiplied by $(V/2k_BT)$, where V is the system volume, k_B is the Boltzmann constant and T is the temperature gives an exact value of γ_1.

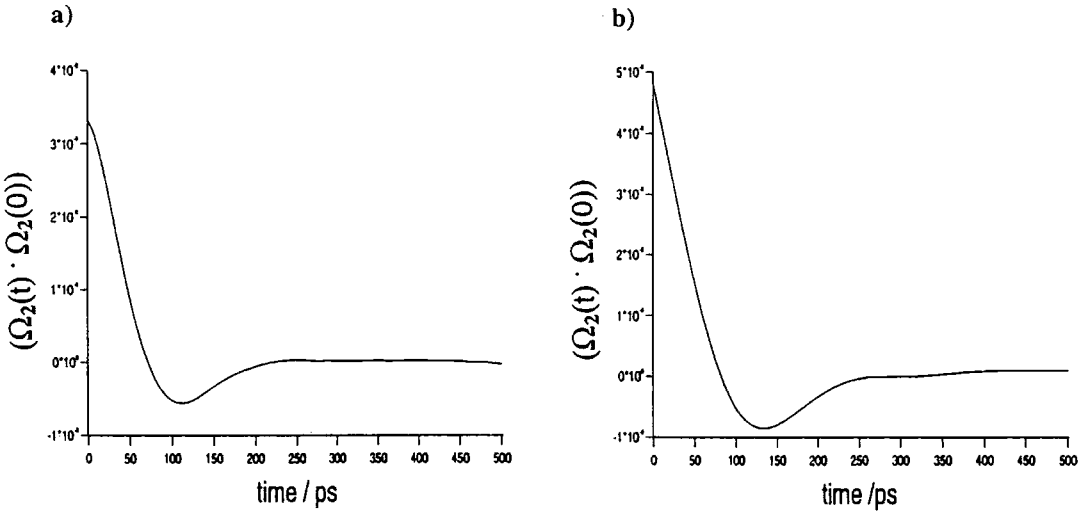

Figure 6.4: Graph showing the director angular velocity autocorrelation function for a) 256 Gay-Berne molecules and b) 2048 Gay-Berne molecules.

The graphs in figures 6.5a and 6.5b show plots of the mean squared displacement of the director in time for the two Gay-Berne systems containing 256 and 2048 molecules respectively. From equation 6.18 it follows that the rotational viscosity can be obtained from the gradient of the graph, which yields a value of $(4k_BT/V\gamma_1)$. Therefore, combining the gradient of the graph with the system volume V, the Boltzmann constant, k_B and the temperature, T, allows an exact value of the rotational viscosity coefficient to be determined for each of the model systems.

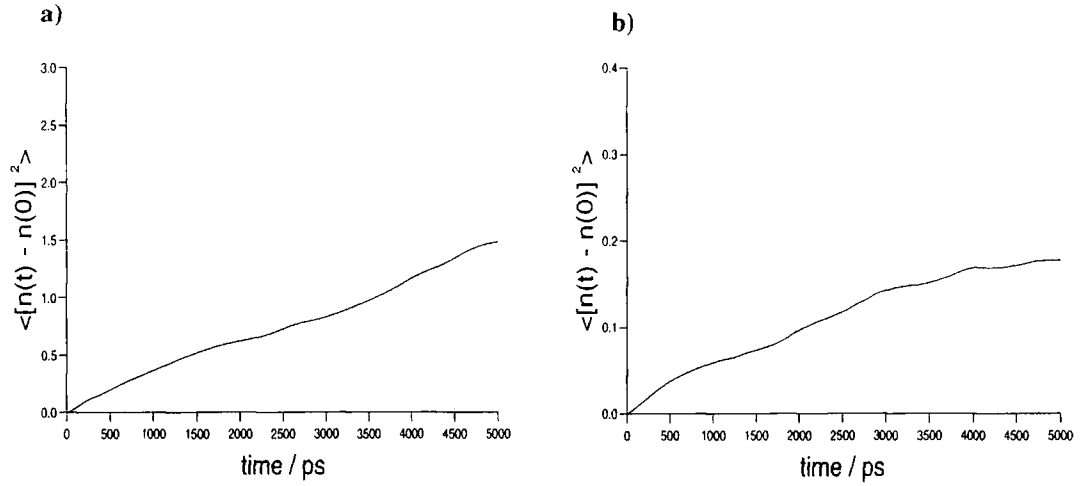

Figure 6.5: Graph showing the mean squared displacement of the director for a) 256 Gay-Berne molecules and b) 2048 Gay-Berne molecules.

Values of the rotational viscosity calculated using both analysis techniques are presented in table 6.1. The results show good agreement (better than 5%) between the values of γ_1 calculated using the two independent methods. There is also good agreement between the values of the rotational viscosity coefficients calculated for the two different system sizes. The values of γ_1, however, do vary slightly with the system size. Therefore, to be confident that system size effects do not significantly influence the overall computed results further simulations are required. The consistency between all the calculated values of γ_1 provides a good indication of the reliability of the two techniques employed.

System size	Volume /m^3	T /K	$< S_2 >$	angular velocity autocorrelation function /$Jm^{-3}s$	mean squared displacement /$Jm^{-3}s$
256	1.48×10^{-25}	400	0.64	1.96 ± 0.69	2.13± 0.32
2048	1.18×10^{-24}	400	0.64	2.00 ± 0.69	2.07± 0.40

Table 6.1: Comparison of computed values of γ_1 for two Gay-Berne systems of different sizes.

The rotational viscosity coefficients calculated in this study can be compared with the computed values of Sarman and the experimentally determined value for

PCH5 given in the literature. The values from this study given in table 6.2 are the average of the values given in table 6.1. The comparison between the various results is good.

System	T /K	γ_1 /Jm^{-3}s
PCH5[†]	298	1.99
GB(256)	400	2.05
GB(2048)	400	2.04
GB(256)Sarman[††]	100	1.60

[†] ref [49], [††] This value was calculated from NEMD.

Table 6.2: Comparison of computed values of γ_1 with experiment and other simulations.

6.4 Conclusions

In this work the rotational viscosity of a nematic liquid crystal system has been calculated using standard equilibrium molecular dynamics simulation methods. Two independent simulation methods (the director angular velocity function and the mean square displacement of the director) have been employed in order to evaluate γ_1 for a pure system of Gay-Berne particles. The results obtained from both these techniques are in good quantitative agreement with each other and consistent with other values of rotational viscosity calculated via simulation for other Gay-Berne systems (see table 6.2). An important advantage of these two methods over the non-equilibrium molecular dynamics technique is that there is no need to constrain the director.

The effects of system size dependency on these calculations have also been investigated by carrying out identical simulations on two model systems, containing 256 and 2048 molecules respectively. Again, the rotational viscosity coefficients compare well with one another, thus confirming the reliability and accuracy of the two independent techniques employed.

This current study describes only preliminary work in the calculation of the

rotational viscosity coefficient for nematic liquid crystal molecules via molecular simulation. However, they provide motivation for developing the technique further to allow the calculation of the rotational viscosity for fully atomistic models. In this work the simulations were carried out for two very simple models containing 256 and 2048 uniaxially symmetrical particles. Even so, these simulations still required the equivalent of $\approx$ 28 CPU hours for calculation of the director angular velocity autocorrelation function, and $\approx$ 264 CPU hours for the calculation of the mean square displacement of the director on state-of-the-art processors. At the present time this is reaching the limit of what can be achieved with a single workstation. Therefore, developing a fully atomistic simulation model is only computationally feasible at the present time on a super computer, since accurate calculations require proper handling of the long range forces which result in a heavy computational load. However, rapid advances in computer speed are expected to greatly increase the accessibility of such calculations within the next few years. This will allow the progress of many new novel simulation techniques, such as the one described in this work, to be employed in molecular engineering applications, thus allowing molecular properties to be determined prior to synthesis.

CHAPTER

7

Summary

The work presented in this thesis has been concerned with the study of molecular interactions of liquid crystal molecules. This work has been carried out in order to gain a better understanding of the complex area of structure-property relationships in liquid crystal chemistry. The questions asked have been: what interactions are present in liquid crystal molecules and how do these interactions lead to particular effects? The main investigative tool in these studies has been computer simulations incorporating atomistic force field potentials.

Computer simulations have been carried out in order to study a range of different liquid crystalline phenomena. The helical twisting power of liquid crystal chiral dopants is one such phenomenon. The method employed relies on Monte Carlo simulations of a fully atomistic model of a chiral dopant in the presence of a twisted nematic solvent composed of Gay-Berne particles. An advantage of the hybrid model used is that the simulated results are not only obtained on a sensible time scale but their values can be compared to real experimental data. Calculations were performed for eighteen different chiral dopant molecules, and the

helical twisting power values obtained were in good agreement with experimental measurements. The aim of this work was to develop a technique for calculating the helical twisting power that could eventually be used in a predictive sense. This was successfully achieved.

At the present time there is one major drawback to HTP calculations: the computational expense. In tackling this problem several interesting new avenues of research can be explored. Firstly, the Gay-Berne solvent potential could be replaced with a cheaper repulsive spherocylinder potential. It has been shown that the repulsive spherocylinder potential is approximately three times faster to simulate than the Gay-Berne potential. However, at the present time a full phase diagram for the former is not known. A second method would be to include both chiral solute molecules in the one simulation, growing one molecule whilst simultaneously shrinking the other. This could potentially provide a more accurate technique for calculating $\Delta\mu$, with fewer separate Monte Carlo simulations required for the mutation of one enantiomer into its mirror image.

Finally, the HTP calculations carried out in this thesis have been restricted to rigid chiral solute molecules. An interesting extension of this work would be to consider how the HTP values would change if the chiral solute molecules were represented as flexible entities. The introduction of molecular flexibility would undoubtably increase the complexity of the calculations, however, because each conformer would have a slightly different HTP value it is expected that the accuracy of the computed HTP would increase.

Another important area of investigation has been that of dipole correlation in the bulk phase. Calculations of the Kirkwood correlation factor, g_1, have been carried out for four very different molecules, PCH5, PCH5-Cl, me5NF and GGP5Cl, in the pre-transitional region of the isotropic phase. The molecular dynamics simulations performed represent the most accurate all atom studies of mesogenic molecules presented to date, and with the exception of GGP5Cl all the molecules produced results that confirm experimental dielectric measurements. The main source of error for the mesogen GGP5Cl was likely to be caused by the combination of highly polar and highly polarisable groups in the one molecule. In such circumstances polarisation effects are expected to be important. The neglect of such interactions in the LCFF used in this work means that it is

difficult to model this molecule as accurately as the others. For PCH5, and me5NF a preferential anti-parallel dipole alignment of the molecules in the bulk is observed, whereas, for the molecules PCH5-Cl and GGP5Cl a preferred parallel dipole alignment is observed. However, it must be stressed, that the picture of dipole correlation in the bulk was found to be extremely complicated. In the case of all four mesogens, several parallel and anti-parallel dipole dimers exist, in addition to some trimers. However, the computed picture of dipole correlation is consistent with the theory of pairwise association of Dunmur and Toriyama. Extensive analysis of the molecular dynamics trajectories, has allowed the identification of the molecular groups responsible for the stabilisation of the dipolar interactions. However, it is still extremely difficult to suggest ways of stabilizing pair configurations that would lead to large effective parallel dipole moments in the bulk.

Throughout this thesis fully atomistic force field models have been employed where computationally possible. Atomistic force field models represent the atoms by a series of potential energy functions whose parameters are chosen to represent *real* molecular systems as closely as possible. Common structural feature present in liquid crystal mesogens are, conjugated phenyl rings, lateral fluorination, ester group, alkyl chains and terminal dipolar groups. These are poorly modelled by existing literature and commercial force fields. In this thesis a new force field (LCFF) has been developed to model mesogenic molecules. New potential parameters were derived by fitting to quantum mechanical data, and the force field was tested by carrying out molecular dynamics simulations of liquid crystal fragments. These simulations yielded good densities and heats of vapourisation in comparison to experimental data.

A final area of interest in this thesis has been the calculation of rotational viscosities of nematic liquid crystal mesogens. Two different techniques have been employed, the mean squared displacement of the director and the director angular velocity autocorrelation function. Good agreement was obtained between the two different methods. This preliminary investigation provides a good basis for; a) a future study of how changes in molecular shape and attractive interactions (by varying the Gay-Berne potential) influence the rotational viscosities; b) future studies of γ_1 in fully atomistic mesogens.

Apart from purely academic interest, all the simulations presented in this thesis have potential applications in industry, especially in the area of molecular engineering. Atom based simulations of this kind are likely to become increasingly important, and will have major uses in the prediction of phases, phase transition temperatures and key material properties. With the knowledge and techniques already developed, coupled with ever increasing computer power, there is a promising future for *computer simulations of liquid crystals.*

BIBLIOGRAPHY

[1] F. Reinitzer, Montash. Chem. **9,** 421 (1888).

[2] F. Reinitzer, Ann. Physik. **27,** 213 (1908).

[3] O. Lehmann, Krist. **18,** 464 (1890).

[4] O. Lehmann, J. Phys. Chem. **56,** 750 (1906).

[5] O. Lehmann, J. Phys. Chem. **4,** 462 (1889).

[6] L. Gattermann and A. Ritschke, Ber. Dtsch. Chem. Ges. **23,** 1738 (1890).

[7] G. Friedel, Ann. Physique. **18,** 273 (1922).

[8] W. Maier and A. Saupe, Z. Nat. **A13,** 564 (1958).

[9] W. Maier and A. Saupe, Z. Nat. **A14,** 882 (1959).

[10] G. H. Heilmeier, L. A. Zanoni, and L. A. Barton, Appl. Phys. Lett **13,** 46 (1968).

[11] J. J. Wysocki, J. Adams, and W. Hass, Phys. Rev. Lett. **20,** 1024 (1968).

[12] M. Schadt and W. Helfrich, Phys. Rev. Lett. **18,** 127 (1971).

[13] D. G. McDonnell, *Thermotropic liquid crystals* (John Wiley and Sons, 1987).

[14] D. Coates, *Thermotropic liquid crystals* (John Wiley and Sons, 1987).

[15] P. J. Collings, *Liquid crystals* (John Wiley and Sons, 1990).

[16] P. J. Collings and M. Hird, *Introduction to liquid crystals* (Taylor and Francis, 1997).

[17] G. W. Gray and J. W. Goodby, *Smectic liquid crystals: Textures and Structures* (Leonard Hill, 1984).

[18] R. B. Meyer, L. Liebert, L. Strzelecki, and P. Keller, J. Phys. Chem. **36,** 69 (1975).

[19] S. Chandrasekhar, B. K. Sadashiva, and K. A. Suresh, Pramana. **7,** 471 (1977).

[20] J. W. Goodby, *Handbook of liquid crystals* (Wiley-VCH, 1998).

[21] H. Bengs, H. Finkelmann, J. Kupfer, H. Ringsdorf, and P. Schuhmacher, Macromolecules. Chem. Rapid. Commun. **14,** 445 (1993).

[22] S. Disch, H. Finkelmann, H. Ringsdorf, and P. Schuhmacher, Macromolecules. **28,** 2424 (1995).

[23] C. Zannoni, *The molecular physics of liquid crystals* (Academic Press, New York, 1979).

[24] R. Eppenga and D. Frenkel, Molec. Phys. **52,** 1303 (1984).

[25] M. P. Allen, G. T. Evans, D. Frenkel, and B. M. Mulder, *Adv. Chem Phys 86* (Wiley, 1993).

[26] M. P. Allen and D. J. Tildesley, *Computer simulations of liquids* (Oxford University Press, Oxford, 1987).

[27] D. A. Cheung, M. R. Wilson, and S. J. Clark, unpublished work.

[28] B. J. Alder and T. Wainwright, Phys. Rev. A **1,** 18 (1970).

[29] J. G. Gay and B. J. Berne, J. Chem. Phys. **74,** 3316 (1981).

[30] N. Metropolis, A. W. Rosenbluth, M. N. Rosenbluth, A. H. Teller, and E. Teller, J. Chem. Phys. **21,** 1087 (1953).

[31] A. R. Leach, in *Molecular Modelling Principle and Applications* (Longmans, 1996), Chap. 3.

[32] J. Vieillard-Baron, J. Chem. Phys. **56,** 4729 (1972).

[33] J. Vieillard-Baron, J. Chem. Phys. **28,** 809 (1974).

[34] A. L. Onsager, NY. Acad. Sci. **51,** 627 (1949).

[35] D. Frenkel and B. M. Mulder, Molec. Phys. **55,** 1171 (1985).

[36] J. A. C. Veerman and D. Frenkel, Phys. Rev. A **41,** 3237 (1990).

[37] J. Corner, Proc. R. Soc. Lond. A **192,** 275 (1948).

[38] B. J. Berne and P. Perchukas, J. Chem. Phys. **56,** 4123 (1972).

[39] A. J. Stone, *The molecular physics of liquid crystals* (Academic Press, New York, 1979).

[40] S. H. Walmsely, Chem. Phys. Lett. **49,** 320 (1977).

[41] A. L. Tsykalo and A. D. Bagmet, Molec. Cryst. Liq. Cryst. **46,** 111 (1977).

[42] M. Bates and G. R. Luckhurst, J. Chem. Phys. (1988).

[43] E. de Miguel, L. F. Rull, M. K. Chalam, and K. E. Gubbins, Molec. Phys. **74,** 405 (1991).

[44] G. R. Luckhurst, R. A. Stephens, and R. W. Phippen, Liq. Cryst. **8,** 451 (1990).

[45] R. Berardi, A. P. Emerson, and C. Zannoni, J. Chem. Soc. Faraday. Trans. **89,** 4069 (1993).

[46] J. Alejandre, J. W. Emsley, and D. J. Tildesley, J. Chem. Phys. **101,** 7027 (1994).

[47] M. P. Allen, M. A. Warren, M. R. Wilson, A. Sauon, and W. Smith, J. Chem. Phys. **105,** 2050 (1996).

[48] J. Stelzer, L. Longa, and H.-R. Trebin, J. Chem. Phys. **103,** 3098 (1995).

[49] S. Sarman and D. J. Evans, J. Chem. Phys. **99,** 9021 (1993).

[50] S. Sarman, J. Chem. Phys. **101,** 480 (1994).

[51] S. Sarman and D. J. Evans, J. Chem. Phys. **99,** 620 (1993).

[52] S. Sarman, J. Chem. Phys. **103,** 393 (1995).

[53] M. R. Wilson, *Handbook of liquid crystals* (Wiley-VCH, 1999).

[54] M. R. Wilson, *Liquid crystals 1: Structure and Bonding* (Springer, 1999).

[55] B. R. Gelin and M. Karplus, BIO **18,** 1256 (1979).

[56] B. R. Brooks, R. E. Bruccoleri, B. D. Olafson, D. J. States, S. Swaminathan, and M. Karplus, J. Comput. Chem. **4,** 187 (1983).

[57] U. C. Singh, P. K. Weiner, and P. A. Kollman, written at University of California, San Francisco, 1987. (unpublished).

[58] P. K. Weiner and P. A. Kollman, J. Comput. Chem. **2,** 287 (1981).

[59] S. J. Weiner, P. A. Kollman, D. T. Nguyen, and D. A. Case, J. Comput. Chem. **7,** 230 (1986).

[60] S. J. Weiner, P. A. Kollman, D. A. Case, U. C. Singh, C. Ghio, G. Alagona, S. Profeta, and P. Weiner, J. Am. Chem. Soc. **106,** 765 (1984).

[61] W. D. Cornell, P. Cieplak, C. I. Bayly, I. R. Gould, K. M. Merz, D. M. Ferguson, D. C. Spellmeyer, T. Fox, J. W. Caldwell, and P. A. Kollman, J. Am. Chem. Soc. **117,** 5179 (1995).

[62] T. A. Halgren, J. Comput. Chem. **17,** 490 (1996).

[63] T. A. Halgren, J. Comput. Chem. **17,** 520 (1996).

[64] T. A. Halgren, J. Comput. Chem. **17,** 553 (1996).

[65] T. A. Halgren and R. B. Nachbar, J. Comput. Chem. **17,** 587 (1996).

[66] T. A. Halgren, J. Comput. Chem. **17,** 616 (1996).

[67] W. L. Jorgensen and C. J. Swensen, J. Am. Chem. Soc. **107,** 569 (1985).

[68] W. L. Jorgensen and C. J. Swensen, J. Am. Chem. Soc. **107,** 1489 (1985).

[69] W. L. Jorgensen, D. S. Maxwell, and J. Tirado-Rives, J. Am. Chem. Soc. **118,** 11225 (1996).

[70] W. L. Jorgensen, J. Phys. Chem. **90,** 1276 (1986).

[71] W. L. Jorgensen and J. Tirado-Rives, J. Am. Chem. Soc. **110,** 1657 (1988).

[72] W. L. Jorgensen, J. Phys. Chem. **90,** 1276 (1986).

[73] N. L. Allinger, M. T. Tribble, M. A. Miller, and D. H. Wertz, J. Am. Chem. Soc. **93,** 1637 (1971).

[74] N. L. Allinger, J. Am. Chem. Soc. **99,** 8127 (1977).

[75] N. L. Allinger, Y. H. Yuh, and J. H. Lii, J. Am. Chem. Soc. **111,** 8511 (1989).

[76] N. L. Allinger, K. S. Chen, and J. H. Lii, J. Comput. Chem. **17,** 642 (1996).

[77] D. J. Cleaver, C. M. Care, M. P. Allen, and M. P. Neal, Phys. Rev. E **54,** 559 (1996).

[78] H. Goldstein, *Classical mechanics* (Addison-Wesley, Reading, 1980).

[79] R. W. Hockney, Phys. Rev. A **9,** 136 (1970).

[80] D. Fincham, CCP5 Quarterly. **2,** 6 (1981).

[81] D. Fincham, CCP5 Quarterly. **10,** 43 (1983).

[82] D. Fincham, CCP5 Quarterly. **12,** 47 (1984).

[83] J. P. Ryckaert, Molec. Phys. **55,** 549 (1985).

[84] K. Singer, A. Taylor, and J. V. L. Singer, Molec. Phys. **33,** 1757 (1977).

[85] J. P. Ryckaert, G. Ciccotti, and H. J. C. Berendsen, J. Chem. Phys. **23,** 327 (1977).

[86] H. C. Anderson, M. P. Allen, A. Bellemans, J. Board, J. H. R. Clarke, M. Ferrario, J. Haile, S. Nose, J. V. Opheusden, and J. P. Ryckaert, CECAM. **1,** 82 (1984).

[87] L. V. Woodcock, Chem. Phys. Lett. **10,** 257 (1971).

[88] H. J. C. Berendsen, J. P. M. Postma, W. F. van Gusteren, A. D. Nola, and J. R. Haak, J. Chem. Phys. **81,** 3684 (1984).

[89] S. Nosé, J. Chem. Phys. **53,** 255 (1984).

[90] P. G. de Gennes and J. Prost, in *The Physics of Liquid Crystals, 2nd edition* (Oxford University Press, 1993), Chap. 6.

[91] P. van de Witte, E. E. Neuteboom, M. Brehmer, and J. Lub, J. Appl. Phys. **85,** 7517 (1999).

[92] H. Yang, H. Yamane, H. Kikuchi, H. Yamane, G. Zhang, X. F. Chen, and K. Tisato, J. Appl. Polymer Science **73,** 623 (1999).

[93] C. Stützer, W. Weissflog, and H. Stegmeyer, Liq. Cryst. **21,** 557 (1996).

[94] S. N. Yarmolenko, L. A. Kutulyas, V. V. Vashchenko, and L. V. Chepeleva, Liq. Cryst. **16,** 877 (1994).

[95] M. P. Allen, Phys. Rev. E **47,** 4611 (1993).

[96] M. P. Allen and A. J. Masters, Molec. Phys. **79,** 277 (1993).

[97] P. J. Camp, Molec. Phys. **91,** 381 (1997).

[98] D. A. Pearlman and B. G. Rao, in *Encylopedia of Computational chemistry* (1988), p. 1036.

[99] W. L. Jorgensen, in *Encylopedia of Computational chemistry* (1988), p. 1060.

[100] A. E. Mark, in *Encylopedia of Computational chemistry* (1988), p. 1070.

[101] A. R. Leach, in *Molecular Modelling Principle and Applications* (Longmans, 1996), Chap. 9.

[102] M. Mezei and D. L. Beveridge, Ann. N. Y. Acad. Sci **482,** 1 (1986).

[103] R. W. Zwanzig, J. Chem. Phys. **22,** 1420 (1954).

[104] C. H. Bennett, J. Comput. Phys. **22,** 245 (1976).

[105] W. L. Jorgensen and C. Ravimohan, J. Am. Chem. Soc. **83,** 3050 (1985).

[106] D. A. Pearlman and P. A. Kollman, J. Chem. Phys. **91,** 7831 (1989).

[107] J. Hermans, J. Phys. Chem. **95,** 9029 (1991).

[108] M. J. Mitchell and J. A. McCammon, J. Comput. Chem. **12,** 271 (1991).

[109] T. P. Straatsma and J. A. McCammon, J. Chem. Phys. **95,** 1175 (1991).

[110] M. Mezei, J. Chem. Phys. **86,** 7084 (1987).

[111] J.Gao, M. Karplus, K. Kuczera, and B. Tidor, Science **244,** 1069 (1989).

[112] M. Karplus and B. Tidor, Biochemistry **30,** 3217 (1991).

[113] L. X. Dang, M. Merz, and P. A. Kollman, J. Am. Chem. Soc. **111,** 8505 (1989).

[114] U. C. Singh, Proc. Natl. Acad. Sci **85,** 4280 (1988).

[115] U. C. Singh and S. J. Benkovic, Proc. Natl. Acad. Sci **85,** 9519 (1988).

[116] S. Boresch and M. Karplus, J. Mol. Biol **254,** 801 (1995).

[117] A. E. Mark and W. F. van Gunsteren, J. Mol. Biol **240,** 167 (1994).

[118] *For a detailed discussion see.* J. T. Brown, Ph.D. thesis, University of Bristol, 1996.

[119] *CAChe Satellite: A Chemists Guide to CAChe for Windows* (Oxford Molecular Group Inc., 1995).

[120] L. Fettre, A. Ferrarini, F. Pacchiele, and P. L. Nordio, Molec. Cryst. Liq. Cryst. **290,** 109 (1996).

[121] G. Gottarelli, M. Hibert, B. Samori, G. Solladie, G. P. Spada, and R. Zimmermann, J. Am. Chem. Soc. **105,** 7318 (1983).

[122] F. J. Vesely, J. Comput. Phys. **47,** 291 (1982).

[123] M. R. Wilson, Liq. Cryst. **21,** 437 (1996).

[124] T. Z. M. Denti, T. C. Beutler, W. F. van Gunsteren, and F. J. Diederich, J. Phys. Chem. **100,** 4256 (1996).

[125] G. Gottarelli, G. P. Spada, R. Bartsch, G. Solladie, and R. Zimmermann, J. Org. Chem. **51,** 589 (1986).

[126] A. Ferrarini, P. L. Nordio, P. V. Shibaev, and V. P. Shibaev, Liq. Cryst. **24,** 219 (1998).

[127] C. McBride, M. R. Wilson, and J. A. K. Howard, Molec. Phys. **93,** 955 (1998).

[128] T. Kihara, J. Phys. Soc. Japan **6,** 289 (1951).

[129] A. Ferrarini, G. J. Moro, and P. L. Nordio, Liq. Cryst. **19,** 397 (1995).

[130] A. Ferrarini, G. J. Moro, and P. L. Nordio, Phys. Rev. E **53,** 681 (1996).

[131] A. Ferrarini, G. J. Moro, and P. L. Nordio, Molec. Phys. **87,** 485 (1996).

[132] L. Feltre, A. Ferrarini, F. Pacchiele, and P. L. Nordio, Molec. Cryst. Liq. Cryst. **290,** 109 (1996).

[133] M. R. Wilson, J. Chem. Phys. **107,** 8654 (1997).

[134] J. W. Emsley, G. R. Luckhurst, and C. P. Stockley, Proc. R. Soc. Lond. A **381,** 139 (1982).

[135] J. W. Emsley, G. R. Luckhurst, and C. P. Stockley, Molec. Phys. **44,** 565 (1981).

[136] M. R. Wilson, "Molecular Modelling," in *Handbook of Liquid Crystals*, D. Demus, J. Goodby, G. W. Gray, H.-W. Spiess, and V. Vill, eds., (Wiley-VCH, Weinheim, 1998), Vol. 1, Chap. III.3.

[137] M. R. Wilson, "Atomistic simulations of liquid crystals," in *Structure and Bonding: Liquid Crystals*, M. Mingos, ed., (Springer-Verlag, Heidelberg, 1999).

[138] M. R. Wilson and M. P. Allen, Molec. Cryst. Liq. Cryst. **198,** 465 (1991).

[139] M. R. Wilson and M. P. Allen, Liq. Cryst. **12,** 157 (1992).

[140] M. R. Wilson, J. Molec. Liq. **68,** 23 (1996).

[141] I. Ono and S. Kondo, Molec. Cryst. Liq. Cryst. **8,** 69 (1991).

[142] G. Krömer, D. Paschek, and A. Geiger, Ber. Bunsenges Phys. Chem. **97,** 1188 (1993).

[143] J. Huth, T. Mosell, K. Nicklas, A. Sariban, and J. Brickmann, J. Phys. Chem. **98,** 768 (1994).

[144] C. W. Cross and B. Fung, J. Chem. Phys. **101,** 6839 (1994).

[145] A. V. Kolmolkin, A. Laaksonen, and A. Maliniak, J. Chem. Phys. **101,** 4103 (1994).

[146] *DL_POLY is a package of molecular simulation routines written by W. Smith and T. R. Forester, copyright The Council for the Central Laboratory of the Research Councils, Daresbury Laboratory at Daresbury, Nr. Warrington (1996). The replicated data form of SHAKE is called RD-SHAKE and is described in section 2.6.8 of the DL_POLY_2.0 reference manual.*

[147] T. L. Hill, J. Chem. Phys. **16,** 399 (1948).

[148] W. L. Jorgensen and J. Tirado-Rives, J. Am. Chem. Soc. **110,** 1666 (1988).

[149] N. Nevins, K. S. Chen, N. L. Allinger, and K. S. Chen, J. Comput. Chem. **17,** 699 (1996).

[150] N. Nevins, J. H. Lii, N. L. Allinger, and K. S. Chen, J. Comput. Chem. **17,** 695 (1996).

[151] N. Nevins and N. L. Allinger, J. Comput. Chem. **17,** 730 (1996).

[152] N. L. Allinger, K. S. Chen, J. A. Katzenellenbogen, S. R. Wilson, and G. M. Anstead, J. Comput. Chem. **17,** 747 (1996).

[153] W. L. Jorgensen, J. D. Madura, and C. J. Swensen, J. Am. Chem. Soc. **106,** 6638 (1984).

[154] G. Kaminski and W. L. Jorgensen, J. Phys. Chem. **100,** 18010 (1996).

[155] M. J. Cook and M. R. Wilson, Liq. Cryst. p. accepted for publication (2000).

[156] M. J. Cook and M. R. Wilson, Liq. Cryst. p. accepted for publication (2000).

[157] E. Garcia, M. A. Glaser, N. A. Clark, and D. M. Walba, Theochem - J. Molec. Struc. **464,** 39 (1999).

[158] W. L. Jorgensen, D. S. Maxwell, and J. Tirado-Rives, *Support material for OPLS-AA force field* (1996).

[159] W. L. Jorgensen and T. B. Nguyen, J. Comput. Chem. **14,** 195 (1993).

[160] *Gaussian 94 is a package written by M. J. Frisch and A. Frisch and J. B. Foresman, copyright Gaussian,Inc., Carnegie office park, Pittsburgh, (1994-1996).*

[161] M. Shibakami and A. Sekiya, Acta Crystallogr. Sect C **51,** 326 (1995).

[162] W. H. Press, B. P. Flannery, S. A.Teukolsky, and W. T. Vetterling, in *Numerical Recipies* (Cambridge University Press, 1988), Chap. 10.

[163] D. M. Pawar, K. K. Wilson, and E. A. Noe, JOC **65,** 1552 (2000).

[164] *DL_POLY is a package of molecular simulation routines written by W. Smith and T. R. Forester, copyright The Council for the Central Laboratory of the Research Councils, Daresbury Laboratory at Daresbury, Nr. Warrington (1996).*

[165] W. L. Jorgensen, E. R. Laird, T. B. Nguyen, and J. Tirado-Rives, J. Comput. Chem. **14,** 206 (1993).

[166] N. D. Lebedeva and Y. A. Katin, Russ. J. Chem. Phys. **46,** 1088 (1972).

[167] D. R. Lide and H. V. Kehiaian, *CRC Handbook of Thermophysical and Thermochemical data* (CRC Press, 1994).

[168] D. A. Dunmur and K. Toriyama, "Dielectric Properties," in *Handbook of Liquid Crystals*, D. Demus, J. Goodby, G. W. Gray, H.-W. Spiess, and V. Vill, eds., (Wiley-VCH, Weinheim, 1998), Vol. 1, Chap. VII.4.

[169] S. Y. Yakovenko, A. A. Muravski, G. Kromer, and A. Geiger, Molec. Phys. **86,** 1099 (1995).

[170] S. Y. Yakovenko, G. Kromer, and A. Geiger, Molec. Phys. **275,** 91 (1996).

[171] S. Y. Yakovenko, A. A. Muravski, F. Eikelschulte, and A. Geiger, Liq. Cryst. **24,** 657 (1998).

[172] M. R. Wilson, Ph.D. thesis, University of Sheffield, 1988.

[173] K. Toriyama and D. A. Dunmur, Molec. Cryst. Liq. Cryst. **139,** 123–142 (1986).

[174] D. A. Dunmur and K. Toriyama, Liq. Cryst. **1,** 169 (1986).

[175] M. R. Wilson and D. A. Dunmur, Liq. Cryst. **5,** 987 (1989).

[176] F. Tournilhac, L. M. Blinov, J. Simon, D. B. Subachius, and S. V. Yablonsky, Synthetic Materials. **54,** 253 (1993).

[177] F. Tournilhac, L. Bosio, J. Simon, L. M. Blinov, and S. V. Yablonsky, Liq. Cryst. **14,** 405 (1993).

[178] M. Mauzac, H. T. Nguyen, F. Tournilhac, and S. V. Yablonsky, **240,** 461 (1995).

[179] S. Hauptmann, T. Mosell, S. Reiling, and J. Brickmann, Chem. Phys. **208,** 57 (1996).

[180] D. A. Dunmur and M. R. Wilson, J. Chem. Soc. Faraday Trans. 2 **84,** 1109 (1988).

[181] M. Bremer, "personal communication,", 1995, (Work carried out at Merck KGaA, Darmstadt).

[182] D. A. Dunmur and K. Toriyama, Molec. Cryst. Liq. Cryst. **264,** 131 (1995).

[183] M. J. Cook and M. R. Wilson, Molec. Cryst. Liq. Cryst. p. accepted for publication (2000).

[184] F. M. Leslie, Advances in Liquid Crystals 4 (1979).

[185] F. M. Leslie, Quart. J. Mech. Appl. Math **19,** 357 (1966).

[186] F. M. Leslie, Arch. Ratl. Mech. Anal **28,** 265 (1968).

[187] J. L. Ericksen, Arch. Ratl. Mech. Anal **23,** 266 (1968).

[188] J. L. Ericksen, Molec. Cryst. Liq. Cryst. **7,** 153 (1969).

[189] M. G. Clark and F. M. Leslie, Proc. R. Soc. Lond. A **361,** 463 (1978).

[190] P. K. Currie, Molec. Cryst. Liq. Cryst. **28,** 335 (1974).

[191] W. Helfrich, J. Chem. Phys. **51,** 4092 (1969).

[192] M. Miesowicz, Bull. Acad. Polon. Sci. Lett., Ser. A, Sci. Math. p. 228 (1936).

[193] D. Demus and G. Pelzl, Zeitschrift Chemie **1,** 21 (1982).

[194] H. Kneppe and F. Schneider, in *Handbook of Liquid Crystals* (Oxford University Press, Oxford, 1998), Chap. 2.

[195] O. Nakagawa, M. Imai, H. Naito, and A. Sugimura, Jpn. J. Appl. Phys **35,** 2767 (1996).

[196] M. Imai, H. Naito, M. Okuda, and A. Sugimura, Molec. Cryst. Liq. Cryst. **262,** 267 (1995).

[197] M. Imai, H. Naito, M. Okuda, and A. Sugimura, Jpn. J. Appl. Phys **33,** 3482 (1994).

[198] M. Imai, H. Naito, M. Okuda, and A. Sugimura, Molec. Cryst. Liq. Cryst. **259,** 37 (1995).

[199] M. Imai, H. Naito, M. Okuda, and A. Sugimura, Jpn. J. Appl. Phys **33,** 119 (1994).

[200] V. Zwetkoff, Acta Physicochimica URSS **10,** 555 (1939).

[201] W. H. de Jeu, in *Physical Properties of Liquid Crystalline Materials* (Gordon and Breach, New York, 1980).

[202] J. Prost and H. Gasparoux, Phys. Lett. A **36,** 245 (1971).

[203] F. Brochard, P. Pieranski, and E. Guyon, Phys. Rev. Lett. **28,** 1681 (1972).

[204] H. Schad, J. Appl. Phys. **54,** 4994 (1983).

[205] P. E. Cladis, Phys. Rev. Lett. **28,** 1629 (1972).

[206] P. R. Gerber, Appl. Phys. **A26,** 139 (1981).

[207] F. J. Bock, H. Kneppe, and F. Schneider, Liq. Cryst. **3,** 217 (1988).

[208] F. M. Leslie, G. R. Luckhurst, and H. J. Smith, Chem. Phys. Lett **13,** 368 (1972).

[209] A. Manabe, to be published. (unpublished).

[210] S. Sarman, Physica A **240,** 160 (1997).

[211] S. Sarman, J. Chem. Phys. **103,** 10378 (1995).

[212] S. Sarman, J. Chem. Phys. **104,** 342 (1996).

[213] S. Sarman, J. Chem. Phys. **108,** 7909 (1998).

[214] D. J. Evans and G. P. Morriss, in *Statistical Mechanics of Nonequilibrium Liquids* (Academic, London, 1990).

[215] *GBMOL: A replicated data molecular dynamics program to simulate combinations of Gay-Berne and Lennard-Jones sites. Author: Mark R. Wilson, University of Durham, (1996).*

APPENDIX

A

Conferences, Courses and Seminars

Conferences

The following is a list of the conferences attended during the course of my Ph.D from 1997-2000.

Sheffield Hallem University, 26th November 1997.
CCP5 workshop: Modelling the behaviour of liquid crystals near to solid substrates.

Hull University, 16-18th December 1997.
BLCS Winter Workshop.

Durham University, 24-27th March 1998.
CCP6 workshop: Optimisation Methods in Chemical Physics.

Durham University,6-9th April 1998.

The Royal Society of Chemistry National Congress and Young Researchers meeting.

Merck House, Poole, 20-21st April 1998.

Merck CASE Conference.

Erice, Sicily, 11-21st June 1998.

NATO ASI Advances in Computer Simulations of Liquid Crystals.

Edinburgh University, 7-9th September 1998.

CCP5 Annual Meeting: Making and Breaking Potentials.

London University, 14th December 1998.

Molecular Modelling: A tool for the modern era.

Durham University, 29-31st March 1999.

BLCS Annual Meeting.

Southampton University, 19-20th April 1999.

Merck CASE Conference.

UMIST, 21-29th June 1999.

Methods in molecular simulation: Summer School.

Daresbury Laboratory, 12th July 1999.

CCP5 workshop: Free energy workshop.

Warwick University, 14th February 2000 .

Southampton University, 10-11th April 2000.

Merck CASE Conference.

Strathclyde University, 17-19th April 2000.
BLCS Annual Meeting.

Courses

The following is a list of the postgraduate courses attended during the first year of my Ph.D.

Practical Nuclear-Magnetic Resonance

An introduction to some of the more practical aspects of modern NMR. Spectrometers-which bits do what; locking and shimming; pulse lengths. Experiments available, and the information available from them. Two-dimensional experiments. Use of applied gradients in pathway selection. Practical difficulties/limitations. Strategy for determination using NMR. Worked examples.

Diffraction and Scattering Methods

Summary of crystallographic terms: Bragg's Law, diffraction theory, space-group symbols and their definition, calculation of structure factors and electron density from measured intensities. Introduction to the practical methods used to measure diffraction data powder, single crystal; 4-circle automated diffractometer; electronic counting; their analysis to solve crystal structures. Allowance for the systematic errors in the experiment; interpretation and application of the crystallographic results. Interpretation of crystallographic papers in the literature.

Molecular Modelling

Definition of Molecular Modelling. Range of chemical applications. Overview of computational methods. Availability of software. Links to experimental results. Energy and force fields in molecular dynamics. Optimistaion of molecular geometry. Conformational space analysis. Simulation of molecular dynamics. Semi empirical methods. Electronic effects in conjugated pi-systems. Ab-initio

calculation. Density functional theory. Current and future developments. Practical computation: Navigation, optimisation, and conformational space analysis. Visulisation of computational results of molecular orbital calculations. Intermolecular interaction. Analysis of a set of problems.

.....

Seminars

The following is a list of the seminars in the chemistry department from 1997-2000. The ones marked with an asterisk were attended.

1997 - 1998

October 8 Professor E. Atkins, Bristol University.

Advances in the control of architecture for polyamides: from nylons to genetically engineered silks to monodisperse oligoamides

October 15 Dr. R. M. Ormerod, Keele University.

Studying catalysts in action

October 21 Professor A. F. Johnson, IRC, Leeds University.

Reactive processing of polymers: science and technology

October 22 Professor R. J. Puddephatt (RSC Endowed Lecture),
University of Western Ontario.

Organoplatinum chemistry and catalysis

October 23 Professor M. R. Bryce, Durham University, Inaugural Lecture.

New Tetrathiafulvalene Derivatives in Molecular, Supramolecular and Macromolecular Chemistry: controlling the electronic properties of organic solids

October 29 Professor B. Peacock, Glasgow University.

Probing chirality with circular dichroism

October 28 Professor A. P. de Silva, The Queen's University, Belfast.

Luminescent signalling systems

November 5 * Dr. M. Hii, Oxford University.
Studies of the Heck reaction

November 11 Professor V. Gibson, Imperial College, London.
Metallocene polymerisation

November 12 * Dr. J. Frey, Southampton University.
Spectroscopy of liquid interfaces: from bio-organic chemistry to atmospheric chemistry

November 19 * Dr. G. Morris, Manchester University.
Pulsed field gradient NMR techniques: Good news for the Lazy and DOSY

November 20 Dr. L. Spiccia, Monash University, Melbourne, Australia.
Polynuclear metal complexes

November 25 Dr. R. Withnall, Greenwich University.
Illuminated molecules and manuscripts

November 26 * Professor R.W. Richards, Durham University, Inaugural Lecture.
A random walk in polymer science

December 2 * Dr. C. J. Ludman, Durham University. *Explosions*

December 3 Professor A. P. Davis, Trinity College Dublin.
Steroid-based frameworks for supramolecular chemistry

December 10 * Sir G. Higginson, former Professor of Engineering in Durham and retired Vice-Chancellor of Southampton University.
1981 and all that

December 10 Professor M. Page, Huddersfield University.
The mechanism and inhibition of beta-lactamases

January 14 * Professor D. Andrews, East Anglia University .
Energy transfer and optical harmonics in molecular systems

January 20 Professor J. Brooke, Lancaster University.
What's in a formula? Some chemical controversies of the 19th century

January 27 Professor R. Jordan, University of Iowa, USA.

Cationic transition metal and main group metal alkyl complexes in olefin polymerisation

January 28 * Dr. S. Rannard, Courtaulds Coatings, Coventry.

The synthesis of dendrimers using highly selective chemical reactions

February 3 Dr. J. Beacham, ICI Technology

The chemical industry in the 21st century

February 4 * Professor P. Fowler, Exeter University.

Classical and non-classical fullerenes

February 11 Professor J. Murphy, Strathclyde University.

February 17 Dr. S. Topham, ICI Chemicals and Polymers

Perception of environmental risk; The River Tees, two different rivers

February 18 * Professor G. Hancock, Oxford University.

Surprises in the photochemistry of tropospheric ozone

February 24 * Professor R. Ramage, Edinburgh University.

The synthesis and folding of proteins

February 25 Dr. C. Jones, Swansea University.

Low coordination arsenic and antimony chemistry

March 4 * Professor T. C. B. McLeish, IRC of Polymer Science Technology, Leeds University.

T*he polymer physics of pyjama bottoms (or the novel rheological characterisation of long branching in entangled macromolecules)*

March 11 Professor M. J. Cook, Dept of Chemistry, East Anglia University.

How to make phthalocyanine films and what to do with them

March 17 Professor V. Rotello, University of Massachusetts, Amherst.

The interplay of recognition & redox processes - from flavoenzymes to devices

March 18 * Dr. J. S. O. Evans, Oxford University.

Materials which contract on heating (from shrinking ceramics to bullet proof vests)

1998 - 1999

October 7 Dr. S. Rimmer, Ctr Polymer, Lancaster University.

New Polymer Colloids

October 9 Professor M. F. Hawthorne, UCLA, USA.

RSC Endowed Lecture

October 21 Professor P. Unwin, Warwick University.

Dynamic Electrochemistry: Small is Beautiful

October 23 Professor J. C. Scaiano, University of Ottawa, Canada.

In Search of Hypervalent Free Radicals, RSC Endowed Lecture

October 26 Dr. W. Peirs, University of Calgary, Alberta, Canada.

Reactions of the Highly Electrophilic Boranes HB(C6F5)2 and B(C6F5)3 with Zirconium and Tantalum Based Metallocenes

October 27 Professor A. Unsworth, Durham University.

What's a joint like this doing in a nice girl like you? In association with The North East Polymer Association

October 28 * Professor J. P. S. Badyal, Durham University.

Tailoring Solid Surfaces, Inaugural Lecture

November 4 * Dr. N. Kaltscoyannis, University College London.

Computational Adventures in d & f Element Chemistry

November 3 * Dr. C. J. Ludman, Durham University.

Bonfire night Lecture

November 10 * Dr. J. S. O. Evans, Durham University.

Shrinking Materials

November 11 Dr. M. Wills, Warwick University.

New Methodology for the Asymmetric Transfer Hydrogen of Ketones

November 12 Professor S. Loeb, University of Windsor, Ontario, Canada.
From Macrocycles to Metallo-Supramolecular Chemistry

November 17 * Dr. J. McFarlane,
Nothing but Sex and Sudden Death!

November 18 Dr. R. Cameron, Department of Materials Science & Metallurgy, Cambridge University.
Biodegradable Polymers

November 24 * Dr. B. G. Davis, Durham University.
Sugars and Enzymes

December 1 Professor N. Billingham, Sussex University.
Plastics in the Environment - Boon or Bane In association with The North East Polymer Association

December 2 Dr. M. Jaspers, Aberdeen University.
Bioactive Compounds Isolated from Marine Inverterates and Cyanobacteria

December 9 Dr. M. Smith Department. of Chemistry, Warwick University.
Multinuclear solid-state magnetic resonance studies of nanocrystalline oxides and glasses

January 19 Dr. J. Mann, Reading University.
The Elusive Magic Bullet and Attempts to find it?

January 20 Dr. A. Jones, Edinburgh University.
Luminescence of Large Molecules: from Conducting Polymers to Coral Reefs

January 27 * Professor K. Wade, Durham University.
Foresight or Hindsight? Some Borane Lessons and Loose Ends

February 3 Dr. C. Schofield, Oxford University.
Studies on the Stereoelectronics of Enzyme Catalysis

February 9 Professor D. J. Cole-Hamilton, St. Andrews University.
Chemistry and the Future of life on Earth

February 10 Dr. C. Bain, Oxford University.

Surfactant Adsorption and Marangoni Flow at Expanding Liquid Surfaces

February 17 Dr. B. Horrocks, Newcastle University.

Microelectrode techniques for the Study of Enzymes and Nucleic Acids at Interfaces

February 23 * Dr. C. Viney, Heriot-Watt University.

Spiders, Slugs And Mutant Bugs

February 24 Dr.. A. K. Duhme, York University.

Bioinorganic Aspects of Molybdenum Transport in Nitrogen-Fixing Bacteria

March 3 Professor B. Gilbert, York University.

Biomolecular Damage by Free Radicals: New Insights through ESR Spectroscopy

March 9 Dr. M. Warhurst, Chemical Policy issues, Friends of the Earth.

Is the Chemical Industry Sustainable?

March 10 Dr. A. Harrison, Edinburgh University.

Designing model magnetic materials

March 17 Dr. J. Robertson, Oxford University.

Recent Developments in the Synthesis of Heterocyclic Natural Products

May 11 * Dr. J. Sodeau, East Anglia University.

Ozone Holes and Ozone Hills

May 12 * Dr. D. Bruce, Exeter University.

The Synthesis and Characterisation of Liquid-Crystalline Transition Metal Complexes

1999 - 2000

October 13 Professor G. Fleet, Oxford University.

Sugar Lactone and Amino Acids

October 19 Professor K. Gloe, TU Dr.esden, Germany.

Tailor Made Molecules for the Selective Binding of Metal Ions

October 20 Professor S. Lincon, University of Adelaide.

Aspects of Complexation and Supramolecular Chemistry

October 25 Professor S. Collins, University of Waterloo, Canada.

Methacrylate Polymerisation using Zirconium Enolate Initiatore: Polymerisation Mechanisms and Control of Polymer Tacticity

October 27 Dr. C. Braddock, Imperial College.

Novel Catalysts for Atom Economic Transformations

November 3 Professor D. W. Smith, University of Waikato, New Zealand.

The Strengths of C-C and C-H bonds in Organic and Organometaliic Molecules: Emperical, Semi-emperical and Ab-initio Calculations.

November 10 Dr. I. Samuel, Durham University.

Improving Organic Light Emitting Diodes by Molecular, Optical and Device Design

November 18 Dr. G. Siligardi, Kings College London.

The use of Circular Dichrosim to Detect and Characterise Biomolecular Interactions in Solution

November 24 Proffeser T. Jones, Imperial College.

December 8 Professor D. Crout, Warwick University.

More Than Simply Sweet: Carbohydrates in Medicine and Biology

January 12 Professor D. Haddleton, Warwick University.

Atom Transfer Polymerisation- Whats the Hype All About?

January 19 Dr. H. Gleeson, Manchester University.

Ferrielectric liquid crystals

January 19 Professor P. R. Fielden, UMIST.

Miniaturised Chemical Analysis (Lab-on-a-chip): Functional or merely Fashionable?

February 2 C Wilson Head of Crystallography, ISIS Rutherford Appleton Laboratory

Protons in Motion, Neutron Diffraction Studies of Hydrogen Atoms in Organic Crystal Structures

February 9 Dr S Moratti, Cambridge University

Shape and Stereoselectivity in Polymers

February 16 Professor Kocienski, Glasgow University

Asymemetric Synthesis Using Planar Chiral TT-Allyl Cationic Complexes

February 23 * Dr N Clark UMIST

The Flow of Polymer Blends

March 1 * Professor D Tildsley, *Computer Simulation of interfaces Fact and Friction*

March 8 Professor J Courtieu, Universite de Paris-Sud Orsay

May 5 Professor R Hochstrasser, University of Pennsylvania USA

RSC Centenary Lecture